2013

Turbulence characteristics in unsteady and non-uniform flows and their impacts on the incipient motion of sediment transport-water resources-river mechanics

Ishraq Hamdan Al-Fadhli

University of Wollongong, ia179@uowmail.edu.au

2013

Turbulence characteristics in unsteady and non-uniform flows and their impacts on the incipient motion of sediment transport-water resources-river mechanics

Ishraq Hamdan Al-Fadhli
University of Wollongong, ia179@uowmail.edu.au

TURBULENCE CHARACTERISTICS IN UNSTEADY AND NON-UNIFORM FLOWS AND THEIR IMPACTS ON THE INCIPIENT MOTION OF SEDIMENT TRANSPORT-WATER RESOURCES-RIVER MECHANICS

A thesis submitted in fulfilment of the requirements for the award of the degree of

MASTER OF ENGINEERING - RESEARCH

From

UNVERSITY OF WOLLONGONG

By

ISHRAQ HAMDAN AL-FADHLI, B.Sc., M. Eng. Prac.

SCHOOL OF CIVIL, MINING AND ENVERIMENTAL ENGINEERING

December 2013

CERTIFICATION

I, Ishraq Hamdan Alfadhli, declare that this thesis titled “Turbulence characteristics in unsteady and non-uniform flows and their impacts on the incipient motion of sediment transport”, submitted in fulfilment of the requirements for the award of Master by research, in the School of Civil Mining and Environmental Engineering, University of Wollongong, is wholly my own work unless otherwise referenced or acknowledged. The document has not been submitted for qualifications at any other academic institution.

Ishraq Hamdan Talib Alfadhli
December 2013

ACKNOWLEDGEMENTS

It is a pleasure to thank my both supervisors (Assoc. Prof/ Shu-Qing Yang and Assoc. Prof/ Muttucumaru Sivakumar) who have taught me the steps that have allowed me to conduct this research. They taught me how to choose articles that relate to my research topic and how to deal with this field. Both of them explained everything in two ways directly and by examples. I am also thankful that Assoc. Prof/ Muttucumaru Sivakumar had an open mind in allowing someone with different background to do this research, and used this to reanalyse every data which required supporting Assoc. Prof/ Shu-Qing Yang's idea. Thanks very much also to Assoc. Prof/ Muttucumaru Sivakumar for spending time and effort to review this thesis and provide me with insightful remarks.

Also, I would like to acknowledge that my study has been conducted under a fully funded scholarship provided by the Iraqi Ministry of Higher Education and Scientific Research. This fully funded scholarship is greatly appreciated.

Many thanks to all people who work in the developing learning centre especially (Dr. Alisa Percy) to check my English Language. Also, I would like to thank librarians who work in the University of Wollongong library, as they were essential in helping me to obtain all resources that I needed. These resources were located in Australia, as well as around the world. I like also to express my thanks to my parents and friends in Iraq for their constant encouragement, understanding and patience and for their moral support. Last, but not least, I would like to express my deepest gratitude to my beloved husband Qasim, who has unconditionally supported me. Thank you for being wonderful husband together with our daughters Maryam, Sarah and Ruqia, you fill my life with happiness and inspiration every day.

RESEARCH PUBLICATIONS

1. Alfadhli, I., Yang, S.Q. and Sivakumar, M. (2012). Does the critical Shields stress for sediment transport depend on channel-bed slope? *Proceeding of 34 th Hydrology and Water Resources Symposium 19-22 November-HWRS*, pp. 117-128, Sydney, Australia.

2. Alfadhli, I., Yang, S.Q. and Sivakumar, M. (2013). Velocity distribution in non-uniform/ unsteady flows and the validity of Log law. *Proceeding of 13 th International Multidisciplinary Scientific GeoConference – SGEM 19-22 June*, pp. 425-432, Albena, Bulgaria.

3. Alfadhli, I., Yang, S.Q. and Sivakumar, M. (2013). Distribution of Reynolds shear stress in steady and unsteady flows. *Proceeding of 13 th International Multidisciplinary Scientific GeoConference – SGEM 19-22 June*, pp. 109-116, Albena, Bulgaria.

4. Alfadhli, I., Yang, S.Q., and Sivakumar, M. (2014). Influence of vertical motion on initiation of sediment movement. *Journal of Water Resources and Protection* (J WARP) Vol.6 No.18.

5. Alfadhli, I., Yang, S.Q. and Sivakumar, M. (2014). Why the observed turbulence intensities in non-uniform flow deviate from those in uniform flow? *Proceeding of 35 th Hydrology and Water Resources Symposium 24-27 February-HWRS*, Perth, Australia.

6. Alfadhli, I., Yang, S.Q. and Sivakumar, M. (2014). The prediction of turbulence intensities in unsteady flow. *Proceeding of 35 th Hydrology and Water Resources Symposium 24-27 February-HWRS*, Perth, Australia.

ABSTRACT

This study investigates turbulence characteristics in steady and unsteady non-uniform flows and how these flows affect the incipient motion of sediment transport. Specifically, it deals with two issues, one relates to the deviation of critical shear stress in non-uniform flow from that in Shield diagram, and the other is associated with the deviation of mean velocity profile and other turbulence characteristics in steady and unsteady non-uniform flows from the classical Log law or other their predictions in uniform flow. New formulas have been developed for the determination of critical shear stress and the prediction of longitudinal velocity and other turbulence characteristics, such as vertical velocity, Reynolds shear stress and turbulence intensities across the water depth in uniform and non-uniform (steady and unsteady) flows.

The deviation of critical shear stress from Shields diagram is often attributed to many factors like measurement errors, sediment gradation/shapes, or channel-bed slopes, but little attention has been paid to the effect of vertical velocity that could be caused by a non-uniformity, seepage or unsteadiness etc. This part has re-examined the measured data available in the literature and found that, the vertical velocity in a channel flow also leads to the deviation of critical shear stress from the standard Shield's diagram. A closer look of the measured data shows that positive/negative deviation of measured critical shear stress from Shields' prediction corresponds to the up/downward vertical velocity; the Shields diagram is valid only when the flow is uniform. A new theory for critical shear stress has been developed, which shows that the decelerating flows promote the mobility of sediment, but accelerating flows constrain its mobility. A unified critical Shields stress for sediment transport has been established, that can

predict the critical shear stress for the initial motion of sediment in both uniform and non-uniform flows.

This study also investigates the deviation of measured mean horizontal velocity profile from the classical Log law. The Log law is applicable in the inner region where $y/h < 0.2$ when compared with the measured longitudinal velocity. However, in the rest of water depth i.e. $y/h \geq 0.2$, the measured horizontal velocity profile deviates from its prediction using Log law. The deviation is negative when the flow is accelerating, or the measured longitudinal velocity profile fall below the Log law; the deviation becomes positive when the flow is decelerating, or the measured longitudinal velocity profile has higher value than the Log law. The reason for this deviation is attributed to the positive or negative value of flow acceleration generated from accelerating or decelerating non-uniform flows, respectively. For this reason, different empirical equations have been established to predict longitudinal velocity in accelerating and decelerating steady and unsteady flows depending on the dimensionless flow acceleration. Based on these developed equations, Log law, Cole's Wake law and Dip law have been combined together to predict the mean velocity profile in uniform and non-uniform steady and unsteady flows across the full depth of a channel. This modification has been confirmed based on experimental data sets available in the literature for both steady and unsteady flows, and a reasonable agreement between the measured and predicted mean velocity profile is obtained.

In a similar manner, new formulas to express the profiles of other turbulence characteristics, such as Reynolds shear stress, turbulence intensities and vertical velocity have been developed for both steady and unsteady non-uniform flows. The newly proposed equations are also dependent on the impact of flow acceleration on the deviation of these turbulence characteristics from those in uniform flow. The validity of

these proposed equations has been verified using published experimental data for smooth and rough rectangular open channels and good agreement between the predicted and observed profiles has been achieved. Based on these developed formulas, the turbulence characteristics in unsteady flow can be easily estimated because the time factor is not included.

In this study, another method to estimate the turbulence intensities profiles in unsteady flow has been found. This prediction depends on the ratio of Reynolds shear stress in non-uniform flow to that in uniform flow. Two empirical equations have been proposed to express the relationship between horizontal and vertical turbulence intensities with the measured Reynolds shear stress based on experimental data available in the literature. These empirical equations are tested using the experimental data of Song (1994), Nezu et al. (1997), Song and Chiew (2001) and Emadzadeh et al. (2010), good agreements have been achieved between the measured and predicted turbulence intensities by applying these relationships.

Based on this research, a total of seven new empirical equations have been developed and verified with literature data. These relationships can be used to predict turbulent structures and sediment transport in steady and unsteady flows and these findings significantly add to the body of scientific knowledge available in this area.

TABLE OF CONTENTS

LIST OF FIGURES

LIST OF TABLES

NOTATIONS

d_{50} Median diameter of sediment particles (mm);

τ_c Critical shear stress (N/m^2);

τ_* Dimensionless critical shear stress;

g Gravitational acceleration (9.81m/s^2);

ρ_s Sediment density (kg /m^3);

ρ_w Water density (kg /m^3);

R_* Dimensionless Particle Reynolds number ($R_* = \frac{u_* d_{50}}{\nu}$);

u_* Critical shear velocity (m/sec);

ν Kinematic viscosity of water and equal = 0.01 (cm^2/s);

S_f Energy slope (%);

R Hydraulic radius $R = \frac{cross\ section\ of\ wetted\ area}{wetted\ perimeter}$ (m);

d_* Dimensionless particle diameter $d_* = \left[\frac{(\rho_s - \rho_w)}{\rho_w} \frac{g d_{50}^3}{\nu^2} \right]^{1/3}$

S_0 Channel bed slope (%);

h Water depth (m);

y The vertical distance measured from the reference level of channel bed;

y_0 The reference bed level;

dh/dx The variation of water depth;

Q Flow discharge in (m^3/s);

U Depth averaged horizontal velocity $U = Q/(B*h)$ (m/s);

$\bar{u}$ Time averaged horizontal velocity at (y) (m/s);

$\bar{u}_h$ Time averaged horizontal velocity at the water surface (m/s);

V Depth averaged vertical velocity across the whole water depth (m/s);

$\bar{v}$ Time averaged vertical velocity at (y) in (m/s);

$\bar{v}_h$ Time averaged vertical velocity at the water surface (m/s);

V_b Vertical velocity in the sediment layer (m/s);

ω Particle's settling velocity (m/s);

ω' Net falling velocity (m/s);

B Flume width (m);

λ Empirical factor for flow without seepage;

λ_s Empirical factor for flow with seepage;

F_r Froude number by using $F_r = U / \sqrt{g * h}$;

n Roughness Coefficient $(n = d_{50}^{1/6} / 21.1)$;

$\bar{a}_1$ Flow acceleration in each point in steady non-uniform flow (m/s^2);

a_1 Depth averaged flow acceleration in steady non-uniform flow (m/s^2);

$\bar{a}_2$ Flow acceleration in each point in unsteady flow (m/s^2);

a_2 Depth averaged flow acceleration in unsteady flow;

t Time (s);

u' Horizontal turbulence intensities (m/s);

v' Vertical turbulence intensities (m/s).

1.1 Background

Sustainable river management is dependent on knowledge of river hydraulics and its application. One important aspect of this knowledge involves the causes of erosion, and sediment transport. Sediment transport is an important aspect of river hydraulics because of its impact on the earth surface, specifically bed forms, banks, estuaries and coastal lines. A sediment particle starts to move by water flow when the boundary shear stress is larger than its critical shear stress. Critical shear stress is the friction force per unit area, it is the force between two surfaces whenever these surfaces move or try to move. As a result of water flow in a river system, particles move in three different ways: movement near the bed (bed load); suspension through the water column (suspended load) and permanent suspension which always remains close to the free surface and it contains smaller particle sizes than the available materials in the bed (wash load). All these types of movement lead to erosion and sediment transport as changes to the river boundary occur. Thereby, sediment transport has a negative impact on water quality and light penetration, but more specifically, the increase of sediment concentrations affect the ecosystem, including fish and other aquatic living creatures' habitats and the process of photosynthesis.

The water flow in a river system can be classified into steady and unsteady flows. The difference between them is that the velocity in unsteady flow varies with time, i.e., $\frac{\partial \bar{u}}{\partial t} \neq 0$ and the reverse is true for steady flow. Unsteady flow can only be classified as non-uniform flow whereas steady flow can be classified into uniform and non-uniform flows. This flow uniformity, on the other hand, refers to the variation of flow velocity with space. Based on the definition of flow uniformity, the flow velocity in uniform flow has a similar value along the open channel, whereas in non-uniform flow, the flow

velocity increases or decreases along the channel. Uniform, unsteady flow, although unlikely to occur in nature, is theoretically possible. Non-uniform flow is classified into accelerating and decelerating flow and these non-uniform flows are represented in both steady and unsteady flows. Accelerating flow refers to an increase in flow velocity along an open channel flow whereas decelerating flow refers to a decrease in flow velocity along an open channel. Thus, these types of non-uniform flows are associated with river hydraulics and their characteristics are important in hydraulic engineering. The effect of accelerating and decelerating non-uniform flows are important because their turbulence characteristics are crucial for understanding how sediment movement and contamination occurs in rivers, lakes and coastal waters.

Phenomena, such as erosion, diffusion of matter, transport, deposition of sediment and flow resistance, are all linked to the characteristics of flow and velocity distributions. In other words, the rate of sediment particles transported by water flow is dependent on the flow characteristics. Therefore, a clear understanding of the link between sediment transport and the two types of non-uniform flows is crucial in modelling local sedimentation process, channel souring, sidewall erosion and flooding, and thus is vital to sustainable river management.

In the past, many laboratory experiments (Cardoso et al., 1991; Nezu et al., 1993; Song & Graf, 1994; Song, 1994; Kironoto & Graf, 1995; Song & Chiew, 2001) and theoretical studies (Yang & Lee, 2007; Yang & Chow, 2008; Yang, 2009) have been done to understand the flow characteristics and turbulence characteristics specifically in non-uniform flows. The experimental studies utilised various equipment, including an Acoustic Doppler Velocimeter (ADV); a Laser Doppler anemometer (LDA) and Hot Film Anemometer (HWA) etc., to measure the velocity profiles in three directions:

longitudinal or horizontal (*x*), vertical (*y*) and lateral direction (*z*). These velocity profiles were measured in both clear water and over smooth or rough bed. Of all the findings, the comprehensive work was done by Song (1994) and Song and Chiew (2001) who proved the existence of vertical velocity in accelerating and decelerating flow. While it is already known that the value of vertical velocity is zero in uniform one dimensional flow, in their studies, they found that accelerating flow is associated with a negative value or downward vertical velocity while decelerating flow is associated with a positive value or upward vertical velocity.

A number of studies concerned with flow characteristics have limited their work to the examination of vertical velocity and Reynolds shear stress distributions in the non-uniform flows. Yang and Lee (2007) limited their theoretical work to show the deviation of Reynolds shear stress distribution in accelerating and decelerating non-uniform flows over a rough bed from those in uniform flow. Yang and Lee (2007) reported that this deviation is related to the presence of upward and downward vertical velocity. Yang and Chow (2008) developed a one-to-one relation between the relative turbulence intensities and relative Reynolds shear stress. However, similar to this relationship in unsteady flow has not been developed. Yang (2009) investigated theoretically the effect of vertical velocity and turbulent structures in accelerating and decelerating flows on sediment transport. This theoretical investigation provides the physical explanation for the impact of non-uniform flow on the vertical velocity and the influence of vertical velocity on mass transport.

Generally, the distributions of turbulence characteristics, such as (longitudinal and vertical velocities, Reynolds shear stress and turbulent intensities) in non-uniform flow are different from those in uniform flow. Turbulent intensities and Reynolds shear stress

have linear distributions in uniform flow with high values near the bed surface and they decrease to have lower value at the free surface. However, these distributions have a fluctuating value above or below the uniform flow distribution dependent on two types of non-uniform flows. Accelerating non-uniform flow hampers the turbulence and Reynolds shear stress (below the uniform flow line) because the water velocity downstream is larger than upstream whereas the decrease of water velocity downstream generates decelerating flow which strengthens the turbulence and Reynolds shear stress (above the uniform flow). The reason for the difference of flow characteristics in uniform and non-uniform flows is related to the different values of vertical velocity that have been proved by Song (1994) and Song & Chiew (2001).

Furthermore, many studies have investigated the influence of non-uniform flow on critical shear stress for sediment transport over a rough bed (Cheng & Chiew, 1999; Afzalimhr et al., 2007; Emadzadeh et al., 2010). Critical shear stress is an important concept in studies about sediment motion as it refers to the incipient motion of sediment particles from the river bed. In uniform flow, the relationship between critical shear stress and grain diameter was first determined by Shields (1936). Applying Shield's diagram of critical shear stress to non-uniform flow, Afzalimhr et al. (2007) and Emadzadeh et al. (2010) demonstrated the values of critical shear stress for accelerating and decelerating non-uniform flows ranged above and below the Shields diagram. Further, Cheng and Chiew (1999) investigated the sediment motion with upward seepage and found the typical Shields diagram is invalid. In the Shields diagram, all their data points have lower value than expected by Shields in uniform flow. As a result, these latter investigations do not confirm to Shield's predictions. The reason for these deviations is related to the shear stress distributions in non-uniform flows.

Moreover, the present study also deals with the characteristics of unsteady flow. Unsteady flow refers to the variation of flow discharge or water depth versus time from the rising stage (before flow discharge reaching its maximum) to the falling stage (after flow discharge reaching its maximum) along the channel. In other words, unsteady flow appears during the passage of a flood in a natural river or open channel flow. The changes of velocity and water depth with respect to time are charted as a hydrograph where the velocity and water depth in the rising stage is shown to move from the base to the peak point and the falling time moves from the peak to the base point. It is clearly seen that the unsteady flow could be easier to work without including the time.

The turbulence characteristics of unsteady flow have been studied by some researchers experimentally. For example, Song (1994) measured the mean velocity and turbulence characteristics of unsteady flow over a gravel bed using an Acoustic Doppler Velocity Profiler or ADVP. Song found that the horizontal point velocity near the water surface reaches its maximum value earlier than the horizontal point velocity near the bottom, and the vertical velocity is always negative even when the experiments have been done using a positive bed slope. His experiment also demonstrated that the value of turbulence intensities in the rising stage is higher than that in the falling stage. Song also measured the distribution of Reynolds shear stress and turbulence intensities in unsteady flow. Reynolds shear stress distribution deviated notably from the linear distribution, but this was not explained in the literature. The similar results for accelerating flow in steady non-uniform were observed by Song and Chiew (2001).

Nezu et al. (1997) studied the turbulence characteristics in unsteady open channel flow over a smooth bed using a two component Laser Doppler Anemometer (LDA). Firstly, they measured the mean horizontal velocity profile near the bed flume (viscosity layer)

to evaluate the friction velocity. They proved that the friction velocity increases in rising flow, whereas it decreases in falling flow. Secondly, Nezu et al. (1997) measured the mean horizontal velocity profile and turbulence characteristics such as Reynolds shear stress and turbulence intensities across the whole water depth from the near bed channel up to the free water surface. They found that turbulence intensities in the horizontal and vertical directions near the water surface become smaller in the rising stage than in the falling stage. Nezu et al. also found that the measurement of Reynolds shear stress in unsteady flow has similar profile to that in uniform flow.

For sediment transport in steady and unsteady flows, Griffith and Sutherland (1977) found that there was no difference. However, Graf and Suszka (1987) and Suszka (1987), who derived a new formula from steady flow condition in order to compare the measurements and the calculations of sediment discharge, found that the measured sediment discharge is always larger than the calculated. This means that it is likely that there is some small difference in sediment discharge between steady and unsteady flow.

1.2 Justification of research

The present study describes a causal relationship between flow velocity and sediment transport. Accelerating and decelerating non-uniform in steady and unsteady flows always occur in natural waterways, but it is difficult to understand them even for the simplest case of gradually varied non-uniform flow in an open channel. This thesis will investigate the critical shear stress for sediment movement in steady / unsteady flows. The critical shear stress in uniform flow is a function of grain diameter as proposed by Shields (1936). However, in a steady non-uniform flow, it was found that the critical shear stress always significantly deviates from the Shields' prediction. The reason for this deviation has not been explained and not understood.

The turbulence characteristics in unsteady flow will be investigated in this study. Many researchers predicted the amount of sediment transport in unsteady flow using uniform flow condition (Yang, 1973; Van Rijn, 1984a, 1984b; Yang & Lim, 2003; Yang, 2005). It is difficult to apply the knowledge from uniform flows to unsteady flow as the two cases are different. As mentioned before, uniform flow means that the flow velocity and water depth have similar value from upstream to downstream. While in the unsteady flow, the flow velocity fluctuates from high to low, and therefore, the uniform and unsteady flows have different applications. All these differences ignored the variation of flow velocity with time. Therefore, the present study deals with two cases, firstly, the case of incipient motion of sediment particles in non-uniform flow and secondly, the turbulence characteristics in steady and unsteady flow.

From the above, it is clear that further research is needed to answer the following:

- Why observed critical shear stress for the incipient motion of sediment transport in non-uniform flow often deviates from the Shields prediction?
- Why the measurements of turbulence characteristics, such as ($\bar{u}, \bar{v}, -\rho\overline{u'v'}, u'$ and v') in steady and unsteady non-uniform flows deviate from those in uniform flow, and what is the impact of flow acceleration on the distribution of these turbulence characteristics?

In this study, the above mentioned questions will be answered based on theoretical considerations.

1.3 Aims and objectives

The overall aim of this research is to investigate the influence of turbulence characteristics in steady and unsteady non-uniform flows on sediment transport in an open channel flow.

The specific objectives of this study are:

1. Critically review literature to understand open channel flow processes with and without sediment movement in order to identify the knowledge gaps in the research area.
2. Why sometimes the Shields curve cannot express the incipient motion of sediment transport and explain the dependence of Shields stress on the variation of water depth along the open channel flow.
3. Establish a universal relationship between dimensionless critical shear stress and particle Reynolds number for both uniform and non-uniform steady flows and verify the newly established equation using the experimental data from literature.
4. Observe the influence of flow acceleration on turbulence characteristics for both steady and unsteady flows.
5. Develop new formulas to express turbulence characteristics in steady and unsteady flows without including the time factor based on the value of flow acceleration and using experimental data available in the literature to compare between the measured turbulence characteristics with the developed model.
6. Establish empirical relations between Reynolds shear stress and turbulence intensities in unsteady flow and investigate these relations using experimental data.

1.4 Scope of the study

To achieve the above mentioned objectives, the following must be considered:

- Using the Wollongong Library Website or other libraries, journals, books and conferences publications will be used in the literature review. Previous studies will be reviewed: how about their experimental setups; their observed relationship with and without sediment transport; and the conclusions and recommendation drawn from their results. This literature review will generate a holistic understanding of how these types of flow work in hydraulic engineering, and it will help to identify the knowledge gaps in their relationship with sediment transport in order to set out the objectives for the current study.
- Theoretical consideration for the influence of vertical velocity on the incipient motion will be provided. This vertical velocity generated from non-uniform steady flow has a different distribution depending on the type of non-uniform flow. The value of vertical velocity is negative when the flow is accelerating while it is a positive value when the flow is decelerating. As a result this vertical velocity affects the settlement of particle velocity, and therefore the original sediment density changes to the concept of "apparent" density. Furthermore, using experimental data available in the literature, the dependence of critical shear stress on the variation of water depth rather than the channel-bed slope will be proven.
- Shields diagram refers to the initial motion of sediment transport in steady uniform flow. This diagram describes dimensionless critical shear stress as an ordinate against the dimensionless particle Reynolds number as an abscissa. In order to extend its application, vertical velocity generating from non-uniform

flows will be included in both formulas based on experimental data of incipient motion available in the literature.

- 2-D unsteady flow varies in space (x and y) and time, thus it is generally complicated. In order to simplify it, the estimation of flow acceleration in steady and unsteady will be investigated. These estimations will be come from the integration of flow acceleration formulas for both steady and unsteady flows. Using experimental data available in the literature, the influence of flow acceleration on the distribution of turbulence characteristics in both steady and unsteady non-uniform flows will be identified. These influences will be illustrated graphically in this study. Along the x-axis, the dimensionless turbulence characteristics, such as mean horizontal and vertical velocity, Reynolds shear stress and horizontal / vertical turbulent intensities ($\bar{u}/u_*, \bar{v}/u_*$, $-\rho\overline{u'v'}/u_*^2, u'/u_*, v'/u_*$), respectively with respect to the shear velocity will be drawn, while the y-axis will present as y/h. In order to prove these influences, the value of dimensionless flow acceleration $a/(u_*^2/h)$ will be determined to compare its value with the deviation of these turbulence characteristics in non-uniform flow from those in uniform flow.
- The full profile of all turbulence characteristics from the bed up to the water surface in steady and unsteady non-uniform flows will be estimated. This estimation depends on the reason for the deviation of turbulence characteristics in non-uniform flow from those in uniform flow. In this study, we will also focus on the deviation of measured longitudinal velocity in the outer region from Log law which can only match well in the inner region. In order to fit with Log law, flow

acceleration generating from non-uniform flows will be included in the classical Log law using experimental data in steady and unsteady non-uniform flows.

- Experimental data in unsteady flows will be used to estimate the full profile of turbulence intensities. This prediction depends on the ratio of the measured Reynolds shear stress in non-uniform flow to that in uniform flow because the distribution of Reynolds shear stress is similar to the distribution of turbulence intensities.

1.5 Thesis structures

Chapter 1 presents the general background of different types of flow and their relations with the sediment transport.

Chapter 2 provides a critical review of literature for the existing research mainly on accelerating and decelerating non-uniform flows. This research reviews thematically unknowns for clear water and flows with sediment transport in non-uniform flows (accelerating and decelerating flows). Each part briefly discussed the works that have been done and has also concluded what is still unknown.

Chapter 3 illustrates the effect of accelerating and decelerating steady non-uniform flows on the incipient motion of sediment transport. This effect deals with the influence of vertical velocity in non-uniform flows on the deviation of critical shear stress value from the Shields diagram. In this chapter, a new formula to determine the vertical velocity in the sediment layer was developed. Experimental data related to the incipient sediment motion was used to extend Shields' diagram to predict the critical shear stress in non-uniform flows.

Chapter 4 provides new formulas to determine the value of flow acceleration in steady and unsteady flows. This chapter shows that there exists a significant responsibility of flow acceleration on the deviation of turbulence characteristics i.e. (longitudinal and vertical velocity, Reynolds shear stress, turbulence intensities and flow acceleration) in steady and unsteady non-uniform flows from those in uniform flow. By adding this influence to uniform flow equations, empirical formulas were established to express the full profile of these turbulence characteristics in uniform and non-uniform steady and unsteady flows.

Chapter 5 summarises the main conclusions of the investigation, based on the influence of non-uniform flows on the incipient sediment motion and the prediction of their turbulence characteristics. Some areas for further research are also suggested.

2.1 Introduction

This chapter reviews the studies on the interaction between water flow and sediment transport to clarify how water flow affects sediment transport. Water flow and sediment transport in an open channel are a familiar sight whether in a natural channel like that of a river or an artificial channel like that of an irrigation ditch. Studying various flows in natural or large man made channels are difficult, however they can be readily studied in laboratory flumes under controlled conditions. Numerous types of channel flows occur, for example, steady and unsteady flows, and they are dependent on water velocity, discharge or flow rate, water depth, and bed and water surface slope along the channel upstream to downstream. This critical review will cover a broad statement for these different types of flow and their relationship with sediment particles and sediment transport.

2.2 Steady and uniform flow

The definition of steady uniform flow implies that the water depth, water area, flow velocity and discharge or flow rate do not change with distance and time along an open channel, and as a result this type of flow is rarely found in natural rivers, as seen in Figure 2.1. This also implies that the energy slope, water surface and channel bed slope are parallel for uniform flow. The depth of uniform flow is called “normal depth”. Chow (1959) suggested that uniform flow should be regarded as steady flow only, since unsteady uniform flow is practically non-existent.

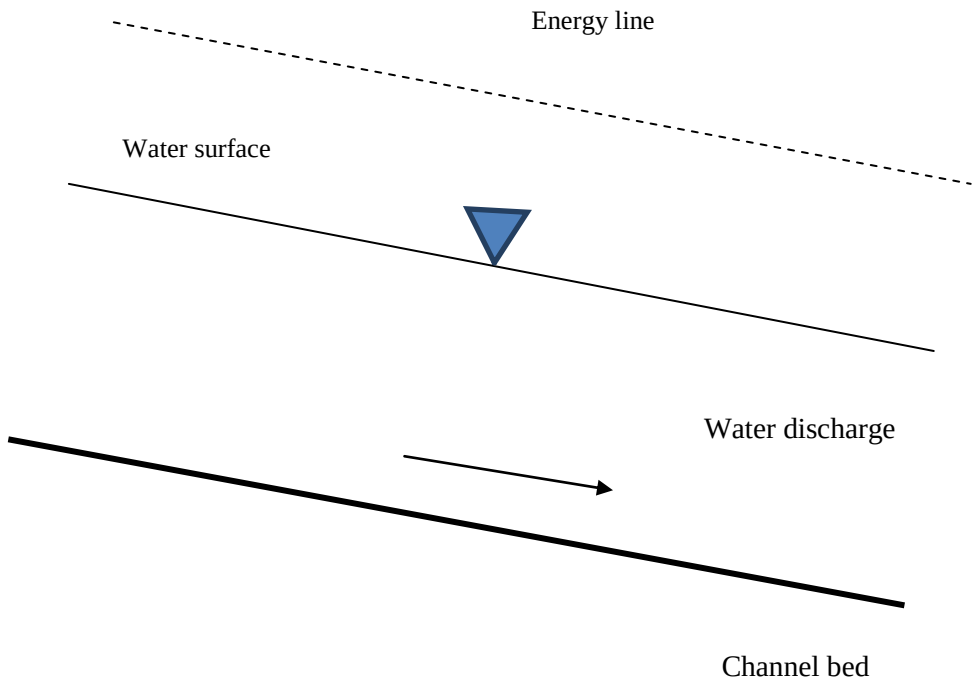

Figure 2.1: Steady uniform flow

In the past, numerous researchers have conducted their research in uniform flows in a laboratory open channel (Nezu, 1977; Nezu &Rodi, 1986; Cardoso et al., 1990; Nezu & Nakagawa, 1993; Kironoto & Graf 1994; Song, 1994; Yang & Lee, 2007); they investigated velocity profiles and turbulence characteristics in uniform flow over a smooth bed. Nezu and Rodi (1986) and Nezu and Nakagawa (1993) measured the longitudinal velocity in rectangular channels with an aspect ratio of $B/h > 6$ (where B and h are channel width and depth water, respectively). They suggested that the water column can be divided in to two different regions: the inner region and the outer region depending on the validity of Log law. They compared their results with the general formula for Log law over a smooth bed (Nezu & Rodi, 1986):

$$\frac{\bar{u}}{u_*} = A\ln\frac{yu_*}{\nu} + B \tag{2.1}$$

where the integral constant B=5.29; $A = 1/k$, where k is the universal von Kármán constant; u_* is shear velocity; ν is the kinematic viscosity; y is the vertical distance measured from the reference level of channel bed; and $\bar{u}$ is the point mean horizontal velocity at y.

Nezu and Nakagawa (1993) found that the Log Law (Equation 2.1) is only valid for the inner region, which is near the flume bed with a limited value of relative water depth $(y/h < 0.2)$, while the Cole's Wake Law is valid for the outer region which is near to the water surface with a limited value $(y/h \geq 0.2)$. They also found that the flow in the inner region is controlled by the inner parameters, such as shear velocity (u_*), the kinematic viscosity (ν) and the bed roughness (k_s) whereas in the outer region the flow is dominated by the maximum velocity and the water depth. These findings are supported by Cardoso et al. (1990) who obtained the same results even when the aspect ratio B/h in their experiments ranges between 4.6 and 7.3.

Kironoto and Graf (1994) measured turbulence characteristics in uniform open channel flow over a rough channel bed in a laboratory with large relative roughness $(0.05 < k_s/h < 0.08)$ and a limited bed slope (0.025% < S_0 <0.125%). They used two types of bed (rough plate with $d_{50} = 4.8mm$) and (gravel bed with $d_{50} = 23mm$).They found that the Log law is valid in the inner region for both types of bed when they compared their result with universal formula for prediction horizontal velocity using Log law's equation over a rough bed (Graf & Altinakar, 1993, p.56):

$$\frac{\bar{u}}{u_*} = A\ln\frac{y+y_0}{k_s} + B \tag{2.2}$$

where k_s is the roughness height = d_{50}; y_0 is the reference bed level = $0.2\,k_s$ and B is the constant of integration. Reynolds (1974) found that the value of B equals to $8.5\pm15\%$ for a rough bed.

Song (1994) measured in a laboratory channel the mean flow and turbulence characteristics of a uniform flow in a rough mobile bed $(0.058 < k_s / h < 0.16)$ with a steep open channel $(0.25\% < S_0 < 1.5\%)$ using an Acoustic Doppler Velocity Profiler (ADVP). Song compared his results of vertical and horizontal turbulence intensities with Kironoto and Graf (1994) and Nezu (1977). For a smooth bed, Nezu (1977) developed a new formula as an exponential law to calculate the full profile of horizontal and vertical turbulence intensities a cross the whole water depth from the bed up to the water surface as expressed below:

$$\frac{u'}{u_*} = 2.3\exp(-y/h) \tag{2.3}$$

$$\frac{v'}{u_*} = 1.27\exp(-y/h) \tag{2.4}$$

where u', v' are horizontal and vertical turbulence intensities, respectively and h = water depth. While for a rough bed, Kironoto and Graf (1994) found other relationships which are expressed as follows:

$$\frac{u'}{u_*} = 2.04\exp(-0.97 * y/h) \tag{2.5}$$

$$\frac{v'}{u_*} = 1.14\exp(-0.76 * y/h) \tag{2.6}$$

Song's data for the horizontal turbulence intensity supports the findings of Kironoto and Graf (Equations 2.5, 2.6), but fell slightly below the curve given by Nezu for smooth beds (Equations 2.3, 2.4). While the vertical turbulence intensity agrees with the exponential law only in the outer region, in the inner region, there is a deviation from Nezu's (1977) and Kironoto and Graf's (1994) results.

Reynolds shear stress distribution in uniform flow follows:

$$\frac{-\overline{u'v'}}{u_*^2} = 1 - \frac{y}{h} \tag{2.7}$$

The above formulas from Equation 2.1 to 2.7 predict the whole profile for mean horizontal velocity, Reynolds shear stress and turbulence intensities. The measured data points of Reynolds shear stress and turbulence intensities decrease with increasing y, which means these values of turbulence characteristics, have higher values near the bed than in the rest of the region. Equations 2.2, 2.5, 2.6 and 2.7 will be modified in Chapter 4, which will be universal to estimate the full profile for these turbulence characteristics in uniform, non-uniform steady and unsteady flows.

2.3 Steady and non-uniform flow

Most flow in natural rivers and open channels are non-uniform or spatially varied flow. Spatially varied flow is measured along one dimension because the hydraulic variables vary only along the length of the river. Even if the flow is steady, spatial variation can result from changes occurring along the channel boundaries for example, channel geometry changes, or from lateral inflows to the channel, or both. The non-uniform flow can be classified into two types: rapidly varied flow and gradual or tranquil varied flow, as shown in Figure 2.2.

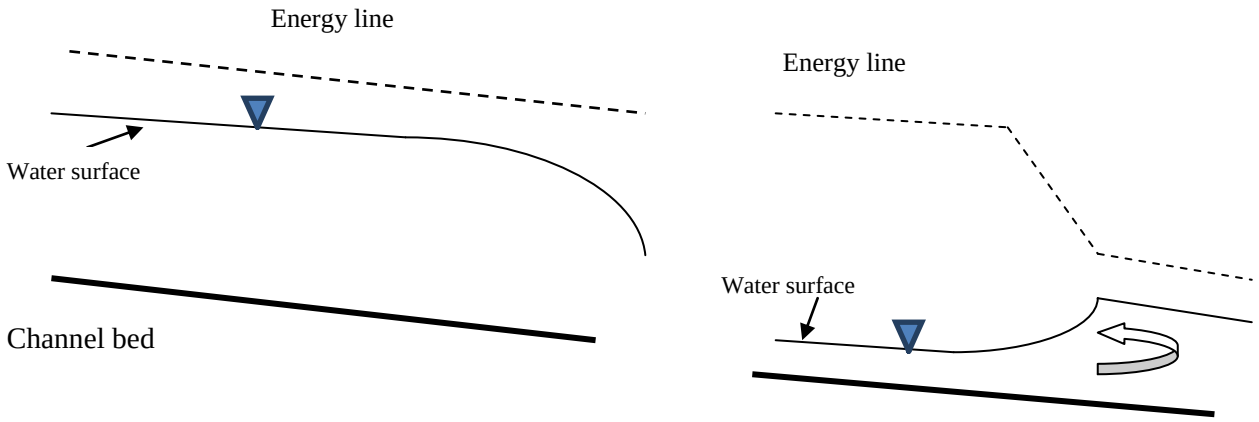

(a) Gradually varied (b) Rapidly varied

Figure 2.2: Steady non-uniform flow.

In a channel, the flow type can change depending on the level of bed slope and the variation of water depth which can alter based on the existence of obstructions. The flow varies rapidly when spatial changes to the flow (depth and velocity) occur abruptly and the pressure distribution is not hydrostatic and it occurs over a short distance near obstacles. Thus, the condition of rapidly varied flow is occurred when the flow depth changes abruptly in the direction of flow within a short length. Rapidly varied flow is

usually a local phenomenon such as hydraulic jump and hydraulic drop. The change of flow from supercritical to subcritical is known as hydraulic jump. The supercritical condition is represented by the value of Froude number which is the ratio of inertial to gravitational forces and it follows the following formula:

$$F_r = \frac{U}{\sqrt{gh}} \tag{2.8}$$

where F_r = Froude number; U = depth averaged flow velocity in a channel (m/s); g = acceleration of gravity (m/s^2); and h = water depth (m). When this value of Froude number is more than one, this means that the inertial forces exceed the gravitational forces. This exceedance of inertial forces relates to the high water velocity along an open channel flow.

Another type of non-uniform flow is gradually or tranquil varied flow, this flow appears when the water surface changes over a long distance and usually connects between uniform flow and rapidly varied flow. The gradually varied flow is referred to subcritical when the flow water velocity is small and as a result the inertial force is less than gravitational forces ($F_r \leq 1$).

These types of non-uniform flows (gradually and rapidly varied flows) can be divided into two types: accelerating and decelerating flows. Generally, non-uniform flow can be generated when the characteristic of a channel changes, such as the cross-sectional shape of a channel or bed slope or bed roughness. All these types of non-uniform flows (accelerating and decelerating flows) for both gradually and rapidly varied flow are demonstrated in Figure 2.3, where (a, b) represent accelerating and decelerating flows in the gradually varied state while (c, d) represent accelerating and decelerating flow in the rapidly varied state.

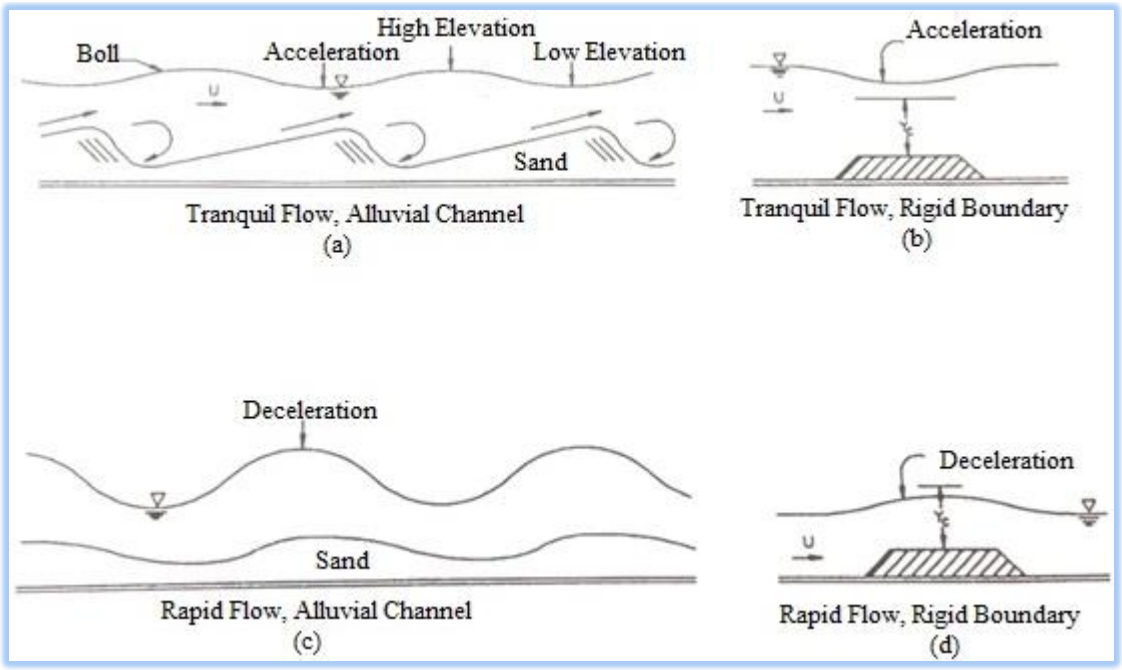

Figure 2.3: Relationship between water surface and bed configuration for gradually or tranquil and rapid flow (Simons & Senturk, 1976 cited in US Army Corps of Engineers, 1996).

As can be seen in Figure 2.3 (a, b), where there is a change in bed level or existing obstructions, the water level is affected. If the bed channel is covered by sand or there is an obstruction at the bottom, then the separation of flow often happens just downstream of the crest of the sand waves. According to Figure 2.3 (a), the water flow will accelerate over the humps, and decelerate over the troughs, while Figure 2.3 (b) shows the occurrence of accelerating flow over an obstruction through the gradually varied flow. In other words, the flow is changed from decelerating to accelerating or vice versa. Figure 2.3 (c, d) explain the phenomena of high turbulent flows for both accelerating and decelerating cases. If the water flow passes over obstructions and humps, this leads to an increase in the water level resulting in decelerating flow, whereas the pools and troughs lead to accelerating flow.

From the above descriptions, various types of non-uniform flows are identified, specifically the characteristics of accelerating and decelerating flow in an open channel. Accelerating flow is an effect of high water velocity along the open channel, and this results in the water depth downstream being lower than upstream, and vice versa for decelerating flow, as shown in Figures 2.4 (a, b).

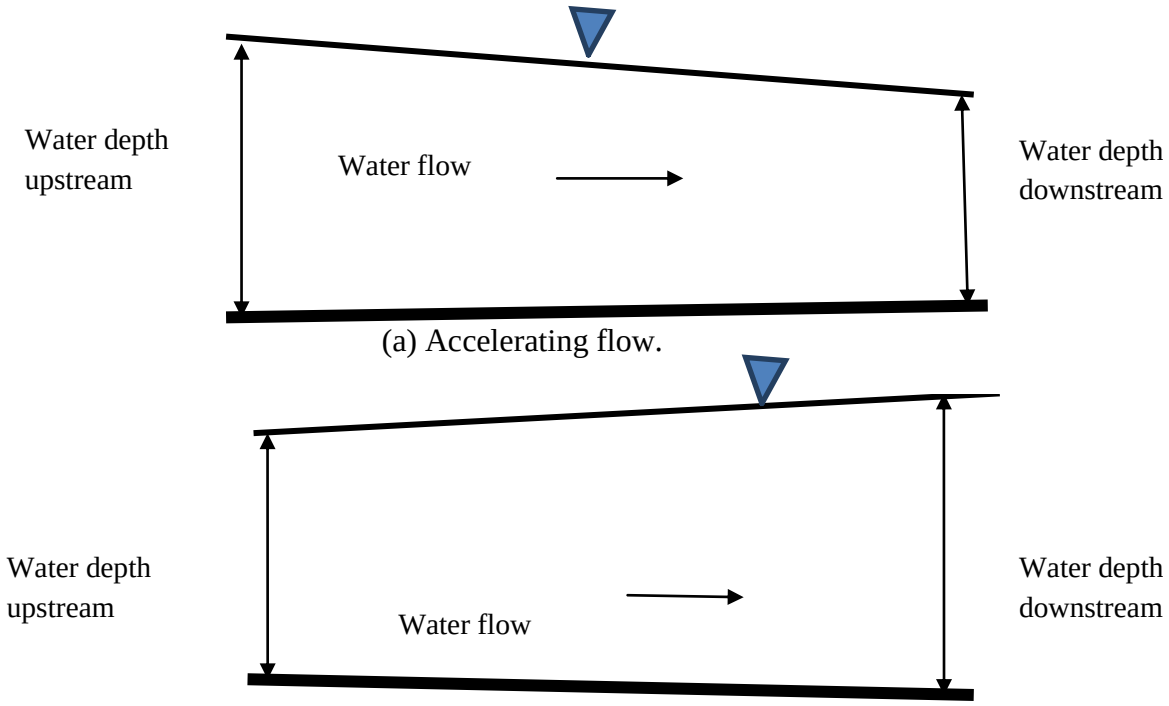

(a) Accelerating flow.

(a) Decelerating flow.

Figure 2.4: Illustration of non–uniform (a) accelerating flow (b) decelerating flow.

This study is particularly concerned with gradually varied flow (accelerating and decelerating non-uniform flows) and their relationship to sediment transport.

Studies into the generation of non-uniform flow as an effect of variation in bed slope have been conducted in both smooth and rough channel conditions. Using a smooth open channel, Cardoso et al. (1991) conducted laboratory experiments on the structure of spatially accelerating flows, where upstream water depth is greater than the downstream depth using a Hot-Film Anemometer. They concluded that the longitudinal

velocity distributions cannot be represented entirely by the universal Log Law except at regions very close to the wall. In other words, they found that the Log Law is only valid for regions close to the bed whereas the Cole's Wake Law is valid for the outer region. They found that accelerating flow leads to a decrease in water depth along the channel when they compared their results with those in uniform flow.

Kironoto and Graf (1995) used the Log Law to fit with the measured velocity profiles of accelerating and decelerating flows over rough plate and gravel beds. They found that the measured velocity profile deviates from the Log law; it becomes higher value than the Log law's prediction when the flow is decelerating and vice versa. They also measured turbulent intensities and Reynolds shear stress near the bed, and found that a decelerating flow promotes turbulence while an accelerating flow constrains turbulence. These results are different to those findings for uniform flow where the Reynolds shear stress and turbulence intensities have linear distributions along the water column. They also measured the longitudinal velocity in different cross-sections, i.e. ($x = 9.89$, 10.39, 11.245, 11.7 and 12.21m, where x is the distance from the flume entrance to the measuring cross section). From these measurements, they illustrated that the velocity profile of accelerating flow is fuller than that of decelerating flow. In the near bed region, the velocity profile of accelerating flow is generally larger, while it is smaller at the near surface region when compared with that of decelerating flow. They also found that the measured turbulence intensities did not fit well with their calculations using the uniform formulas (see Equations 2.5 and 2.6). However, their research has limitations because it was conducted with a small aspect ratio where $B/h < 2.9$ and limited bed slope (-0.85%, -0.75%, -0.5%, 0.75% and 1.25%).

Using a rough open channel with a gravel bed, Song (1994) measured the velocity and turbulence characteristics of accelerating and decelerating flow using an Acoustic

Doppler Velocity profiler (ADVP) which has 3 transducers, two of them were installed with a relevant angle and the third one was put in a horizontal position. Using this equipment, horizontal and vertical velocities and their fluctuations were measured instantaneously. Song's experiments were conducted in a 16.8 m long, 0.6m wide and 0.8 m height and the bed channel was covered by gravel with different size distribution d_{50}=12.3mm, d_{16}= 0.9cm and d_{84}=1.65cm. To generate accelerating and decelerating flows, Song (1994) used different positive and negative bed slope ranging from -0.93% to 0.9% with high water discharge between 145 L/s to 60 L/s in the negative bed slope and low water discharge from 90 L/s to 55 L/s in the positive bed slope. The aim of his research was to describe the turbulence characteristics of both types of non-uniform flows in equilibrium boundary layer conditions. Song (1994) measured two dimensional velocities at a point downstream where the flow was fully developed. He concluded that the vertical velocity is much smaller than horizontal velocity. He also found that vertical velocity is non-zero which means that negative vertical velocity is found in accelerating flow while positive vertical velocity is found in decelerating flows.

Song (1994) also discussed the turbulent characteristics in non-uniform flow. He found that the measured data points of Reynolds shear stress and turbulence intensities were higher and lower than those in uniform flow. These findings are the same as Kironoto and Graf's (1995) observations even when there were significant variations in bed slope and water discharge.

Using a rough channel bed with $d_{50} = 2.6$mm and using an Acoustic Doppler Velocimeter (ADV), Song and Chiew (2001) measured turbulence characteristics in non-uniform flow in different across sections along the channel. The ADV was installed vertically to measure the water velocity in three dimensions with different cross-

sections. Their experiments were conducted in an 18m long, 0.6m wide and 0.8m high open channel where the bed slope ranged from -0.2% to 0.75%. Their results showed that turbulent characteristics fluctuate above and below those in uniform flow as observed previously in the literature. Song and Chiew (2001) found the same as Song (1994) observations that vertical velocity in non-uniform flow has different values. However, although their research demonstrated different values, they did not discuss the influence of non-uniform flow on vertical velocity.

Yang and Lee (2007) and Yang and Chow (2008) discussed the influence of non-uniform flow on vertical velocity. They expressed the vertical velocity at the free water surface as:

$$\bar{v}_h = -\bar{u}_h * \Delta S \tag{2.9}$$

where $\bar{v}_h$ and $\bar{u}_h$ are mean velocities at the free surface in longitudinal and vertical directions, respectively; and ΔS refers to the difference between the free water surface slope and bed slope along the channel. Using Equation 2.9, the authors demonstrated that the values of vertical velocity fluctuated in non-uniform flows. This fluctuation refers to variations between the free water surface and bed slope along the channel, as shown in Figure 2.5. In uniform flow, the value of ΔS is zero, when the surface water slope is equal to the bed slope due to consistent water depth along the channel. In this case, $\bar{v}_h$ is equal to zero. In accelerating non-uniform flow, the value of ΔS is positive when the water surface slope is higher than the bed slope due to a decrease in water depth along the channel, and based on Equation 2.9, this case generates a negative value of $\bar{v}_h$. While the positive value of ΔS in decelerating non-uniform flow generates positive $\bar{v}_h$ due to the increase of water depth along the channel.

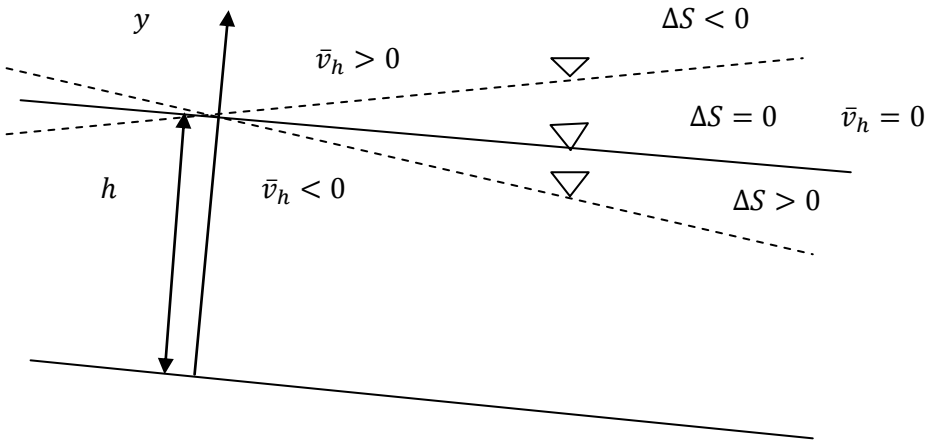

Figure 2.5: Sketch for non-uniform flow (Yang & Chow, 2008).

Therefore, it is clearly seen the existence of vertical velocity in non-uniform flow whether positive or negative value is related to variations between water depth and bed slope along the channel.

More recently, turbulence intensities in steady and non-uniform flow have been expressed depending on the value of Reynolds shear stress (Yang and Chow, 2008). The relationship between the deviations occurring in Reynolds shear stress and turbulence intensities, which can be evaluated as follows:

$$\frac{u'}{u'_{uf}} = F\left(\frac{-\overline{u'v'}}{-\overline{u'v'}_{uf}}\right) \tag{2.10}$$

$$\frac{v'}{v'_{uf}} = G\left(\frac{-\overline{u'v'}}{-\overline{u'v'}_{uf}}\right) \tag{2.11}$$

where F and G as functions; and $u^{'},v^{'}$ are turbulence intensities in x and y directions respectively. Yang and Chow verified these developed relationships using Song's (1994) experimental data sets in uniform and non-uniform steady flows.

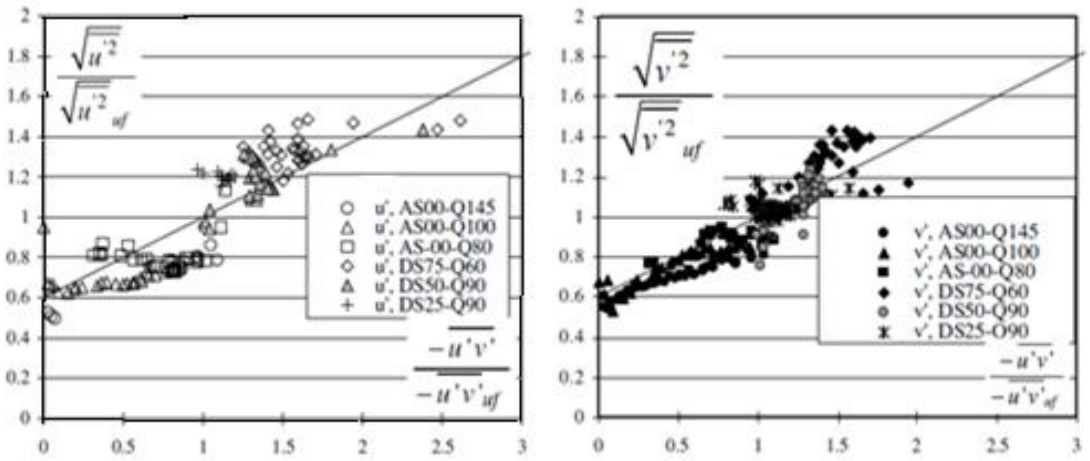

Figure 2.6: The relationship between the relative turbulence intensities and the relative Reynolds shear stress based on Song, 1994 experimental data (Yang and Chow, 2008).

Figure 2.6 indicates that there is a relationship between the measured Reynolds shear stress $(-\rho\overline{u^{'}v^{'}})$ and the value of horizontal and vertical turbulence intensities $u^{'},v^{'}$ respectively, and this relationship can be approximated by:

$$y = 0.6 + 0.4x \tag{2.12}$$

Equation 2.12 is applicable for the prediction of horizontal and vertical turbulence intensities in steady non-uniform flows based on the measured Reynolds shear stress, where y represents the relative horizontal and vertical turbulent intensities as $(u^{'}/u^{'}_{unf.})$ $(v^{'}/v^{'}_{unf.})$ respectively; the subscript "$unf.$" denotes these turbulence intensities in uniform flow and x is the relative Reynolds shear stress as $(-\overline{u^{'}v^{'}}/-\overline{u^{'}v^{'}}_{unf.})$. From

Equation 2.12, if $-\overline{u'v'} = -\overline{u'v'}_{unf.}$, $y = 1$, this indicates that turbulence intensities are identical to that of uniform flow. Obviously, if the value of ($-\overline{u'v'} / -\overline{u'v'}_{unf.}$) is higher than 1, then y is also higher than 1. This means that if the measured Reynolds shear stress is higher than in uniform flow, then the corresponding turbulent intensities will be higher than uniform flow. Conversely, if ($-\overline{u'v'} / -\overline{u'v'}_{unf.}$) <1, Equation 2.12 gives $y < 1$, all data points must be located below uniform flow. In the present study, Yang and Chow's work will be extended to define the relationship between Reynolds shear stress and turbulence intensities as well as developing a new method to express the value of turbulence intensities in unsteady flow.

2.4 Unsteady flow

Natural rivers and open channels often encounter unsteady flow. This type of flow depends on time and velocity. If the velocity at a point changes with time, the flow is unsteady. Methods for analysing unsteady flow account for time explicitly as an important variable. The turbulence characteristics across the water depth in an open channel unsteady flow will be predicted in Chapter 4. Therefore, the velocity and the distributions of turbulence characteristics, such as horizontal and vertical velocity, Reynolds shear stress and turbulence intensities must be identified in the literature. This section outlines the experimental findings that demonstrated the non-liner distribution of turbulence characteristics in unsteady flow and this is similar to those distributions in steady non-uniform flow.

Nezu and Nakagawa (1991 & 1993) observed velocity profiles and turbulent characteristics in unsteady open channel flow over a rough bed using a Laser Doppler Anemometer (LDA). They used a new circulation system to measure turbulence

characteristics. They found that Log Law was valid in the inner region for unsteady flow distributions when they analysed their results of the mean velocity with linear distribution in the semi-log plot.

Nezu et al. (1997) measured turbulence characteristics in an unsteady open channel flow over a smooth bed using the two components Laser Doppler Anemometer (LDV) and water wave gauge. They found that the observed values of friction velocity, turbulence intensity and Reynolds shear stress increase in the rising and decreases in the falling periods.

Over a gravel bed and using an Acoustic Doppler velocity profile (ADVP), Song (1994) measured: two dimensional velocities in an entire water column; turbulence characteristics through negative and positive bed slope; and flow rate. Downward vertical velocity is found even when the bed slope is positive. He also demonstrated that the value of turbulence intensity in the rising period is larger than that in the falling period. The measurements of Reynolds shear stress in the flow with a larger negative bed slope had a clear concave form and a maximum value near the bed while Reynolds shear stress for the positive bed slope was less concave. He also found the measurements of Reynolds stress are larger in the rising period than in the falling period which is similar to Nezu et al.'s (1997) observation.

Bagherimiyab and Lemmin (2011) measured mean velocity in accelerating and decelerating unsteady open channel flow. They described two types of non-uniform flow, accelerating and decelerating flows in two ways, with and without fine sediment using a combination of an Acoustic Doppler and Imaging method (ADVP) with an optical method (PTV) for suspended sediment particle tracking. They found that the measurement of mean horizontal velocity profile and Log law are applicable in the inner

layer (near the flume bed) whereas the higher shear velocity was observed more in accelerating flow than in decelerating flow for comparable water depths.

It is clearly illustrated from all the experimental findings described above that turbulence characteristics in unsteady flows have non-linear distributions and this is similar to those distributions in steady non-uniform flow. In order to simplify the study of an unsteady flow, new equations for the estimation of these turbulence characteristics will be developed based on the main reason for the deviation of turbulence characteristics from the uniform flow line.

2.5 Turbulence characteristics in steady and unsteady flows

The turbulence characteristics of open channel flows are of great interest in hydraulic engineering. This topic is important because turbulence characteristics are crucial for predictions of sediment transport in rivers, lakes and coastal waters where the effect of flow is significant. For several decades, the accurate predictions of the mean horizontal and vertical velocities, Reynolds shear stress and turbulence intensities in fully developed open channel uniform and non-uniform flows have challenged scientists and hydraulic engineers. As discussed before, these turbulence characteristics in uniform and non-uniform flows have been widely studied. The increase or decrease of flow velocity along the open channel affects on the turbulence and thus the distributions of these turbulence characteristics in this type of flow are different from those in uniform flow. Unfortunately, the underlying mechanism for this difference has not been well revealed, and the prediction for these turbulent characteristics based on the reason for this difference is not available in the literature.

In uniform flows, many researchers developed formulas to predict longitudinal velocity in the entire water column. Prandtl (1925) investigated the most popular formula which

is called the Log law (see Equation 2.1) to predict the mean longitudinal velocity distribution near the boundary layer of plate $(y/h < 0.2)$ with mixing length hypothesis in fully developed open channel flow. Equation 2.1 is only applicable for smooth bed and then this equation was modified by Grass (1971) to be applicable for a rough bed by taking into account particle diameters (see Equation 2.2).

In Equations 2.1 and 2.2, there are two constant (A and B) shown in Table 2.1 and these can be calculated from the experimental results. From the numerical investigations, Reynolds (1974, p.187) investigated the constant value of integration B for smooth and rough beds. Nikuradse (1932) measured the velocity distribution over flat plates and circular pipes. The findings from his measurements verified accuracy of the mean velocity profile in pipes as calculated with a Log law. Keulegan (1938) found the value of A is similar to Nikuradse result, but the other constant depends on the nature of the bed surface. For a smooth open channel, many researchers have obtained different values for these two constants when they plotted their measured velocity profiles as $\bar{u}/u_*$ versus $\ln(u_* y/\nu)$, for instance, Klebanoff (1954), Townsend (1956), Huffman and Bradshaw (1972), Steffier et al. (1985), and Nezu and Rodi (1986). It is clearly seen from these investigations, the value of A has a range of variation between 2.43 and 2.5, and the value of B from 4.9 to $8.5 \pm 15\%$.

A handful of researchers checked the validity of Log law in an unsteady flow over a smooth bed (Nezu et al. 1997) and over a rough bed (Song, 1994). They found that the Log law is applicable for y/h <0.2. Therefore, the Log law formula is widely used to express the longitudinal velocity profile near the boundary layer in open channel and pipes over a smooth and rough bed for both steady and unsteady flows.

However, the experimental data from flat boundary layer flows (Coles, 1956; Monty et al., 2009) and pipe flows (Zagarola, 1996 etc.) suggested that the Log law may be not always be correct in describing the velocity distribution. This was also observed in open channel flows over 100 years ago by river engineers, such as Francis (1878), who discovered from their measurement in rivers that maximum velocity does not appear at the free surface as the Log law predicts, but occurs below the free surface. This effect, also called "dip-phenomenon", remains an open question for researchers who still debate its mechanism. Consequently, an article in Science (Cipra, 1996) commented that: "… the law of the wall was viewed as one of the few certainties in the difficult field of turbulence, and now it should be dethroned. Generations of engineers who learned the law will have to abandon it". In open channel flows, the same phenomenon has been known for a long time, but the mechanism is still unclear.

Log law was extended by Coles (1956) to predict the velocity profile in boundary layer flows. Coles introduced an additional term (i.e. wake term) as an empirical correction function to express the deviation of measurement velocity from the prediction of Log law. Cole's Wake law has the following formula:

$$\frac{\bar{u}}{u_*} = \frac{1}{k}\ln(\frac{y}{y_0}) + B + \frac{2\prod}{k}\sin^2(\frac{\pi}{2}\frac{y}{h}) \tag{2.13}$$

where $\prod$ is the wake strength parameter and its value for different researchers is presented in the last column of Table 2.1. For example, in an open channel uniform flow, Nezu & Nakagawa (1993, p.51), Coleman and Alonso (1983) and Cardoso et al. (1990) obtained different values of $\prod$ shown in Table 2.1 over a smooth bed while Kironoto and Graf (1995) found Π value in the range of -0.08 to 0.15 over a gravel bed with non-uniform flow. In unsteady flow, Song (1994) found the Π-value for a run

with small bed slope is smaller than one with larger bed slope. For small slope, i.e. S_0 = -0.6%, the values of Π ranges between -0.007 to 0.129, while for large slope, i.e. S_0 = 0.3% its values are larger than 0.206. However, Nezu et al. (1997) found that the value of Π increases with an increase of time and attains a maximum ($\Pi \cong$ 0.3-0.4) before the flow depth attains a peak. From all these previous findings, it is clearly seen that the average value of Π is not universal for all cases of flow over smooth or rough beds.

Table 2.1: Different values of A, B and Π in different bed conditions.

Researchers	*A*	*B*	Π
Reynolds (1974)		5 for smooth bed $8.5 \pm 15\%$ for rough bed	--
Nikuradse (1932)	2.5	5.5	--
Klebanoff (1954)	2.44	4.9	--
Townsend (1956)	2.44	7	--
Huffman and Bradshaw (1972)	2.44	5	--
Steffier et al. (1985)	2.5	5.5	--
Nezu & Rodi (1986)	2.43	5.29	--
Nezu & Nakagawa (1993)	2.5	5.1	0.55
Coleman & Alonso (1983)	--	--	0.31
Cardoso et al. (1990)	--	--	-0.077
Kironoto & Graf (1995) (non-uniform steady flow)	--	--	(-0.08) – (0.15)
Song (1994) (unsteady flow)	--	--	(-0.007) – (0.129) for small bed slope. >0.206 for large bed slope.
Nezu et al. (1997) (unsteady flow)	--	--	0.3-0.4

From the brief review, it is concluded that the Log law is applicable only in the inner region with $(y/h < 0.2)$ while the velocity profile in the rest of the water column i.e. $(y/h \geq 0.2)$ can be predicted using Cole's Wake law. Therefore, the Log law cannot express the velocity distribution accurately in the outer region. Whilst significant advances have been made by using Cole's Wake law, the mechanism of Cole's Wake law and the associated wake strength parameter are not fully understood.

Yang et al. (2004) discussed the dip phenomenon, in which the maximum longitudinal occurs below the water surface. They suggested that the Cole's Wake law is not able to describe the entire velocity profile when the dip-phenomenon exists. Therefore, Yang et al. (2004) modified the Log law by adding a term to express the dip phenomenon instead of the Cole's Wake law based on Reynolds equations:

$$\frac{\bar{u}}{u_*} = \frac{1}{k}\ln(\frac{y}{y_0}) + \frac{\alpha}{k}\ln(1-\frac{y}{h}) \tag{2.14}$$

where α is the dip correction factor and can be determined by:

$$\alpha = 1.3\exp(-\frac{z}{h}) \tag{2.15}$$

where z is the distance from the sidewall in z direction. It is clearly seen from Equation 2.14 that a dip model consists of two logarithmic distances, one from the bed (i.e. Log law) and the other from the free surface i.e. $\ln(1-y/h)$, and a deviation-correction factor α that can be determined empirically using Equation 2.15. Similarly, the Yang et al. (2004) model is unable to fit the cases where measured velocity is locally higher than the prediction of Log law. Therefore, further research is needed to develop a general expression of velocity in open channel flow to be universal for all types of flow; uniform, steady and unsteady non-uniform flow.

Turbulence characteristics such as Reynolds shear stress and turbulence intensities have been measured in both steady and unsteady flows. In unsteady flow, Song (1994) found that the measurements of Reynolds shear stress and turbulence intensities along the water column have clearly concave distributions. For a steady non-uniform flow, Song used positive and negative bed slopes to generate accelerating and decelerating flow. The measured data show that the distributions of these turbulence characteristics are not linear in either an accelerating or a decelerating flow. The concave distributions of

Reynolds shear stress and turbulence intensities are observed in accelerating flow where the bed slope was negative; while convex distributions are observed for decelerating flow with positive bed slope. In accelerating flow, the maximum value of measured data points occurs close to the bed surface while in decelerating flow its maximum value occurs above the bed surface (at $y > 0$). In both of these accelerating and decelerating non-uniform flows, the minimum value of measured data points occurs at the water surface. Song (1994) also confirmed the linear distribution for steady uniform flow when he compared with the non-uniform flow. From this comparison, the measurements of Reynolds shear stress and turbulent intensities are smaller in accelerating flow, but larger in decelerating flow when compared with the linear distribution in uniform flow.

Based on these similarities in the distributions of Reynolds shear stress and turbulence intensities, Yang and Chow (2008) found a relationship between Reynolds shear stress and turbulence intensities in non-uniform flow. They developed an empirical equation to express this relationship based on experimental data available in the literature.

The measurement of vertical velocity has a similar distribution in steady and unsteady flow. Song (1994) and Song and Chiew (2001) demonstrated different values for vertical velocity generating from steady non-uniform flow. Song (1994) used large negative and small positive bed slopes but the results showed the flow is always accelerating with negative vertical velocity distribution along the water column.

It is possible from experiments that these turbulence characteristics have similar distributions for both steady and unsteady non-uniform flows. Based on the review outlined above, the classical Log law is applicable when the flow is uniform as almost all flows in rivers are unsteady or non-uniform flows. In the literature, however, there is no universal model to express the velocity in the complex flow conditions. Thus more

research is needed to clarify why the Log law cannot predict the measured longitudinal velocity well in non-uniform flows, and how we can ignore the time in unsteady flow using only its variation with space. More investigation is needed for the deviation of other turbulence characteristics in non-uniform stead and unsteady flows from that in uniform flow. Besides, although these researchers have found the difficulty of Log law and other developed equations in uniform flow to match with the measured mean velocity and other turbulence characteristics, but none of them has proposed a universal formula that can predict the full profile for longitudinal and vertical velocities, Reynolds shear stress and turbulence intensities in non-uniform flows, which further justifies this research.

2.6 The influence of water flow on the initiation of sediment transport

Sediment transport has been the most challenging issue to hydraulic and river engineers as it deals with the inter-motion of water and sediment particles. It is important to study it because sediment transport determines the evolution of rivers, coastlines and the earth surface. Many studies over the past decades have been conducted, and it is well known that sediment transport can be affected by a variety of factors, such as the velocity, uniformity and steadiness of water flow, particle size and channel slope, etc. (Neil, 1967; Yang, 1973; Yang, 2005; Afzalimehr et al., 2007; Lamb et al., 2008). The velocity, uniformity and steadiness of a water flow play a significant role for sediment movement, and these factors will form the basis of the present study.

In sediment transport, a key focus of research is on the initial motion of bed sediment, which refers to the very beginning of particle movement. There is a condition for this movement; if the shear stress on a particle exceeds a certain value, sediment particles begin to move (Chien & Wan, 1999; Yang, 1996). This has been referred as the critical

shear stress: it means that in moving water, sediment starts to move as a result of a friction force created on individual sediment particles (Julien, 1995). This force causes sediment particles to be suspended or rolled through the channel bed. The vertical and horizontal drag forces are shown in Figure 2.7.

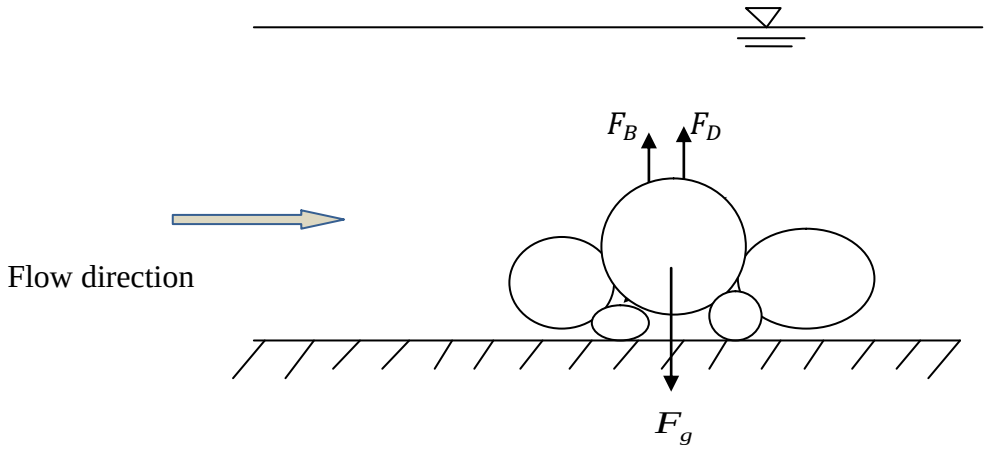

Figure 2.7: The vertical forces affect on the sediment particle.

Figure 2.7 shows three types of vertical forces that affect sediment particles through their movement inside the water:

- Gravity force (F_g) which is the weight of sediment that can be expressed as follows:

$$F_g = \frac{\pi}{6} d^3 g \rho_s \tag{2.16}$$

in which d is the particle diameter and ρ_s is the density of the particle.

- Buoyancy force (F_B) is an upward acting force exerted by a fluid that opposes an object's weight and has the following formula:

$$F_B = \frac{\pi}{6} \rho_w d^3 g \tag{2.17}$$

where ρ_w is the density of water.

- Drag force (F_D) or fluid resistance refers to forces which act on a solid object in the vertical direction, and can be expressed as:

$$F_D = \frac{1}{2}\rho_w \omega^2 C_d A \tag{2.18}$$

where C_d is the drag coefficient, and ω is the fall velocity of the particle.

The drag force is a resistive force acting on a particle that undergoes settling and the fall velocity of a particle is reached when there is a balance between drag force (F_D) and submerged weight of the particle $(F_g - F_B)$, i.e., when:

$$C_d \pi \frac{d^2}{4} \frac{\rho_w \omega^2}{2} = \pi \frac{d^3}{6} g(\rho_s - \rho_w) \tag{2.19}$$

where Equation 2.19 describes a spherical particle's falling velocity ω in still water (without any momentum) and this equation will be used in Chapter 3 to investigate a relationship between vertical velocity generated from non-uniform flow and fall particle velocity.

Before this can be investigated, it is first necessary to understand the different values of vertical velocity generated from uniform and non-uniform flows. In 2-D uniform flow, the value of time averaged vertical velocity is equal to zero, however, the instantaneous vertical velocity is not be zero. This statement is true due to the consistency of water depth and flow velocity upstream to downstream. In decelerating non-uniform flow, the measured data of vertical velocity is zero near the boundary layer, and it takes a linear positive distribution along the water column when the water depth upstream is higher than downstream. In contrast, accelerating non-uniform flow generates negative value of vertical velocity along the water column when the water depth upstream is less than

downstream (Song, 1994; Song & Chiew, 2001). From this explanation, it is clearly seen that the vertical velocity generated from non-uniform flow affects sediment transport. The first ever study which relates to sediment transport in uniform flow was done by Shields (1936). When Shields did his experiment, he presented the results according to the dimensionless groups given as dimensionless critical shear stress τ_* and Reynolds particle number R_* as presented in Equations 2.20 and 2.21:

$$\tau_* = \frac{\tau_c}{(\rho_s - \rho_w)gd_{50}} = \frac{\rho_w u_*^2}{(\rho_s - \rho_w)gd_{50}} \tag{2.20}$$

$$R_* = \frac{u_* d_{50}}{\nu} \tag{2.21}$$

where τ_c is the critical shear stress at incipient motion; d_{50}= median diameter of sediment particles (m) which means the total sediment passing sieve about 50% from these diameters; ν = kinematic viscosity of water; u_*= critical shear velocity for incipient motion (m/s); g = gravitational acceleration (m/s^2); and ρ_s , ρ_w = sediment and water density (kg/m^3) respectively.

Shields conducted flume experiments on the initial motion and bed load transport of sediment as affected by the specific gravity of the sediment. He used different types of sediment, such as Barite, Amber and Lignite ranging between a median size of 0.36-3.44 mm. Shields presented his results according to the dimensionless critical shear stress as a function of grain diameter as a shaded zone for the beginning of sediment movement in what has come to be called the Shields diagram (see Figure 2.8) .

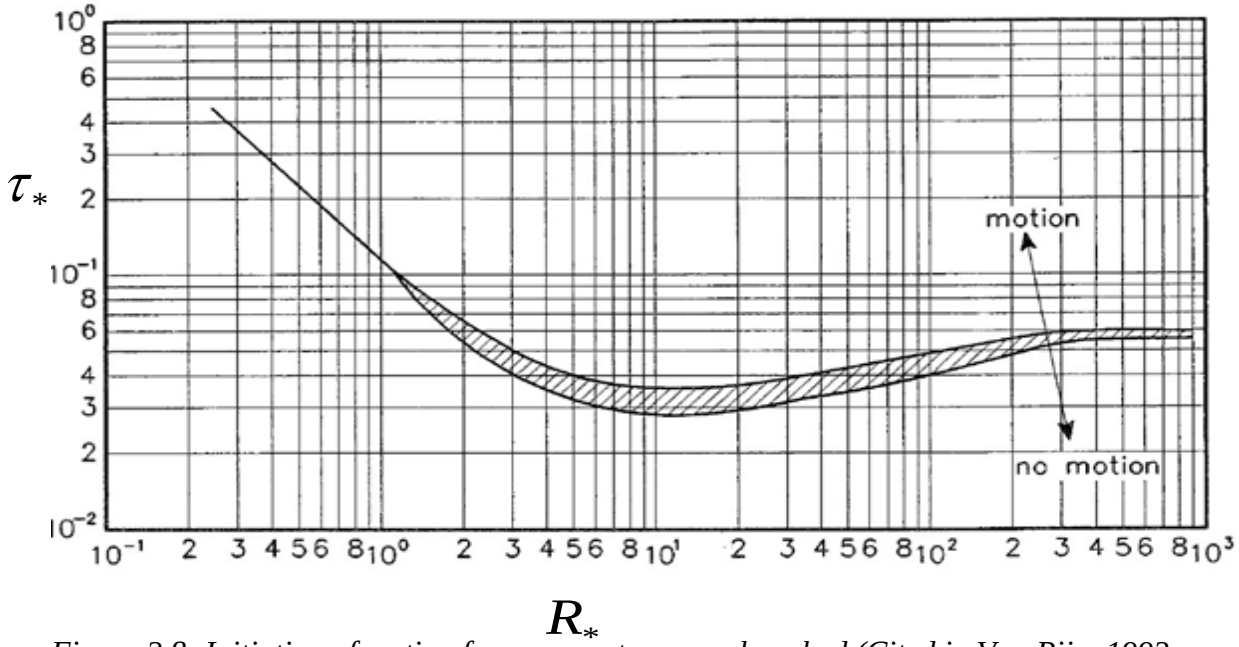

Figure 2.8: Initiation of motion for a current over a plane bed (Cited in Van Rijn, 1993, p.4.5).

Figure 2.8 described the dimensionless critical shear stress as a function of particle diameter. Specifically, the value of critical shear stress varies with the sediment sizes. This value varies from 0.039 for fine gravel to 0.05 for very coarse gravel to 0.054 for boulders in the constant τ_* region in which R_* is greater than 100.

In Shields diagram, the dimensionless Reynolds particle number (R_*) can be replaced by the dimensionless particle diameter d_* (see Equation 2.22), resulting in Figure 2.9 as discussed by Julien (1995):

$$d_* = [\frac{\rho_s - \rho_w}{\rho_w} \frac{g d_{50}^3}{\nu^2}]^{1/3} \tag{2.22}$$

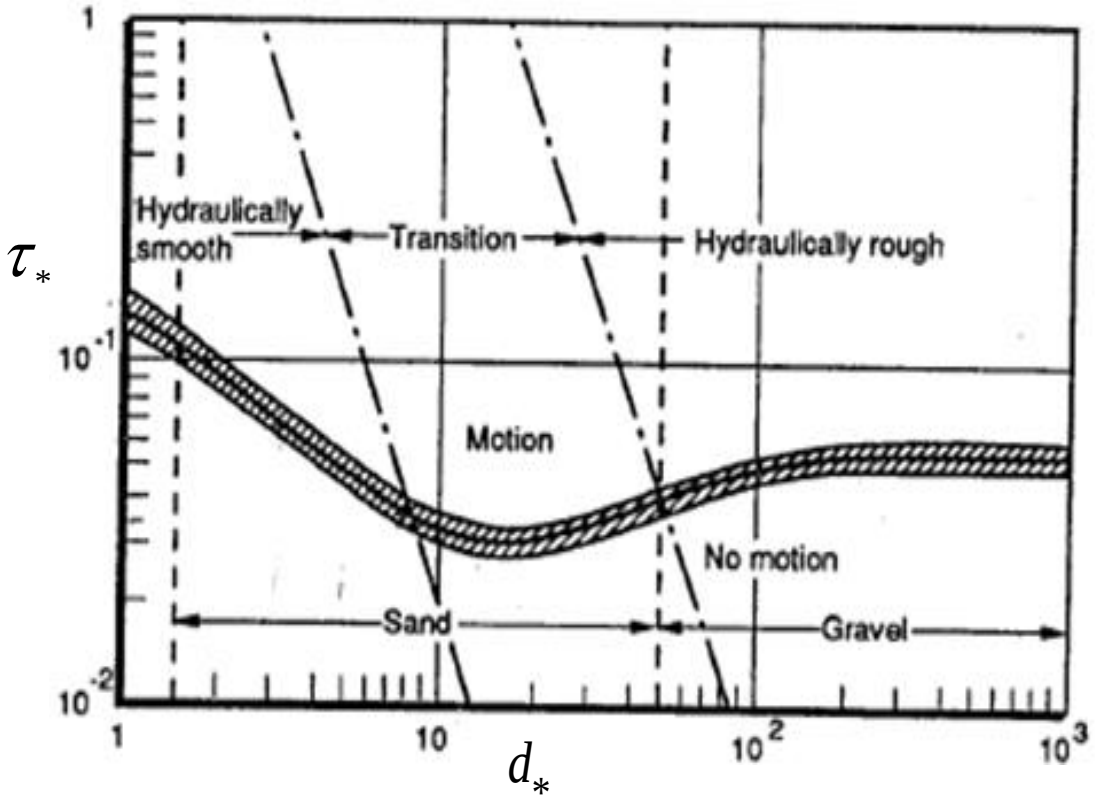

Figure 2.9: Particle motion diameter. (Cited in Julien, 1995).

2.7 The invalidity of Shields prediction for critical shear stress

Particle incipient motion and its relationship with critical shear stress is a significant issue in river engineering. Many researchers have investigated this issue by conducting experiments to evaluate the relationship between critical shear stress and various dependent conditions in uniform and non-uniform flows.

Shields (1936) found that the critical shear stress increases with finer grain sizes more than coarser sizes. But other studies show the dependence of critical shear stress on a channel slope (Paintal, 1971; Hammond et al., 1984; Bathurst, 1987). These studies examined the data from natural streams and laboratory flumes; they found that critical Shields stress increases as the slope of the channel increases, or sediment particles become more stable on a steeper slope. This dependence is also confirmed by Chiew

and Parker (1994) who proved experimentally and theoretically the influence of bed slope on the threshold condition for sediment motion. They found that the critical shear stress decrease with increase bed slope. Their results achieved theoretically by analysing forces acting on a sediment particle resting on a non-horizontal bed slope; while their experimental results were conducted under a closed conduit flow. All these findings contradict the prediction of standard models which posit that there would be reduced stability as the slope increases as a result of the influence of the downstream gravitational force resulting from positive bed slope (Lamb et al., 2008, p1).

Based on the published data, Lamb et al. (2008, p1) proved that critical shear stress is as a function of bed slope. They studied the cause of this discrepancy by using a simple force-balance model as well as "increased drag from channel walls and bed morphology, variable friction angles, grain emergence, flow aeration, and changes to the local flow velocity and turbulent fluctuations" (2008, p1). They argued that Shields stress at incipient motion varies with the particle Reynolds number but is approximately constant when Reynolds number is greater than 100. By considering the effects of particle emergence, logarithmic velocity profile, flow aeration, turbulent fluctuations, and quadratic velocity profile, the critical Shields stress (τ_*) as a function of channel slope (S = tan β) was predicted on a model and this model predicted that $(\tau_*) = 0$ where the bed slope angle is equal to the friction angle.

These findings imply that incipient motion is affected by channel slope in a significant manner basically because velocity fluctuations increase the drag and lift forces that are exerted on the particle thereby increasing the mobility for all channel slopes. Although they used different forces, such as buoyancy, lift, drag and gravity which have influence on sediment particles, the vertical velocity generated from non-uniform flow or the

forces generated from ground water were not taken into account. From the results above, both of authors i.e. Chiew and Parker (1994) and Lamb et al. (2008) have different investigations; the first one confirmed the threshold particle is reduced when the bed slope increases while the second one found the opposite. Therefore, further research is needed to explore the reasons for this dependence.

For non-uniform flow, the incipient sediment motion has also been presented on the Shields diagram and all values for critical shear stress fluctuate below and above this diagram (Afzalimehr et al., 2007; Emadzadeh et al., 2010). The influence of decelerating non-uniform flow on incipient motion over a gravel bed has been investigated by Afzalimehr et al. (2007) who found that the value of critical shear stress in decelerating flow becomes lower than that expected by Shields (1936). In addition to this investigation, Emadzadeh et al. (2010) have shown the effect of accelerating and decelerating non-uniform flow on incipient motion over a sand bed. They illustrated that the value of critical shear stress in accelerating flow is higher than that in decelerating flow and is located above the Shields diagram. The current study will focus on this deviation from the Shields diagram, which relates to the influence of non-uniform flow on the initiation of sediment motion. The physical and theoretical influence of non-uniform flow will be illustrated based on the negative and positive value of vertical velocity generated from accelerating and decelerating non-uniform flows.

2.8 Summary

In this chapter, sediment transport and turbulence characteristics in uniform and non-uniform flows were reviewed. The sediment transport in uniform flow has been widely investigated using the Shields diagram. This diagram was developed to describe the threshold condition for sediment transport in terms of a critical shear stress or a critical

velocity at which the forces or moments resisting motion of an individual grain are overcome. However, in non-uniform flow, there is no general investigation for the deviation of the initial motion of sediment transport from the Shields diagram. Because this diagram was originally applied to uniform flow, it is not surprising that researchers who have applied it to non-uniform flow have found different results. These researchers found the value of critical shear stress in accelerating non-uniform flow is higher than the Shields diagram, while in decelerating non-uniform flow, it is lower.

A number of researchers attributed this deviation to the channel bed slope. Modifications to this diagram have been developed based on the acting force on sediment, such as proximity to the bed, buoyancy, lift, drag and gravity (Lamb et al., 2008). According to these descriptions, they found that the value of critical shear stress increases with the steeper channel. However, in their analysis, they did not take the influence of fall settling velocity for sediment particle into account.

In this chapter, turbulence characteristics in (uniform and non-uniform) steady and unsteady flows were also reviewed. Longitudinal and vertical velocity, Reynolds shear stress and turbulence intensities are the most important flow parameters or turbulence characteristics investigated in the literature. Many studies have found that the Log law's formula is only applicable to predict the longitudinal velocity in the inner region of the water column, which is very close to the boundary layer $(y/h < 0.2)$ and in the rest of the whole region i.e. $(y/h \geq 0.2)$, the measured velocity deviates from the Log law. Other researchers have obtained the mean velocity in the outer region using the Cole's Wake law; the mechanism of Cole's Wake law is not fully understood. Other investigations have demonstrated the deviation of the measurements of Reynolds shear stress, turbulence intensities and vertical velocity in non-uniform steady and unsteady

flows from those in uniform flow. Some researchers attributed these deviations to the vertical velocity but there are no developed equations including this reason.

Therefore, in the next two chapters, all the reviewed gaps in this chapter will be covered. In Chapter 3, the Shields formulas will be modified to be universal for uniform and non-uniform steady flows. In these modifications, the relationship between vertical velocity and settling particle velocity will be taken into account. While in Chapter 4, the Log law will be modified to be universal for all types of flow, such as uniform and non-uniform steady and unsteady flows. Formulas for the prediction of these turbulence characteristics in uniform flow will also be modified for both steady and unsteady non-uniform flows. In these modified formulas, the reason for the deviations of these turbulence characteristics in non-uniform flow from those in uniform flow will be included.

CHAPTER 3 CRITICAL SHEAR STRESS IN NON- UNIFORM FLOW

3.1 Background

The initiation of sediment motion is one of the most important topics in sedimentology and geomorphology as well as hydraulic/hydrological engineering. Generally there are two methods available in the literature to express the incipient motion, i.e., the shear stress approach and velocity approach (Yang, 1996). As sediment transport is a direct result of forces acting on a particle, the shear stress approach that represents the forces per unit area on a particle has been widely used by researchers and scientists. The earliest one who used the shear stress approach is probably Shields (1936) who used the dimensional analysis to determine the dimensionless parameters and the well-known Shields diagram was developed using the dimensionless Shields stress i.e. (τ_* - see Equation 2.20). Based on the experimental data, Shields found that τ_* depends only on the particle Reynolds number (R_* - see Equation 2.21).

The Shield diagram shows that the dimensionless shear stress τ_* at incipient motion varies with R_*, but it approaches a constant value (i.e., $\tau_* \approx 0.045$) when $R_* > 100$. The minimum value of $\tau_* \approx$ 0.032~0.033, and the corresponding value of R_* is about 10. The original Shields diagram has been reproduced and modified by many researchers; a comprehensive review has been done by Buffington and Montgomery (1997), Julien (1995) and others, in which some significant deviations of the observed critical shear stress from the standard Shields curve were observed. This has attracted extensive attention in the research community. Several investigators (Garde & Ranga Raju, 1985; Lavelle & Mofjeld, 1987; Wilcock, 1992; Buffington & Montgomery, 1997) re-analyzed the critical Shields stress, and they attribute the data scatter to the different definitions of critical condition.

As it is difficult to define precisely the status of sediment particles, thus it depends more or less on the experimental observers' subjective judgment, thus criteria like "individual initial motion", "several grains moving" and "weak movement" has been introduced to express the incipient motion (Yang, 1996).

The other reason of divergence is attributed to sediment characteristics, in which grain shape, orientation; exposure, protrusion etc. can affect the critical Shields stress (e.g. Wiberg & Smith, 1987; Wilcock, 1988; Kirchner et al., 1990; Johnston et al., 1998). It is understandable that when the material is non-uniform, it is very difficult to determine the condition of incipient motion, for example, the coarse particles could move relatively easily and the smaller ones move less readily because they will be sheltered (Garde & Ranga Raju, 1985), but in reality, to simplify the experimental works and also the calculation of Shields stress, the characteristic diameter of sediment particle (d_{50}) is generally used to represent the grain size in a mixture for critical condition.

Over eight decades, the incipient motion of sediment transport has been extensively investigated again and again (Buffington & Montgomery, 1997), and it is certain that the Shields diagram cannot exactly predict the threshold of sediment transport in some circumstances. As mentioned, the reason of invalidity is not fully understood, some of them ascribe the large scatters to sediment's characteristics, some researchers believe these deviations are caused by the flow conditions i.e., non-uniformity (Afzalimhr et al., 2007).

Probably, Iwagaki (1956) was the first one who linked the wide scatter in Shields diagram with flow's non-uniformity, as he observed that when the same sediment was applied, the observed critical shear stress in non-uniform flows is highly different from that in uniform flows even when the same "subjective judgment criteria" was applied. Neill (1967) also observed very large critical shear stress deviation compared to Shields

diagram. Afzalimhr et al. (2007) confirmed experimentally that in decelerating flows, the critical shear stress is considerably below the Shields' prediction, and their experimental data are in complete disagreement with the Shields diagram. Similar results are obtained by Andrews and Kuhnle (1993), and Dey and Raju (2002), etc. It was suggested concluded that "…there is no universal value for τ_*" (Afzalimhr et al., 2007). Buffington and Montgomery (1997) also suggested "less emphasis should be given on choosing a universal τ_*".

A number of researchers have made attempts to explain the large discrepancy between predicted and measured critical shear stress using channel's characteristics, such as the channel shape and bed slope (Andrews, 1994; Chiew & Parker, 1994; Church et al., 1998; Patel & Ranga Raju, 1999; Dey & Debnath, 2000; Dey & Raju, 2002; Mueller et al., 2005). For example, Graf and Suszka (1987) found that "the well-known Shields criterion is insufficient for large slope". Among these researchers, the work done by Lamb et al. (2008) is comprehensive; they re-visited and examined almost all published datasets. It was found that the critical Shields stress for incipient motion of sediment in open-channel flow increases with channel slope, this is contrary to people's intuition that predicts increased mobility with increasing channel slope due to the added gravitational force in the downstream direction. But Chiew and Parker's (1994) experiments in very steep channels show that the critical shear stress is decreased, contrary to Lamb et al.'s (2008) conclusion.

Therefore, the brief literature review shows that more research is needed to clarify why the critical shear stress for sediment motion depends on channel-bed slope and non-uniformity, and why Shields diagram cannot predict the critical shear stress well. Besides, although these researchers have found the difficulty of using Shields diagram in practical application, but none of them has proposed a modified diagram that can

predict the universal τ_*, which further justifies this research. Thus, the specific objectives for this particular chapter are:

1) Investigate why sometimes the Shields curve cannot express the incipient motion of sediment transport;
2) Explain the dependence of Shields stress on the variation of water depth along the open channel flow;
3) Establish a universal relationship between dimensionless critical shear stress and the particle Reynolds number, by including both flow non-uniformity and channel-bed slope;
4) Verify the newly established equations using data from literature.

3.2 Theoretical considerations of the influence of vertical velocity on the critical shear stress

In this study, we hypothesized that the upward/downward velocity caused by non-uniformity or seepage play an important role for the invalidity of Shields' diagram. It is ubiquitous as shown in Figure 3.1 that a river flow always interchanges with groundwater. The suctions injections caused by groundwater happen in flood/dry seasons alternatively. It is reasonable to infer that the upward flow increases the sediment particles' mobility, or the threshold shear stress required is reduced due to the upward motion. Its influence of upward velocity on sediment mobility can be seen from its effective settling velocity when its ambient water has an upward velocity, i.e.

$$\omega'(y) = \omega - V_b(y) \tag{3.1}$$

where ω = particle's settling velocity and ω' = the net falling velocity at the distance y from the bed, V_b = vertical velocity at the sediment layer. A spherical particle's falling velocity ω in still water ($V_b = 0$) can be expressed as:

$$C_d \pi \frac{d^2}{4} \frac{\rho_w \omega^2}{2} = \pi \frac{d^3}{6} g(\rho_s - \rho_w) \tag{3.2}$$

where d is the particle diameter, C_d is the drag coefficient which is a function of the particle Reynolds number; g is the gravitational acceleration; ρ_s and ρ_w are the densities of sediment and flowing water, respectively.

It can be seen that if the upwards velocity V_b is the same as the particles' falling velocity ω, the net vertical velocity of the particle becomes zero, thus the particle can be suspended in the flowing water like a neutrally buoyant particle. In such case, it is impossible to expect that the Shields diagram is valid to predict the critical shear stress. Likewise, if the particles in Figure 3.1 are subject to the downward suction, then the net falling velocity ω' is higher than ω, and it seems that the particle become heavier, also in such case the threshold critical shear stress is unpredictable using the existing Shields diagram.

The above simple discussion clearly shows that the presence of vertical velocity V_b in a sediment layer could lead to the invalidity of Shields diagram. This inference has been confirmed experimentally by many researchers like Ramakrishna Rao and Nagaraj (1999) and others who observed the critical shear stress subject to injection and suction flows, and a comprehensive literature review can be found from Lu et al. (2008). The influence of seepage on the critical shear stress has been discussed by many researchers, the parameters used to express the seepage include (i) the hydraulic gradient, e.g., Cheng and Chiew (1999); (ii) the pressure variation (e.g., Francalanci et al., 2008); or (iii) the apparent water density due to the pressure variation. But, there is no research

available to investigate the role of vertical velocity on the incipient motion of sediment transport.

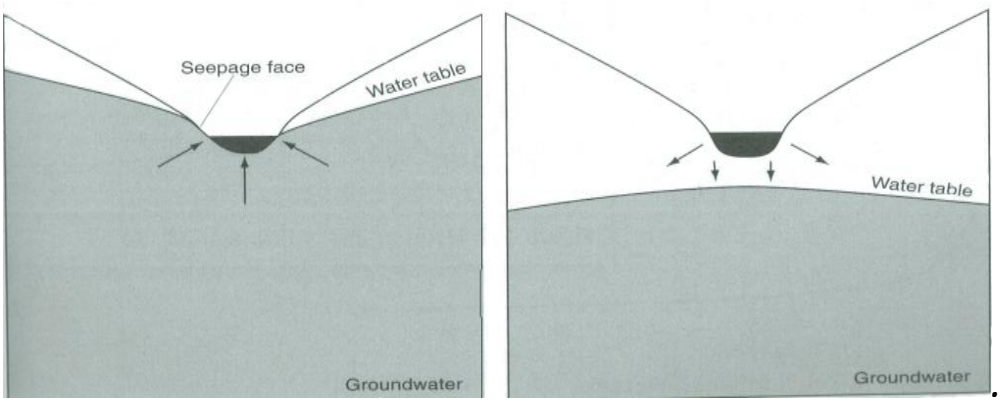

Figure 3.1: The upward and downward vertical velocity generating from seepage face (a) injection seepage (b) suction seepage (Ladson, 2008, p99).

In this study, the reduction of settling velocity as shown in Equation 3.1 can be achieved by introducing "apparent sediment density". It is assumed that the presence of vertical velocity can alter the net settling velocity, the upward velocity promotes sediment's mobility, the critical shear stress is assumed similar to lightweight material without seepage. Similarly, the downward velocity increases the net sediment falling velocity or its apparent density, subsequently its stability.

The introduction of apparent sediment density is similar to Francalanci et al.'s (2008) treatment. Instead of alteration in sediment density, they modified the water's density to eliminate the variation of pressure. Their results shows that the higher pressure yields higher "apparent water density", and lower pressure corresponds to lower "apparent water density". In this study, the concept of apparent sediment density is introduced and the parameter of settling velocity is modified by the presence of vertical velocity in the sediment layer. Therefore, it is necessary to establish a relationship between the apparent sediment density and the settling velocity. In other words, after the

introduction of apparent density, the effect of pressure variation or seepage on sediment transport is eliminated, a "lightweight particle" with settling velocity ω' should have same effect on its mobility as a real sediment particle whose settling velocity is ω' in the environment without seepage/pressure variation, and vice versa. Hence, the introduction of apparent density can simplify this mathematical treatment for the complex interaction between horizontal and vertical motions in open channel flows. In the environment with ambient velocity, the modified settling velocity and apparent density can be expressed in the following:

$$C_d \pi \frac{d^2}{4} \frac{\rho_w \omega'^2}{2} = \pi \frac{d^3}{6} g(\rho_s' - \rho_w) \tag{3.3}$$

where ρ_s' is the apparent density of sediment.

From Equations 3.2 and 3.3, one can obtain

$$\frac{\rho_s' - \rho_w}{\rho_s - \rho_w} = \left(\frac{\omega - V_b}{\omega} \right)^2 \tag{3.4}$$

Equation 3.4 shows that if V_b is equal to zero, then ρ_s' is the same as the sediment's density in reality, if V_b is upwards or positive then ρ_s' is less than the density of sediment ρ_s, and particles behave in the same way as plastic sands; if $V_b = \omega$, then ρ_s' is same as the density of water and the particles are neutrally buoyant. But, if V_b is downward or negative, the apparent density of sediment is higher than the density of natural sediment, or the sediment's stability is increased like heavy metals.

As the vertical velocity V_b in Figure 3.1 has the similar effect for the particles' stability as the buoyancy effect, i.e., the submerged weight of the particles is no longer $\rho_s - \rho_w$, but $\rho_s' - \rho_w$, thus the general expression for the modified Shields parameter should be:

$$\tau_*^{'} = \frac{\tau_c^{'}}{(\rho_s^{'} - \rho_w)gd_{50}} \tag{3.5}$$

Substituting Equation 3.4 into Equation 3.5, one obtains:

$$\tau_*^{'} = \frac{\tau_c}{(\rho_s - \rho_w)gd_{50}}\left(\frac{\omega}{\omega - V_b}\right)^2 \tag{3.6}$$

Equation 3.6 can be rewritten as follows

$$\frac{\tau_*^{'}}{\tau_*} = \left(\frac{1}{1-Y}\right)^2 \tag{3.7}$$

where $Y = V_b / \omega$

Equation 3.6 or 3.7 generally expresses the critical shear stress with the presence of vertical velocityV_b, and it is useful to show why the vertical velocity, *V* is ubiquitous in open channel flows and how the vertical velocity can be induced by unsteady/non-uniform flows.

3.3 Influence of non-uniform flow on the critical Shields stress

It has been shown that the existence of vertical velocity will modify the particles' mobility or stability. If the non-uniform flows can change the particles' Shields number, this means vertical velocity may exist in non-uniform flows. In other words, if the new modified Shields' parameter shown in Equation 3.6 is universal, one must be able to detect the existence of vertical velocity V_b in non-uniform flows theoretically and experimentally.

In natural streams and laboratory flumes, the uniform flow is very rare; most of them are non-uniform or unsteady. As shown in Figure 3.2, even the flow rate is constant, the flow could still be either accelerating or decorating dependent of water depth variation, i.e., d*h*/d*x* (≠ 0). The 3-D continuity equation can be written as follows:

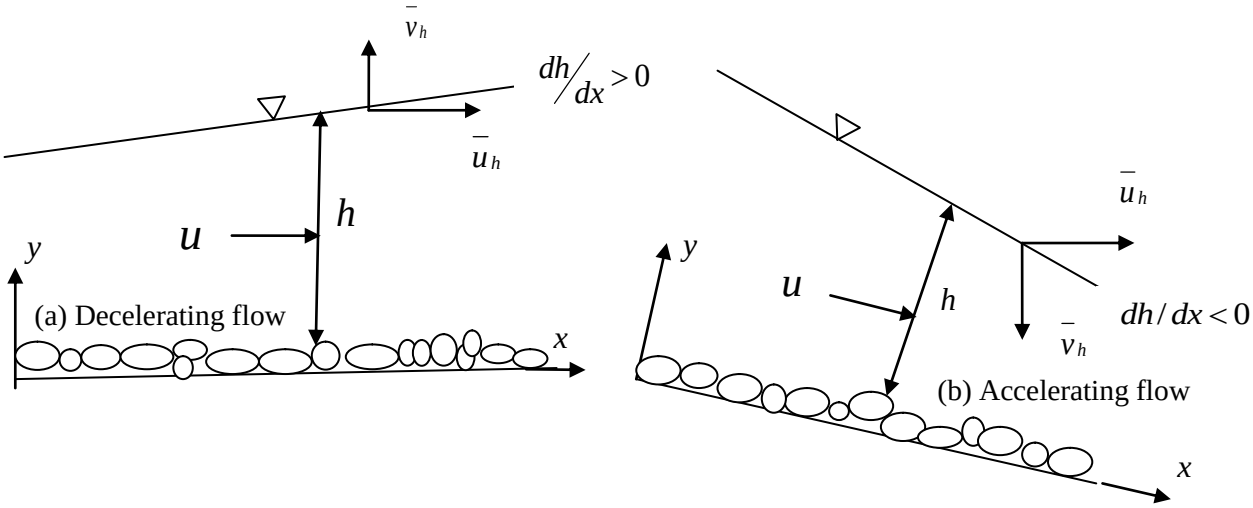

Figure 3.2: Non-uniform flows in open channel and the variation of water depth, in which u and v are mean velocities in x and y direction, respectively.

$$\frac{\partial \bar{u}}{\partial x} + \frac{\partial \bar{v}}{\partial y} + \frac{\partial \bar{w}}{\partial z} = 0 \tag{3.8}$$

where $\bar{u}$, $\bar{v}$ and $\bar{w}$ are the time-averaged local velocity at any point in the fluid in x , y and z directions respectively. $\partial \bar{w}/\partial z = 0$ because it is on the central line (symmetrical condition).

Integration of Equation 3.8 with respect to y yields

$$\bar{v} = -\int_0^h \frac{\partial \bar{u}}{\partial x} dy \tag{3.9}$$

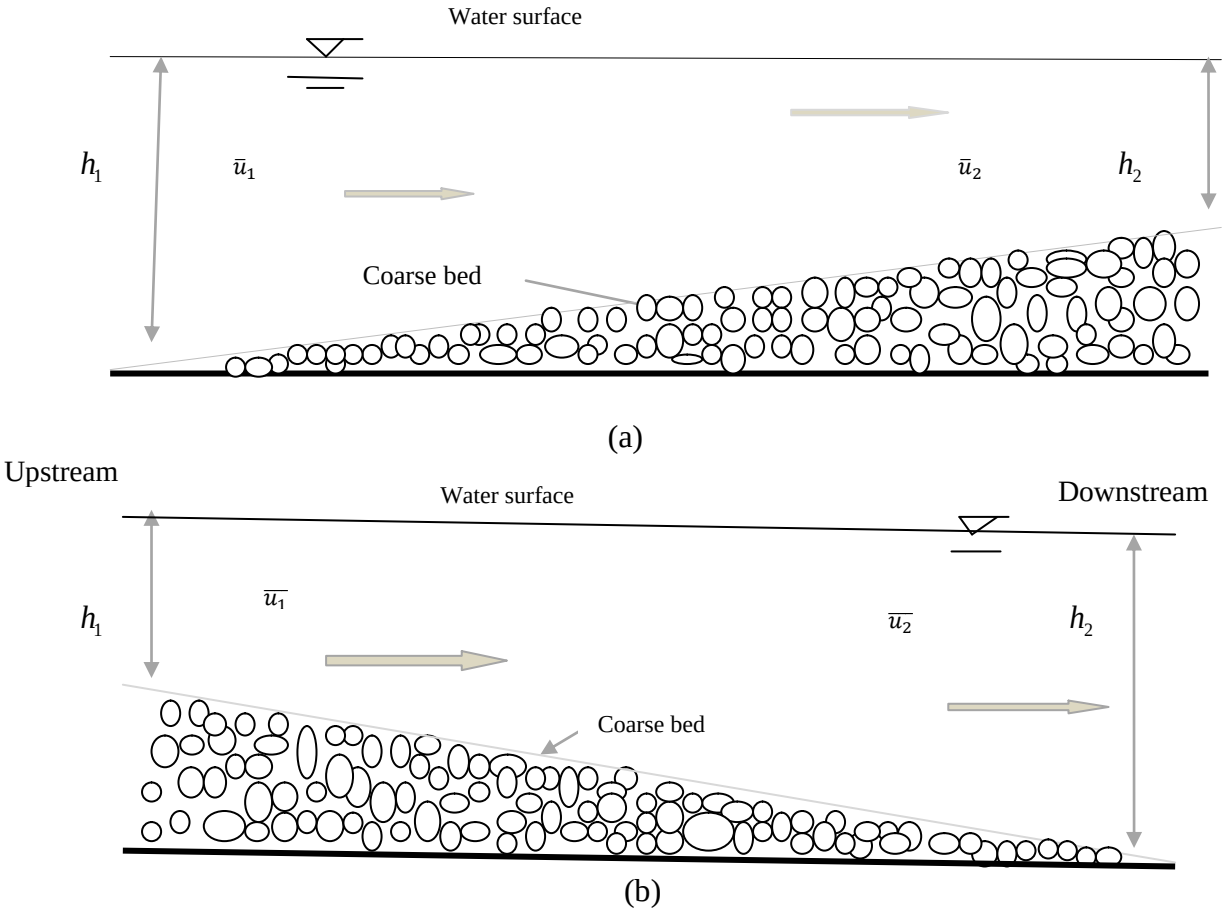

Figure 3.3: Generating non- uniform flow (a) accelerating flow (b) decelerating flow by providing coarse bed level.

Figure 3.3 proves the influence of physical phenomena on non-uniform flows and vertical velocity. For example, if the flow is accelerating (Figure 3.3 a), mean horizontal velocity increases along the channel $(\bar{u}_2 > \bar{u}_1)$ or $\partial\bar{u}/\partial x > 0$ while water depth decreases along the flow direction or $(h_2 < h_1)$. In decelerating flow shown in Figure 3.3 b, the mean horizontal velocity decreases along the channel $(\bar{u}_2 < \bar{u}_1)$ or $\partial\bar{u}/\partial x < 0$ while water depth increases $(h_2 > h_1)$. According to this description, Equation 3.9 generates a

negative downward vertical velocity when the flow is accelerating flow and a positive upward vertical velocity when the flow is decelerating.

Therefore, it is clear that there exists vertical velocity in a non-uniform flow (accelerating and decelerating flows); the increase of velocity in flow direction generates a negative value or downward vertical velocity, and vice versa.

Hence, the presence of vertical velocity is ascertained in non-uniform flows or unsteady flows. Next, it is necessary to quantify whether the velocity in Equation 3.9 is negligible when compared with the sediment settling velocity. The quantity of vertical velocity can be estimated as follows in rectangular channels:

$$Q = BU\,h \tag{3.10}$$

where Q = discharge and this value is constant for a steady flow; U is the depth averaged mean streamwise velocity along the water column, h is the water depth and B is the channel width. The derivation of Equation 3.10 with respect to x gives,

$$\frac{d(Uh)}{dx} = \frac{d}{dx}\int_0^h \bar{u}dy = 0 \tag{3.11}$$

The vertical velocity $\bar{v}_h$ at the free surface can be obtained from Equation 3.9 using the Leibniz's rule, i.e.

$$\bar{v}_h = -\int_0^h \frac{\partial \bar{u}}{\partial x}dy = -\frac{d}{dx}\int_0^h \bar{u}dy + \bar{u}_h\frac{dh}{dx} \tag{3.12}$$

where $\bar{u}_h$ is the horizontal velocity at the surface in the x direction. By inserting Equation 3.11 into Equation 3.12, one obtains:

$$\bar{v}_h = \bar{u}_h\frac{dh}{dx} \tag{3.13}$$

Equation 3.13 shows that the decelerating flow generates $\bar{v}_h > 0$ as $dh/dx > 0$, but the accelerating flows yield the negative $\bar{v}_h$ as $dh/dx < 0$, thus one can conclude that the

vertical velocity do exist in the main flows. Its existence can be extended from the upper boundary to the lower boundary. Subsequently the flow across the porous boundary can be induced, the velocity on the solid-liquid interface surface may be very small, its importance for sediment incipient movement, entrainment and suspension should not be underestimated (Francalanci et al., 2008).

Julien (1995) replaced the Reynolds number (R_*) in Shields' diagram is replaced by the dimensionless particle diameter (d_*):

$$d_* = \left[\frac{\rho_s - \rho_w}{\rho_w} \frac{g d_{50}^3}{\nu^2} \right]^{1/3} \tag{3.14}$$

After the introduction of similarly, this apparent parameter needs to be expressed in the following form for flows with the presence of vertical velocity:

$$d_*^{'} = \left[\frac{\rho_s^{'} - \rho_w}{\rho_w} \frac{g d_{50}^3}{\nu^2} \right]^{1/3} \tag{3.15}$$

Inserting Equation 3.4 into Equation 3.15, one has

$$d_*^{'} = \left[\frac{\rho_s - \rho_w}{\rho_w} \left(\frac{\omega - V_b}{\omega} \right)^2 \frac{g d_{50}^3}{\nu^2} \right]^{1/3} \tag{3.16}$$

$$\text{or } \frac{d_*^{'}}{d_*} = (1 - Y)^{2/3} \tag{3.17}$$

Therefore, the empirical equation of Shields curve by Yalin and Silva (2001) can be modified with the following form:

$$\tau'_* = 0.13 d_*^{'-0.392} \exp(-0.015 d_*^{'2}) + 0.045[1 - \exp(-0.068 d_*^{'})] \tag{3.18}$$

The fall velocity ω can be calculated by Julien (1995)

$$\frac{\omega d_{50}}{\nu} = 8\left[\sqrt{1 + 0.0139 d_*^3} - 1\right] \tag{3.19}$$

CHAPTER 3 CRITICAL SHEAR STRESS IN NON- UNIFORM FLOW

In order to explain the observed dependence of critical shear stress on the variation of water depth, the variation of water depth's formula will be derived first and the dependence will be explained later. The formula for the variation of water depth for non-uniform flows can be evaluated by using a derivative of the total Energy equation which is a function of (x) as shown below:

$$E = Z + h + \alpha \frac{U^2}{2g} \tag{3.20}$$

where E is the total energy; Z is the elevation; α is a coefficient which is assumed to be 1; h is the water depth; and U is the depth averaged horizontal water velocity which can be obtained from the Continuity equation as shown in Equation 3.10:

$$U = \frac{Q}{Bh} \tag{3.21}$$

where Q is the water discharge (m^3/s); B is the flume width (m); and h is the water depth (m). In this case, the water discharge can be assumed to be constant along the channel. After inserting Equation 3.21 into Equation 3.22, the total energy equation can be rewritten as:

$$\frac{dE}{dx} = \frac{dz}{dx} + \frac{dh}{dx} + \alpha \frac{d}{dx}\left(\frac{Q^2}{2gh^2B^2}\right) \tag{3.22}$$

where:

$\frac{dE}{dx} = -S_f$ (Energy slope)

$\frac{dz}{dx} = -S_0$ (Bed slope)

Rearrange Equation 3.22 by using the definition for each concept to obtain:

$$-S_f = -S_0 + \frac{dh}{dx} - \frac{Q^2}{gh^2B^2}\frac{dh}{dx} \tag{3.23}$$

$$\text{Since } F_r{}^2 = \frac{U^2}{gh} = \frac{Q^2}{gh^3B^2} \tag{3.24}$$

After substituting the square of Froude number formula F_r^2 in Equation 3.23, the formula for the variation of water depth (dh/dx), which is called the Governing equation for water surface profiles, can be obtained:

$$\frac{dh}{dx} = \frac{S_0 - S_f}{1 - U^2/gh} \tag{3.25}$$

In order to explain the dependence of critical shear stress on the variation of water depth, Equation 3.25 clearly shows that dh/dx depends on the channel slope S_0 and almost all flows in rivers are non-uniform flows; this is probably why the field data shows the dependence of critical shear stress on the channel slope (Lamb et al., 2008).

Although the incipient of motion of uniform flow have been extensively investigated, to the authors' knowledge there is no study on the influence of vertical velocity on incipient motion of sediment particles, this vertical flow can be especially important when it is large enough to induce discernible seepage, and the average vertical velocity can be written in a similar way as shown in Equation 3.13, i.e.,

$$V = U\frac{dh}{dx} \tag{3.26}$$

The depth average streamwise velocity is introduced because all experiments report their mean *U*, rather than $\bar{u}_h$, thus Equation 3.26 is convenient to use. The near bed vertical velocity can be induced by the groundwater and the surface variation as shown

in Equation 3.26, the joint effect can be proportional to V and the nominal seepage velocity V_s.

It should be stressed that the near bed velocity above the interface between the fluid and porous media $\lambda V + \lambda_s V_s$ is different from V_b that is the water velocity in the sediment layer. Based on the continuity principle, the water velocity in the porous media can be express by:

$$V_b = \frac{\lambda V + \lambda_s V_s}{1 - \varepsilon_0} \tag{3.27}$$

where λ and λ_s are the coefficients, V_s = nominal seepage velocity defined by Darcy ($V_s = ki$, k = hydraulic conductivity, i = hydraulic gradient), ε_0 = porosity of granular materials. Generally in laboratory flumes the second term of Equation 3.27 is negligible (i.e., $V_s = 0$), but in natural streams both the river flow and underground water flow can generate the velocity at the river bed, thus two terms co-exist in Equation 3.27.

3.4 Re-analyse the data on the original Shields diagram

To verify whether Equation 3.18 is applicable to non-uniform flows, we have comprehensively compiled 329 datasets from Neil (1967); White (1970); Everts (1973); Carling (1983); Graf and Suszka (1987); Cheng and Chiew (1999); Shvichenko and Pender (2000); Sarker and Hossain (2006); Afazlimhr et al. (2007); Kavcar and Wright (2009); Emadzadeh et al. (2010); Gaucher et al. (2010); and Liu and Chiew (2012). The hydraulic conditions of these experimental data sets are summarized in Table 3.1. In order to prove the Shields diagram cannot predict the threshold condition in non-uniform flow, the available datasets in the literature related to the incipient sediment motion have been re-analysed and re-plotted in the form of the Shields diagram based on the original definitions, as shown in Figure 3.4. It can be seen that the observed

critical shear stress highly deviates from the standard Shields curve. Similar discrepancy has been noticed and reported by many researchers (e.g., Buffington and Montgomery, 1997, Lamb et al. 2008, etc.), this discrepancy cannot be simply attributed to measurement errors. All the calculated critical shear stresses are present in Figure 3.4, in which the three lines represent the average Shields number and its upper/lower limits of error band, the middle one is produced by Equation 3.18 and the two additional curves are defined by $\pm 100\%$ error band (Sturm, 2010, p420) and (Julien, 1995, p116).

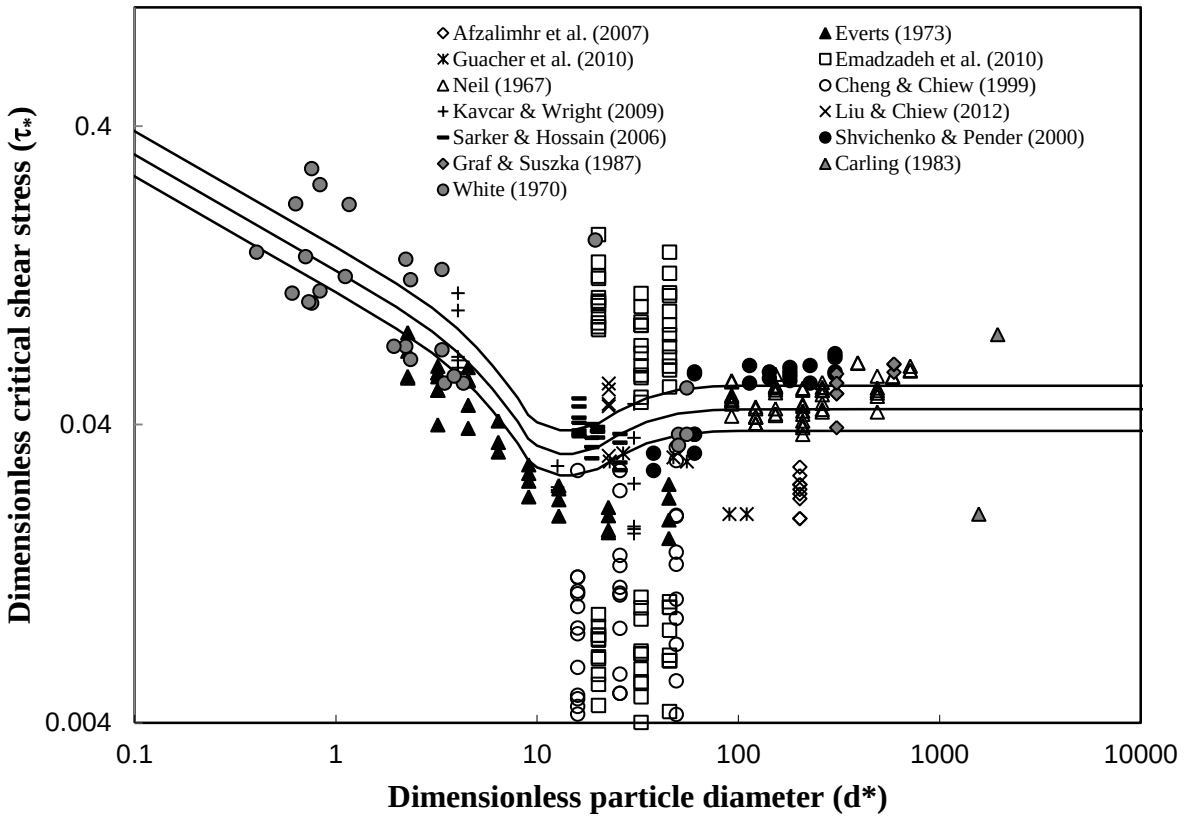

Figure 3.4: The experimental data of incipient sediment motion on the Shield's diagram.

CHAPTER 3 CRITICAL SHEAR STRESS IN NON- UNIFORM FLOW

Table 3.1: Summary of hydraulic conditions of open channel flow for the 329 datasets:

Researchers	d_{50} (mm)	S_0	h (m)	U (m/s)	Fall velocity ω (m/s) Eq. (3.19)	No. of data sets
Afzalimhr et al. (2007)	8	0.0075	0.13-0.19	0.73-0.86	0.338	5
		0.015	0.17-0.21	0.72-0.8		4
Everts (1973)	1.79	0.005	0.022-0.064	0.288-0.38	0.156	4
	0.895	0.005	0.023-0.088	0.24-0.28	0.1048	4
	0.508	0.005	0.026-0.082	0.221-0.239	0.07118	4
	0.359	0.005	0.0094-0.08	0.15-0.23	0.0529	4
	0.254	0.005	0.0329-0.08	0.206-0.219	0.0366	3
	0.18	0.005	0.034-0.075	0.192-0.196	0.023	2
	0.127	0.005	0.01-0.0795	0.13-0.189	0.0131	3
	0.18	0.005	0.028-0.053	0.32-0.35	0.0437	3
	0.127	0.005	0.036-0.073	0.13-0.307	0.0268	4
	0.09	0.005	0.023-0.07	0.25-0.27	0.0150	4
Emadzadeh et al. (2010)	1.8	(±0.007)-(±0.015)	0.146-0.205	0.279-0.44	0.1565	24
	0.8	(±0.007)-(±0.015)	0.16-0.222	0.149-0.32	0.097	24
	1.3	(±0.007)-(±0.015)	0.156-0.237	0.195-0.3	0.13	24
Cheng & Chiew (1999)	1.95	0.01	0.027-0.06	0.219-0.399	0.1634	15
	1.02	0.01	0.031-0.076	0.164-0.315	0.114	16
	0.63	0.01	0.03-0.06	0.09-0.237	0.083	19
Neil (1967)	6.2	0.01	0.0519-0.2	0.6-0.8	0.287	10
	8.5	0.01	0.0305-0.2	0.64-0.833	0.33	10
	10.6	0.01	0.064-0.183	0.746-0.96	0.37	8
	20	0.01	0.0366-0.17	0.915-1.15	0.51	6
	23.8	0.01	0.0519-0.13	1.08-1.34	0.56	2
	29.1	0.01	0.058-0.137	1.25-1.42	0.62	3
	5	0.01	0.064-0.177	0.561-0.655	0.28	8
	16	0.01	0.07-0.159	1.05-1.16	0.458	2
	6.4	0.01	0.0488-0.19	0.284-0.366	0.13	10
Gaucher et al. (2010)	0.91	0.01	0.24	0.29	0.105	1
	1.06	0.01	0.2	0.35	0.116	1
	1.88	0.01	0.162	0.43	0.16	1
	2.2	0.01	0.152	0.46	0.174	1
	3.57	0.01	0.14	0.5	0.224	1
	4.36	0.01	0.125	0.56	0.245	1
Kavcar & Wright (2009)	0.16	0.01	0.235-0.275	0.236-0.288	0.019	6
	0.5	0.01	0.246-0.261	0.26-0.276	0.07	4
	1.2	0.01	0.242-0.295	0.338-0.412	0.125	6
Liu & Chiew (2012)	0.9	0.01	0.12-0.14	0.28-0.35	0.105	5
Graf & Suszka (1987)	12.2	0.0075-0.015	0.102-0.2	0.23-1.6	0.48	6
	23.5	0.015-0.025	0.12-0.17	1.27-1.59	0.58	3
Sarker & Hossain (2006)	0.64	0.00026-0.00056	0.089-0.21	0.3-0.59	0.084	7
	0.74	0.00026-0.0005	0.1-0.2	0.31-0.32	0.092	4
	0.79	0.00035-0.0005	0.1-0.18	0.32-0.34	0.096	4
	1.02	0.00042-0.00063	0.12-0.14	0.31-0.35	0.113	4

Researchers	d_{50} (mm)	S_0	h (m)	U (m/s)	Fall velocity ω (m/s) Eq. (3.19)	No. of data sets
Carling (1983)	62	0	0.21	0.163	0.94	1
	77	0	0.22	0.124	1.05	1
Shvichenko & Pender (2000)	1.5-12	0.0019-0.0287	0.002-0.65	0.1-1.07	0.14-0.41	21
White (1970)	0.016-2.2	0.02	0.02-0.07	0.0018-0.23	0.00023-0.17	26

The data in Figure 3.4 are briefly outlined as follows:

1. Afzalimhr et al. (2007) conducted experiments in a rectangular laboratory channel (14m long, 0.6m width and 0.5m depth) using an Acoustic Doppler Velocimeter (ADV) for velocity measurements. The sediment size of $d_{50} = 8$ mm was used for their observation. They generated decelerating non-uniform flow using large channel slope, different from Lamb et al's (2008) prediction, their experimental data reveal that the value of critical shear stress is smaller than Shields' prediction by at least 50%.

2. Experimental data from Everts (1973) contain 35 runs, different sediment sizes d_{50} (1.79, 0.895, 0.508, 0.359, 0.245, 0.18 and 0.127 mm) with specific gravity of 2.65 and 11 runs for d_{50} =(0.18, 0.127 and 0.09 mm) with specific gravity of 4.7 were used in his experiment, also all his data points are located below Shields' prediction.

3. Cheng and Chiew (1999) conducted their experiments to prove experimentally the effect of upward seepage on the critical conditions of incipient motion. They produced 50 datasets in a glass sided horizontal flume with 7.6m long, 0.21m wide and 0.4m deep using the uniform particle size $d_{50} =$ 0.63, 1.02 and 1.95 mm, and the seepage velocity (injection) was measured. They proved that the upward seepage reduces significantly the critical shear stress required by Shields curve.

4. Gaucher et al.'s (2010) experiments were conducted in a horizontal, rectangular glass walled flume with dimensions of 6m long, 0.5 m wide and 0.7 m deep. Different types of non-cohesive materials were used ranged from d_{50} =0.91 to 4.36 mm.

5. The experiments by Emadzadeh et al. (2010) were conducted in accelerating and decelerating flow conditions, in a rectangular flume of 14m long, 0.6m wide and 0.6m deep. The sediment size d_{50} =1.8, 0.8 and 1.3 mm was used for a total 72 data sets. In order to achieve non-uniform flow conditions, negative and positive bed slope (±0.7%, ±0.9%, ±1.25% and ±1.5%) were used. They found that the critical shear stress and Shields parameter for incipient motion in accelerating flow are higher than those predicted by Shields in uniform flow while their values in decelerating flow are considerably lower than that in accelerating flow.

6. The experiments by Neil (1967) were conducted in a flume 0.9m wide and 5m long with different particle sizes and densities. Among the data obtained, 11 data points are obviously above the Shields curve.

7. Kavcar and Wright (2009) conducted experiments in a 7.5m long, 0.6m wide flume with both injection and suction seepage using sediment particle of d_{50} =0.16, 0.5 and 1.2mm.

8. Liu and Chiew (2012) observed the critical shear stress for sediment with a median diameter of 0.9mm in the presence of downward seepage. Their experiment was conducted in a glass-sided flume that was 30m long, 0.7m wide and 0.6m deep. Base on the overall view on seepage effects on the initiation of sediment motion, they proved that the upward seepage (injection) decreases the critical shear velocity while the downward seepage (suction) increases it.

9. The data sets of 9 flume tests were conducted by Graf and Suszka (1987) in 16.8m long, 0.6m wide and 0.8m high over a smooth steel floor with gravel sediment relatively

uniform size distribution to determine the critical shear stress and compared it with the Shields value.

10. Shvidchenko and Pender (2000) did a flume study of the effect of relative depth on the incipient motion of coarse uniform sediments to derive a relationship between the critical stress, grain size ratio, and grain Reynolds number.

11. The data field was selected from Carling (1983) who investigated the threshold values of the shear stress for a given grain size in a narrow natural stream and in a broad stream.

12. The determination of threshold have been made in a recirculating flume 6m long and 0.3m wide by White (1970) who described this determination under flows of water for beds of mineral grains of uniform size with diameter between (0.016-2.2) mm.

13. Nineteen flume experiments from Sarker and Hossain (2006) are also included. They investigated the initiation of sediment motion under non-uniform sediment mixtures.

3.5 Dependence of critical shields stress on channel slope

In the literature, many researchers attribute the deviations from the Shields curve to the influence of critical shear stress on channel's slope. For example Chiew and Parker (1994) proposed that

$$\frac{\tau_*^{'}}{\tau_*} = \cos\phi\left(1-\frac{\tan\phi}{\cos\theta}\right) \tag{3.28}$$

where ϕ = angle of streamwise bed slope, θ = angle of repose. Equation 3.28 shows that the Shields number decreases with the increase of bed slope.

However, the formula given by Lamb et al. (2008) shows that the steep channel has a higher Shields number with the following form:

$$\tau_*^{'} = \exp[0.0249X^4 + 0.107X^3 + 0.199X^2 + 0.476X - 3.57] \quad (3.29)$$

where $X = 0.407ln(142S)$, and the slope S is in the regime $10^{-4} < S < 0.5$.

Figure 3.5 shows the comparison of the data listed in Table 3.1 and Equations 3.28 and 3.29, it can be seen that these equations cannot express the data points, as shown in Figure 3.5 the measured critical shear stress could be largely different even the sediment and channel slope are set to constant. Hence, one can conclude that the invalidity of Shields prediction cannot be simply explained by the dependence of channel slope, and more research works need to be carried out for the phenomenon.

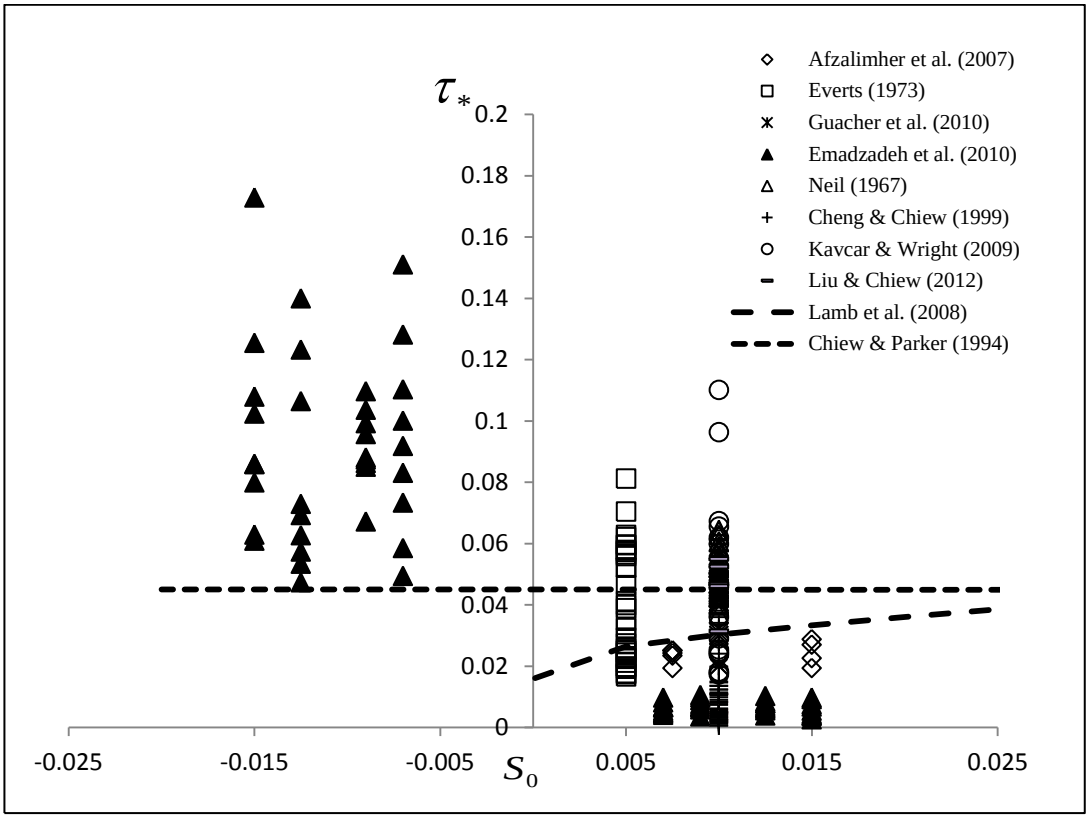

Figure 3.5: Dependence of critical shear stress on the channel slope.

3.6 Effect of seepage on critical shields stress

Figure 3.5 shows that particles of the same size and same channel slope behave largely different, and none of the existing theory can explain the invalidity of Shields curve. Equation 3.27 states that the scatter could be caused by either groundwater or the main flow, or both of them. To simplify the discussion, the effect of seepage on the critical shear stress is discussed first. The experimental data by Cheng and Chiew (1999), Kavcar and Wright (2009) and Liu and Chiew (2012) are presented in Figure 3.6.

The modified Shields number in Equation 3.5 should remain unchanged if the apparent sediment density is introduced, i.e.

$$\tau_*^{'} = \frac{\tau_c^{'}}{(\rho_s^{'} - \rho)gd_{50}} = \frac{\tau_c}{(\rho_s - \rho)gd_{50}} \tag{3.30}$$

Using Equation 3.4, one obtained the critical shear stress in the following form:

$$\frac{\tau_c^{'}}{\tau_c} = (1 - Y)^2 \tag{3.31}$$

Figure 3.6 also includes the critical shear stress predicted by Equation 3.31 and the empirical factor i.e. λ_s is found to be (i.e., λ_s = 8.5). The determined values of $\tau^{'}_c / \tau_c$ for all these selected data can be found in Appendix A. Therefore, the good agreement between the measured and predicted critical shear stress indicates that the introduction of apparent sediment density is acceptable.

Different from Equation 3.31, Cheng and Chiew (1999) expressed their data using the following empirical way:

$$\frac{\tau_c^{'}}{\tau_c} = 1 - \left(\frac{V_s}{V_{sc}}\right)^m \tag{3.32}$$

where V_{sc} is the critical seepage velocity in a quick state and m = 1~2 and depends on the characteristics of sediments, and V_{sc} was determined by:

$$V_{sc} = k\left(\frac{\rho_s}{\rho} - 1\right)(1 - \varepsilon_0) \tag{3.33}$$

It is clearly seen that Equations 3.31 and 3.32 are functionally similar to each other.

Francalanci et al. (2008) also developed an empirical equation to express the critical shear stress under the influence of seepage, it has the following form:

$$\frac{\tau_c^{'}}{\tau_c} = \frac{\rho_s - \rho(1 + V_s / k)}{\rho_s - \rho} \tag{3.34}$$

Comparing Equations 3.31, 3.32 and 3.34, one can find that the conditions for $\tau_c' = 0$ are, respectively, $V_s = \omega$; $V_s = V_{sc}$ and

$$V_s = k(\frac{\rho_s}{\rho} - 1) \tag{3.35}$$

From the physical interpretation, it is apparent that Equation 3.31 gives the reasonable limit for $\tau_c' = 0$. Equations 3.34 and 3.35 may not be correct, because the calculated V_{sc} could be less or larger than ω, if $V_{sc} > \omega$, it implies that streamwise force is still needed to initiate the particles' movement even all particles are in a suspended state, it is totally unacceptable; if $V_{sc} < \omega$, it indicates that the streamwise force could be zero to move the particles when particles are not in the suspended mode, it is also impossible. Therefore, only Equations 3.31 gives a reasonable condition for $\tau_c' = 0$.

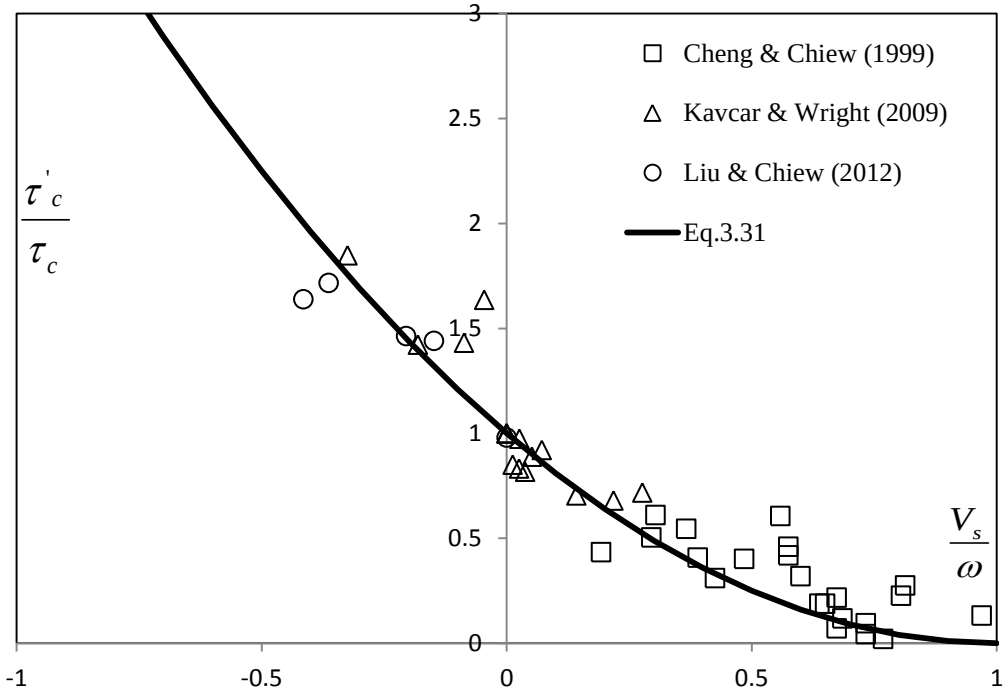

Figure 3.6: Comparison of experimental results on threshold condition under injection and suction seepage with Equation 3.31 where $Y = V_s/\omega$.

3.7 Effect of non-uniformity on the critical shear stress

Figure 3.4 shows that the Shields' curve could be totally invalid sometimes, these noticeable deviations imply that the non-uniformity could affect the predictability of Shields curve. Afzalimhr et al.'s (2007) data points locate below the curve as the flow was decelerating, whilst Emadzadeh et al.'s (2010) measured critical shear stress was far higher than the Shields' prediction. The former was conducted in decelerating flows, and the latter in accelerating flows. Therefore the large deviation from Shields curve shown in Figure 3.4 may be mainly caused by the vertical velocity as predicted by Equation 3.27, and the *V* could be induced by flow's non-uniformity.

To ascertain whether the deviations from Shields curve are caused by the non-uniformity, the data shown in Table 3.1 are used to determine the water depth variation dh/dx using Equation 3.25.

Manning coefficient (n) can be assessed using the Strickler's formula:

$$n = \frac{d_{50}^{1/6}}{21.1} \tag{3.36}$$

The energy slope S_f in Equation 3.25 was determined from the Manning equation using the Manning coefficient and hydraulic radius *R*.

$$S_f = \frac{n^2 U^2}{R^{4/3}} \tag{3.37}$$

For all data listed in Table 3.1, the calculated dh/dx could be either positive or negative and the data shown in Figure 3.4 is replotted in Figure 3.7, in which if the obtained value of d*h*/d*x* is positive, then the data point is represented by the sign "+", if the obtained value of d*h*/d*x* is negative, then the data point is marked by "-". It is interesting to note from Figure 3.7 that all data points above the Shields curve have been marked by "-", indicating the flows were accelerating, whilst almost all data points below the Shields curve have the sign of "+", implying that the flow is decelerating. Therefore it is clear that the non-uniformity plays an important role for the deviation of measured critical shear stress from the Shields curve. Figure 3.7 reveals that the presence of vertical velocity is the main cause responsible for the deviation of observed critical shear stress from the Shields curves, the accelerating flow increases particles' stability, and decelerating flow increases sediment's mobility. In Figure 3.7, the calculated positive dh/dx ranges from 0.000237 to 0.0526, the negative values vary from -0.024 to -0.00073, it is needed to investigate whether the higher d*h*/d*x* has the higher deviation.

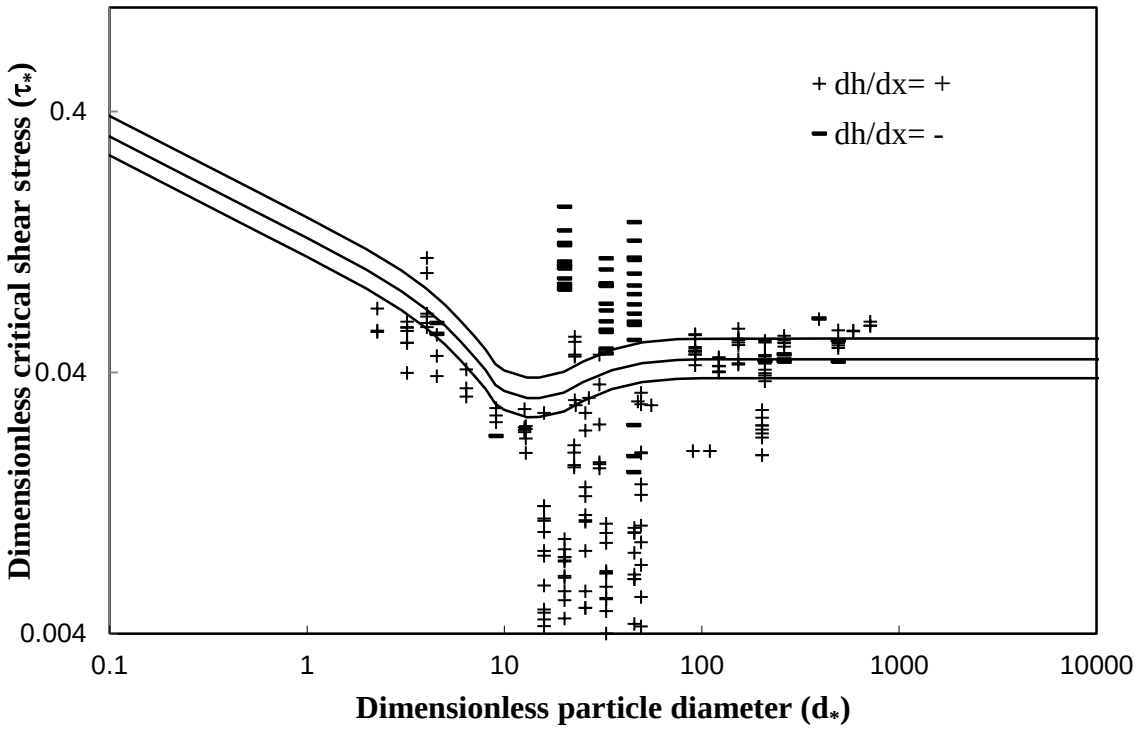

Figure 3.7: The variation of water depth dh/dx has different values based on the influence of vertical velocity on the initial motion, where (-0.024< dh/dx <0.0526) for all data sets from Figure 3.4.

3.8 The modification of Shields' diagram

To investigate whether all data points shown in Figure 3.4 can be expressed by Equation 3.18, we analyze the datasets without artificial seepage or its effect of groundwater variation is negligible ($V_s = 0$), i.e., only those data is analyzed in which V_b is caused by the non-uniformity in the main flow. Therefore, Equations 3.26 and 3.27 can be simplified as follows:

$$Y = \frac{V_b}{\omega} = \frac{\lambda U}{(1-\varepsilon_0)\omega}\frac{dh}{dx} \tag{3.38}$$

Experiments by Everts (1973); Afazlimhr et al. (2007); Emadzadeh et al. (2010); and Gaucher et al, (2010) are analyzed. They reported that their measured critical shear stress is lower than Shields' prediction. Besides, the datasets by Neil (1967) and Emadzadeh

et al. (2010) are examined; they claimed that higher values of critical shear stress were observed.

In these studies, flow discharge Q or mean flow velocity U; flow depth h or hydraulic radius R; median sediment size d_{50}; bed slope S_0 were comprehensively measured. The experimental data sets from the collected data related to the non-uniform flow are plotted in Figure 3.8 in which the empirical factor λ is found to be 8.5 for both accelerating and decelerating flow. The comparison of the measured and predicted critical shear stress in Figure 3.8 shows that the agreement is reasonably good, and it could be better if different λ is used in the fitting as λ could be a function of sediment gradation and shapes etc. In this research we only assume that sediment particle size is uniform and can be represented by d_{50}.

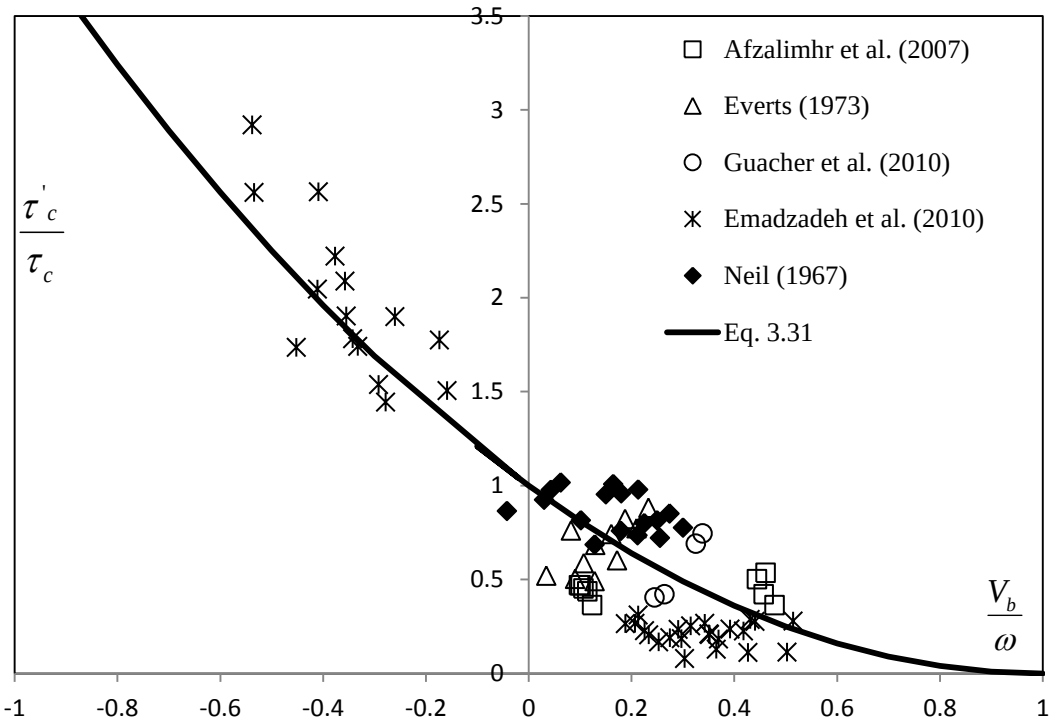

Figure 3.8: Comparison of experimental results on threshold condition without seepage with Equation 3.31 where $Y = \frac{V_b}{\omega}$.

Figure 3.9 shows the comparison of Equation 3.18 and the measured critical shear stress, the datasets i.e. Sarker and Hossain (2006), Shvidchenko and Pender (2000), Graf and Suszka (1987), White (1970) and Carling (1983) are included. It can be seen that even the observed critical shear stress largely deviates from Shields diagram represented by the solid line ($Y = V_s/\omega = 0$), all data points can be covered by Equation 3.18 when the parameter Y is introduced.

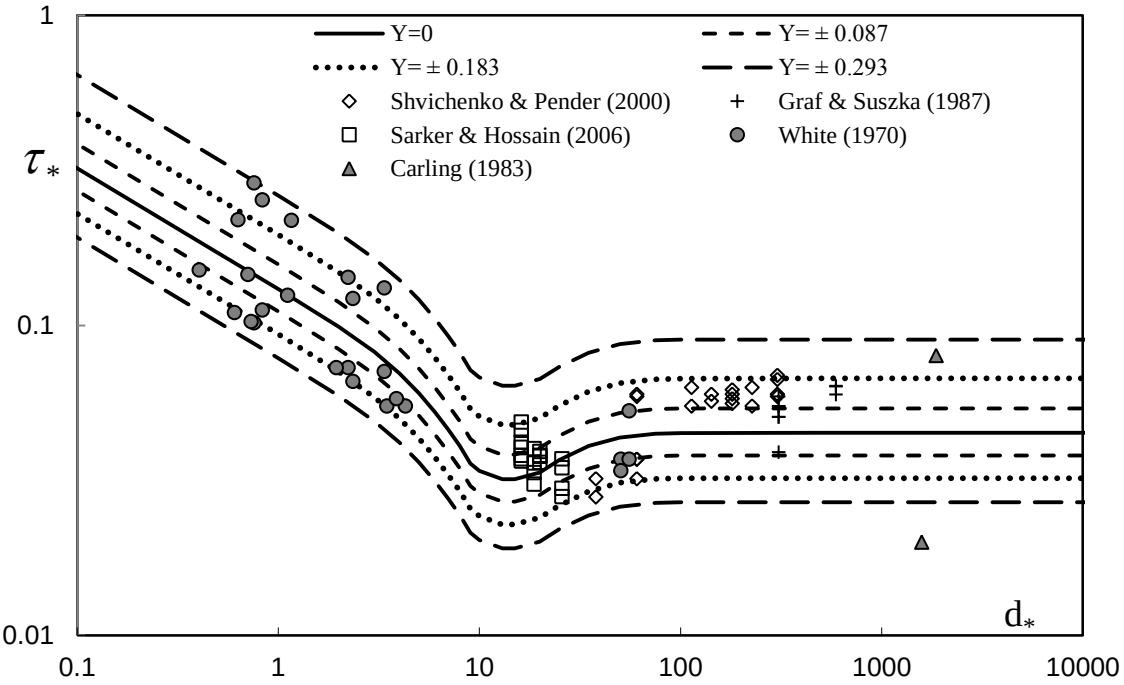

Figure 3.9: Influence of wall-normal velocity on critical shear stress, the symbols are measured results and lines are the calculated results from Equation 3.18 by changing Y.

3.9 Discussions

Different from previous studies that attribute the invalidity of Shields diagram to the channel slope, this study discovers that the Shields diagram is valid only for a uniform flow which rarely occurs in laboratory or nature. A universal Shields curve is developed by introducing the apparent sediment density. The relationship between the density and

flows' acceleration is established, thus it provides a useful tool to predict incipient motion of sediment for both uniform, non-uniform, or unsteady flows. The flow's non-uniformity is included in the parameter of *Y*; this inclusion makes the model to unite many phenomena like the initiation of sediment movement subject to seepage. The inclusion in the Shields' diagram also makes it possible to explain some odd phenomena observed by previous researchers, for example, many researchers found the dependence of critical Shields stress on the bed slope using other laboratory and natural streams data (Lamb et al., 2008), but it is still an open question whether the Shields number increases or decreases with the bed slope increment, thus it is worthwhile to explore the reasons for this dependence.

Equations 3.26 and 3.27 indicate that in almost all cases, there exists the vertical velocity caused by either the exchange of groundwater and river water or flow's non-uniformity. Therefore, the widely observed dependence like those reported by Lamb et al. (2008) is possibly caused by the parameter Y ($\neq 0$), to ascertain the statement, we only need to check whether the data used Lamb et al. (2008) is obtained in uniform flows. All data used by Lamb et al. to support their claim are listed in Table 3.2; here only the laboratory data are included as the field data were certainly collected from non-uniform conditions. The last column of Table 3.2 shows the length of flumes, and from it one can see that almost half of the researchers used the flumes whose length was less than 10m. Kirkgöz and Ardiçlioğlu (1997) measured the developing zone of a flume and found that to achieve the uniform flows a channel should be longer than 10m as there are developing zones from the flume's entrance and its tailgate. Even for those data from flumes longer than 10m, the flow could be non-uniform also when the parameter dh/dx is checked. Therefore we can conclude that it is likely that the data

were generated in non-uniform conditions, this could be contributed to the misleading interpretation of the dependence of critical shear stress on the channel slope.

Table 3.2: Previously reported data selected from Lamb et al. (2008):

Source	d_{50} (mm)	τ_*	R_*	Flume length (m)
Neil (1967)	6.2, 8.5, 10.6, 20, 23.8, 29.1, 5, 16, 6.4	0.04-0.06	184.3-4800	5
Shvidchenko & Pender (2000)	1.5, 2.4, 3.4, 4.5, 5.65, 7.15, 9, 12	0.025-0.065	40-2000	6.5
Ikeda (1982)	0.42 1.3	0.02 0.047	8.7 72	4
Wilcock & Mcardell (1993)	5.3	0.02	219	7.9
Paintal (1971)	7.95, 2.5	0.05, 0.05	638, 112	15
Everts (1973)	3.57, 1.79, 0.895, 0.508, 0.395, 0.254, 0.127, 0.18, 0.09	0.018-0.07	1.3-162	16.8
Ashida & Bayazit (1973)	22.5, 12, 6.4	0.0386-0.1178		20
Graf & Suszka (1987)	12.2, 23.5	0.05-0.07	800-5000	16.8
Wilcock (1987)	1.83 1.83 0.67 5.28	0.03 0.036 0.023 0.037	61 12 332 115	23
Fernandz Luque & Van Beek (1976	0.9, 1.5, 1.8, 3.3	0.021-0.047	12-127	8

We took Chiew and Parker's (1994) as an example; their observation is opposite to Lamb et al. (2008). Their channel slope was specially designed to vary within a range of -10^o to 31^o, but their channel lengths were 4m and 2m only. Obviously, their experiments were conducted in the uniform flow conditions as the 2~3m length is too short to form the uniform flow that needs the transitional sections from the head tank and tailgate. In other words, both conclusions drawn by Lamb et al. (2008) and Chiew

and Parker (1994) are not very convincing as they did not check the parameter of d*h*/d*x*, and the data they used may be generated from non-uniform conditions.

3.10 Summary

This chapter investigates the influence of vertical motion on initiation of sediment motion and the validity of the Shields curve. This deviation could be often caused by many factors like measurement errors, sediment gradation/shapes, or channel-bed slopes. Different from previous investigations, this chapter analyzes the effect of vertical velocity on the critical shear stress by re-examining 329 datasets available in the literature. Based on our research, we can draw the following conclusions:

1) There exist vertical velocity on the channel bed and this vertical velocity could be induced by seepage, non-uniformity, or unsteadiness, the amount of the vertical velocity may be very small, but its influence to sediment inception should not be underestimated. The joint effect can be expressed by Equation 3.27.
2) The upward velocity promotes sediment mobility and downward velocity promotes sediment stability. The sediment's mobility or stability can be equivalently expressed by its apparent sediment density which is able to eliminate the effect of vertical velocity as shown in Equation 3.4. For non-uniform or unsteady flows, Equation 3.4 indicates that the sediment tends to move in decelerating flows, but it becomes more difficult to move in accelerating phase or flows.
3) The Shields diagram is valid only when the flow is uniform, but after the introduction of apparent sediment density, the Shields diagram could be extended to express complex flows. A unified critical Shields stress for sediment

transport has been established, that can predict the critical shear stress in both uniform and non-uniform flows well.

4) Strictly speaking, the existing theory of sediment transport from its threshold to entrainment till suspension is only valid in uniform flows (Y = 0), but some previous researchers extend it to non-uniform flows, and some modifications for the diagram have been made. A new parameter Y has been proposed to check whether the data were collected from uniform flows, this parameter should be used in experimental and analytical investigations to gauge the flow's unsteadiness or non-uniformity.

5) According to available experimental data in the incipient motion in non-uniform flow or in seepage cases, good agreements between the measured and predicted values can be achieved. More research is needed to determine the coefficients λ_s and λ in Equation 3.27.

CHAPTER 4 THE PREDICTION OF TURBULENCE CHARACTERISTICS IN STEADY AND UNSTEADY FLOWS

4.1 Introduction

Unsteady flow is a recurrent phenomenon in nature, turbulence characteristics of unsteady flows are difficult to understand due to their dependence of time and space. It is important to understand unsteady flow because its turbulence characteristics are crucial for predicting sediment transport and pollution dispersion in river systems where the influence of unsteadiness is more significant. It is difficult to predict unsteady flow in practice and no widely accepted theory has been established. In general, the unsteady flow is complicated because of its variation with time and space but steady flow only varies with space. In this chapter, the full profile of turbulence characteristics including longitudinal and vertical velocity distributions, Reynolds shear stress and turbulence intensities will be predicted.

As mentioned in Chapter 2, the distributions of these turbulence characteristics in steady and unsteady non-uniform flows are different from those in uniform flow. From experimental data sets available in the literature, the measured data points of Reynolds shear stress, horizontal and vertical velocities and turbulence intensities in non-uniform and decelerating flows deviate from those in uniform flow. In accelerating non-uniform flow, the measured data points for these turbulence characteristics have less value than those predicted using uniform flow while these data points have higher value when the flow is decelerating. Therefore, more research is needed to investigate the reason for this deviation.

Thus, the specific objectives for this chapter are:

1. Observe the influence of flow acceleration on turbulence characteristics for both steady and unsteady flows;
2. Develop universal formula to express the longitudinal velocity distribution across the water depth in a channel in uniform, non-uniform steady and unsteady flows by combining Log law, Cole's Wake law and Dip law;
3. Develop new formulas to express the other turbulence characteristics in steady and unsteady flows without including the time based on the value of flow acceleration;
4. Establish a new relationship between Reynolds shear stress and turbulence intensities in unsteady flow;
5. Verify the developed empirical equations using available experimental data.

4.2 The relationship between the flow acceleration and velocity distribution

In the literature, it has already been discussed that the consistency of flow velocity and water depth in open channel flows from upstream to downstream generate the uniform flow. However, in steady non-uniform, unsteady flows, the upstream flow velocity and water depth are different from downstream. These differences relate to flow acceleration. Generally, the flow acceleration i.e. a means that there is a difference in velocities in two adjacent measuring stations or different time at the same location. Based on this definition, the flow acceleration is equal to zero when the flow is uniform while in steady and unsteady non-uniform flows, the flow acceleration is different. When the flow velocity increases along the open channel the flow acceleration is increased or has a positive value and this type of flow is accelerating steady and

unsteady non-uniform flows. In contrast, the flow acceleration is less than zero or has a negative value when the flow is decelerating steady and unsteady non-uniform flow due to the decrease of flow velocity along the channel. According to this, flow acceleration is the most important parameter to distinguish the flows, thus it is possible to develop empirical formulas to predict the turbulence characteristics using the flow acceleration.

The distinction of velocity profiles in a uniform flow with those of accelerating and decelerating flows is shown in Figures 4.1 to 4.4, where the velocity profiles of (S_0=0.75%, Q=50L/s; S_0= - 0.25%, 932, t=15s) and (AGB5, DGC3) were measured by Song (1994) and Kironoto and Graf (1995), respectively in the form of $\bar{u}/u_*$ against $y + y_0/k_s$, in which y is the vertical distance measured from the reference level y_0; $y_0 = 0.2 * k_s$ is the reference bed level; and $k_s = d_{50}$ (from Kironoto and Graf's definition) while $y_0 = 0.25 * k_s$ from Song's definition. In these figures, the first letter in AGB5 and DGC3 denotes accelerating and decelerating flow respectively; the letter of G refers to the gravel bed; the letters B and C are series numbers used by the authors and 3 and 5 were the measuring cross-section which were 11.245m and 12.21m from the flume entrance. More details of Kironoto and Graf's (1995) experimental setup and experimental procedure have been described in Kironoto's thesis (1992). While in Song's definitions, S_0 is bed slope, Q is flow discharge, 932 is the hydrograph's number and t is time.

Figure 4.1 shows that the measured velocity profiles match well in the inner region with the Log law as no influence for the flow acceleration (a = 0, where a is the depth averaged flow acceleration) and in the outer region there is a small deviation from the predicted value. While in Figure 4.2, the measured data points bend down from the straight line of Log law prediction as the flow acceleration (a > 0) is positive; and they

bend up over the Log law prediction (see Figure 4.3) when the flow acceleration ($a < 0$) is negative. Similar case can be found in accelerating unsteady flow as shown in Figure 4.4.

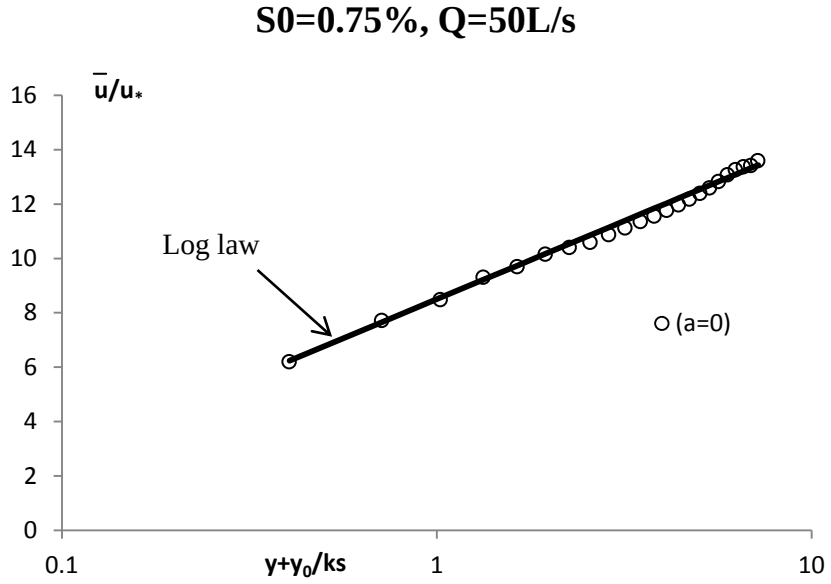

Figure 4.1: Comparison between measured velocity profile with Log law's prediction in uniform flow based on Song's (1994) experimental data.

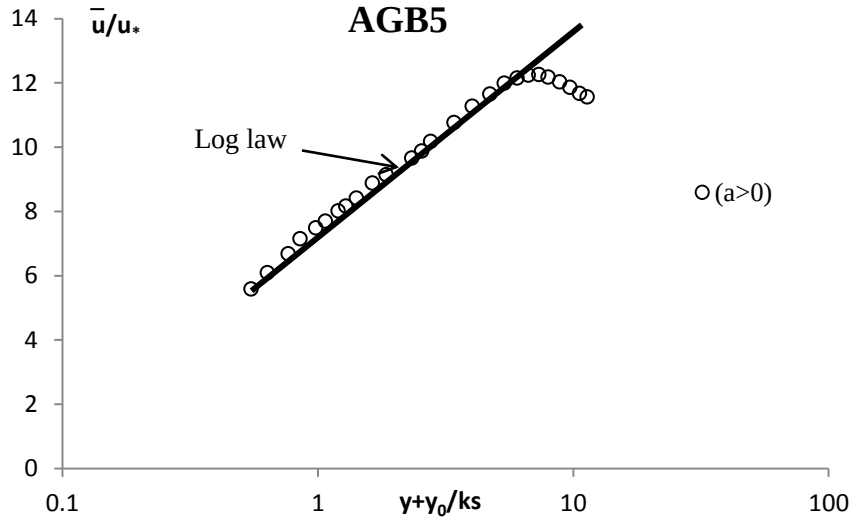

Figure 4.2: Comparison between measured velocity profile with Log law's prediction in accelerating non-uniform steady flow based on Kironoto and Graf's (1995) experimental data.

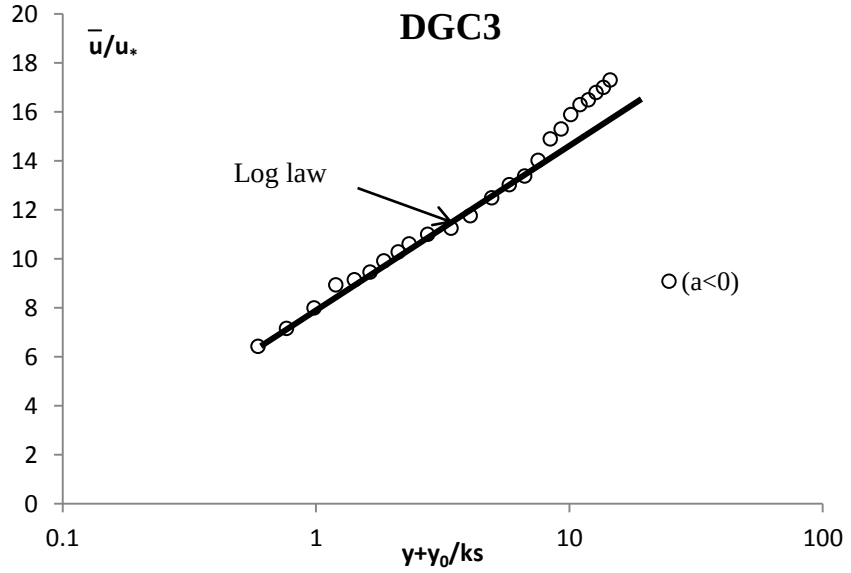

Figure 4.3: Comparison between measured velocity profile with Log law's prediction in decelerating non-uniform steady flow based on Kironoto and Graf's (1995) experimental data.

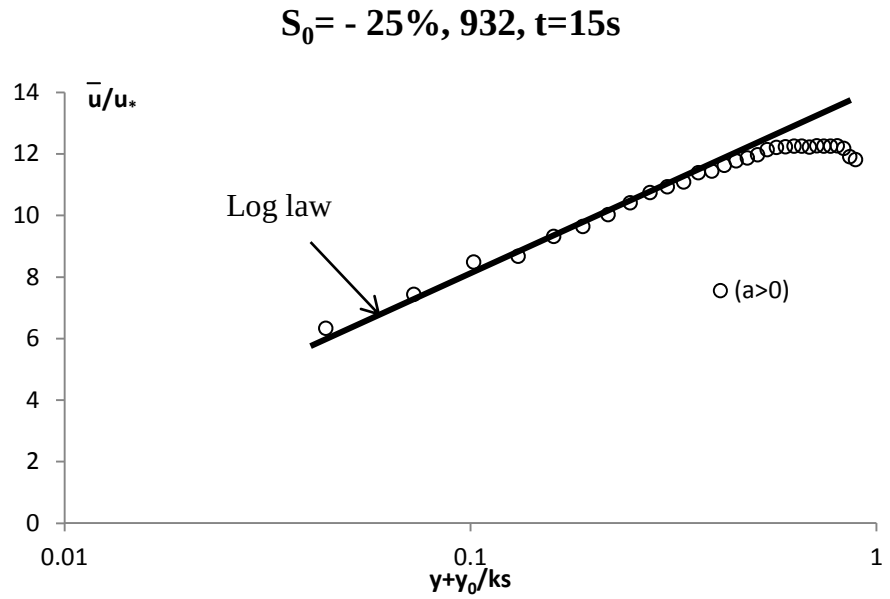

Figure 4.4: Comparison between measured velocity profile with Log law's prediction in accelerating unsteady flow based on Song's (1995) experimental data.

.

The comparisons in the above four figures clearly show that the Log law is valid only in flows where the acceleration is zero, the deviation from the Log law is negative in accelerating flows $(a > 0)$, while it becomes positive in a decelerating flow. The reason for this deviation was explained by Yang and Lee (2007) based on the Reynolds

equation, and they concluded that the presence of vertical velocity or wall-normal velocity $(\bar{v})$ is responsible for the invalidity of Log law. They found that the Log law is valid if $\bar{v}=0$ (uniform flow); and the Coles model becomes valid only when $\bar{v}>0$ (decelerating flow), and the maximum velocity occurred below the water surface if and only if $\bar{v}<0$ (accelerating flow). But in practice, the formula proposed by Yang and Lee are very difficult to use because the wall-normal velocity is generally too small in quantity to measure. Therefore, to help river engineers to solve their practical problems easily, it is necessary to develop a formula that is valid for all flow conditions and a readily measurable parameter such as the mean streamwise velocity, rather than the wall-normal velocity is used.

To simplify such as an expression, the Log law together with Cole's Wake law and Dip law are combined to express the longitudinal velocity across the whole water depth from the bed to the water surface for both steady and unsteady flows.

$$\frac{\bar{u}}{u_*}=\frac{1}{k}\ln(\frac{y+y_0}{k_s})+k_1\sin^2(\frac{\pi}{2}\frac{y}{h})+k_2\ln(1-\frac{y}{h}) \tag{4.4}$$

where k_1 and k_2 are coefficients to be determined empirically. The first term in Equation 4.4 refers to the Log law while the second and third terms are Cole's Wake law and Dip law, respectively. Obviously, k_1 and k_2 are a function of flow acceleration, and they become zero if the acceleration is zero (uniform flow), terms 2 and 3 on the right hand side of Equation 4.4 are negligible in the inner region, but they are noticeable in the main flow region. Due to $\ln(1-y/h)\to-\infty$ as $y/h\to 1$, Therefore, Equation 4.4 is invalid in a very thin layer near the free surface just like the classical Log law that becomes invalid at the layer closer to the boundary, i.e. $y=0$. In Equation 4.4, k_1 and

k_2 are empirical coefficients and will be evaluated from their relationships with the flow acceleration instead of the wall-normal velocity. As mentioned before, the wall-normal velocity is equivalent to predict the longitudinal velocity but the flow acceleration is more direct and simpler in the mathematical treatment. Therefore, in this study, the value of flow acceleration (a) is needed to confirm the validity of Equation 4.4. For this purpose a simple expression of flow acceleration should be established.

4.3 Determination of flow acceleration for both steady and unsteady flow

This chapter makes an attempt to express the turbulence characteristics in steady non-uniform flow or unsteady flow, to achieve this, appropriate expression of flow acceleration is needed; the point and instantaneous acceleration can be written as follows:

Steady flow $$\bar{a}_1 = \bar{u}\frac{\partial \bar{u}}{\partial x} + \bar{v}\frac{\partial \bar{u}}{\partial y} + \bar{w}\frac{\partial \bar{u}}{\partial z} \tag{4.5}$$

Unsteady flow $$\bar{a}_2 = \frac{\partial \bar{u}}{\partial t} + \bar{u}\frac{\partial \bar{u}}{\partial x} + \bar{v}\frac{\partial \bar{u}}{\partial y} + \bar{w}\frac{\partial \bar{u}}{\partial z} \tag{4.6}$$

where Equation 4.5 describes the acceleration in steady flow whereas Equation 4.6 describes the variation of unsteady flow. In these equations, the variation of velocity in the lateral direction becomes zero if only 2-D flow is considered. Therefore, Equations 4.5 and 4.6 reduce to:

$$\bar{a}_1 = \bar{u}\frac{\partial \bar{u}}{\partial x} + \bar{v}\frac{\partial \bar{u}}{\partial y} \tag{4.7}$$

$$\bar{a}_2 = \frac{\partial \bar{u}}{\partial t} + \bar{u}\frac{\partial \bar{u}}{\partial x} + \bar{v}\frac{\partial \bar{u}}{\partial y} \tag{4.8}$$

In steady and unsteady equations, the term of $\bar{v}\frac{\partial \bar{u}}{\partial y}$ can be rewritten as:

$$\bar{v}\frac{\partial \bar{u}}{\partial y} = \frac{\partial \overline{\bar{u}\bar{v}}}{\partial y} - \bar{u}\frac{\partial \bar{v}}{\partial y} \tag{4.9}$$

The continuity equation for two dimensional open channel flows (2-D) is:

$$\frac{\partial \bar{v}}{\partial y} = -\frac{\partial \bar{u}}{\partial x} \tag{4.10}$$

Substitution of Equation 4.10 into Equation 4.9 obtains:

$$\bar{v}\frac{\partial \bar{u}}{\partial y} = \frac{\partial \overline{\bar{u}\bar{v}}}{\partial y} - \bar{u}\left(-\frac{\partial \bar{u}}{\partial x}\right) \tag{4.11}$$

Substitution of Equation 4.11 into Equations 4.7 and 4.8 obtain:

$$\bar{a}_1 = \bar{u}\frac{\partial \bar{u}}{\partial x} + \frac{\partial \overline{\bar{u}\bar{v}}}{\partial y} + \bar{u}\frac{\partial \bar{u}}{\partial x} \tag{4.12}$$

$$\bar{a}_2 = \frac{\partial \bar{u}}{\partial t} + \bar{u}\frac{\partial \bar{u}}{\partial x} + \frac{\partial \overline{\bar{u}\bar{v}}}{\partial y} + \bar{u}\frac{\partial \bar{u}}{\partial x} \tag{4.13}$$

Equations 4.12and 4.13 can be expressed as the following:

$$\bar{a}_1 = \frac{\partial \bar{u}^2}{\partial x} + \frac{\partial \overline{\bar{u}\bar{v}}}{\partial y} \tag{4.14a}$$

$$\bar{a}_2 = \frac{\partial \bar{u}}{\partial t} + \frac{\partial \bar{u}^2}{\partial x} + \frac{\partial \overline{\bar{u}\bar{v}}}{\partial y} \tag{4.14b}$$

In this study, the depth averaged flow acceleration is used as the characteristic acceleration for both steady and unsteady non-uniform flow, it is defined as:

$$a = \frac{1}{h}\int_0^h \bar{a}dy \tag{4.15}$$

where a is the depth averaged flow acceleration in steady and unsteady flows. Then, insert Equations 4.14a and 4.14b into Equation 4.15 one has:

$$a_1 = \frac{1}{h}\int_0^h \frac{\partial \bar{u}^2}{\partial x}dy + \frac{1}{h}\int_0^h \frac{\partial \bar{u}\bar{v}}{\partial y}dy \tag{4.16}$$

$$a_2 = \frac{1}{h}\int_0^h \frac{\partial \bar{u}}{\partial t}dy + \frac{1}{h}\int_0^h \frac{\partial \bar{u}^2}{\partial x}dy + \frac{1}{h}\int_0^h \frac{\partial \bar{u}\bar{v}}{\partial y}dy \tag{4.17}$$

where a_1 and a_2 refer to the depth averaged flow acceleration in steady and unsteady non-uniform flows, respectively. Using the Leibnitz theorem to integrate the first term of $\frac{1}{h}\int_0^h \frac{\partial \bar{u}}{\partial t}dy$ from Equation 4.17 with the limiting conditions $y = 0$ and $y = h$ to obtain:

$$\frac{1}{h}\int_0^h \frac{\partial \bar{u}}{\partial t}dy = \frac{1}{h}\left(\frac{d}{dt}\int_0^h \bar{u}dy - \bar{u}_h \frac{dh}{dt}\right)$$

$$= \frac{dU}{dt} - \frac{\bar{u}_h}{h}\frac{dh}{dt} \tag{4.18}$$

where U is the depth averaged longitudinal velocity; $\bar{u}_h$ is the longitudinal velocity at the water surface i.e. ($y = h$); and dh/dt, dU/dt are the derivative of water depth and velocity with respect to time. The term of $\partial \bar{u}^2 / \partial x$ in Equations 4.16 and 4.17 can be integrated with respect to water depth y from the channel bed $(y = 0)$ to the free water surface $(y = h)$ as follows:

$$\frac{1}{h}\int_0^h \frac{\partial \bar{u}^2}{\partial x}dy = \frac{1}{h}\left(\frac{d}{dx}\int_0^h \bar{u}^2 dy - \bar{u}_h^{\,2}\frac{dh}{dx}\right)$$

$$= \beta\frac{dU^2}{dx} - \frac{\bar{u}_h^{\,2}}{h}\frac{dh}{dx} \qquad (4.19)$$

where β is the momentum flux correction factor that takes into the non-uniform of flow velocity across the inlet and outlet. The value of β ranges between 1.01 and 1.04 (Cengel & Cimbala, 2010, p.249) and in this study, the value of β is assumed to be 1.03.

The integration of $\partial\overline{uv}/\partial y$ in both Equations 4.16 and 4.17 with respect to *y* from $y = 0$ to $y = h$ using the Leibnitz theorem yields:

$$\frac{1}{h}\int_0^h \frac{\partial \overline{uv}}{\partial y}dy = \frac{1}{h}\int_0^h d\overline{uv}$$

$$= \frac{1}{h}(\bar{u}_h\bar{v}_h - \bar{u}_0\bar{v}_0) \qquad (4.20a)$$

At the bed surface when $y = y_0$ (where y_0 is a function of d_{50}), the longitudinal velocity, i.e. $\bar{u}_0$ is zero while the vertical velocity $\bar{v}_0 = V_b$ (in which V_b is the vertical velocity at the interface between porous media), $V_b = V = 0$ if there is no seepage effect and $V_b \neq 0$ if there is either suction or injection seepage flux. Therefore, Equation 4.20a becomes:

$$\frac{1}{h}\int_0^h \frac{\partial \overline{uv}}{\partial y}dy = \frac{1}{h}\bar{u}_h\bar{v}_h \qquad (4.20b)$$

Then, the final equation to predict the flow acceleration in steady and unsteady non-uniform flows can be expressed as the following:

$$a_1 = (\beta \frac{dU^2}{dx} - \frac{\bar{u}_h^2}{h}\frac{dh}{dx}) + (\frac{1}{h}\bar{u}_h\bar{v}_h) \tag{4.21}$$

$$a_2 = (\frac{dU}{dt} - \frac{\bar{u}_h}{h}\frac{dh}{dt}) + (\beta \frac{dU^2}{dx} - \frac{\bar{u}_h^2}{h}\frac{dh}{dx}) + (\frac{1}{h}\bar{u}_h\bar{v}_h) \tag{4.22}$$

The depth averaged flow acceleration a_1 and a_2 are calculated using Equations 4.21 and 4.22 respectively given the following basic data: longitudinal velocity at the water surface, $\bar{u}_h$; vertical velocity at the water surface, $\bar{v}_h$; the variation of water depth with time, dh/dt; the variation of water depth along the longitudinal direction, dh/dx; water depth, h; the variation of depth averaged longitudinal velocity with time, dU/dt; and the variation of depth averaged longitudinal velocity squared along the channel, dU^2/dx. All these parameters should be known from experimental data sets available in the literature in order to predict the values of flow acceleration in steady and unsteady flows.

For steady flow, the value of dU^2/dx can be determined by the derivation of Energy equation with respect to x:

$$E = Z + h + \frac{U^2}{2g} \tag{4.23}$$

where E is the total energy and Z is the elevation. From the derivation of Equation 4.23, one obtains:

$$\frac{dE}{dx} = \frac{dZ}{dx} + \frac{dh}{dx} + \frac{1}{2g}\frac{dU^2}{dx} \tag{4.23a}$$

Then

$$-S_f = -S_0 + \frac{dh}{dx} + \frac{1}{2g}\frac{dU^2}{dx} \tag{4.24}$$

where dh/dx is the variation of water depth along the open channel, S_0 is the bed slope, and these two terms can be evaluated from the experimental data sets. S_f is the energy slope and can be determined from the Manning Equation:

$$U = \frac{1}{n}R^{2/3}S_f{}^{1/2} \tag{4.25}$$

where U is depth averaged mean horizontal velocity; and R is the hydraulic radius and its value can be computed by the flow area in open channel divided by the wetted perimeter. n is the Manning coefficient, for a smooth bed the value of n ranges between 0.01 to 0.013 (Mays, 2005) while in a rough bed it can be evaluated from Strickler's formula as follows:

$$n = \frac{d_{50}^{1/6}}{21.1} \tag{4.26}$$

where d_{50} is the median particle size in meter.

For an unsteady flow, the value of dU^2/dx can be calculated by (Henderson, 1966, p.287):

$$S_f = S_0 - \frac{\partial h}{\partial x} - \frac{1}{2g}\frac{\partial U^2}{\partial x} - \frac{1}{g}\frac{\partial U}{\partial t} \tag{4.27}$$

where dU/dt is the derivative velocity with time.

In this chapter, the flow acceleration is the main factor; therefore, its calculation is summarized as follows:

1. The vertical velocity at the water surface $\bar{v}_h$ should be known in order to determine the flow acceleration using Equations 4.21 and 4.22. While the longitudinal velocity at the water surface $\bar{u}_h$ can be known from experimental results and if this value cannot be measured due to high turbulence and water level fluctuation near the water surface, it is best done by extrapolating the measured velocity to free surface, provided accurate velocity profiles data is available just below the surface.

2. In steady and unsteady flows experimental results, water depth (h), flow discharge (Q), averaged depth mean velocity (U), bed slope (S_0) and the variation of water depth (dh/dx) should be known. The value of energy slope S_f can be estimated using Manning Equation (see Equation 4.25) and after that applying the value of S_f in Equation 4.24 to obtain the value of dU^2/dx. For unsteady flow, a similar calculation is performed using Equation 4.27 instead of Equation 4.24 to calculate dU^2/dx.

3. The value of (dU/dt) and (dh/dt) can be known from the variations of two mean velocities and water depth in specific time.

4. After applying the values of $\bar{u}_h, \bar{v}_h, dh/dx, dU^2/dx, dh/dt$ and dU/dt in Equation 4.21 and 4.22, the acceleration in steady/unsteady flows, i.e. a can be calculated.

4.4The influence of flow acceleration on turbulence characteristics in steady and unsteady flow

In order to verify that flow acceleration is responsible for the deviation of the measured turbulence characteristics in non-uniform flow from that in uniform flow, Song's (1994) experimental data is used as it may be one of the most comprehensive datasets in the literatures, all parameters needed for Equations 4.21 and 4.22 were measured and documented. Song measured turbulence characteristics, such as mean horizontal and vertical velocity, Reynolds shear stress and horizontal and vertical turbulence intensities $(\bar{u},\bar{v},-\rho\overline{u'v'},u',v')$, respectively in steady and unsteady non-uniform flows using an Acoustic Doppler Velocity Profiler (ADVP). Song's experiments were performed in a 16.8m long, 0.6m wide and 0.8m high flume, in which the bed consisted of nearly uniform gravels with d_{50}=12.3mm. Song generated the non-uniform flow by adjusting the bed slope and regulating the tail gate. He used negative bed slope to generate accelerating while a positive bed slope generated decelerating flow. Song measured the full profiles across the depth for all turbulence characteristics as well as the vertical velocity. Therefore, Song's experimental data is considered to be one of the best and available literature is used in this thesis to develop formulas which will be used to determine these turbulence characteristics for both steady and unsteady flows. Based on Song's (1994) data, Equations 4.21 and 4.22 are used to determine the flow acceleration in steady and unsteady flows. In his experiments, the values of h, S_0, U and dh/dx were measured as well as the full profile of longitudinal (horizontal) and vertical velocity across the water depth as well as Reynolds shear stress and turbulence intensities. The velocities at the water surface can be obtained by extrapolating from the measured velocity to the water surface.

From h, S_0, U and dh/dx, the value of dU^2/dx is estimated using Equation 4.24 and 4.27 after calculating the energy slope using Equation 4.25.

In order to prove the influence of flow acceleration on the deviation of these turbulence characteristics in non-uniform flow from those in uniform flow, the measured full profile of turbulence characteristics for example, horizontal velocity $\bar{u}$ and vertical velocity $\bar{v}$, Reynolds shear stress $-\rho\overline{u'v'}$ and horizontal and vertical turbulence intensities u' and v', respectively, are normalized with the shear velocity and they are plotted as $\bar{u}/u_*$, $\bar{v}/u_*$, $-\overline{u'v'}/u_*^2$, u'/u_* and v'/u_* versus y/h as shown in Figures 4.5 to 4.9, where the acceleration is normalized by u_*^2/h.

The typical profiles in accelerating and accelerating flows are shown in Figures 4.5 to 4.9, in which "A" means accelerating steady; "D" denotes decelerating steady; "AU" refers to accelerating unsteady; "S" represents the bed slope; "Q" is flow discharge; "t" means time; and "931 or 936" is the hydrograph's number in Song's experimental datasets. For example AS-25-Q80 means that the flow is accelerating steady, the bed slope is -25% and discharge is 80L/s, while AUS-60-931, t=15&17s means that the flow is accelerating unsteady, bed slope = -60%, number of hydrograph =931 and t=15&17s refer to the time that averages the profiles obtained at t=15 and 17s.

First, the measured $\bar{u}/u_*$ versus $y + y_0/k_s$ is plotted in Figure 4.5 using the open and solid symbols and the solid line is presented the Log law using Equation 2.2. For each flow condition, the values of $a_1/(u_*^2/h)$ and $a_2/(u_*^2/h)$ refer to the dimensionless flow acceleration in steady and unsteady flows respectively. The calculated values of $a/(u_*^2/h)$ are shown in legend of Figure 4.5.

It can be seen clearly that the measured longitudinal velocity from the inner region in steady and unsteady flows matches well with Log law's prediction but in the main flow region ($y/h \geq 0.2$), the measured velocity becomes larger than its prediction using Log law when the flow is decelerating or it has lower value when the flow is accelerating. Based on this observation, it is reasonable to conclude that the flow acceleration causes the velocity deviations from Log law's prediction. It also demonstrates that the large deviation from Log law is correspondent to the higher value of dimensionless $a/(u_*^2/h)$, no matter whether it is negative or positive. For example, in the decelerating flow (DS75-Q=80) the calculated $a/(u_*^2/h)$ = -6, it gives larger deviation than in DS50-Q=70 where $a/(u_*^2/h)$ = -2.9. The similar influence of flow acceleration is also found when the flow is accelerating. It can be seen that the velocity profiles from unsteady flows are similar to those from steady flows, thus it is possible to establish a universal formula to express the velocity distribution of steady and unsteady flows. In Figure 4.5, it clearly seen that the measured velocity in decelerating flows positively deviate from the Log law, but the deviation becomes smaller near the free surface, or the profile slightly bends down, this is why in Equation 4.4 the dip-term and wake function are kept in the expression. Therefore, it seems that the flow acceleration is a controlling parameter which can affect the shape of the measured longitudinal velocity profile.

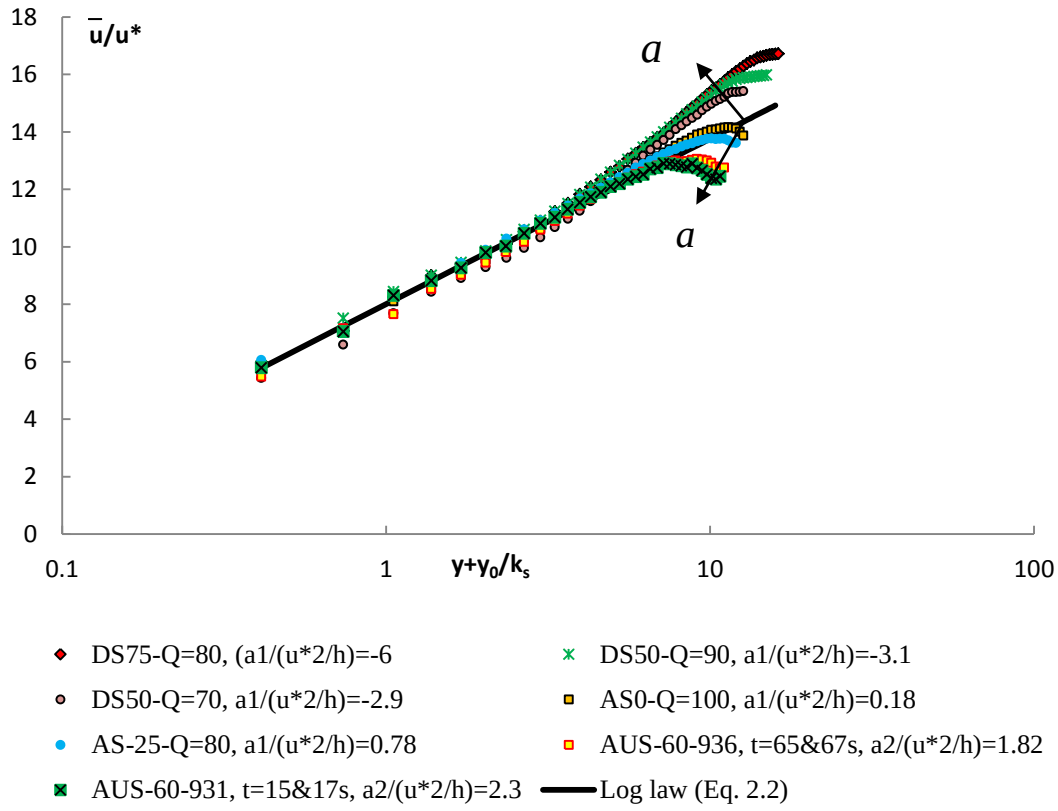

Figure 4.5: The influence of dimensionless flow acceleration on the deviation of measured longitudinal velocity in accelerating and decelerating steady and unsteady flows from Log law based on Song's experimental data sets.

Secondly, Figure 4.6 shows the influence of flow acceleration on the deviation of Reynolds shear stress in non-uniform flow from that in uniform flow, where the open and solid symbols represent the measured Reynolds shear stress in non-uniform flow; while the straight solid line is the predicted Reynolds shear stress in uniform flow using Equation 2.7. The full profiles for $(-\overline{u'v'}/u_*^2)$ are plotted in Figure 4.6 for varying flow condition using dimensionless velocity with respect to the shear velocity (u_*) in $'x'$ axis against the vertical measured distance y with respect to the water depth as $'y'$ axis, where the acceleration is normalized by u_*^2/h. The calculated values of $a/(u_*^2/h)$ are shown in legend of Figure 4.6.

It can be seen that the measured Reynolds shear stress in non-uniform flow becomes zero as y/h approaches to the water surface, and its value becomes 1 as y/h approaches to the bed surface $(y=0)$, these indicate that at $y=0$ and $y=h$, the measured Reynolds shear stress in non-uniform flows becomes identical to a uniform flow. However, between these two extremes, the measurement of data points in accelerating and decelerating steady and unsteady flows locate on both sides of the solid line or Equation 2.7. Reynolds shear stress in the accelerating steady flow (AS0-Q80) is systematically larger than the values of Equation 2.7 and accelerating unsteady flow (AUS-45-936, t=11&13s) are systematically smaller than the values of Equation 2.7, and that in the decelerating flow, i.e., (DS90-Q=80) is systematically larger than the values of Equation 2.7.

Based on this observation, it is reasonable to conclude that the flow acceleration causes the Reynolds shear stress deviations from the uniform flow's prediction; it also demonstrates that the large deviation from the uniform flow line is corresponding to the higher value of dimensionless $a/(u_*^2/h)$, no matter whether it is negative or positive. For example, in the accelerating steady flow (AS0-Q=80) the calculated dimensionless flow acceleration =0.39, it gives lower deviation than in AUS-60-936, t=65&67s where the flow acceleration is equal to 1.82. The similar influence of flow acceleration is found when the flow is decelerating. From this comparison, it can be seen that the Reynolds shear stress profiles in unsteady flows are similar to those in steady flows, thus it is possible to establish a unify formula to express the Reynolds shear stress distribution of steady and unsteady flows. In Figure 4.6, it clearly shows that the large acceleration can generate higher deviation than the smaller one. In order to confirm this

relationship, the difference between the measured data points in non-uniform and uniform flows is defined as:

$\Delta - \overline{u'v'}/u_*^2 = (-\overline{u'v'}/u_*^2)_{nonunf.} - (-\overline{u'v'}/u_*^2)_{unf.}$, in which the subscript ($nonunf.$) is the dimensionless Reynolds shear stress in non-uniform flow while the subscript ($unf.$) is the dimensionless Reynolds shear stress in uniform flow. In Figure 4.6, the average $\Delta - \overline{u'v'}/u_*^2$ between (AS0-Q=80) and Equation 2.7 is equal to -0.23 while in (AUS-60-936, t=65&67s) the value of $\Delta - \overline{u'v'}/u_*^2$ is -0.53. Regardless the negative sign in these two values of $\Delta - \overline{u'v'}/u_*^2$, it is clearly seen that the lower value of $\Delta - \overline{u'v'}/u_*^2$ is closer to the uniform flow than the higher one. While with regard to these negative values, they demonstrate that the measurements of Reynolds shear stress in accelerating flow are smaller than those in uniform flow. In contrast, in decelerating flow, Figure 4.6 shows a higher deviation obtained from the profile of DS90-Q=80 and Equation 2.7 than that obtained from (DS50-Q=70) and Equation 2.7, which is attributed to value of $\Delta - \overline{u'v'}/u_*^2$ in (DS90-Q=80) is 0.14, bigger than the average $\Delta - \overline{u'v'}/u_*^2$ of 0.018 in (DS50-Q=70). In decelerating flow, these differences become in positive values because their measured data points are higher than those in uniform flow. From these values, it clearly shows that the measured Reynolds shear stress in decelerating flows positively deviate from the uniform flow line, but this deviation becomes negative, or the profile slightly trends below the uniform flow when the flow is accelerating. Therefore, Equation 2.7 needs to be modified depending on the influence of flow acceleration.

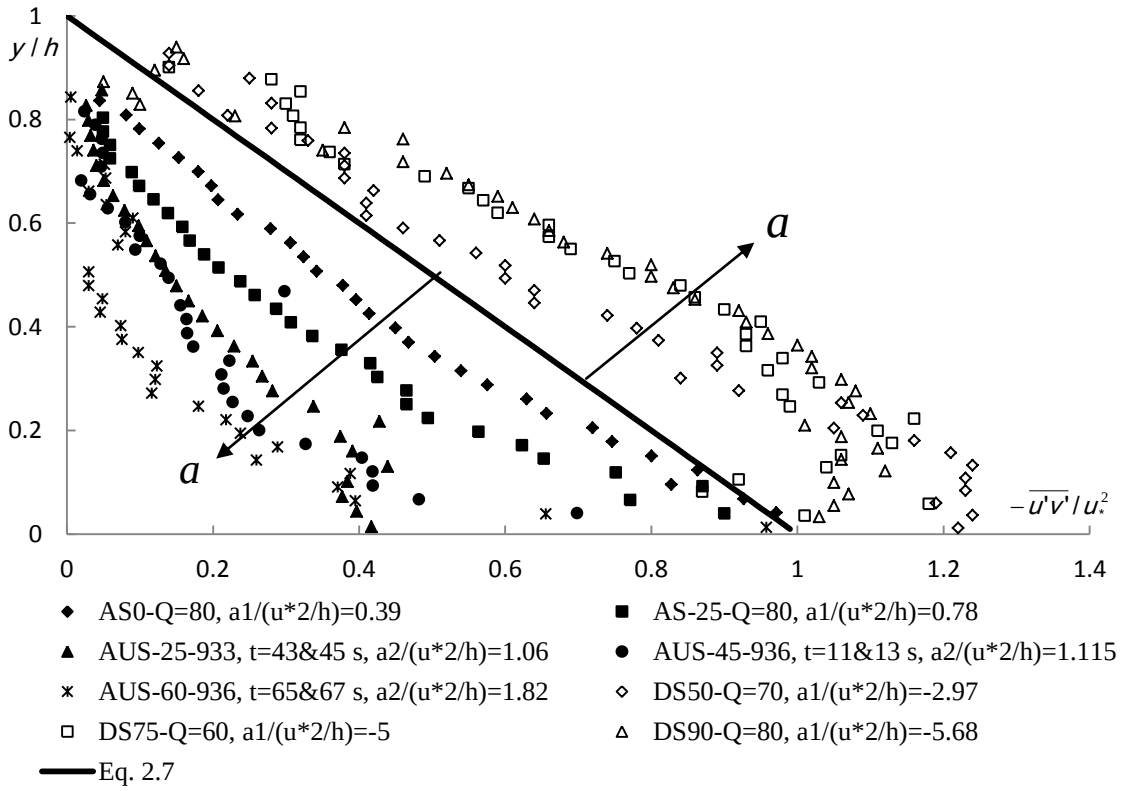

Figure 4.6: The influence of dimensionless flow acceleration on the deviation of measured Reynolds shear stress in accelerating and decelerating steady and unsteady flows from uniform flow based on Song's experimental data sets.

Moreover, the responsibility of flow acceleration on the deviation of horizontal and vertical turbulence intensities in non-uniform flow from those in uniform flow is demonstrated in Figures 4.7 and 4.8. In these figures, the full profiles for horizontal and vertical turbulence intensities i.e. (u'/u_* and v'/u_*), respectively in accelerating and decelerating steady and unsteady flows are plotted in Figures 4.7 and 4.8 for varying flow conditions using dimensionless velocity with respect to the shear velocity (u_*) in 'x' axis against the vertical measured distance y with respect to the water depth as 'y' axis, where the acceleration is normalized by u_*^2/h.

Figures 4.7 and 4.8 show the influence of flow acceleration on the deviation of these turbulence intensities in non-uniform flows from that in uniform flow, where the open and solid symbols represent the measured turbulence intensities in non-uniform flow, i.e., (u'/u_* and v'/u_*) against y/h while the curve solid lines are the predicted horizontal and vertical turbulence intensities in uniform flow using Equations 2.5 and 2.6, respectively. The calculated values of $a/(u_*^2/h)$ are shown in legends of Figures 4.7 and 4.8, it can be clearly shown the deviation of turbulence intensities in non-uniform flow from that in uniform flow curve, the measured data points in accelerating steady and unsteady flow appear below the curve line with concave distributions but the data points in the decelerating flow are located above the curve line with convex distributions. Horizontal and vertical turbulence intensities in the accelerating steady flow (AS0-Q=80) and accelerating unsteady flow (AUS-60-936, t=65&67s) are systematically smaller than the values of Equations 2.5 and 2.6, and that in the decelerating steady flow, i.e. (DS50-Q=90) is systematically larger than the values of Equations 2.5 and 2.6. Thus, Equations 2.5 and 2.6 are needed to be modified based on this deviation in order to be applicable for the predictions of these turbulences in non-uniform flows.

Based on the above observation, it is reasonable to conclude that the flow acceleration causes the turbulence intensity deviations from the uniform flow's prediction. For each flow condition, the flow accelerations in steady and unsteady flow are determined using Equations 4.21 and 4.22 respectively. From these values, it also demonstrates that the large deviation from the uniform flow is corresponding to the higher value of dimensionless $a/(u_*^2/h)$, no matter whether it is negative or positive. For example, in the decelerating steady flow (DS90-Q=80) presented in Figures 4.7 and 4.8, the

calculated dimensionless flow acceleration $a/(u_*^2/h)$=-5.68, it gives higher deviation than in DS50-Q=90 where the flow acceleration $a/(u_*^2/h)$ is equal to -3.1. Similar influence of flow acceleration is also found when the flow is accelerating. From these values, it can be seen that the high dimensionless flow acceleration can generate higher deviation than the smaller one. From Figures 4.7 and 4.8, it can be also seen that the fill profiles of dimensionless turbulence intensities in unsteady flow are similar to those from steady flows, therefore it is possible to establish a unify formula to predict the distribution of turbulence intensity in steady and unsteady flows. From the above investigation, it clearly shows that the measured turbulence intensities in decelerating flows positively deviate from the uniform flow curve or their profiles trend up the uniform flow, but this deviation becomes negative or the profile trends below the uniform flow curve when the flow is accelerating. Therefore, it can be noticed that all profiles of turbulence intensity is significantly affected by the influence of dimensionless flow acceleration.

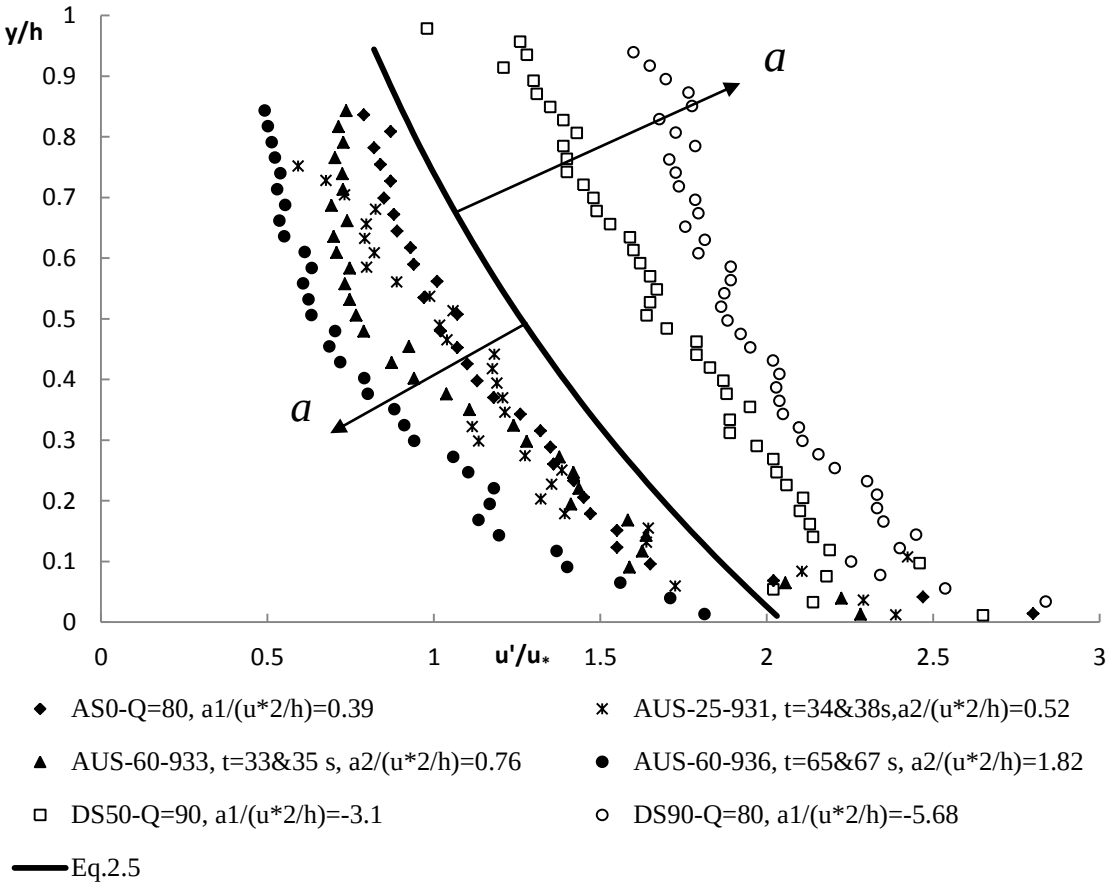

Figure 4.7: The influence of dimensionless flow acceleration on the deviation of measured horizontal turbulence intensities in accelerating and decelerating steady and unsteady flows from uniform flow based on Song's experimental data sets.

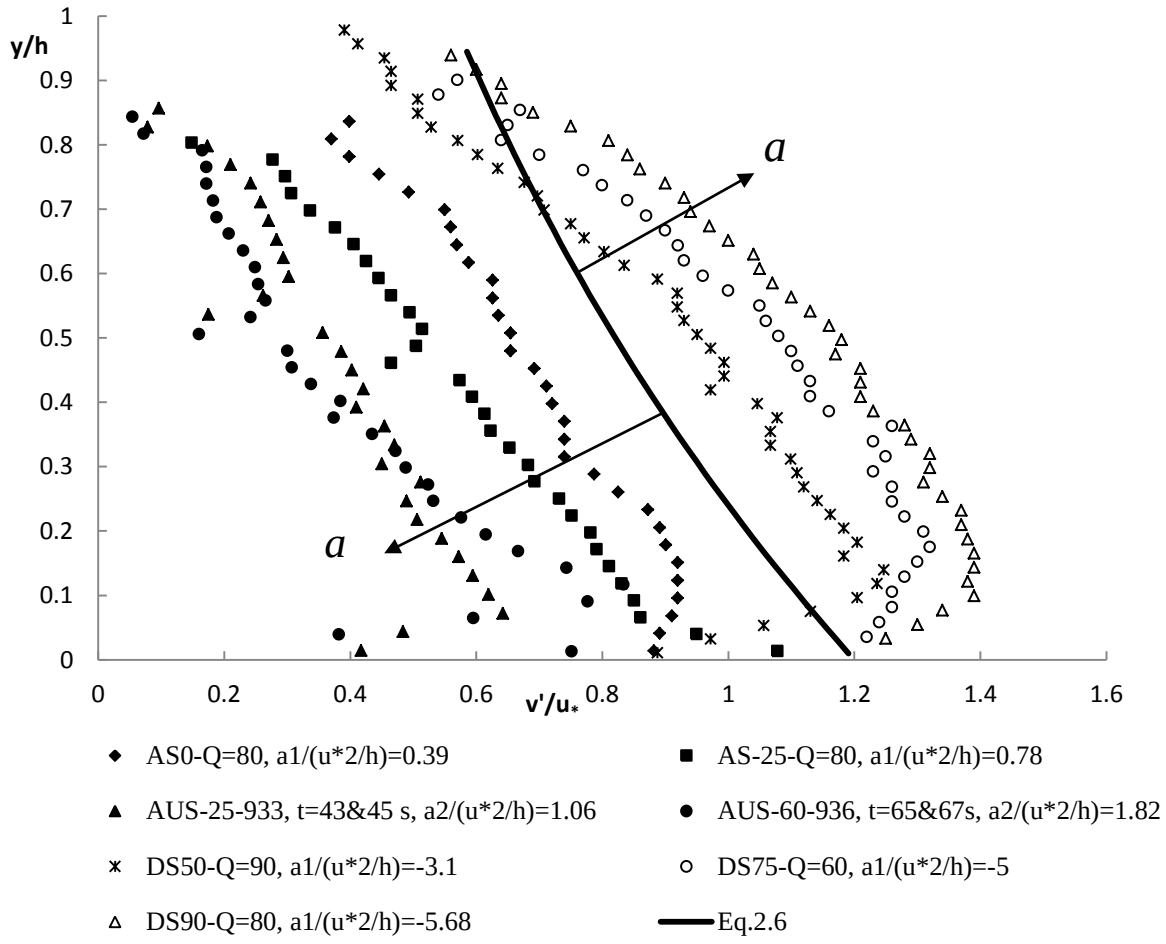

Figure 4.8: The influence of dimensionless flow acceleration on the deviation of measured vertical turbulence intensities in accelerating and decelerating steady and unsteady flows from uniform flow based on Song's experimental data sets.

The most important parameter generated from non-uniform flow is the existence of vertical velocity. The typical profiles of this velocity ($\bar{v}/u_*$) in accelerating and decelerating steady and unsteady flows presented in Figure 4.9. In 2-D uniform flow the time averaged vertical velocity is zero while in the non-uniform flow, this vertical velocity equals to zero when there is no seepage force acting and it becomes non-zero in the main region. In decelerating flow, the measured data points of vertical velocity along the water column are positive whereas they become negative when the flow is accelerating. In general, it can be seen from the above discussion made for other

turbulence characteristics that the flow acceleration has a responsibility for this deviation from uniform flow. The average difference of $\Delta\bar{v}/u_*$ in decelerating flow (DS90-Q=80) is 0.083 which gives higher deviation with the value of $a/(u_*^2/h)$ = -5.68 than that in (DS50-Q=90) with $\Delta\bar{v}/u_*$ and $a/(u_*^2/h)$ are equal to 0.0339 and -3.1 respectively. While in accelerating flow, the large difference is determined in AS-75-Q=80 with the value of $\Delta\bar{v}/u_*$= -0.149 but the smaller one gives -0.057 in AUS-25-932. It is clearly seen that the flow acceleration can affect on the turbulence characteristics distribution in non-uniform flow. Therefore, the next stage is to link between the uniform flow equations and the influence of flow acceleration on these turbulence characteristics in order to establish new equations to express the full profile of turbulence characteristics in steady and unsteady non-uniform flow based on the existence of flow acceleration.

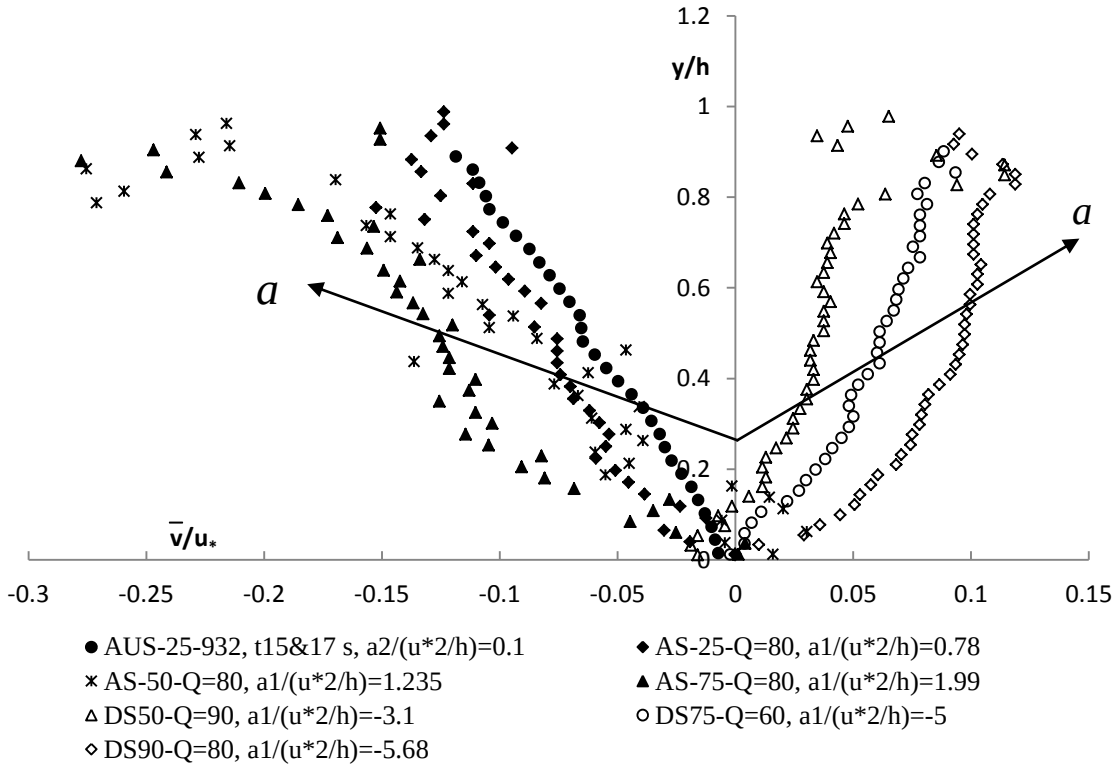

Figure 4.9: The influence of dimensionless flow acceleration on the deviation of measured vertical velocity in accelerating and decelerating steady and unsteady flows from uniform flow based on Song's experimental data sets.

4.5 Distribution of longitudinal mean velocity

After demonstrating the impact of flow acceleration on the deviation of longitudinal mean velocity in steady and unsteady flows from that in the Log law, one needs to assess the dependence of coefficients in Equation 4.4 on the flow acceleration, i.e. k_1 and k_2 which should depend on a dimensionless parameter including flow acceleration, water depth and shear velocity i.e. $a/(u_*^2/h)$. To yield the best agreement between Equation 4.4 and the measured velocity profiles, one can obtain k_1 and k_2 from experimental data in steady and unsteady flows. For example, k_1 and k_2 can be evaluated from the velocity defect between the measured and Log law predicted velocities $\Delta\bar{u}/u_*$ (i.e. $\Delta\bar{u}/u_* = (\bar{u}_{measure} - \bar{u}_{Loglaw})/u_*$). This difference indicates the

amount of deviation from the measured mean velocity and the Log law. Figures 4.10-4.12 describe these differences $\Delta\bar{u}$ against y/h for steady and unsteady flows. Figures 4.10 and 4.11 shows the difference between the measured longitudinal velocities in non-uniform flow and their calculations using the classical Log law based on Song's (1994) experiments in accelerating steady and unsteady flows, while Figure 4.12 includes the data points of $\Delta\bar{u}$ from Song's (1994) experimental data in decelerating steady flow.

In Figure 4.12, the positive deviation from the simple Log law gives a negative flow acceleration with various values for k_1 and k_2, for example, the values of k_1 and k_2 = 3.3 and 0.2 respectively when the dimensionless flow acceleration is equal to -5.68 while the values of k_1 and k_2 are 1.4 and 0.2 respectively when $a_1/(u_*^2/h)$ = -2.683. In decelerating flow, the value of k_2 is equal to 0.2 for different flow conditions and this small value can have the influence to match between the measured and calculated velocities. Figures 4.10 and 4.11 indicate the accelerating flow in steady and unsteady flows. For both figures, the negative deviation of longitudinal velocity in steady and unsteady flows from the predicted velocity can also generate positive values for k_1 and k_2. For example, k_1=2.5 and k_2=1.7 when the value of dimensionless acceleration $a_1/(u_*^2/h)$ in steady flow = 2.2, and these values of k_1 and k_2 reduce to be 1.3 and 0.9 respectively when the value of $a_1/(u_*^2/h)$ = 0.78. A similar case can result from unsteady flow in Figure 4.10, and as expected the values of k_1 and k_2 can be obtained as 1.1 and 1.2 when $a_2/(u_*^2/h)$ =1.115 while these values of k_1 and k_2 are 2.3 and 1.9 when $a_2/(u_*^2/h)$ =2.7.

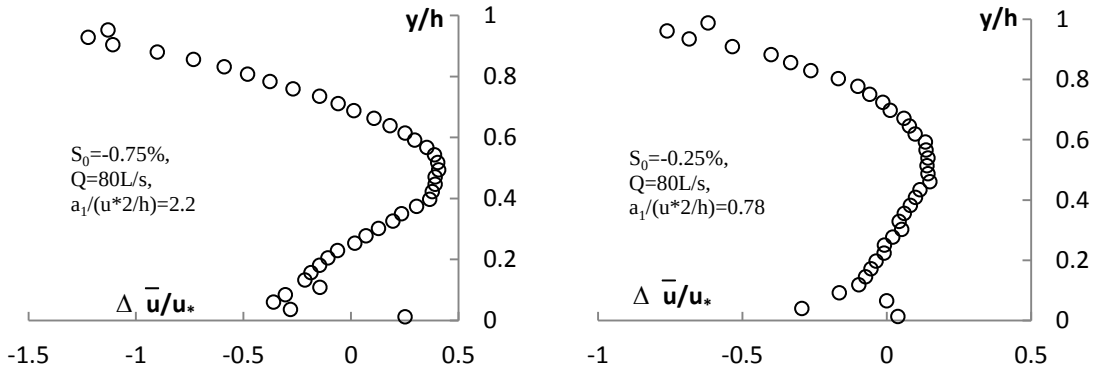

Figure 4.10: The difference between measured velocity and Log law based on Song's (1994) experimental data sets in accelerating steady flow.

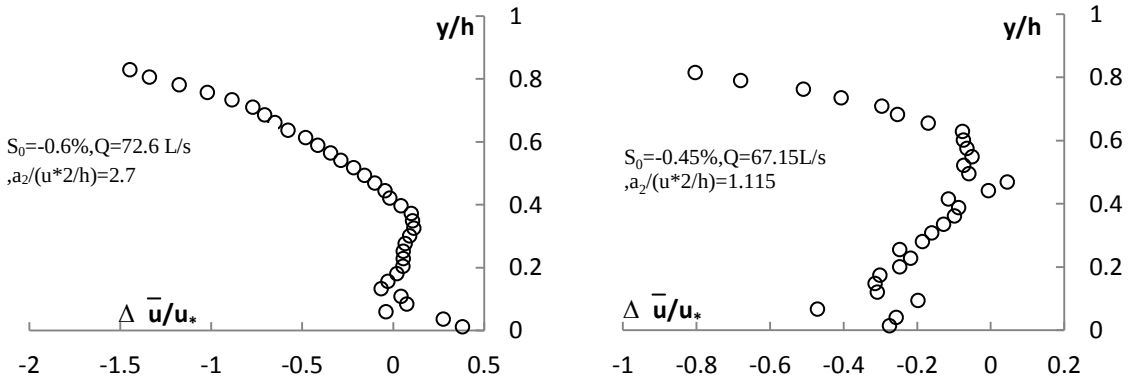

Figure 4.11: The difference between measured velocity and Log law based on Song's (1994) experimental data sets in accelerating unsteady flow.

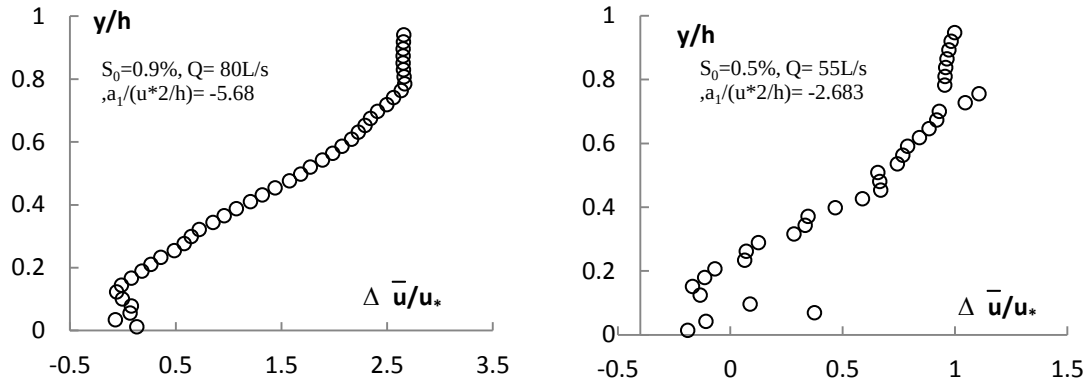

Figure 4.12: The difference between measured velocity and Log law based on Song's (1994) experimental data sets in decelerating steady flow.

From the above figures, it is understandable that the high flow acceleration can give high empirical values of k_1 and k_2. By fitting the velocity difference, one may obtain the expressions of k_1 and k_2. For accelerating flow, the values of k_1 and k_2 were obtained from Song's (1994) experimental data as shown in Figures 4.13 and 4.14, in which only data from accelerating flows in both steady and unsteady flows were selected, and the following empirical expressions are obtained:

$$k_1 = 1.4[a/(u_*^2/h)]^{0.7} \tag{4.28}$$

$$k_2 = [a/(u_*^2/h)]^{0.7} \tag{4.29}$$

In the acceleration shown in Figures 4.13 and 4.14, the following sets of data from Song's measurements were used: the water depth h; the variation of water depth with the longitudinal direction dh/dx; bed slope S_0; and longitudinal and vertical velocity profiles $\bar{u}(y)$ and $\bar{v}(y)$ from the reference level to the free surface, respectively. Note that the longitudinal and vertical velocity at the water surface, i.e., $\bar{u}_h$ and $\bar{v}_h$ are assessed by extrapolating the measured velocity profile to the surface level. The energy slope S_f can be estimated using Equation 4.25. From the calculated values of S_f, S_0 and dh/dx, the value of dU^2/dx can be calculated in steady and unsteady flows using Equations 4.24 and 4.27, respectively. Based on these calculated and measured values, the acceleration in steady flow i.e. a_1 can be determined.

The acceleration in an unsteady flow has similar calculation to the steady flow, only the value of dU^2/dx can be estimated from Equation 4.27 after calculate dU/dt from the derivation of depth averaged flow velocity with time. After applying the values of $\bar{u}_h$,

$\bar{v}_h$, h, dh/dx, dU^2/dx, dh/dt and dU/dt in Equation 4.22, the acceleration in unsteady flow a_2 can be determined.

In Figures 4.13 and 4.14, the empirical values of k_1 and k_2 are plotted against $a/(u_*^2/h)$. The solid symbols in both Figures 4.13 and 4.14 denote the data obtained from unsteady flows, and the open symbols represent the same but in steady flow. A clear dependence of these coefficients k_1 and k_2 on the dimensionless acceleration can be observed and solid lines can be drawn based on the data points presented in each figure. If a =0, then k_1 and k_2 =0, Equations 4.28 and 4.29 were obtained. In Figures 4.13 and 4.14, significant similarity is observed between dimensionless flow acceleration in steady and unsteady flow and these similar values of flow acceleration give similar values for k_1 and k_2. Thus, this is the reason why the acceleration symbol (a) is used in Equations 4.28 and 4.29 without any subscript relating to the steady or unsteady flow. From these figures, it is clear that the values of k_1 and k_2 increase with the flow acceleration.

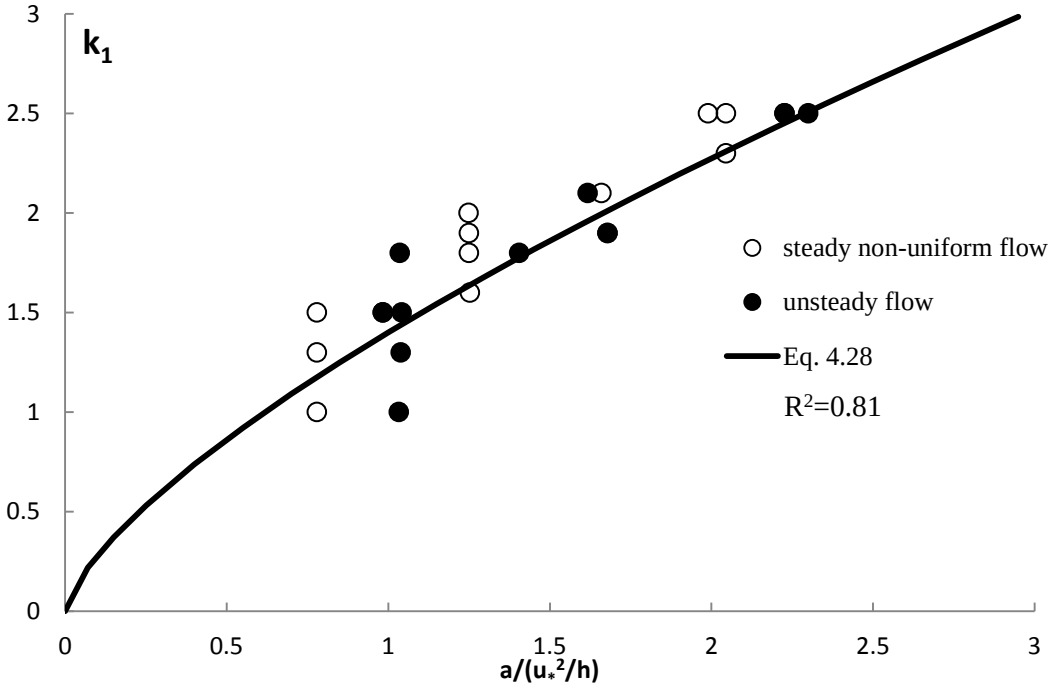

Figure 4.13: Relationship between k_1 and dimensionless flow acceleration $a/(u_*^2/h)$ in steady and unsteady flow based on Song's (1994) experimental data sets.

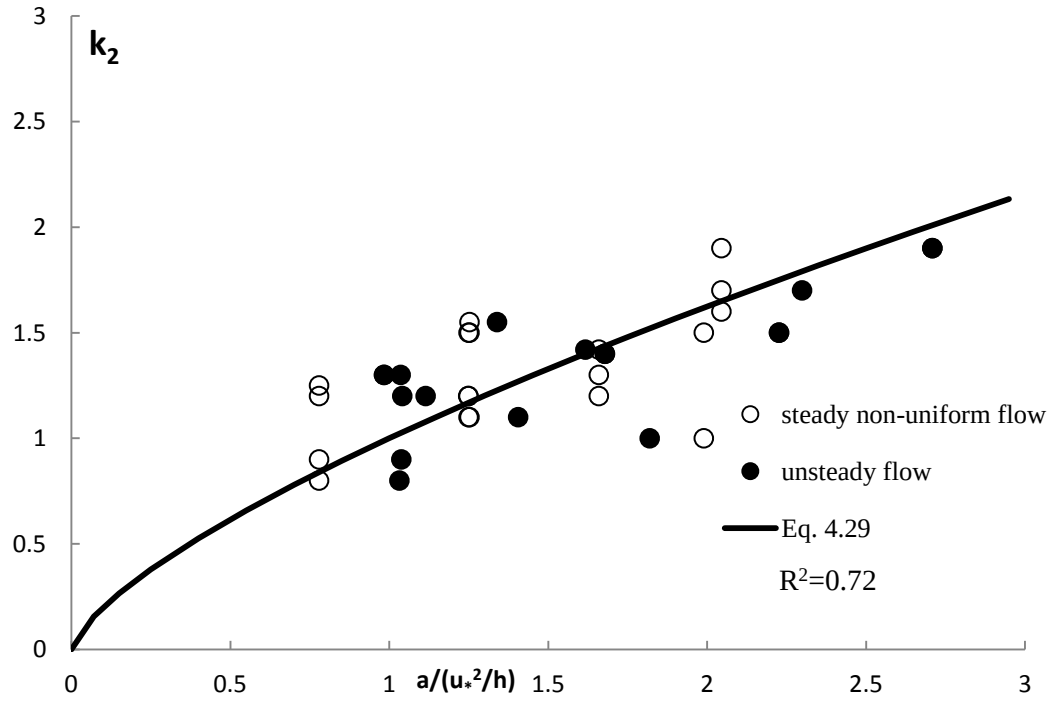

Figure 4.14: Relationship between k_2 and dimensionless flow acceleration $a/(u_*^2/h)$ in steady and unsteady flow based on Song's (1994) experimental data sets.

Song (1994) reported that the flow in his experiments was accelerating in unsteady flows. Therefore, there is no decelerating unsteady data available to compare with decelerating steady flows. Based on the similarities between accelerating in steady and unsteady flow, it is reasonable to assume that there exist some similarities between decelerating steady and unsteady flow.

For decelerating flows, the empirical equations for k_1 and k_2 can be obtained with the similar method as shown in Figure 4.15, and the k_1 can be evaluated as an exponential function of negative flow acceleration:

$$k_1 = \exp\{-0.27*[a/(u_*^2/h)]\} - 1 \tag{4.30}$$

It was found by analysing Song's data that k_2 is very small and $k_2 \approx 0.2$.

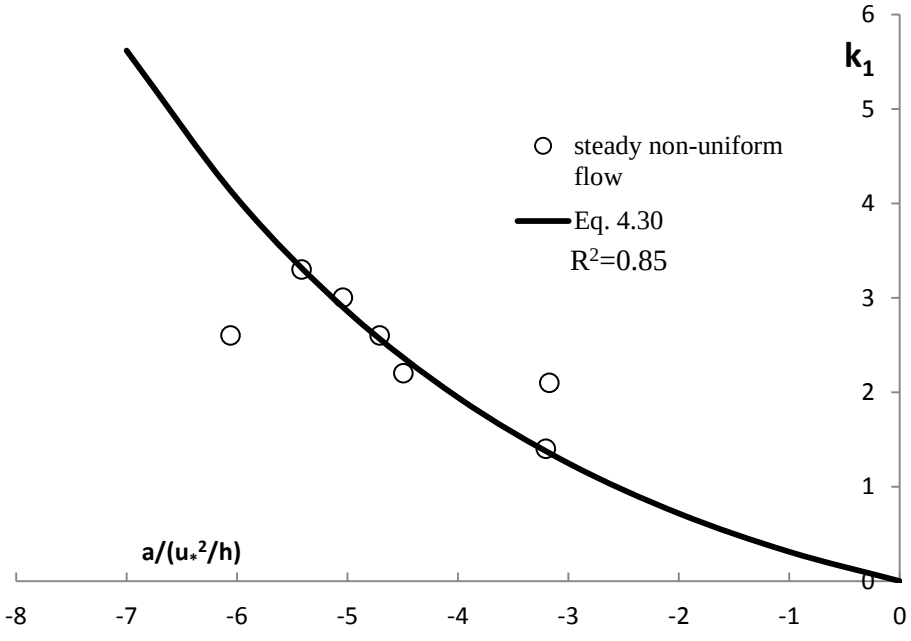

Figure 4.15: Relationship between k_1 and dimensionless flow acceleration $a/(u_*^2/h)$ in decelerating steady flow based on Song's (1994) experimental data sets.

In Figure 4.15, the open symbols represent the predicted value of dimensionless flow acceleration against the calculated value for k_1 in decelerating steady flow and the solid line refers to Equation 4.30 which represents the best fit for these measured data points. Consequently, if the flow acceleration in steady or unsteady flows is known and then the values of k_1 and k_2 can be estimated based on Equations 4.28, 4.29 and 4.30 for both accelerating and decelerating flows.

In order to check the validity of Equation 4.4 with these empirical values for k_1 and k_2, the remaining datasets in Song's (1994) experiments except those shown in Figures 4.13- 4.15 are plotted in Figures 4.16, 4.17 and 4.18, where S_0 refers to the bed slope, NO refers to the number of each hydrograph and (t) is time. In each figure, the value of acceleration is labelled. Taking into account the positive and negative value of flow acceleration generating from accelerating and decelerating in steady and unsteady flow, all signs of k_1 and k_2 are found to be positive irrespective of whether the value of flow acceleration is negative or positive.

In order to demonstrate the performance of Equation 4.4 and the two empirical values of k_1 and k_2 obtained from their relationship with the flow acceleration, in each figure the relative error between the measured and predicted longitudinal velocity profile is determined as $E = \left| \bar{u}_m - \bar{u}_c \right| / \bar{u}_m * 100$, where the subscript m and c are the measured velocities respectively. As can be seen from Figure 4.16, the average value of E is less than 4% error band between the measurement and calculations velocity profiles in accelerating unsteady flow.

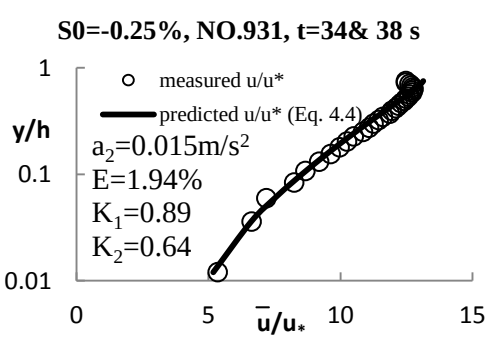
S0=-0.25%, NO.931, t=34& 38 s
measured u/u*
predicted u/u* (Eq. 4.4)
a2=0.015m/s2
E=1.94%
K1=0.89
K2=0.64
y/h
u/u*

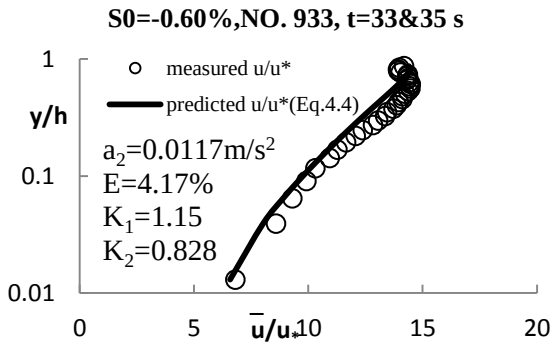
S0=-0.60%,NO. 933, t=33&35 s
measured u/u*
predicted u/u*(Eq.4.4)
a2=0.0117m/s2
E=4.17%
K1=1.15
K2=0.828
y/h
u/u*

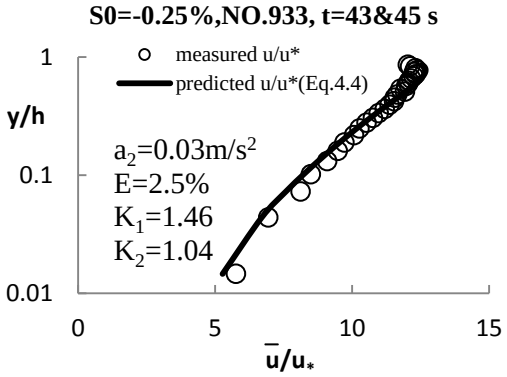
S0=-0.25%,NO.933, t=43&45 s
measured u/u*
predicted u/u*(Eq.4.4)
a2=0.03m/s2
E=2.5%
K1=1.46
K2=1.04
y/h
u/u*

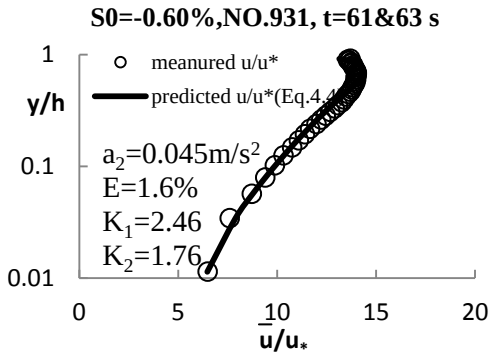
S0=-0.60%,NO.931, t=61&63 s
meanured u/u*
predicted u/u*(Eq.4.4)
a2=0.045m/s2
E=1.6%
K1=2.46
K2=1.76
y/h
u/u*

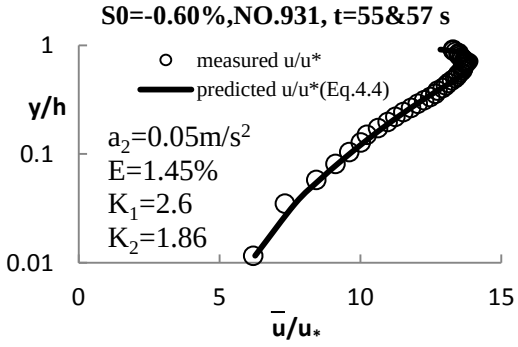
S0=-0.60%,NO.931, t=55&57 s
measured u/u*
predicted u/u*(Eq.4.4)
a2=0.05m/s2
E=1.45%
K1=2.6
K2=1.86
y/h
u/u*

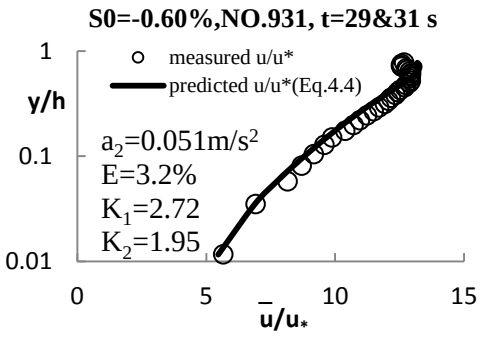
S0=-0.60%,NO.931, t=29&31 s
measured u/u*
predicted u/u*(Eq.4.4)
a2=0.051m/s2
E=3.2%
K1=2.72
K2=1.95
y/h
u/u*

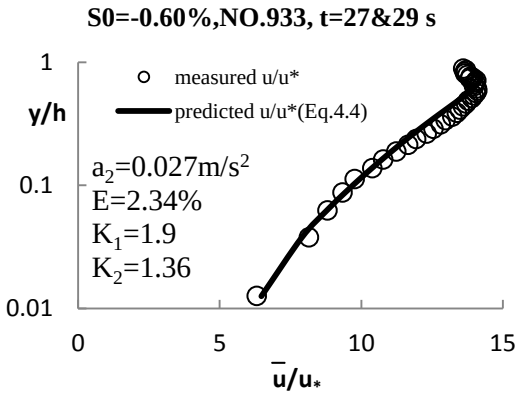
S0=-0.60%,NO.933, t=27&29 s
measured u/u*
predicted u/u*(Eq.4.4)
a2=0.027m/s2
E=2.34%
K1=1.9
K2=1.36
y/h
u/u*

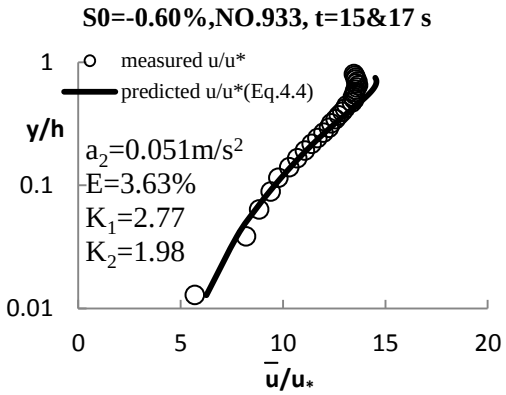
S0=-0.60%,NO.933, t=15&17 s
measured u/u*
predicted u/u*(Eq.4.4)
a2=0.051m/s2
E=3.63%
K1=2.77
K2=1.98
y/h
u/u*

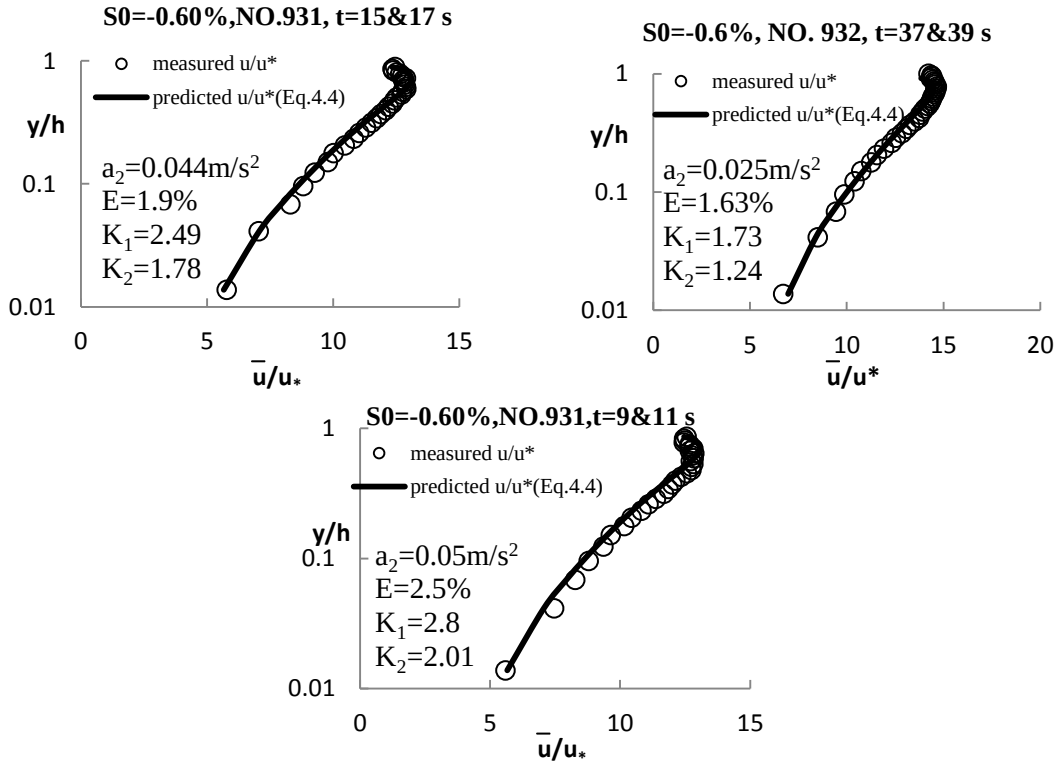

Figure 4.16: Comparison of measured and predicted mean horizontal velocity profile in accelerating unsteady flow based on Song's (1994) experimental data.

Figure 4.16 shows the comparison between the measured and predicted velocity profiles against the relative water depth y/h, where data are represented in the open circles, and Equation 4.4 by solid lines. These data sets are taken from different bed slopes, hydrographs and times. In each graph, the determined values of a, E, k_1 and k_2 are presented. From the relative error labelled in Figure 4.16, it is clearly seen that a reasonable agreement is achieved between the measured longitudinal velocity and Equation 4.4. Therefore, it can be observed that these three laws (Log, Wake and Dip) are indeed needed to capture the correct shape of the velocity profile.

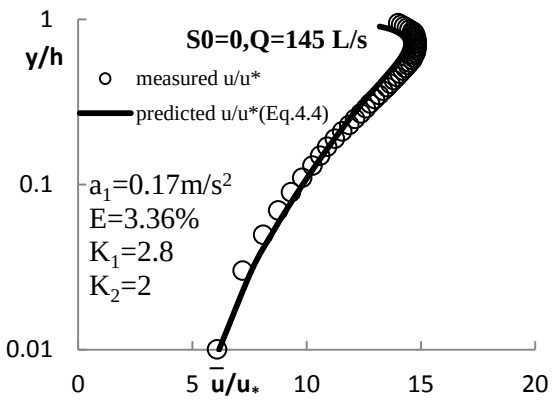
S0=0,Q=145 L/s
measured u/u*
predicted u/u*(Eq.4.4)
a1=0.17m/s2
E=3.36%
K1=2.8
K2=2
y/h
ū/u*

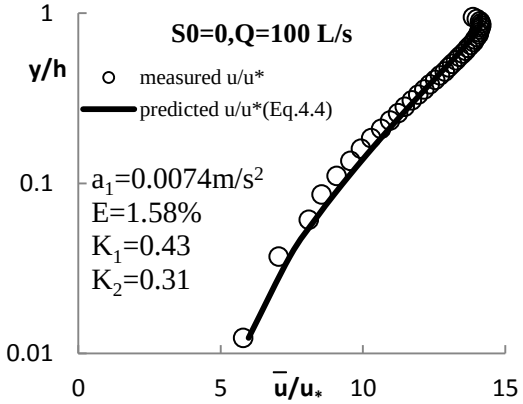
S0=0,Q=100 L/s
measured u/u*
predicted u/u*(Eq.4.4)
a1=0.0074m/s2
E=1.58%
K1=0.43
K2=0.31
y/h
ū/u*

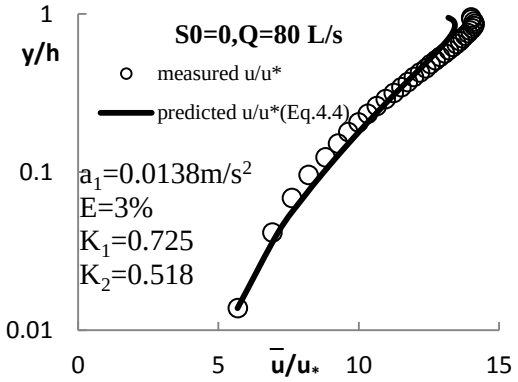
S0=0,Q=80 L/s
measured u/u*
predicted u/u*(Eq.4.4)
a1=0.0138m/s2
E=3%
K1=0.725
K2=0.518
y/h
ū/u*

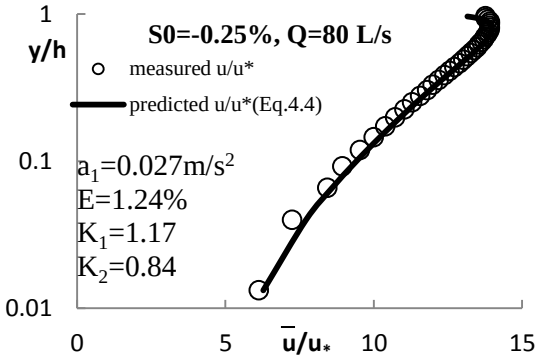
S0=-0.25%, Q=80 L/s
measured u/u*
predicted u/u*(Eq.4.4)
a1=0.027m/s2
E=1.24%
K1=1.17
K2=0.84
y/h
ū/u*

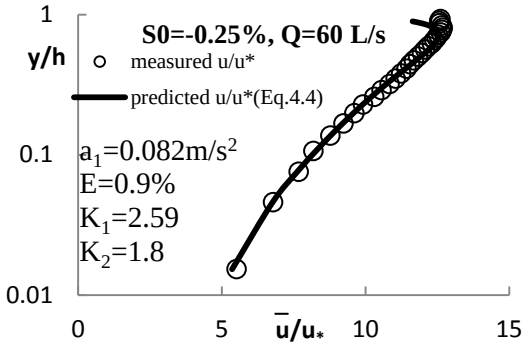
S0=-0.25%, Q=60 L/s
measured u/u*
predicted u/u*(Eq.4.4)
a1=0.082m/s2
E=0.9%
K1=2.59
K2=1.8
y/h
ū/u*

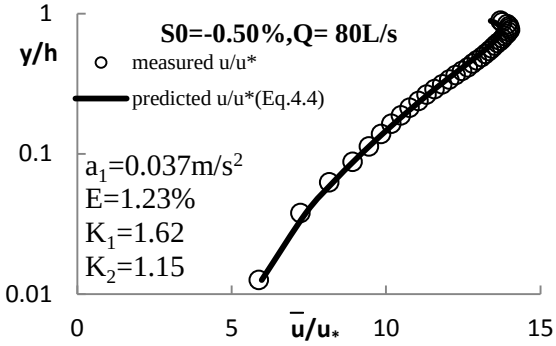
S0=-0.50%,Q= 80L/s
measured u/u*
predicted u/u*(Eq.4.4)
a1=0.037m/s2
E=1.23%
K1=1.62
K2=1.15
y/h
ū/u*

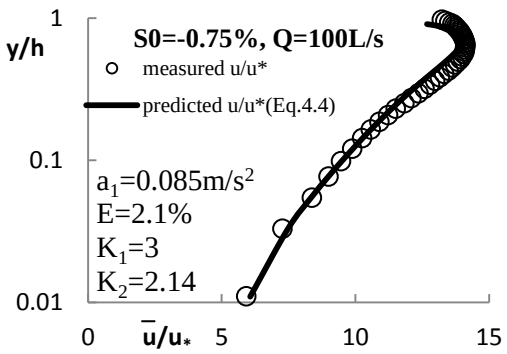
S0=-0.75%, Q=100L/s
measured u/u*
predicted u/u*(Eq.4.4)
a1=0.085m/s2
E=2.1%
K1=3
K2=2.14
y/h
ū/u*

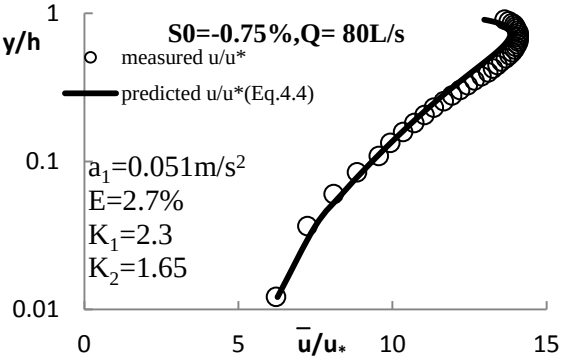
S0=-0.75%,Q= 80L/s
measured u/u*
predicted u/u*(Eq.4.4)
a1=0.051m/s2
E=2.7%
K1=2.3
K2=1.65
y/h
ū/u*

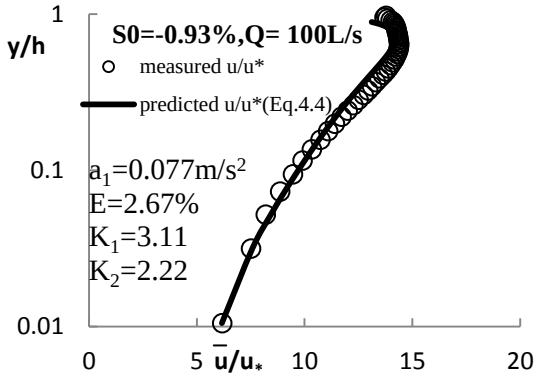

Figure 4.17: Comparison of measured and predicted mean horizontal velocity profile in accelerating steady flow based on Song's (1994) experimental data.

The comparison between the measured and predicted velocity profiles in accelerating steady flow is presented in Figure 4.17. Based on this comparison, the average value of E is also less than 4% which gives a good agreement between the measured and estimated velocity using the influence of flow acceleration. It can be seen that the proposed Equation 4.4 is able to capture the velocity negative deviation well.

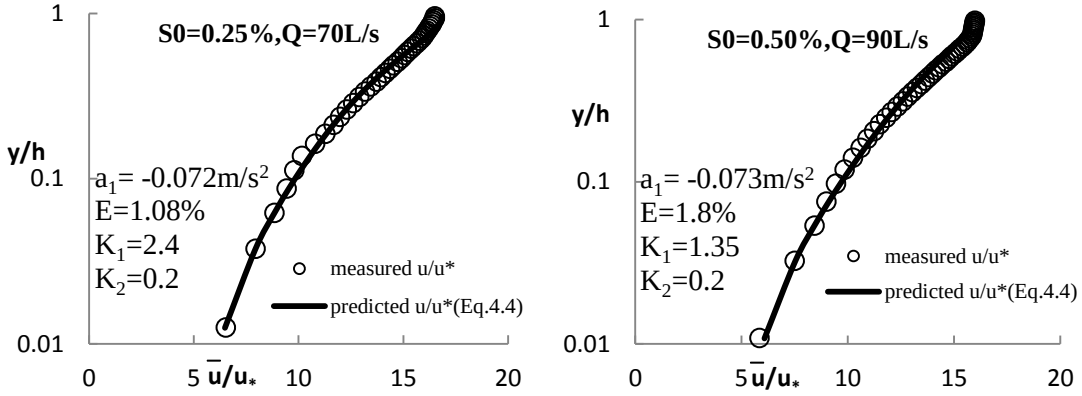

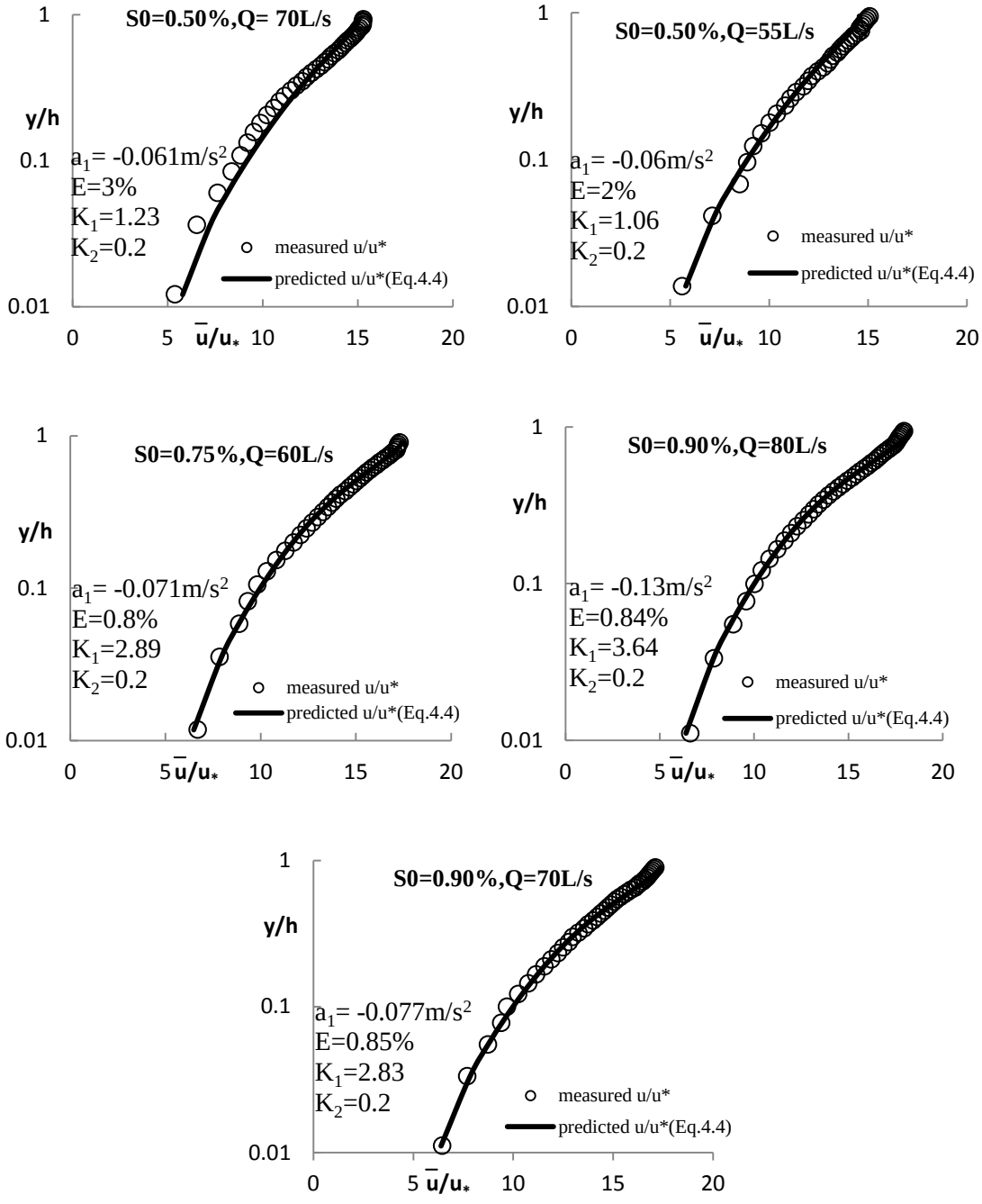

Figure 4.18: Comparison of measured and predicted mean horizontal velocity profile in decelerating steady flow based on Song's (1994) experimental data.

Figure 4.18 shows the comparison between the measurement and calculation of velocity profiles in decelerating steady flow. This comparison depends on Equation 4.4 and the values of k_1 and k_2 after estimating the value of flow acceleration using Equation 4.21. The value of k_2 is assumed to be constant (0.2) for different flow conditions. k_2 is an

empirical coefficient in the Dip law, which plays an important role in the outer region. This law is negligible in the inner region since $\ln(1-y/h)\approx 0$ for small y. Here, $\ln(1-y/h)$ is always negative when $y/h<1$. This negative value with small value of k_2 = 0.2 gives small negative value for the third term of Equation 4.4 but it is really needed to match with the measured data at the water surface.

Figure 4.18 demonstrates that the Cole's Wake law and Dip law are working together with Log law to predict the full longitudinal mean velocity profile in decelerating steady flow. The best evidence for this demonstration is shown by the value of error measure E of less than 4% between the predicted and the measured velocity profile. In general, it can be seen from the above comparisons that Equation 4.4 is able to capture the velocity distribution in the entire profile that includes the inner and outer regions depending on the value of flow acceleration.

4.6 Distributions of turbulent shear stress

In the previous sections, the longitudinal mean velocity profiles for different flow conditions have been modelled using the dimensionless flow acceleration as a main factor. In order to determine other turbulence structures, such as Reynolds shear stress ($-\rho\overline{u'v'}$), turbulence intensities (u', v') and vertical velocity ($\bar{v}$), other empirical equations have to be developed for each turbulence characteristics to express empirically the relationship between the dimensionless flow acceleration and the value of k_i where the subscript "i" denotes the type of turbulence characteristics, for example, for Reynolds shear stress profile, the symbol $k_{-\rho\overline{u'v'}}$ is used. As discussed before, the distributions of Reynolds shear stress are linear in a uniform flow while they deviate being a convex or concave distribution in decelerating or accelerating in both steady and

unsteady flows, respectively. This deviation from the uniform is generated from the effect of flow acceleration on the Reynolds shear stress distribution. The measured Reynolds shear stress bends down from the standard linear distribution as the flow is accelerating ($a > 0$), it bends up over the uniform flow line as the flow is decelerating. After demonstrating the impact of flow acceleration in steady and unsteady flow on the deviation of Reynolds shear stress in steady and unsteady flows with uniform flow, one may conclude that the difference of Reynolds shear stress in non-uniform steady and unsteady flows to that in uniform flow is proportional to $(1-y/h)$ and y/h respectively as the difference between these two types of flow must become zero at these boundary conditions, where $y/h \approx 0$. Thus the proportionality $k_{-\rho\overline{u'v'}}$ should depend on dimensionless flow acceleration i.e. $a/(u_*^2/h)$. Therefore, these empirical formulas are proposed as follows:

$$(-\frac{\overline{u'v'}}{u_*^2})_{nonunf.} = (-\frac{\overline{u'v'}}{u_*^2})_{unf.} \pm k_{-\rho\overline{u'v'}} * (1-y/h)^{1.5} * y/h \qquad (4.31)$$

where $(-\overline{u'v'}/u_*^2)$ is the normalised Reynolds shear stress with respect to the shear velocity, the subscript "$unf.$" refers to the Reynolds shear stress in uniform flow (i.e. dimensionless stress equals to $1-y/h$) while the subscript "$nonunf.$" refers to the Reynolds shear stress in non-uniform flows. In Equation 4.31, the value of $k_{-\rho\overline{u'v'}}$ has two signs, one positive and the other negative. The positive one can be used when the flow is decelerating while the negative sign will be used when the flow is accelerating for both steady and unsteady flows. In other words, when the value of the second term on the right hand side of Equation 4.31 is positive the predicted value of dimensionless Reynolds shear stress $(-\overline{u'v'}/u_*^2)$ is higher than those in uniform flow, and therefore,

this flow is decelerating. In contrast, the negative sign gives lower value than those in uniform flow, and thus this flow is accelerating. This is consistent with other researchers' observations, the distribution of Reynolds shear stress in non-uniform flow deviate from the standard linear distribution, i.e. $(1-y/h)$ (Song, 1994; Kironoto & Graf, 1995; Song & Chiew, 2001).

To yield the best agreement between Equation 4.31 and the measured Reynolds shear stress, one can determine $k_{-\rho\overline{u'v'}}$ from experimental data in steady and unsteady flows. For example, the value of $k_{-\rho\overline{u'v'}}$ can be evaluated from Reynolds shear stress defect between the measured Reynolds shear stress in uniform and non-uniform flows, i.e. $\Delta(-\overline{u'v'}/u_*^2) = (\overline{u'v'}_{nonuf.} - \overline{u'v'}_{unf.})/u_*^2$. This difference indicates the value of deviation from the measured Reynolds shear stress from the uniform line. By fitting the Reynolds shear stress, one may obtain the expression of $k_{-\rho\overline{u'v'}}$. For accelerating and decelerating flows, $k_{-\rho\overline{u'v'}}$ obtained from Song's (1994) experimental data as shown in Figures 4.19 and 4.20, in which only the data from accelerating flows in both steady and unsteady flows are selected, the empirical expressions of are obtained:

$$k_{-\rho\overline{u'v'}} = -\ln\{1+5.8*[a/(u_*^2/h)]\} \qquad \text{(Accelerating flow)} \qquad (4.32)$$

$$k_{-\rho\overline{u'v'}} = \exp\{-0.2*[a/(u_*^2/h)]\} - 1 \qquad \text{(Decelerating flow)} \qquad (4.33)$$

The acceleration in an unsteady flow has similar calculation to the steady flow, only the value of dU^2/dx can be estimated from Equation 4.27 after calculate dU/dt from the derivation of depth averaged flow velocity with time. After applying the values of

$\bar{u}_h, \bar{v}_h$, h, dh/dx, dU^2/dx, dh/dt and dU/dt in Equation 4.22, the acceleration in unsteady flow a can be calculated.

From Equations 4.32 and 4.33, the observed value of $k_{-\rho\overline{u'v'}}$ is negative when the flow is accelerating because the distribution of Reynolds shear stress in accelerating non-uniform flow is lower than those in uniform flow (see Figure 4.19). While this empirical value of $k_{-\rho\overline{u'v'}}$ is positive (see Figure 4.20) when the flow is decelerating because the data points for Reynolds shear stress in this flow are higher than those in uniform flow.

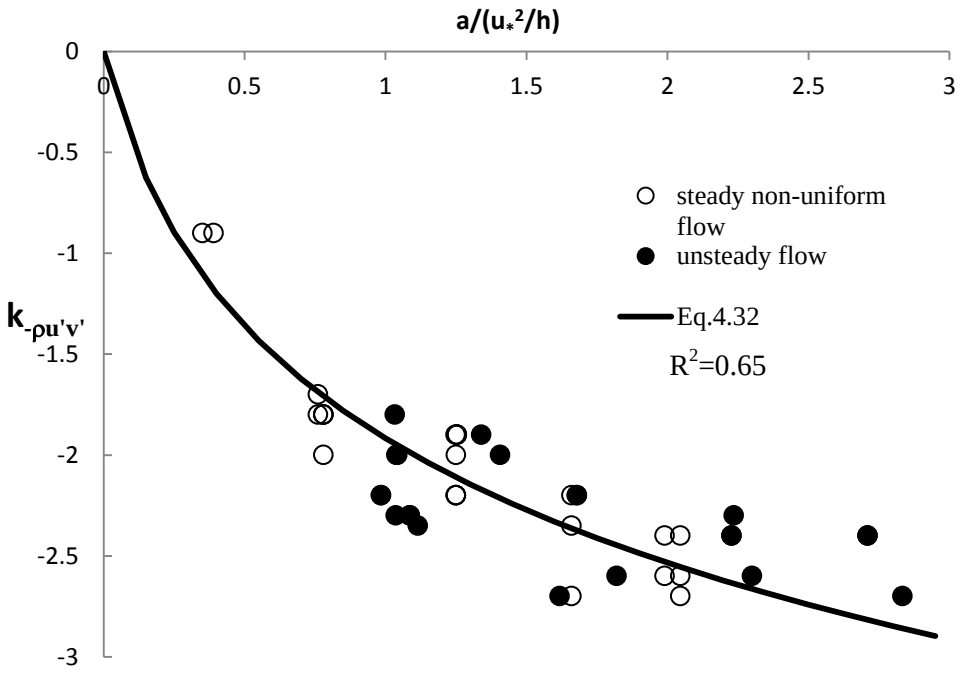

Figure 4.19: Relationship between dimensionless flow acceleration and the value of $k_{-\rho\overline{u'v'}}$ for Reynolds shear stress $(-\overline{u'v'}/u_*^2)$ in accelerating steady and unsteady flow based on selected data sets from Song's (1994) experimental data, where a solid line represents Equation 4.32.

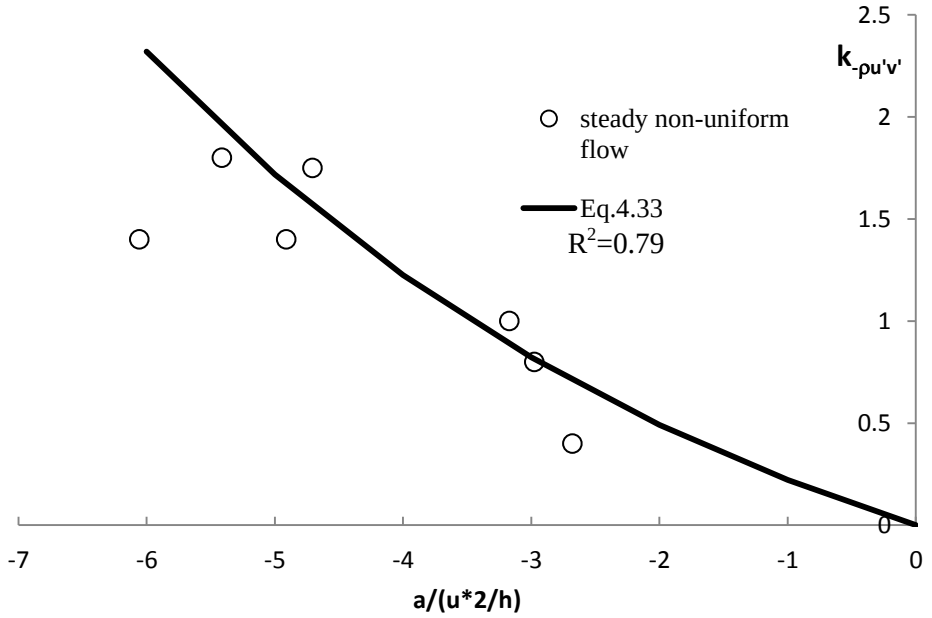

Figure 4.20: Relationship between dimensionless flow acceleration and the value of $k_{-\rho\overline{u'v'}}$ *for Reynolds shear stress* $(-\overline{u'v'}/u_*^2)$ *in decelerating steady flow based on selected data sets from Song's (1994) experimental data, where a solid line represents Equation 4.33.*

In Figure 4.19 and 4.20, the empirical values of $k_{-\rho\overline{u'v'}}$ are plotted against $a/(u_*^2/h)$. The solid symbols in both Figures 4.19 and 4.20 denote the data obtained from unsteady flows, and the open symbols represent the same but in steady flow. In Figure 4.20, there is no decelerating unsteady data available to compare with decelerating steady flows because Song (1994) reported that the flow in his experiments was accelerating in unsteady flow.

A clear dependence of the coefficient of $k_{-\rho\overline{u'v'}}$ on the dimensionless acceleration can be observed and solid lines can be drawn based on the data points and the condition that if a=0, then $k_{-\rho\overline{u'v'}}$=0 in both accelerating and decelerating flows, Equations 4.32 and 4.33 were obtained. In Figures 4.19 and 4.20, significant similarity is observed between dimensionless flow acceleration in steady and unsteady flows and these similar values

of flow acceleration give similar values for $k_{-\rho\overline{u'v'}}$. Thus, this is the reason why the acceleration symbol (a) is used in Equations 4.32 and 4.33 without any subscript relating to the steady or unsteady flow. When the flow is accelerating for both steady and unsteady cases, a positive a gives a negative value of $k_{-\rho\overline{u'v'}}$ and the vice versa for decelerating flow. While if a=0, then $k_{-\rho\overline{u'v'}}$=0 and as a result the second term of Equation 4.31 is negligible and this is uniform flow. It is clear that the values of $k_{-\rho\overline{u'v'}}$ increase with the flow acceleration. Consequently, if the flow acceleration in steady or unsteady flows is known and then the value of $k_{-\rho\overline{u'v'}}$ can be estimated based on Equations 4.32 and 4.33 for both accelerating and decelerating flows.

In order to check the validity of Equation 4.31 with these empirical values of $k_{-\rho\overline{u'v'}}$, the remaining datasets in Song's (1994) experiments except those shown in Figures 4.19 and 4.20 are plotted in Figures 4.21, 4.22 and 4.23 where S_0 refers to the bed slope, NO refers to the number of each hydrograph and (t) is time. In each figure, the value of acceleration is labelled. Taking into account the positive and negative values of flow acceleration generating from accelerating and decelerating in steady and unsteady flow, the value of $k_{-\rho\overline{u'v'}}$ is positive when the value of flow acceleration is decreased along the channel while it becomes negative when the acceleration is increased.

In order to demonstrate the performance of Equation 4.31 and the empirical value of $k_{-\rho\overline{u'v'}}$ obtained from its relationship with the flow acceleration, the value of relative error (E) is determined between the measured and predicted values, i.e. $E = \left| \overline{u'v'}_m - \overline{u'v'}_c \right| / \overline{u'v'}_m * 100$, where the subscripts m and c are the measured and calculated values of Reynolds shear stress.

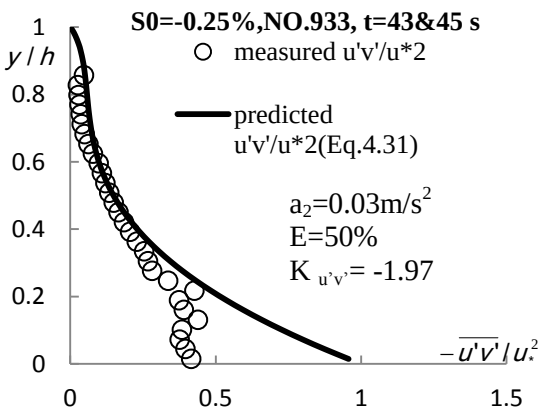
S0=-0.25%,NO.933, t=43&45 s
measured u'v'/u*2
predicted u'v'/u*2(Eq.4.31)
a2=0.03m/s2
E=50%
K u'v'= -1.97
y / h
$-\overline{u'v'}/u_*^2$

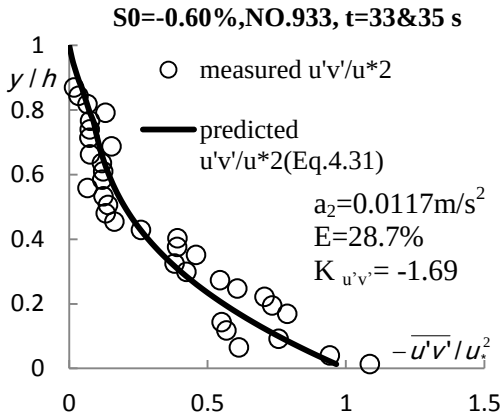
S0=-0.60%,NO.933, t=33&35 s
measured u'v'/u*2
predicted u'v'/u*2(Eq.4.31)
a2=0.0117m/s2
E=28.7%
K u'v'= -1.69
y / h
$-\overline{u'v'}/u_*^2$

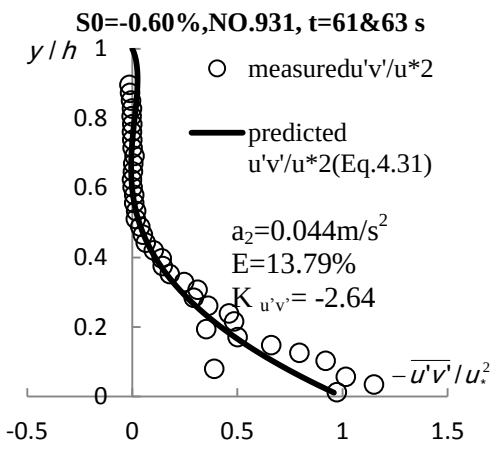
S0=-0.60%,NO.931, t=61&63 s
measuredu'v'/u*2
predicted u'v'/u*2(Eq.4.31)
a2=0.044m/s2
E=13.79%
K u'v'= -2.64
y / h
$-\overline{u'v'}/u_*^2$

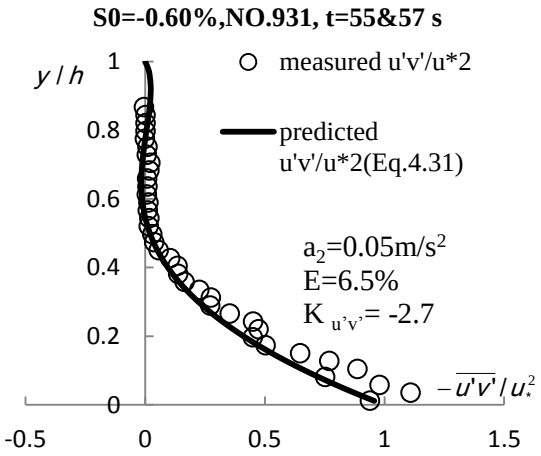
S0=-0.60%,NO.931, t=55&57 s
measured u'v'/u*2
predicted u'v'/u*2(Eq.4.31)
a2=0.05m/s2
E=6.5%
K u'v'= -2.7
y / h
$-\overline{u'v'}/u_*^2$

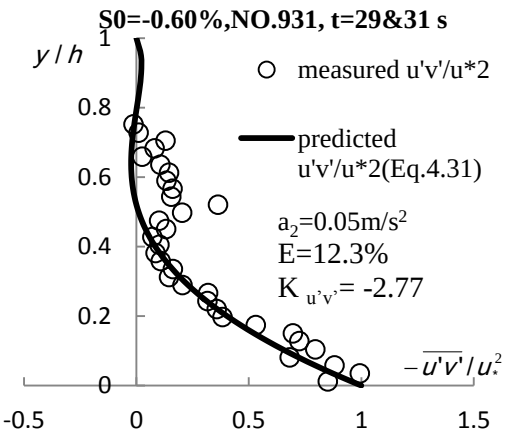
S0=-0.60%,NO.931, t=29&31 s
measured u'v'/u*2
predicted u'v'/u*2(Eq.4.31)
a2=0.05m/s2
E=12.3%
K u'v'= -2.77
y / h
$-\overline{u'v'}/u_*^2$

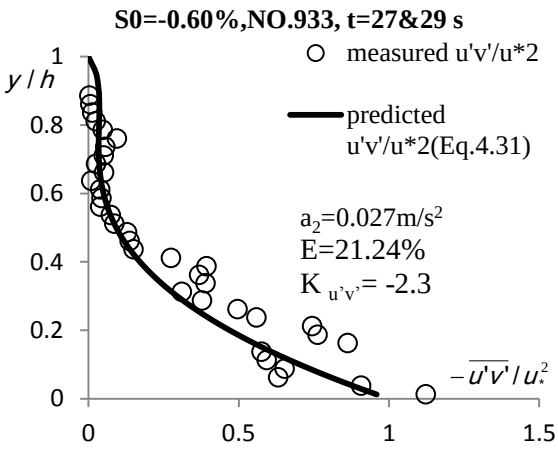
S0=-0.60%,NO.933, t=27&29 s
measured u'v'/u*2
predicted u'v'/u*2(Eq.4.31)
a2=0.027m/s2
E=21.24%
K u'v'= -2.3
y / h
$-\overline{u'v'}/u_*^2$

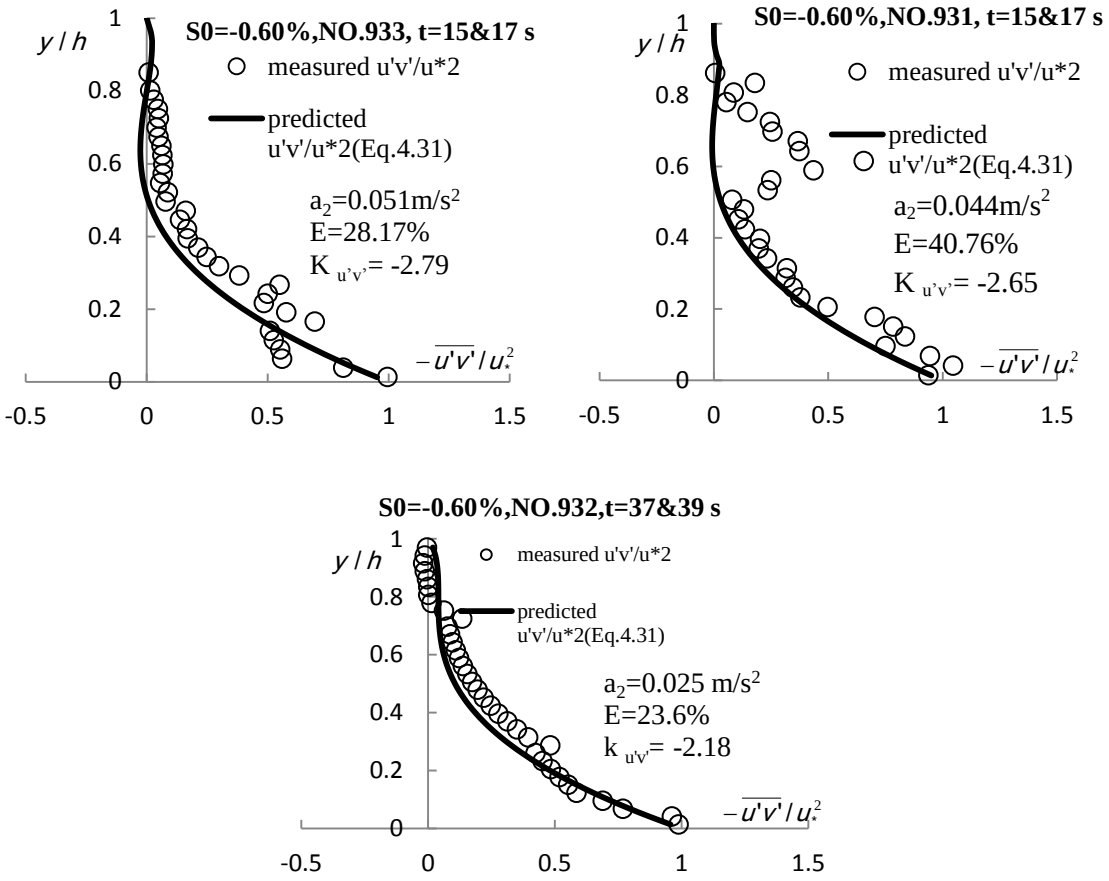

Figure 4.21: Comparison of measured and predicted Reynolds shear stress profile in accelerating unsteady flow based on Song's (1994) experimental data.

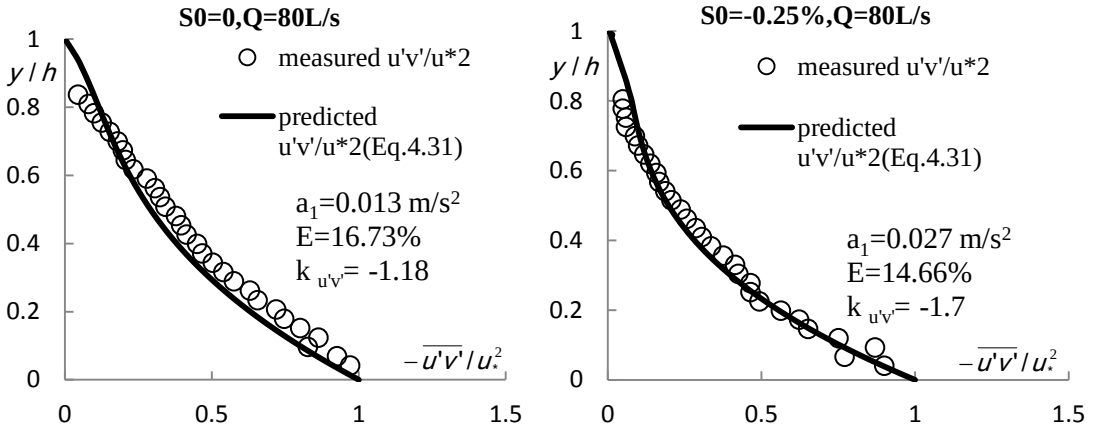

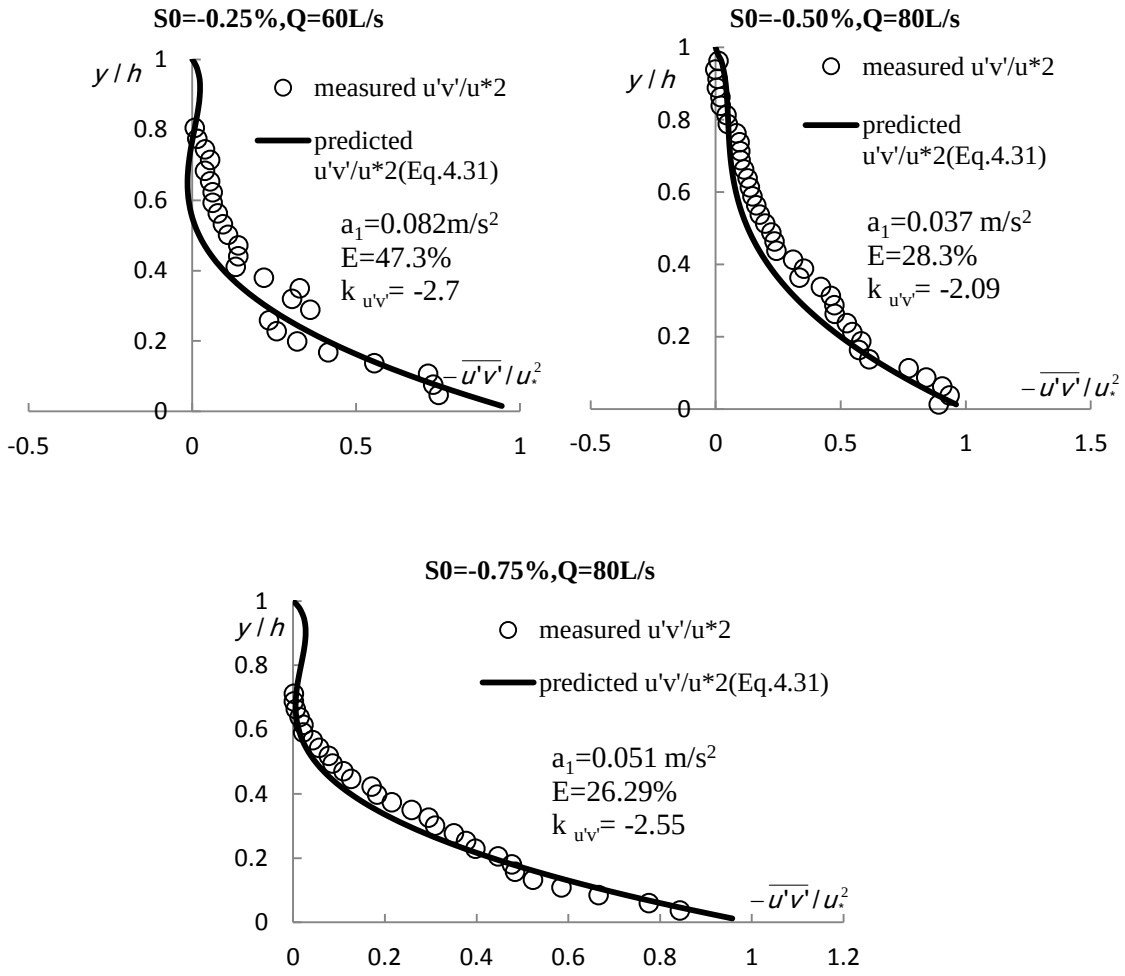

Figure 4.22: Comparison of measured and predicted Reynolds shear stress profile in accelerating steady flow based on Song's (1994) experimental data.

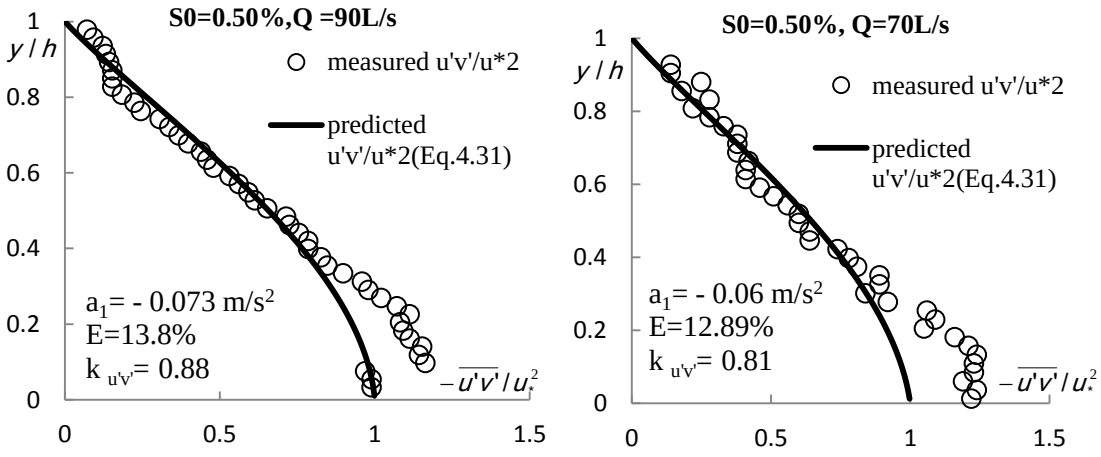

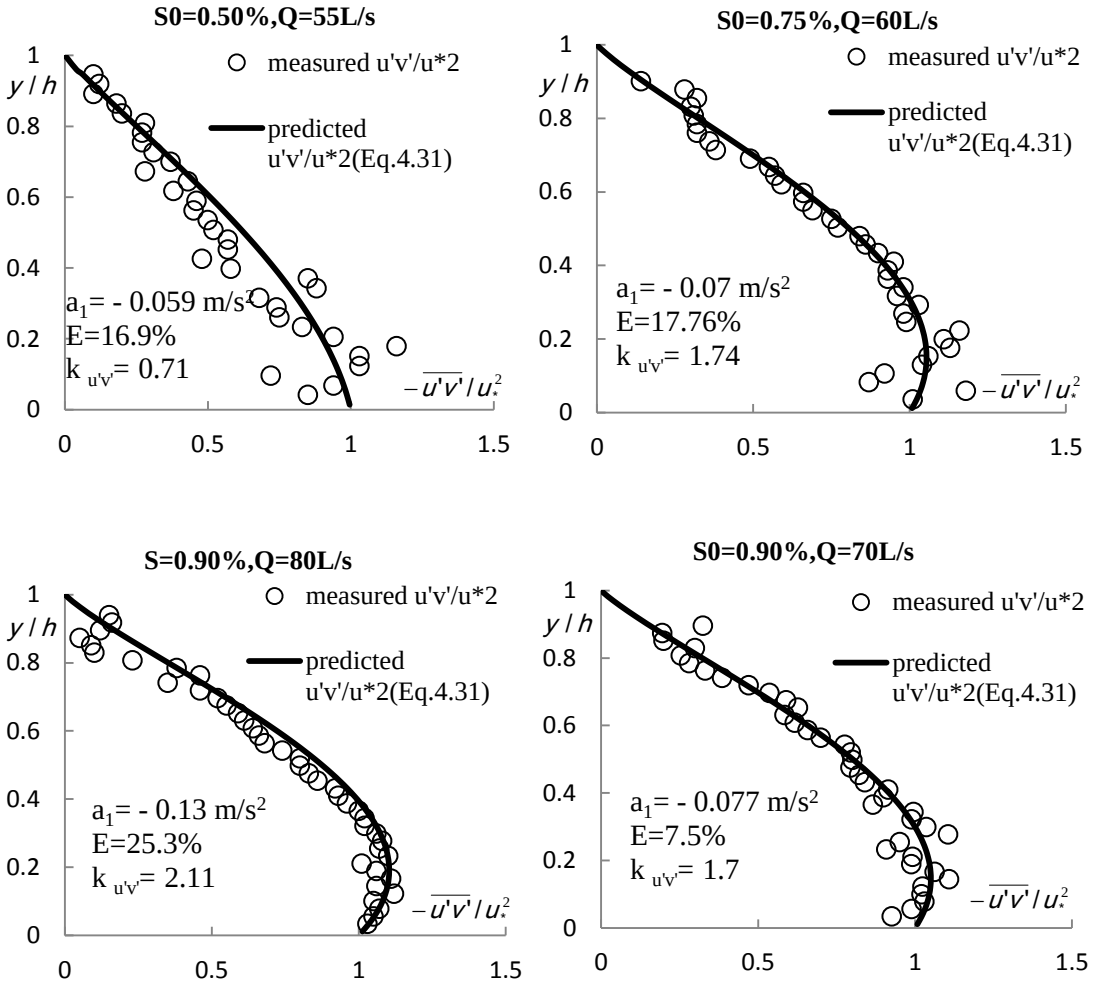

Figure 4.23: Comparison of measured and predicted Reynolds shear stress profile in decelerating steady flow based on Song's (1994) experimental data.

In Figures 4.21, 4.22 and 4.23, the calculated Reynolds shear stress profiles using Equation 4.31 are plotted as a solid line and the open circles denote to the measured data points in accelerating (steady and unsteady) and decelerating steady flow, respectively. To demonstrate the influence of flow acceleration on the deviation of Reynolds shear stress in non-uniform flow from that in uniform flow, the value of E is determined for each figure. The average values of E in Figures 4.21, 4.22 and 4.23 are less than 50%, 47% and 17% respectively indicating that the proposed model agreed the existing datasets in decelerating and accelerating steady and unsteady flows, especially when the value of flow acceleration is known. Overall, the agreement is fairly good. It

can be found that the predicted formulas can give similar profiles to the measurements of Reynolds shear stress, concave distribution when the applying negative value of $k_{-\rho\overline{u'v'}}$ and convex distribution when the value of $k_{-\rho\overline{u'v'}}$ is positive.

4.7 Distribution of turbulence intensities

In this section, the empirical formulas to predict the horizontal and vertical turbulence intensities will be discussed. As mentioned before, the full profiles of these turbulence intensities in non-uniform flows have a curve form, which they deviate from the uniform flow distribution being a convex distribution when the flow is decelerating, or they have a concave distribution when the flow is accelerating. The reason for this deviation is related to the impact of flow acceleration on the distribution of horizontal and vertical turbulence intensities. The measurements of turbulence intensities bend down from their distribution in uniform flow as the flow is accelerating ($a > 0$), they bend up over the uniform flow's prediction as the flow is decelerating. After demonstrating the influence of flow acceleration on the deviation of these turbulence intensities in steady and unsteady flows from that in the uniform flow, one may conclude that the difference of turbulence intensity in uniform and non-uniform flows is proportional to $(1-y/h)$ when the flow is decelerating and y/h when the flow is accelerating. The difference must become zero at the water surface, i.e. $y = h$ when the flow is decelerating and it becomes less than zero when the flow is accelerating. Therefore, this proportionality k_u or k_v should depend on a dimensionless parameter including flow acceleration, water depth and shear velocity, i.e. $a/(u_*^2/h)$. Thus, these empirical formulas for horizontal and vertical turbulence intensities are expressed as follows:

$$(\frac{u'}{u_*})_{nonunf.} = (\frac{u'}{u_*})_{unf.} - k_{u'}(y/h)^{0.75} \quad \text{(Accelerating flow)} \quad (4.34)$$

$$(\frac{u'}{u_*})_{nonunf.} = (\frac{u'}{u_*})_{unf.} + k_{u'}(1-y/h)^{0.75} \quad \text{(Decelerating flow)} \quad (4.35)$$

$$(\frac{v'}{u_*})_{nonuf.} = (\frac{v'}{u_*})_{uf.} - k_{v'}(y/h)^{0.5} \quad \text{(Accelerating flow)} \quad (4.36)$$

$$(\frac{v'}{u_*})_{nonuf.} = (\frac{v'}{u_*})_{uf.} + k_{v'}(1-y/h)^{0.5} \quad \text{(Decelerating flow)} \quad (4.37)$$

where u'/u_* and v'/u_* are the normalized horizontal and vertical turbulence intensities, with respect to the shear velocity, respectively, and the subscripts "$unf.$" and "$nonunf.$" are the symbols for the prediction of these turbulence intensities in uniform and non-uniform flows, respectively. In Equations 4.34/4.35 and 4.36/4.37, the values of $k_{u'}$ and $k_{v'}$ are different in accelerating and decelerating non-uniform flows. For both type of turbulence intensities, it can be used as a negative value when the flow is accelerating or a positive one when the flow is decelerating for both steady and unsteady flows. In other words, when the values of second term on the right hand side of Equations 4.34 and 4.36 are negative the predicted values of dimensionless horizontal (u'/u_*) and vertical (v'/u_*) turbulence intensity are lower than those in uniform flow, and therefore, this flow is accelerating. In contrast, the positive sign gives higher value than those in uniform flow, and thus this flow is decelerating. This observation is similar what other researchers achieved, the distribution of turbulence intensities in non-uniform flow deviate from the standard distribution, i.e. Equations 2.5 and 2.6 (Song, 1994; Kironoto & Graf, 1995).

The relative water depth y/h in the second term on the right hand side of Equations 4.34 and 4.35 is another difference between these empirical Equations 4.34 and 4.35. The overall turbulence intensity profile decreases with an increase y and its maximum value is near to the bed surface. As shown in Figure 4.24a, the difference between accelerating non-uniform and uniform flows i.e. ($\Delta u^{'}/u_{*}$) is nearly zero at the bed, and along the water column this value increases with the negative value. While in Figure 4.24b, the maximum of $\Delta u^{'}/u_{*}$ appears at the bed and then decreases at the water surface when this difference, i.e. $\Delta u^{'}/u_{*}$ determined between decelerating and uniform flow. This means that the value of ($\Delta u^{'}/u_{*}$) ≈0 in accelerating flow when $y/h \approx 0$; while ($\Delta u^{'}/u_{*} > 0$) or nearly to be 1 in decelerating flow when $y/h \approx 0$. This is the reason for taking different relative water depth i.e. (y/h) in Equation 4.34 and (1-y/h) in Equation 4.35. A similar observation can also be found in the prediction of vertical turbulence intensities shown in Equations 4.36 and 4.37.

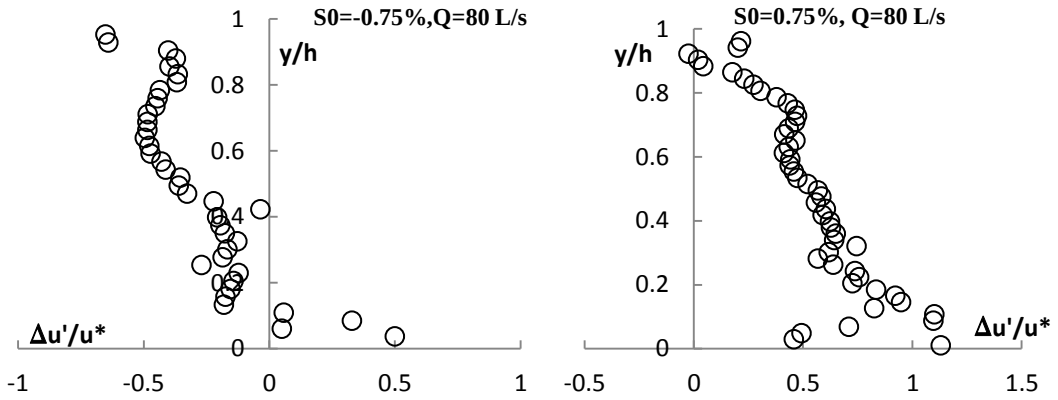

(a) (b)

Figure 4.24: The difference between measured horizontal turbulence intensities in non-uniform and uniform flow based on Song's (1994) experimental data sets in (a) accelerating steady flow and (b) decelerating steady flow.

To yield the best agreement between the developed Equations, i.e. 4.34/4.35, 4.36/4.37 and the measured horizontal and vertical turbulence intensities, one can determine $k_{u'}$ and $k_{v'}$ from experimental data in steady and unsteady flows. For example, the values of $k_{u'}$ and $k_{v'}$ can be evaluated from horizontal and vertical turbulence intensities defect between the measured horizontal and vertical turbulence intensities in uniform and non-uniform flows, i.e. $\Delta(u'/u_*) = (u'_{nonunf.} - u'_{unf.})/u_*$ and $\Delta(v'/u_*) = (v'_{nonunf.} - v'_{unf.})/u_*$. These differences indicate the value of deviation from the measured these turbulence intensities and the uniform curve. By fitting turbulence intensities, one may obtain the expression of $k_{u'}$ and $k_{v'}$. For accelerating and decelerating flows, $k_{u'}$ and $k_{v'}$ obtained from Song's (1994) experimental data as shown in Figures 4.25/4.26 and 4.27/4.28, in which only the data from accelerating flows in both steady and unsteady flows are selected, the empirical expression of the value of $k_{u'}$ and $k_{v'}$ can be approximated as follows:

$$k_{u'} = -\ln\{1 + 0.7*[a/(u_*^2/h)]\} \quad \text{(Accelerating flow)} \quad (4.38)$$

$$k_{u'} = \exp\{-0.12*[a/(u_*^2/h)]\} - 1 \quad \text{(Decelerating flow)} \quad (4.39)$$

$$k_{v'} = -\ln\{1 + 0.5*[a/(u_*^2/h)]\} \quad \text{(Accelerating flow)} \quad (4.40)$$

$$k_{v'} = \exp\{-0.08*[a/(u_*^2/h)]\} - 1 \quad \text{(Decelerating flow)} \quad (4.41)$$

where a is the flow acceleration in steady and unsteady non-uniform flows. Its calculation in unsteady flow is similar to the steady flow, only the determined value of depth averaged flow velocity with time dU/dt as well as the estimation of dU^2/dx using Equation 4.27. After known the flow parameters, i.e. $\bar{u}_h, \bar{v}_h$, h, dh/dx, dU^2/dx,

dh/dt and dU/dt from experimental datasets, the flow acceleration in steady and unsteady flow can be calculated using Equations 4.21 and 4.22, respectively.

In Equations 4.38/4.39 and 4.40/4.41, the investigated values of $k_{u'}$ and $k_{v'}$ shown in Figures 4.25 and 4.27, respectively, are negative when the flow is accelerating because the measured data points of horizontal and vertical turbulence intensities in accelerating non-uniform flow are lower than those in uniform flow. Whereas these empirical values of $k_{u'}$ and $k_{v'}$ are positive (see Figures 4.26 and 4.28) when the flow is decelerating because its distribution in this flow is higher than those in uniform flow.

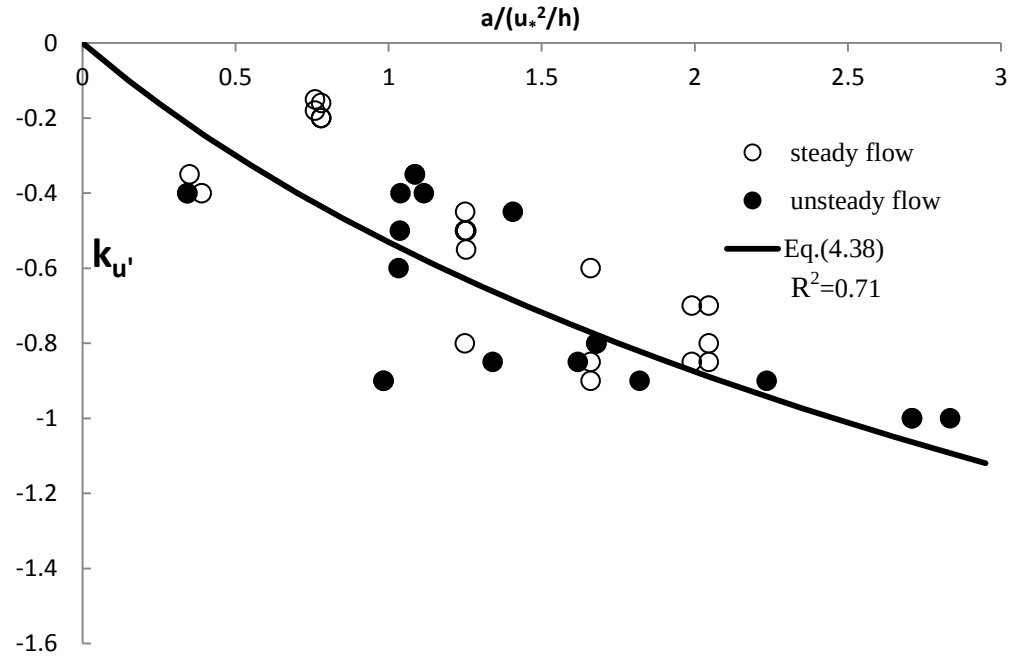

Figure 4.25: Relationship between dimensionless flow acceleration and the value of $k_{u'}$ for horizontal turbulence intensities (u'/u_*) in accelerating steady and unsteady flow based on selected data sets from Song's (1994) experimental data, where a solid line represents Equation 4.38.

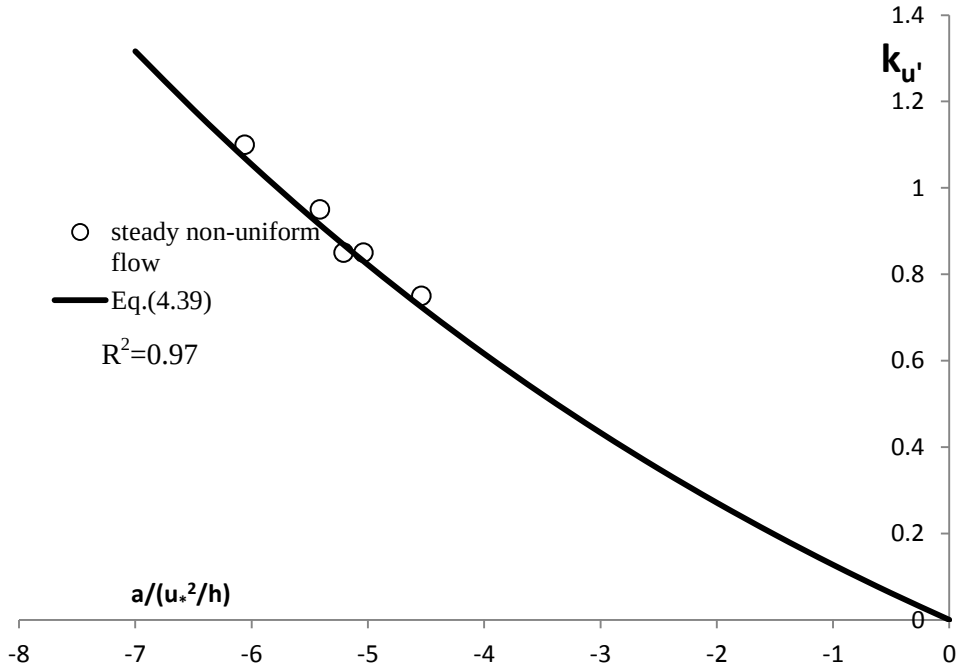

Figure 4.26: Relationship between dimensionless flow acceleration and the value of $k_{u'}$ for horizontal turbulence intensities (u'/u_*) in decelerating steady flow based on selected data sets from Song's (1994) experimental data, where a solid line represents Equation 4.39.

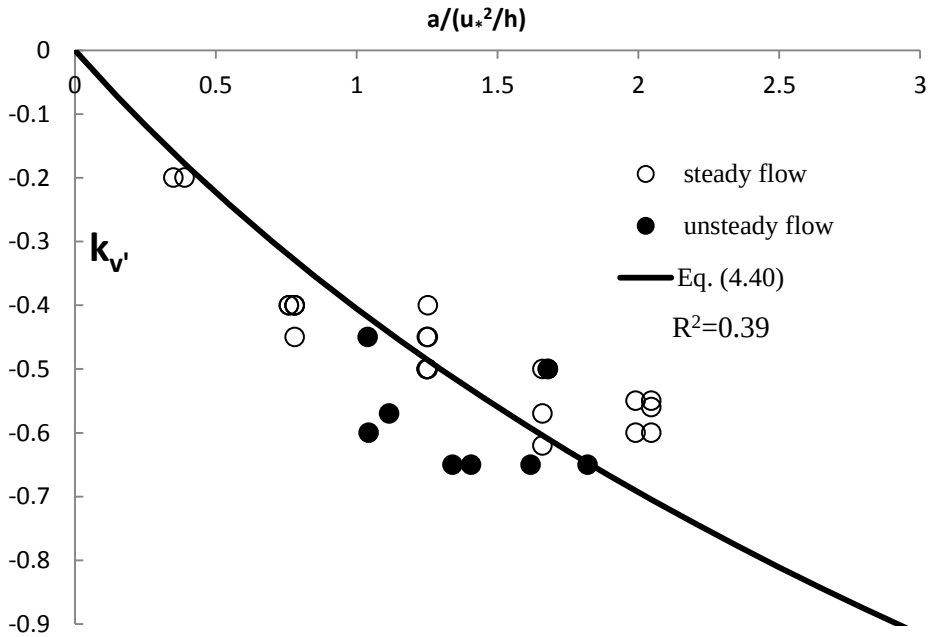

Figure 4.27: Relationship between dimensionless flow acceleration and the value of for vertical turbulence intensities (v'/u_*) in accelerating steady and unsteady flow based on selected data sets from Song's (1994) experimental data, where a solid line represents Equation 4.40.

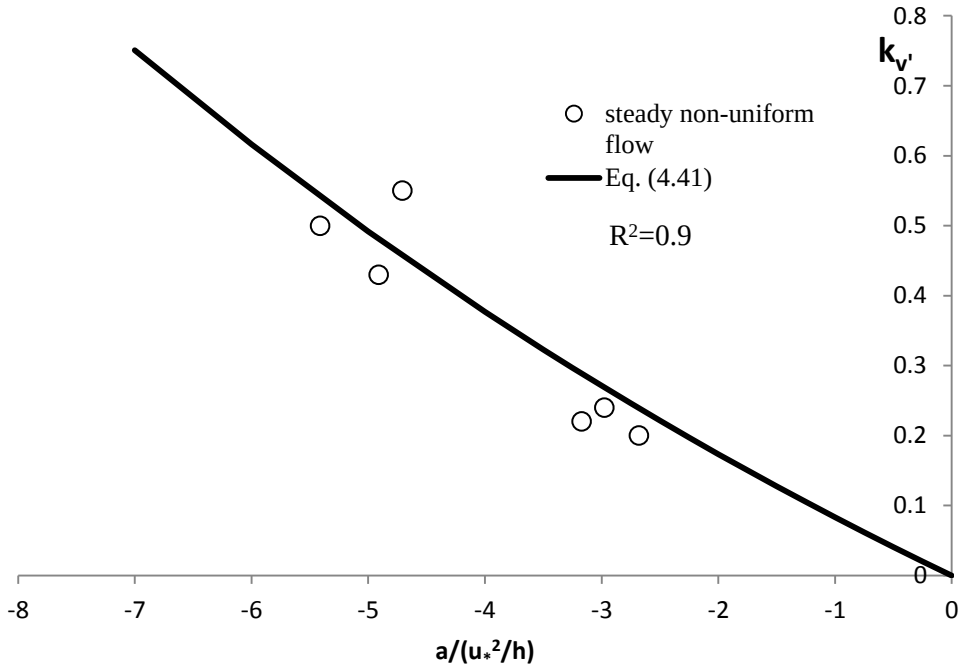

Figure 4.28: Relationship between dimensionless flow acceleration and the value of $k_{v'}$ *for vertical turbulence intensities* (v'/u_*) *in decelerating steady flow based on selected data sets from Song's (1994) experimental data, where a solid line represents Equation 4.41.*

In Figures 4.25/4.26 and 4.27/4.28, the open and solid symbol represent the determined values of dimensionless flow acceleration, i.e. $a/(u_*^2/h)$ against the predicted values of $k_{u'}$ and $k_{v'}$ in steady and unsteady flows, respectively and the solid line refers to Equations 4.38/4.39 and 4.40/4.41 which represents the best fit for these plotted data points. In Figures 4.26 and 4.28, there is no decelerating unsteady flow datasets available to compare with decelerating steady flows because Song (1994) reported that the flow in his experiments was accelerating in unsteady flows.

Based on the developed model of Equations 4.38/4.39 and 4.40/4.41, it is clearly seen the dependence of the empirical value of $k_{u'}$ and $k_{v'}$ on the dimensionless flow acceleration. The solid lines presented in Figures 4.25/4.26 and 4.27/4.28 are drawn based on the data points and the condition that if a=0, then $k_{u'}$, $k_{v'}$=0 in both

accelerating and decelerating flows, Equations 4.38/4.39 and 4.40/4.41 were obtained. In Figures 4.25 and 4.27, some similarities are observed between dimensionless flow acceleration in steady and unsteady flows and these similar values of flow acceleration give similar values for $k_{u'}$ and $k_{v'}$. Thus, this is the reason why the acceleration symbol (a) is used in Equations 4.38/4.38 and 4.40/4.41 without any subscript relating to the steady or unsteady flow. When the flow is accelerating for both steady and unsteady cases, a positive a gives a negative values of $k_{u'}/k_{v'}$ and the vice versa for decelerating flow. While if a=0, then $k_{u'}$, $k_{v'}$=0 and as a result the second term of Equations 4.34/4.35 and 4.36/4.37 are negligible and this is uniform flow. It is clear that the values of $k_{u'}$ and $k_{v'}$ increase with the flow acceleration. Consequently, if the flow acceleration in steady or unsteady flow is known, then the value of $k_{u'}/k_{v'}$ can be estimated based on Equations 4.38/4.39 and 4.40/4.41 for both accelerating and decelerating flows.

In order to verify the applicability of Equations 4.34/4.35, 4.36/4.37 with these empirical values of $k_{u'}$ and $k_{v'}$ obtained from Equations 4.38/4.39 and 4.40/4.41, the remaining datasets in Song's (1994) experiments except those shown in Figures 4.25-4.28 are plotted in Figures 4.29- 4.34. In each figure, S_0 is the bed slope, Q is the flow discharge, NO refers to the number of hydrograph in unsteady flow and (t) refers to the time compared with unsteady flow. The open circles represent the measured u'/u_* and the solid lines represent the proposed values. The calculated values of flow acceleration, i.e. a (m/s^2), and the observed values of $k_{u'}$ and $k_{v'}$ from Equations 4.38 and 4.41 are presented in each figure. Based on the calculations of a and $k_{u'}/k_{v'}$, the observations of $k_{u'}$ and $k_{v'}$ is positive values when the flow acceleration is decreased along the open channel while it becomes negative when the acceleration is increased.

In order to illustrate the performance of Equations 4.34/4.35 and 4.36/3.37 for the prediction of horizontal and vertical turbulence intensities, respectively and the empirical values of $k_{u'}$ and $k_{v'}$ obtained from their relationship with the flow acceleration, the value of relative error (E) is determined between the measured and predicted values, i.e. $E = \left| u'_m - u'_c \right| / u'_m * 100$, where the subscripts m and c are the measured and calculated values of horizontal and vertical turbulence intensity.

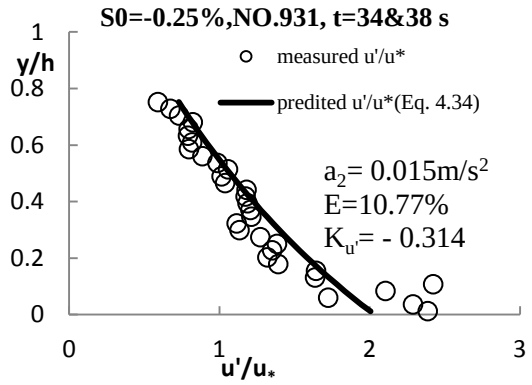

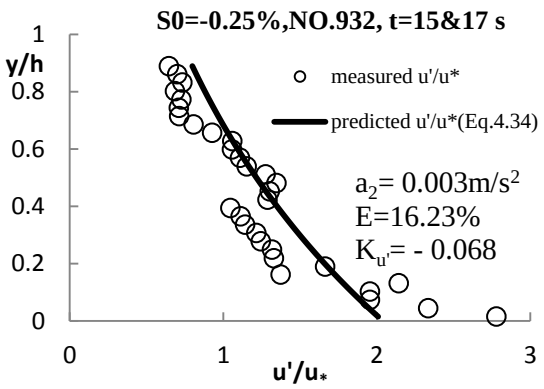

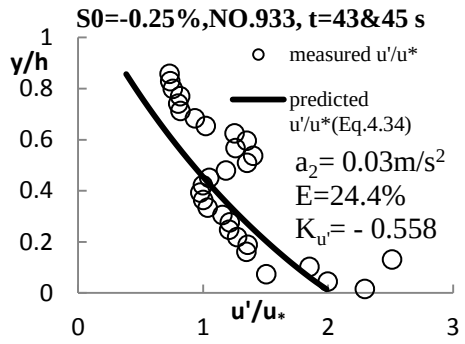

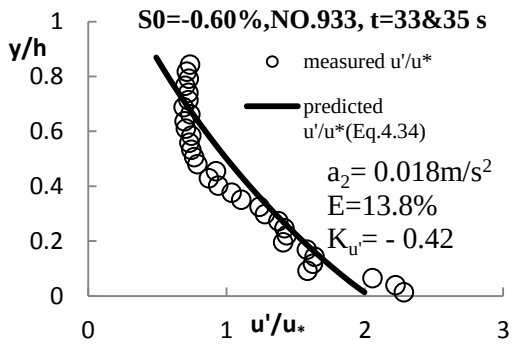

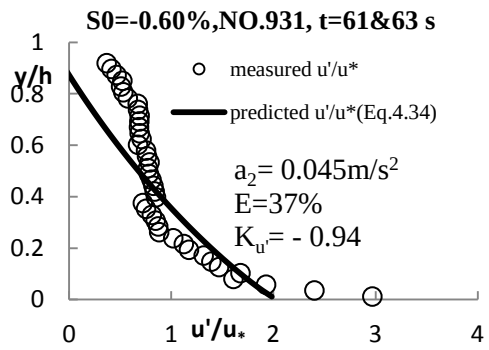

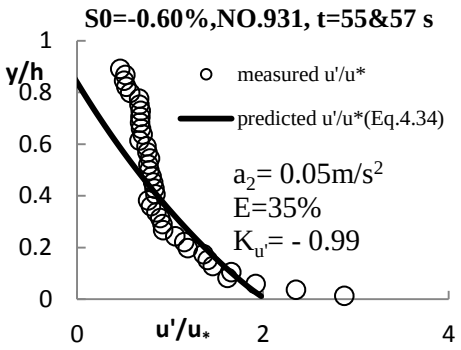

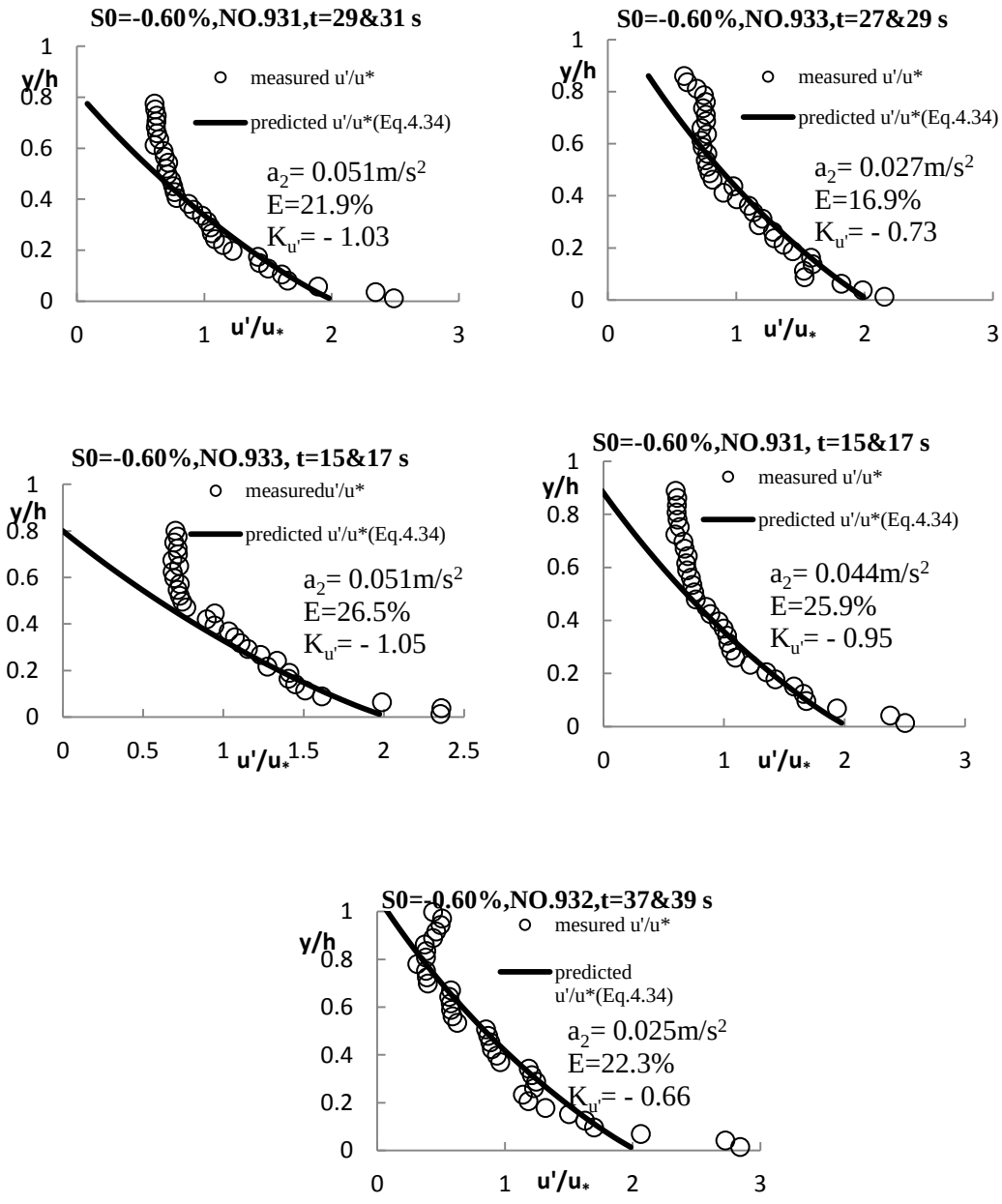

Figure 4.29: Comparison of measured and predicted horizontal turbulence intensities profile in accelerating unsteady flow based on Song's (1994) experimental data.

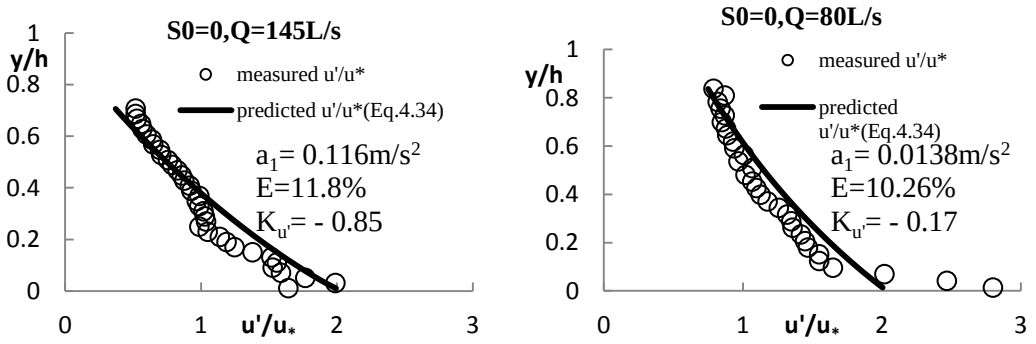

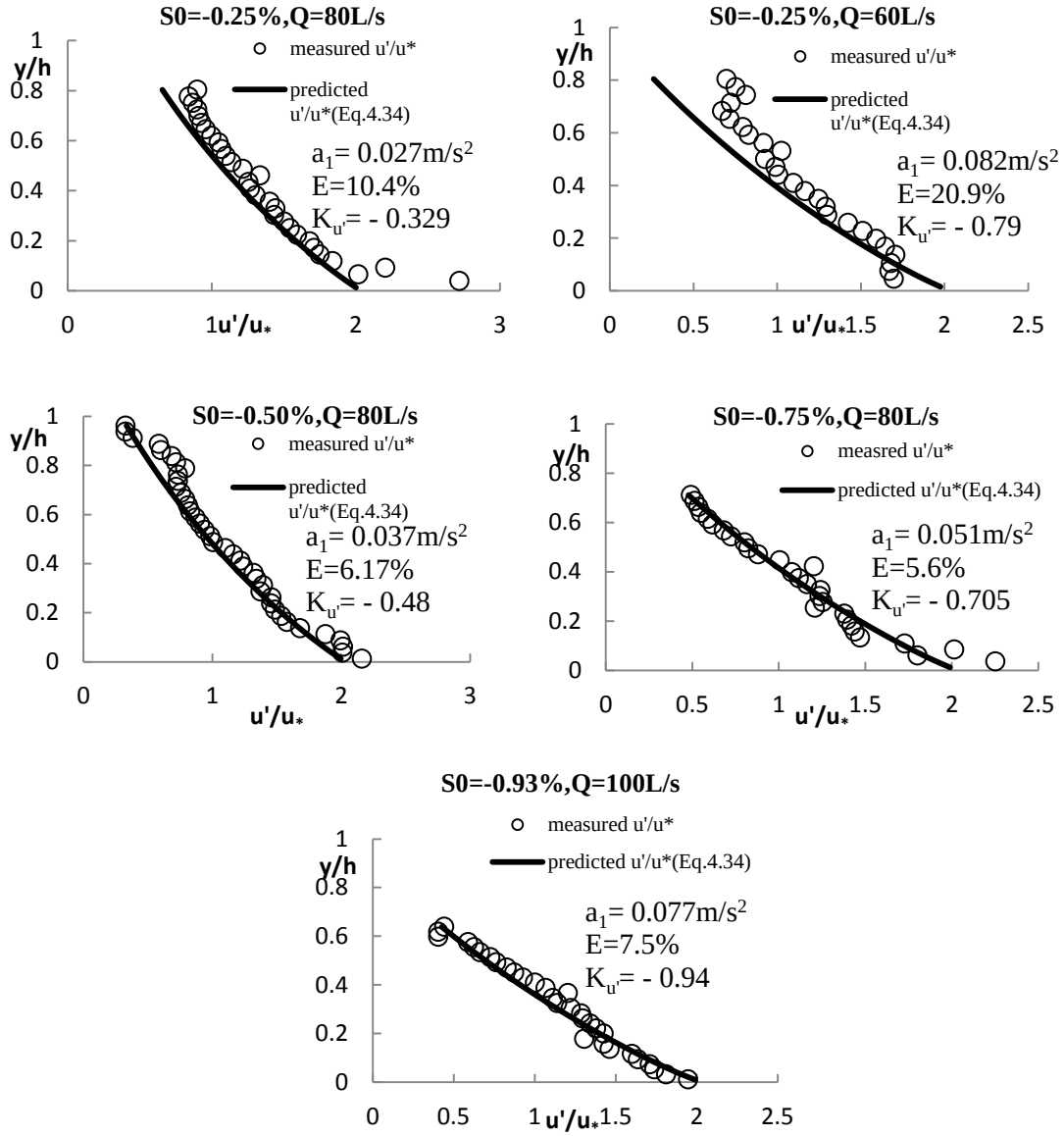

Figure 4.30: Comparison of measured and predicted horizontal turbulence intensities profile in accelerating steady flow based on Song's (1994) experimental data.

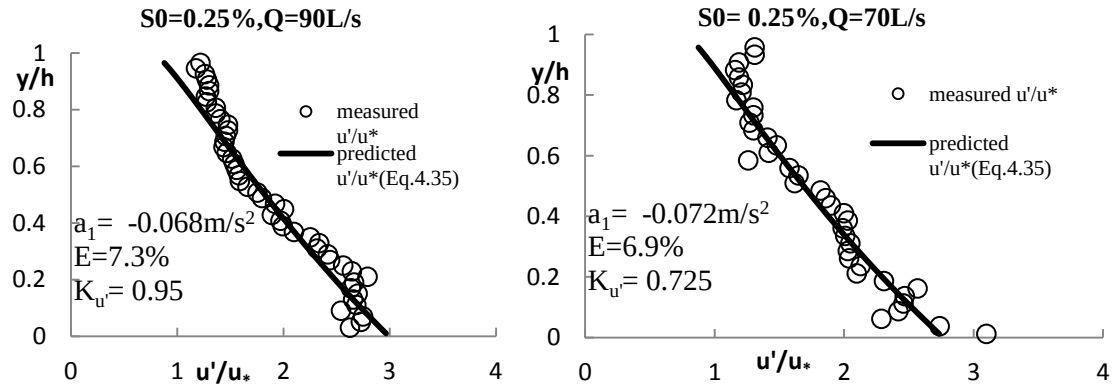

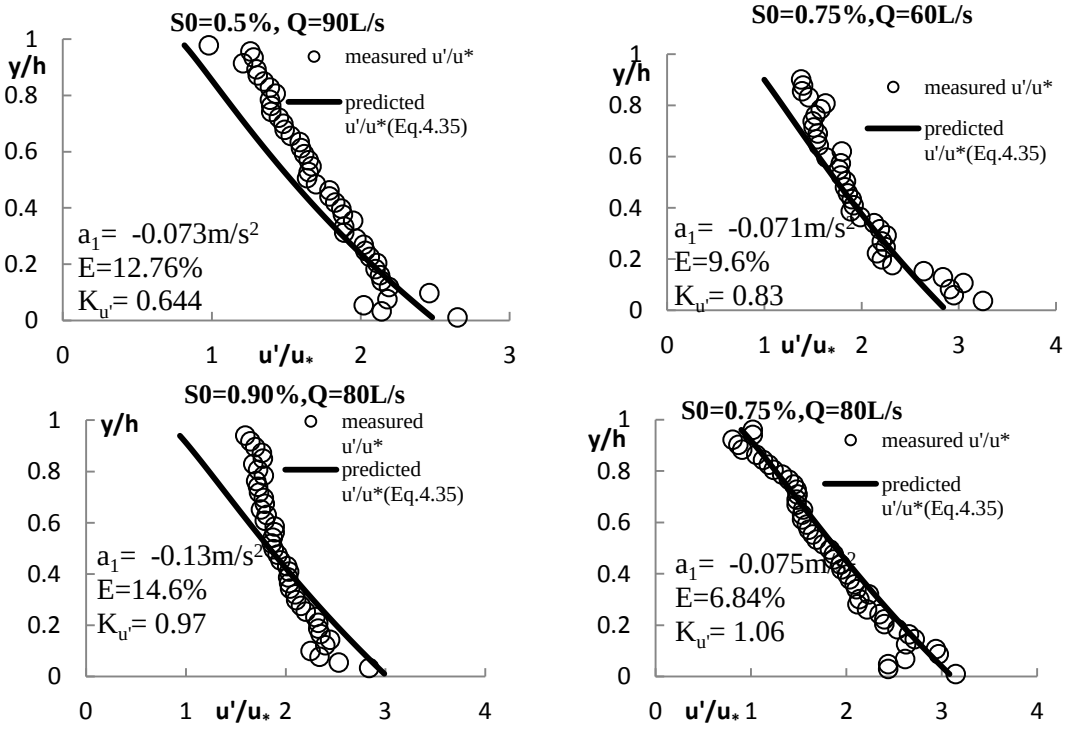

Figure 4.31: Comparison of measured and predicted horizontal turbulence intensities profile in decelerating steady flow based on Song's (1994) experimental data.

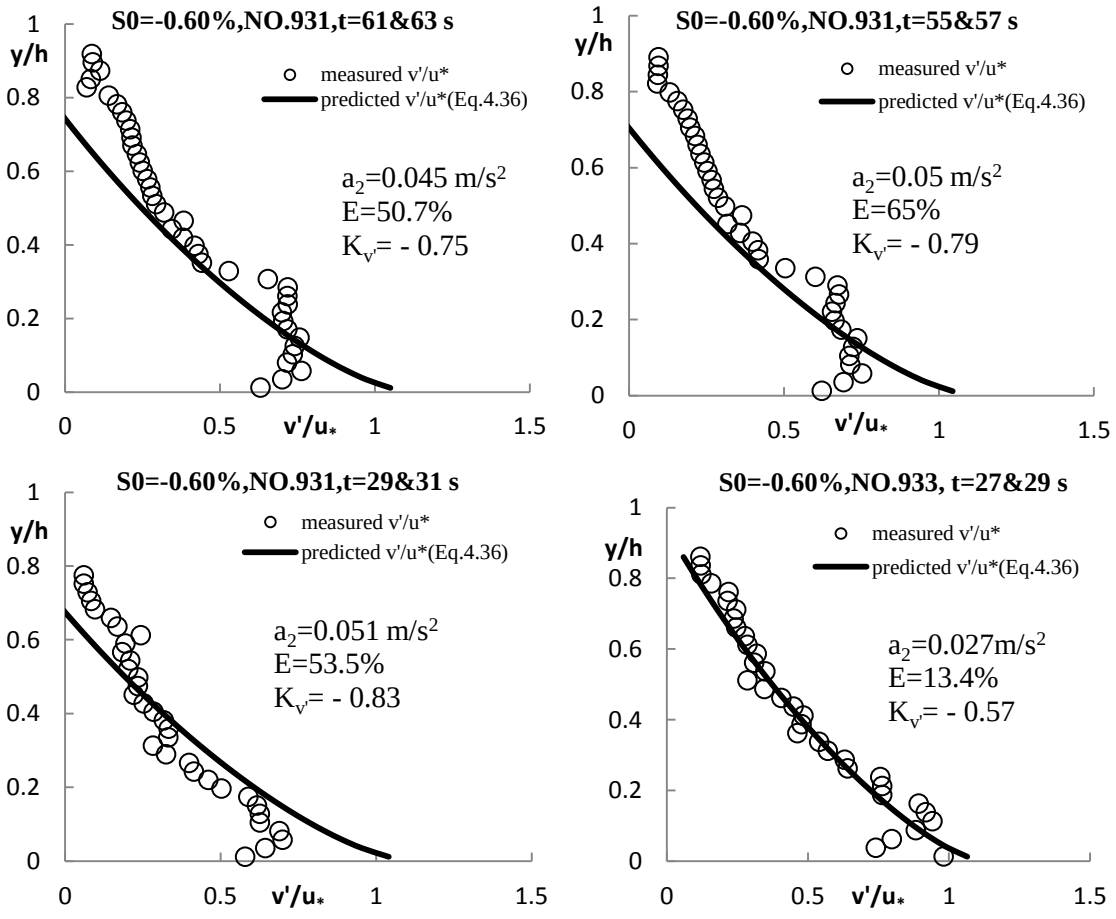

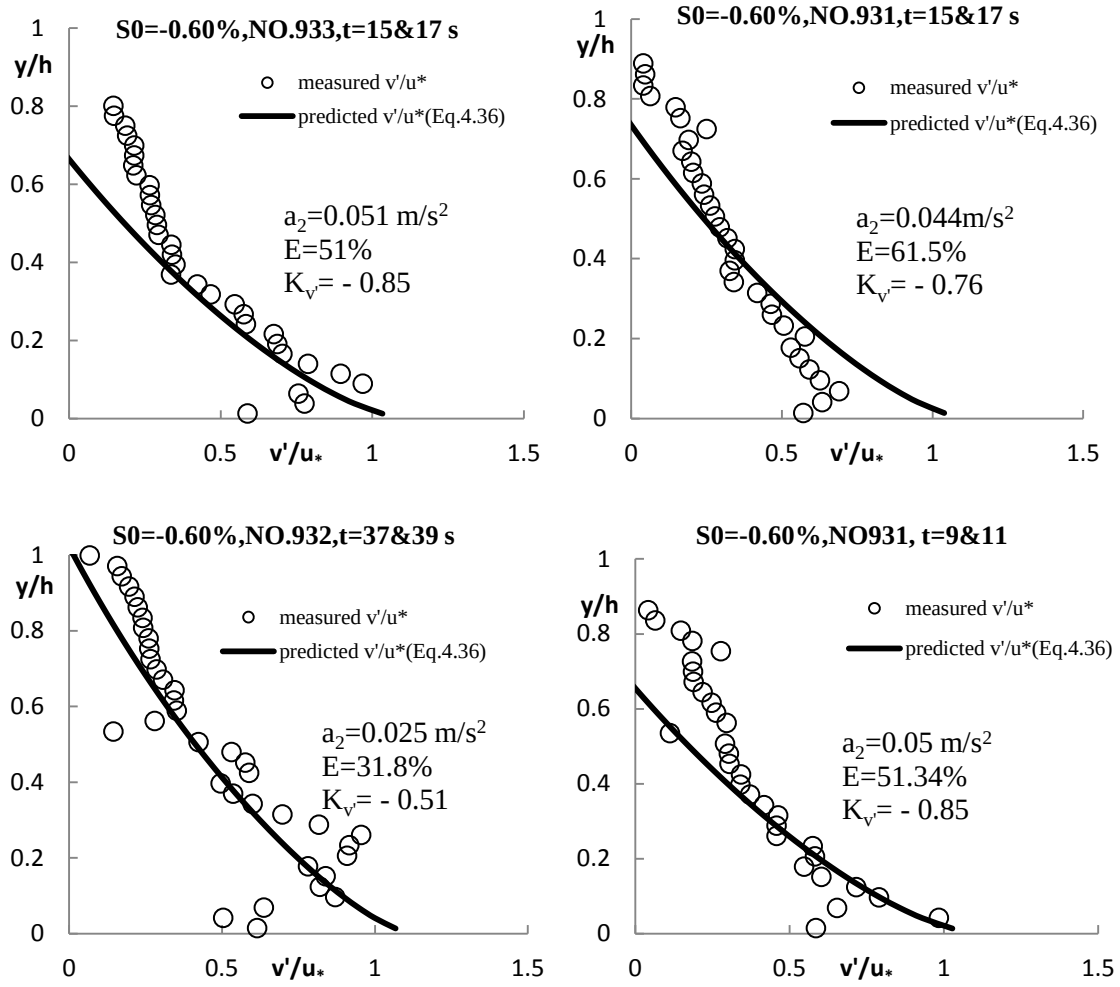

Figure 4.32: Comparison of measured and predicted vertical turbulence intensities profile in accelerating unsteady flow based on Song's (1994) experimental data.

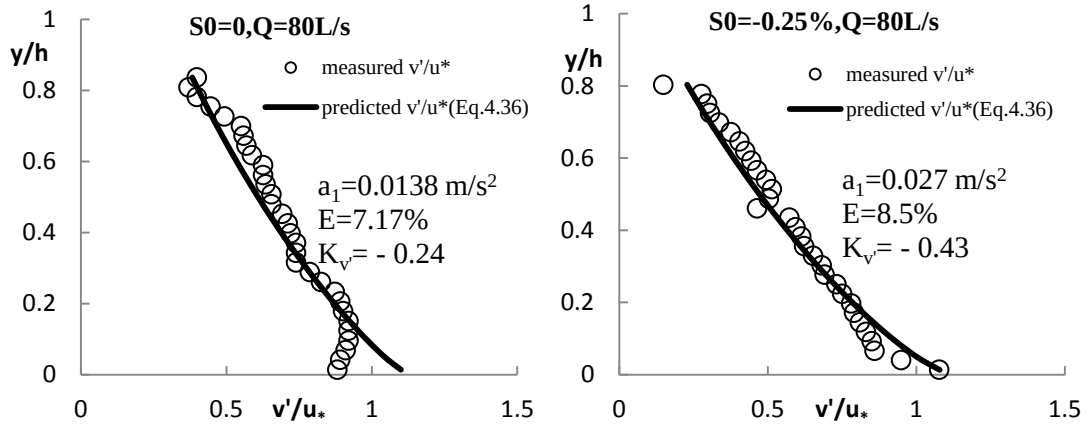

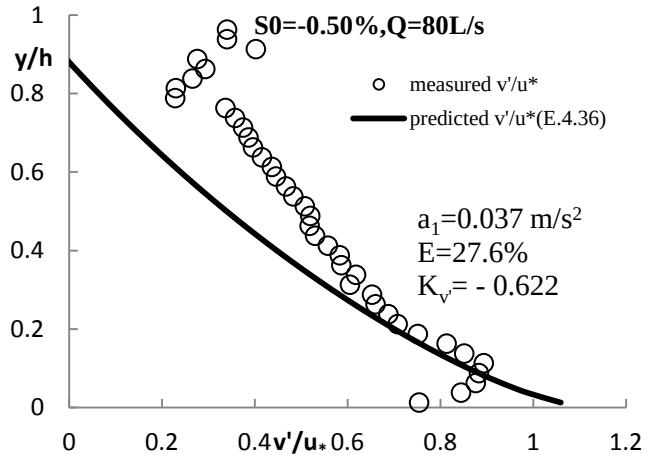

Figure 4.33: Comparison of measured and predicted vertical turbulence intensities profile in accelerating steady flow based on Song's (1994) experimental data.

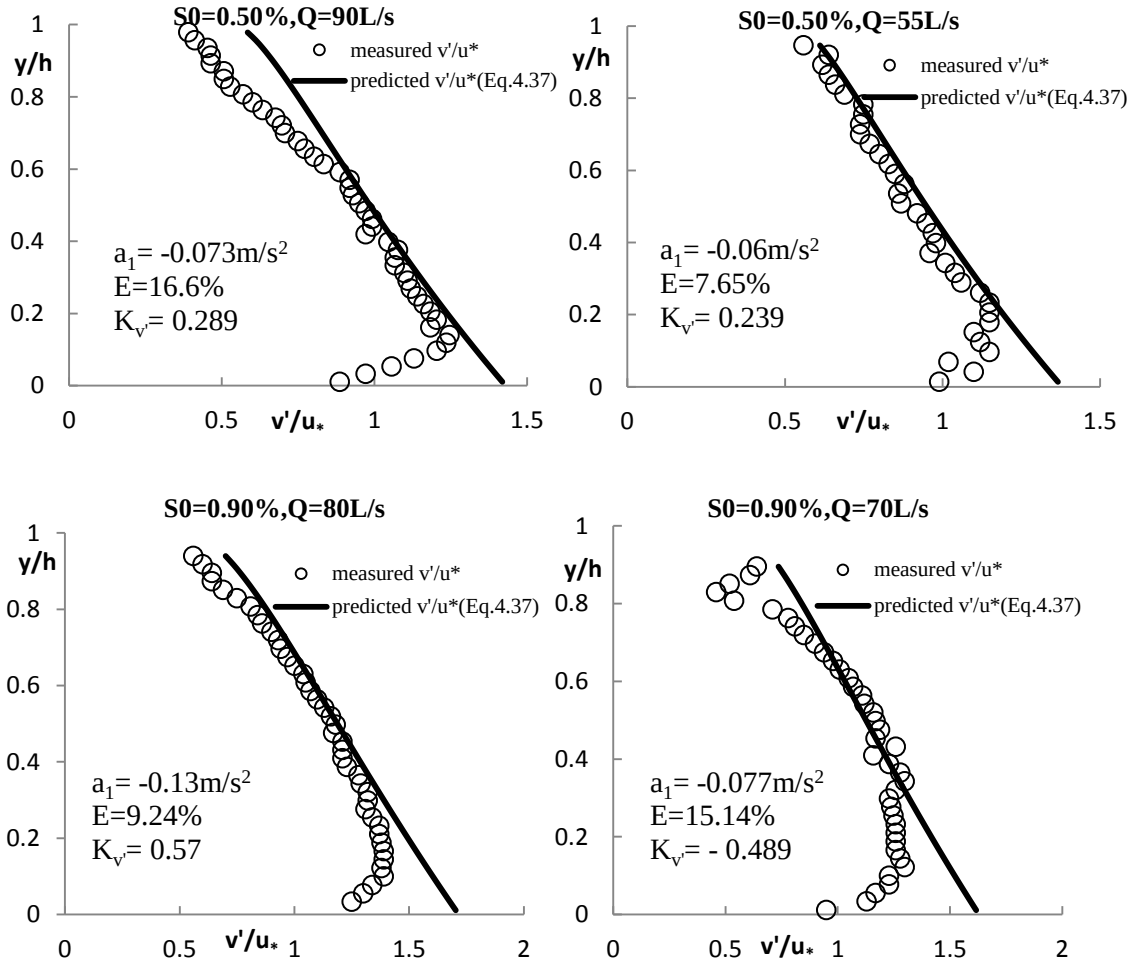

Figure 4.34: Comparison of measured and predicted vertical turbulence intensities profile in decelerating steady flow based on Song's (1994) experimental data.

In Figures 4.29-4.31 the determined horizontal turbulence intensity profiles using Equations 4.34 and 4.35 are plotted as solid lines and the open circles denote to the measured data points in accelerating (steady and unsteady) and decelerating steady flow, respectively. A Similar plot is drawn in Figures 4.32-4.34 for the prediction of vertical turbulence intensity in non-uniform flows using Equations 4.36 and 4.4.37. To demonstrate the influence of flow acceleration on the deviation of these turbulence intensities in non-uniform flow from that in uniform flow, the value of E is determined for each figure. The average values of determined E in Figures 4.29-4.31 and 4.32-4.34 are less than 37% and 15%, respectively, which give a reasonable agreement for steady and unsteady flows even though the some of the comparison shown in Figures 4.29-4.34 are very poor. These newly proposed equations agree quite well with measured data points in accelerating and decelerating flows, especially when the value of flow acceleration is existed. Overall, it can be found that the predicted formulas can give similar profiles to the measurements of horizontal and vertical turbulence intensities, concave distribution when the applying negative values of $k_{u'}$ and $k_{v'}$ determined from positive flow acceleration and convex distribution when the values of $k_{u'}$ and $k_{v'}$ is positive with a negative a.

4.8 Distribution of vertical velocity profile

Vertical velocity profile is one of the turbulence characteristic, which is expected to be different for uniform and non-uniform flows. In a uniform flow, the value of mean vertical velocity is equal to zero while the instantaneous vertical velocity may not be zero; and in non-uniform flow, this vertical velocity is zero at the bed when there is no seepage force and then it increases linearly till the water surface with a negative or positive value (Song, 1994; Song & Chiew, 2001). This deviation from the uniform

flow is generated from the impact of flow acceleration on the vertical velocity distribution. The measured vertical velocity deviates positively from the standard zero distribution as the flow is decelerating ($a < 0$), its value deviates negatively from its zero distribution in uniform flow as the flow is accelerating ($a > 0$). After prove the influence of flow acceleration on the deviation of vertical velocity in steady and unsteady flows from that in the uniform flow, one may conclude that the difference of vertical velocity in uniform and non-uniform flows is proportional to y/h as the difference must become zero at this boundary condition. Therefore, the proportionality k_v should depend on the dimensionless flow acceleration, i.e. $a/(u_*^2/h)$. The proposed distribution of vertical velocity can be expressed as follows:

$$(\frac{\bar{v}}{u_*})_{nonunf.} = (\frac{\bar{v}}{u_*})_{unf.} \pm \frac{y/h}{k_v} \tag{4.42}$$

where $\bar{v}/u_*$ is the normalised vertical velocity with respect to the shear velocity, and the subscripts "*unf* " and "*nonunf* " refer to the vertical velocity in uniform and non-uniform flows, respectively. In Equation 4.42, the value of k_v has two signs, one positive and the other negative. The positive one can be used when the flow is decelerating while the negative sign will be used when the flow is accelerating for both steady and unsteady flows. In other words, when the value of the second term on the right hand side of Equation 4.42 is positive the predicted value of dimensionless vertical velocity ($\bar{v}/u_*$) is higher than those in uniform flow, and therefore, this flow is decelerating. In contrast, the negative sign gives lower value than those in uniform flow, and thus this flow is accelerating. This is consistent with other researchers' observations, the distribution of vertical velocity in non-uniform flow deviate from the

standard zero distribution in uniform flow, i.e. $\bar{v}/u_* = 0$ (Song, 1994; Kironoto & Graf, 1995; Song & Chiew, 2001).

In order to verify Equation 4.42 with the measured vertical velocity, one can determine k_v from experimental data in steady and unsteady flows. For instance, the value of k_v can be evaluated from vertical velocity defect between the measured vertical velocity in uniform and non-uniform flows, i.e. $\Delta(\bar{v}/u_*) = (\bar{v}_{nonuf.} - \bar{v}_{unf.})/u_*$. This difference indicates the value of deviation from the measured vertical velocity from its distribution in uniform flow. By fitting the vertical velocity, one may obtain the expression of k_v. For accelerating and decelerating, k_v obtained from Song's (1994) experimental data as shown in Figures 4.35 and 4.36, in which only the data from accelerating flows in both steady and unsteady flows are selected, the empirical expression of these can be presented as follows:

$$k_v = -5 * \ln\{1 + [a/(u_*^2/h)]\} \qquad \text{(Accelerating flow)} \qquad (4.43)$$

$$k_v = \exp\{-0.36 * [a/(u_*^2/h)]\} - 1 \qquad \text{(Decelerating flow)} \qquad (4.44)$$

where a is the flow acceleration in steady and unsteady flows which can be determined using Equations 4.21 and 4.22, respectively. From Equations 4.43 and 4.44, the observed value of k_v is negative when the flow is accelerating because the distribution of vertical velocity in accelerating non-uniform flows is less than those in uniform flow (negative value) presented in Figure 4.35. While this empirical value of k_v is positive (see Figure 4.36) when the flow is decelerating because the data points for vertical velocity in this flow are larger than those in uniform flow (positive value).

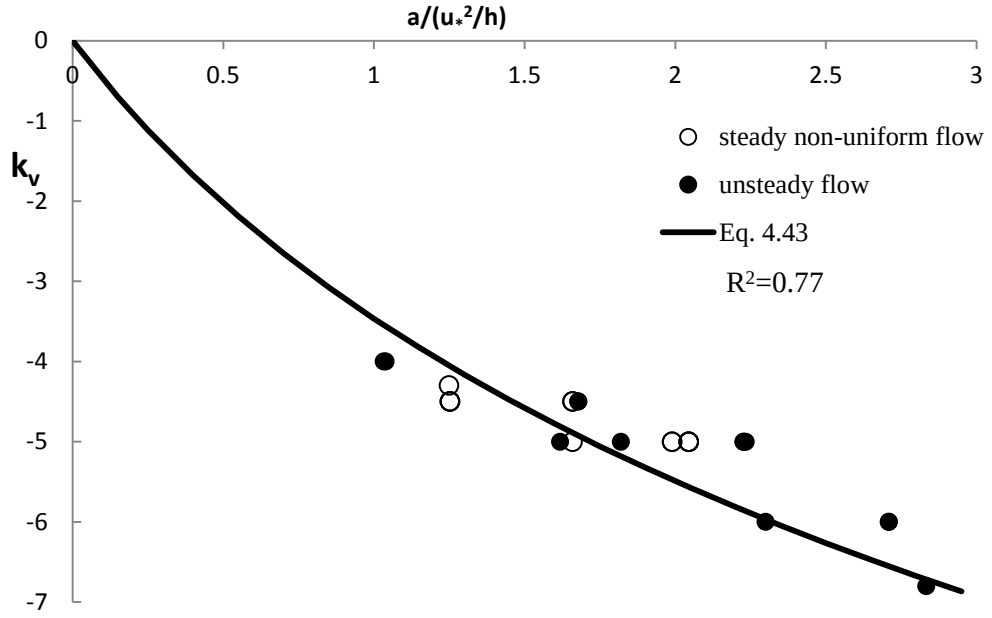

Figure 4:35: Relationship between dimensionless flow acceleration flow acceleration and the value of k_v for vertical velocity (v/u_*) in accelerating steady and unsteady flow based on selected data sets from Song's (1994) experimental data, where a solid line represents Equation 4.43.

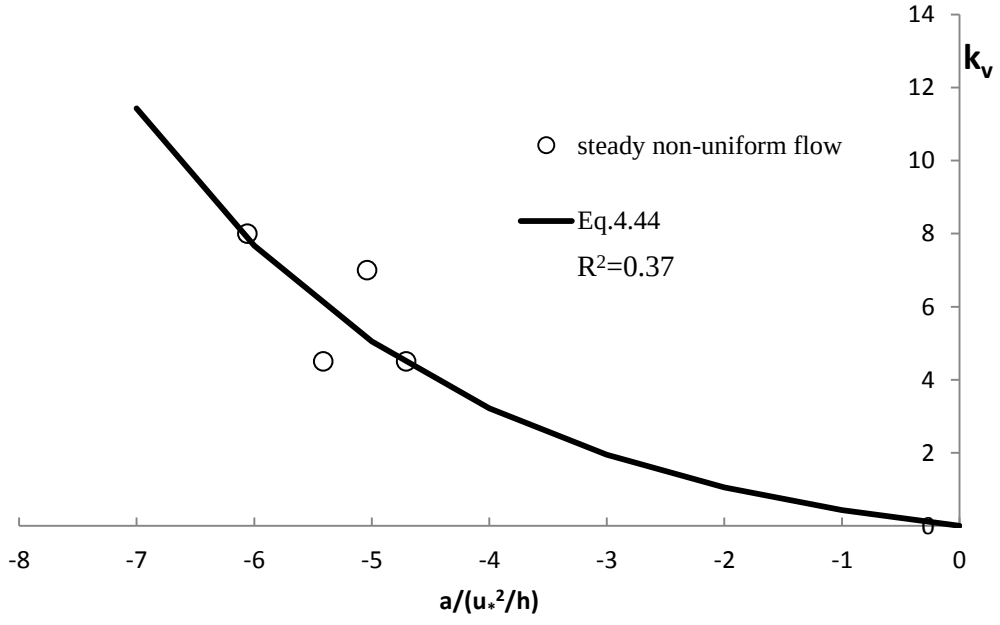

Figure 4.36: Relationship between dimensionless flow acceleration flow acceleration and the value of k_v for vertical velocity (v/u_*) in decelerating steady flow based on selected data sets from Song's (1994) experimental data, where a solid line represents Equation 4.44.

In Figures 4.35 and 4.36, the empirical values of k_v are plotted against $a/(u_*^2/h)$. The solid symbols in both figures 4.35 and 4.36 denote the data obtained from unsteady flows, and the open symbols represent the same but in steady flow. In Figure 4.36, there is no decelerating unsteady data available to compare with decelerating steady flows because Song (1994) reported that the flow in his experiments was accelerating in unsteady flow.

A clear dependence of the coefficient of k_v on the dimensionless acceleration can be observed and the solid line can be drawn based on the data points and the condition if a =0, then k_v =0 in both accelerating and decelerating flows, Equations 4.43 and 4.44 were obtained. In Figures 4.35 and 4.36, some similarities is observed between dimensionless flow acceleration in steady and unsteady flows and these similar values of flow acceleration give similar values for k_v. Therefore, this is the reason why the acceleration symbol (a) is used in Equations 4.43 and 4.44 without any subscript relating to the steady or unsteady flow. When the flow is accelerating for both steady and unsteady cases, a positive a gives a negative value of k_v and the vice versa for decelerating flow. While if a =0, then k_v =0 and as a result the second term of Equation 4.42 is negligible and this is uniform flow. It is clear that the values of k_v increase with the flow acceleration. Consequently, if the flow acceleration in steady or unsteady flows is known and then the value of k_v can be estimated based on Equations 4.43 and 4.44 for both accelerating and decelerating flows.

In order to check the validity of Equation 4.42 with these empirical values of k_v, the remaining datasets in Song's (1994) experiments except those shown in Figures 4.35 and 4.36 are plotted in Figures 4.37, 4.38 and 4.39 where S_0 refers to the bed slope, NO refers to the number of each hydrograph and (t) is time. In each figure, the value of acceleration is labelled as well as the predicted value of k_v using Equations 4.43 and 4.44. Taking into account the positive and negative values of flow acceleration generating from accelerating and decelerating in steady and unsteady flow, the value of k_v is positive when the value of flow acceleration is decreased along the channel while it becomes negative when the acceleration is increased.

In order to demonstrate the performance of Equation 4.42 and the empirical value of k_v obtained from its relationship with the flow acceleration, the value of relative error (E) is determined between the measured and predicted values , i.e., $E = \left| \bar{v}_m - \bar{v}_c \right| / \bar{v}_m * 100$, where the subscripts m and c are the measured and calculated values of vertical velocity.

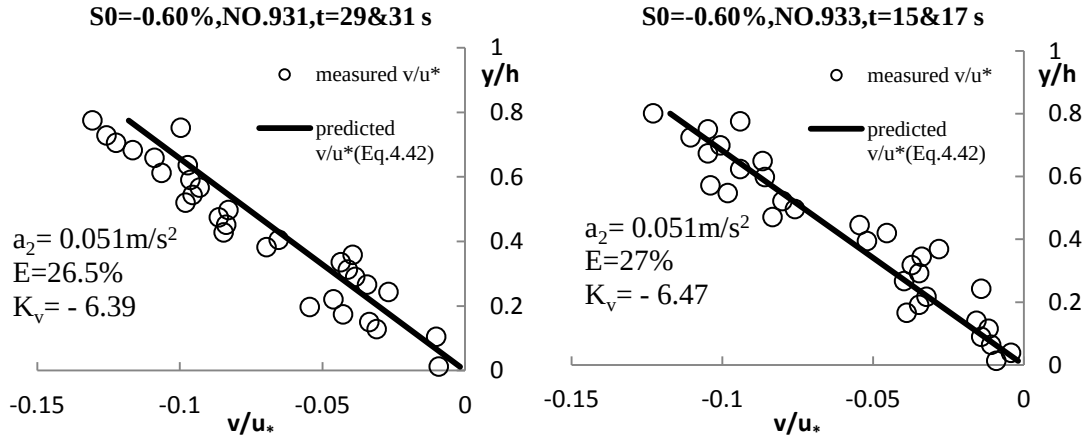

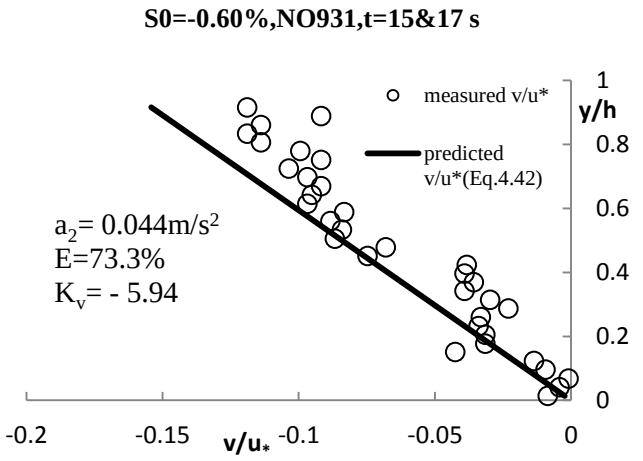

Figure. 4.37: Comparison of measured and predicted vertical velocity profile in accelerating unsteady flow based on Song's (1994) experimental data.

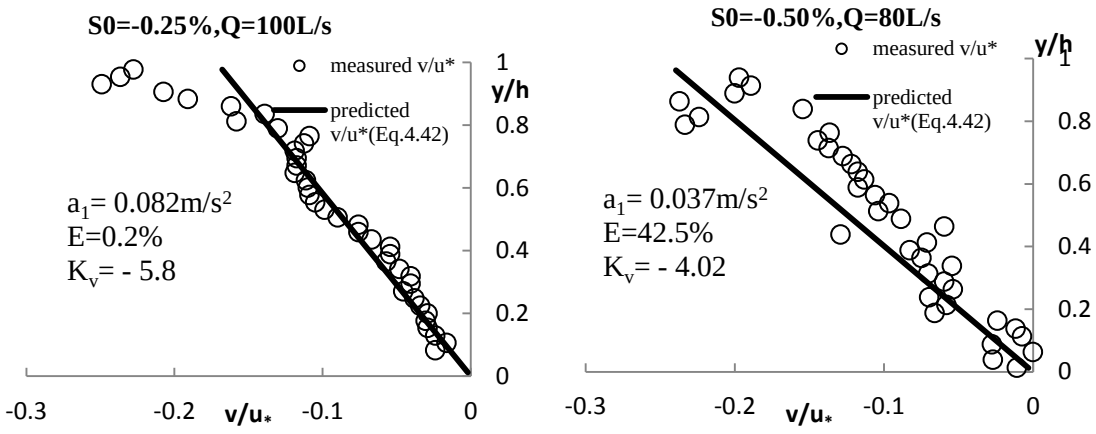

Figure 4.38: Comparison of measured and predicted vertical velocity profile in accelerating steady flow based on Song's (1994) experimental data.

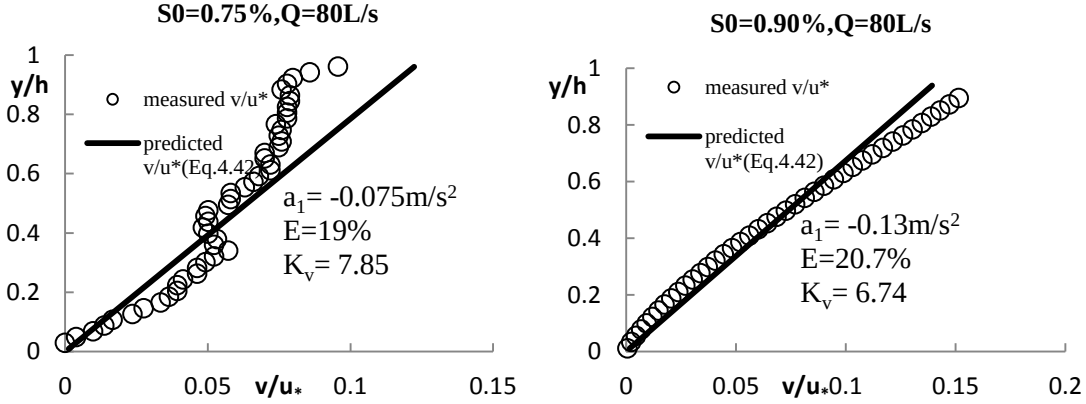

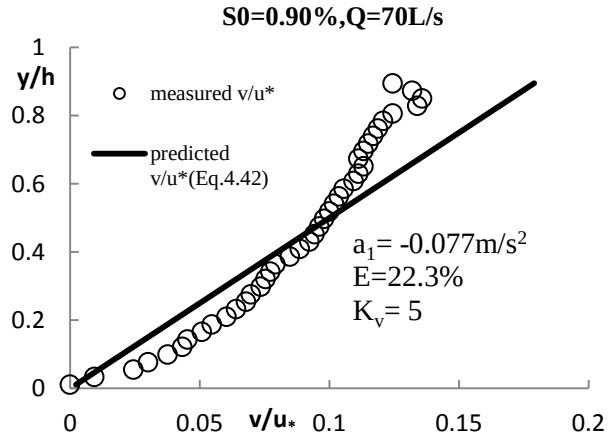

Figure 4.39: Comparison of measured and predicted vertical velocity profile in decelerating steady flow based on Song's (1994) experimental data.

In Figures 4.37, 4.38 and 4.39, the predicted vertical velocity profiles using 4.42 are plotted as a solid line and the open circles denote to the measured data points in non-uniform steady and unsteady flows. To demonstrate the influence of flow acceleration on the deviation of vertical velocity in accelerating and decelerating non-uniform flows from that in uniform flow, the value of E is determined for each figure. The average values of determined E in Figures 4.37, 4.38 and 4.39 using Equation 4.42 are less than 27% which gives a reasonably good agreement between the measured and predicted vertical velocity distributions. Overall, the agreement is fairly good. It can be found that the predicted formulas can give similar profiles to the measurements of vertical velocity, negative values when the applying negative value of k_v and positive value when the value of k_v is positive.

4.9 Comparison with Kironoto and Graf's (1995) experimental data

One of the widely cited measurements was that of Kironoto and Graf (1995), who measured mean horizontal velocity, Reynolds shear stress and turbulence intensities in laboratory channels with rough and gravel beds using Prandtl tubes with 3mm and 5mm outside diameters respectively. The turbulence characteristics were measured in a rectangular channel of 16.8m in length, 0.6m in width and 0.8m in height. Two types of bed roughness were used, such rough plate with d_{50} = 4.8mm and gravel bed with d_{50} = 23mm. Their measurement were conducted in non-uniform open channel steady flow, using negative bed channel to generate accelerating non-uniform flow and using positive bed channel to generate decelerating flow. The flow acceleration was not measured in each flow condition and we cannot determine it because there is no vertical velocity profile reported which is needed in its calculation (see Equation 4.21). Therefore, the values of flow acceleration are assumed in this comparison.

Figures 4.40- 4.42 compare Equations 4.4, 4.31, 4.34, 4.35, 4.36, 4.37 and 4.42 with Kironoto and Graf's experimental data sets, in which the solid lines represent the calculated velocity, Reynolds shear stress and horizontal and vertical turbulence intensities, and the open circles are the measurement of these turbulence characteristics. In Kironoto and Graf's experiment, there are different labels for each figure. "A and D" denote accelerating and decelerating flow respectively, "G and P" are gravel and rough plate," A, B and C" are the flow series and "1, 3 and 5" represent the section number of measuring profiles. For example, DGC3 means that the flow was decelerating, the bed roughness is due to gravel (d_{50}=23mm), C refers to flow series, and 3 is the number of measuring cross section which is located at x=11.245m from the flume entrance.

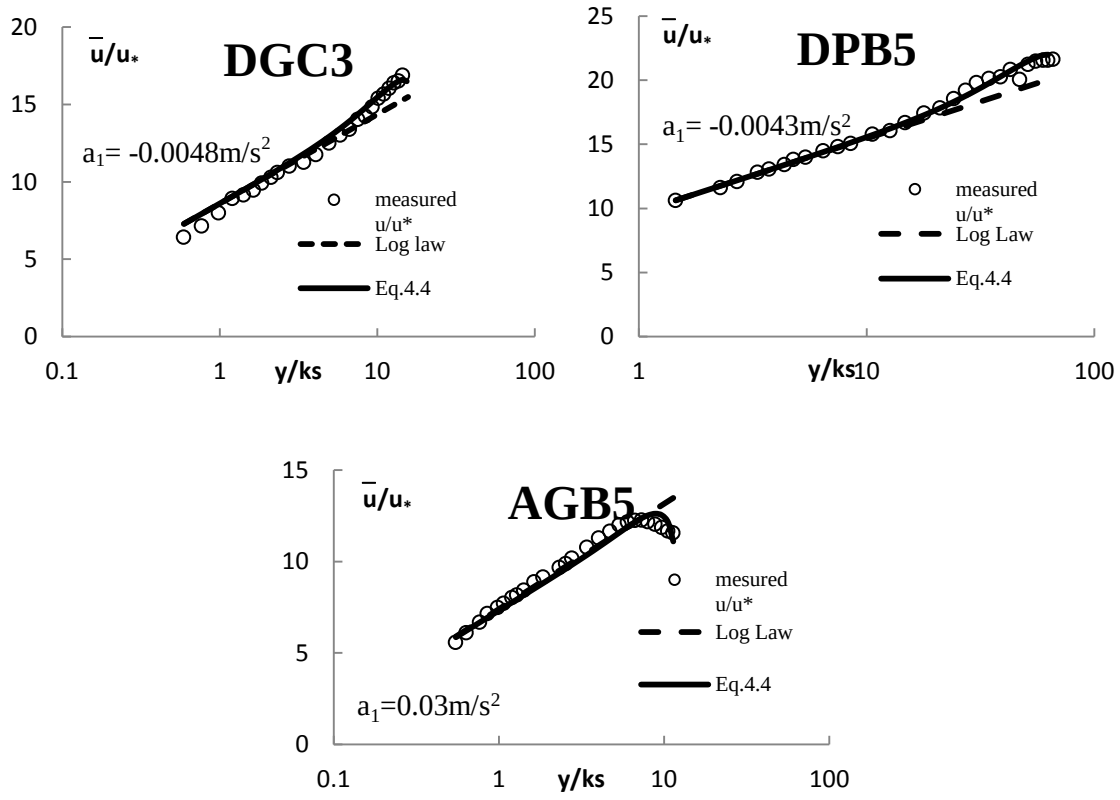

Figure 4.40: Comparison of measured and computed velocity profiles for non-uniform flow (data from Kironoto and Graf's paper).

A typical result is shown in Figure 4.40, in which the measured $\bar{u}/u_*$ is obtained from Kironoto and Graf's (1995) data and represented by the open circles, the classical Log law is represented by the dashed line and Equation 4.4 is represented by the solid lines. To confirm the validity of Equation 4.4, the relative error between the measured data points and their calculations is defined as $E = |\bar{u}_m - \bar{u}_c| / \bar{u}_m * 100$, where the subscript c refers to the calculated velocity using Equation 4.4 and the subscript m refers to the measured experimental data. From Figure 4.40, the determinations of an average E between the measurements and calculations values are presented in Table 4.1.

Table 4.1: Comparison on the determination of relative error between the experimental measurement and present study.

Series run	Kironoto and Graf E (%)	Proposed Equation E (%)
AGB5	3.7	3.08
DPB5	3.15	1.08
DGC3	4.16	2.08

The second column of Table 4.1 shows the values of E obtained from experiment data points and their calculations using Log law formula (see Equation 2.2) and the third column shows the relative error between the measurements and their calculations using the present model developed in this study (see Equation 4.4). It is clearly seen that relative errors in Kironoto and Graf (1995) are bigger than those in the present study, which means Equation 4.4 can capture the measured velocity better than using only the Log law.

It can be seen from Figure 4.40 that the newly developed Equation 4.4 with the values of k_1 and k_2 (obtained from Equations 4.28 and 4.29 for accelerating flow and from Equation 4.30 for decelerating flow) yields similar results that are very close to the measured data when the flow acceleration exists. This is very encouraging indeed.

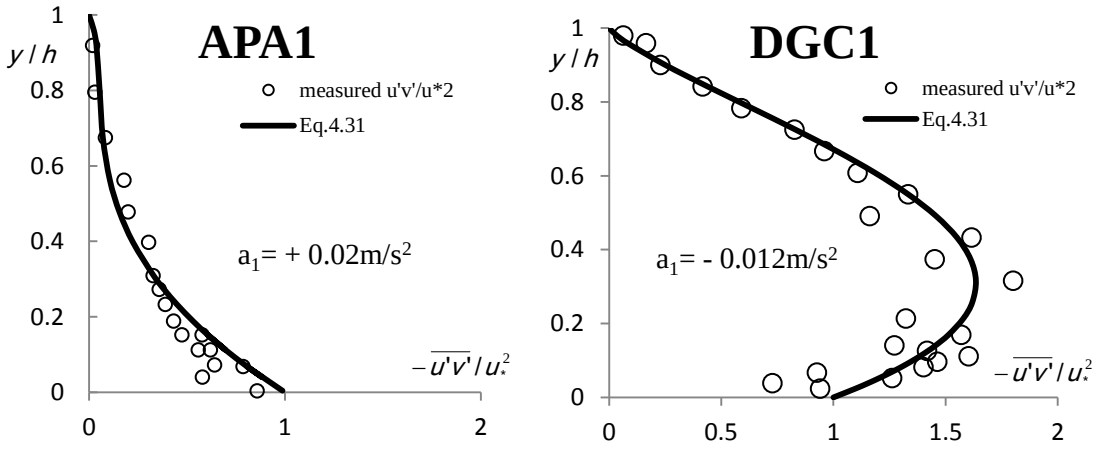

Figure 4.41: Comparison of measured and computed Reynolds shear stress profile for non-uniform flow (data from Kironoto and Graf's paper).

Figure 4.41 shows the comparison between the measured and calculated Reynolds shear stress distribution. Equation 4.31 depends on the value of $k_{-\rho\overline{u'v'}}$ which can be obtained from two empirical Equations 4.32 and 4.33 for both accelerating and decelerating flows respectively. The measured Reynolds shear stress agrees reasonably well with that predicted using the proposed equations. From APA1 and DGC1 in Figure 4.41, the average E is 27% and 13.7%, respectively indicating that the proposed model agreed with the existing dataset in accelerating and decelerating non-uniform flow, especially when it is influenced by flow acceleration. Therefore, it can be seen from Figure 4.41 that Equation 4.31 with the values of $k_{-\rho\overline{u'v'}}$ are able to predict the Reynolds shear stress profiles for both accelerating and decelerating flows and give a clear concave form when the flow is accelerating and a convex form when the flow is decelerating.

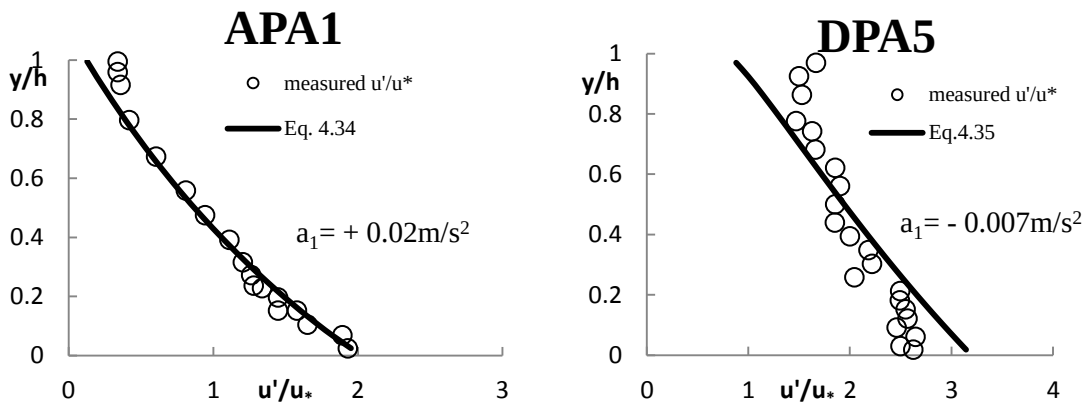

Figure 4.42: Comparison of measured and computed horizontal turbulence intensities profiles for non-uniform flow (data from Kironoto and Graf's paper).

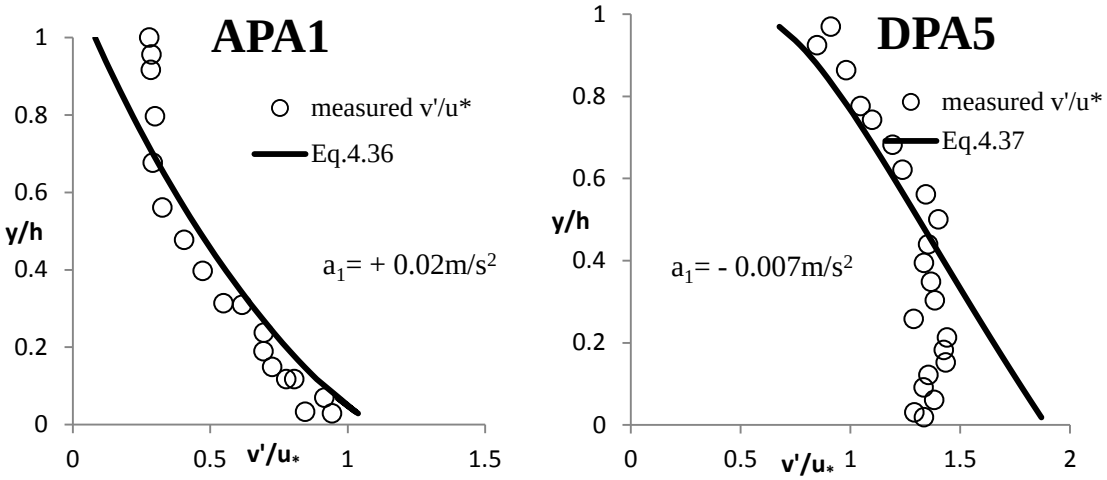

Figure 4.43: Comparison of measured and computed vertical turbulence intensities profiles for non-uniform flow (data from Kironoto and Graf's paper).

The comparisons of measured and predicted horizontal and vertical turbulence intensities in accelerating and decelerating non-uniform flows are presented in Figures 4.42 and 4.43. In these figures, the open circles present the measured data obtained from Kironoto and Graf (1994) and the solid lines presents Equations 4.34 and 4.35 for horizontal turbulence intensities and Equations 4.36 and 4.37 for vertical turbulence intensities. To demonstrate the performance of Equations 4.34 - 4.37, the relative error is defined for each comparison. From Figures 4.42 and 4.43, it is found that the average

value of E is 9% in accelerating flow (APA1) and 17.3% in decelerating flow (DPA5). While the relative error in vertical turbulence intensity is 22% in accelerating flow and 16.5% in decelerating flow. Based on these small relative errors, it can be seen that the agreement is reasonable for the prediction of turbulence intensities profiles in non-uniform flows. This means that Equations 4.34 - 4.37 with the value of k obtained from the effect of flow acceleration, is able to capture the turbulence intensities profiles well and gives a reasonably good description about these turbulence distribution in the entire water depth.

4.10 Comparison with Nezu et al.s' (1997) experimental data

Nezu et al. (1997) measured turbulence characteristics in unsteady flow in an open channel 10m long, 0.4m wide and 0.5m deep. They conducted their experiments over a smooth channel. They measured horizontal mean velocity, Reynolds shear stress and horizontal and vertical turbulence intensities using a Laser Doppler Anemometer (LDA). The base discharge (Q_b) was set to 2.5 and 5L/s in SC3 and SD3 while the peak discharge (Q_p) was ranged from (7.3 to 16.1) L/s. The channel slope was set to 0.001 and 0.0016. Using these flow conditions one can investigate the validity of Log law. They compared their measurements of Reynolds shear stress and turbulence intensities with empirical formulas which are used to predict these characteristics in uniform flow. They found that the values of vertical (v'/u_*) turbulence intensities tend to deviate near the free surface from somewhat less than the predicted formulas in uniform flow, and these deviations can be noted more in dimensionless vertical turbulent intensity (v'/u_*) than those deviations in dimensionless horizontal turbulent intensity (u'/u_*). They also determined that the values of Reynolds shear stress normalized by the shear velocity may not be affected by the unsteadiness of flow when they compared their

measurements with the determined Reynolds shear stress using the uniform formula. The reason for this relates to low flow conditions that generate weakly unsteady flow as compared with Song's flow conditions. The comparison of the experimental condition between Song (1994) and Nezu et al. (1997) are shown in Table 4.2. From this comparison, it is clearly seen that the bed slope and flow discharge selected by Song to generate unsteady flow are larger than those used by Nezu et al.

Table 4.2: Comparison of the values of bed slope and flow discharge between Song (1994) and Nezu et al. (1997).

Researchers	Bed slope (%)	Flow discharge (L/s)
Song (1994)	-0.6 -0.45	(55.6-120.3) (68.2-90.5)
Nezu et al. (1997)	0.16 0.1	(5-15.4) (2.5-7.3)

In Nezu et al. (1997) experimental data sets, the flow acceleration and vertical velocity profiles for each flow condition were not reported. In order to check the validity of the new equations developed in the current study, the value of flow acceleration should be assumed. The assumed value of flow acceleration ranges between 0.002 and $0.0035 m/s^2$, which is another evidence generating weakly unsteady flow when comparing this assumed value with Song's experimental data.

To confirm this assumption, Figures 4.44, 4.45 and 4.46 show the comparisons between the measured and calculated turbulence characteristics using the assumed value of flow acceleration to compute the value of k for each turbulence characteristics. In each figure, there is a label which refers to the series name (SC3T1) and (t) refers to the rising time (i.e. 36 and 48 s) and the falling time (i.e. 84 and 96 s). In Nezu et al.'s

experiments, the type of unsteady flow whether accelerating or deceleration was not reported, therefore the assumed value of flow acceleration is always positive to match with their findings. In these comparisons, the proposed equations are represented as solid lines, Nezu et al.'s equations are presented as dashed lines and the measured data sets are the open circles. The comparison of measured mean velocity is not included because the authors already matched their measured data with the Log law.

For comparison, Nezu et al.'s (1997) equations for the prediction of Reynolds shear stress and turbulence intensities in uniform flow are included in Figures 4.44, 4.45 and 4.46 and are represented as the dashed lines while the proposed Equations 4.31, 4.34 and 4.36 are presented as the solid lines. After the comparison of the measured and predicted these profiles plotted in Figures 4.44 - 4.46, it can be seen that the proposed model generally yields good agreement. The detailed relative error is listed in Table 4.3. The last two columns of Table 4.3 show a comparison of the percentage relative error E for the predicted and measured data points. The third column indicates the value of average E determined from the measurements of turbulence characteristics selected from Nezu et al.'s experimental results and the proposed Nezu et al.'s equations (see Equations 2.3, 2.4 and 2.7) and the forth column refers to the relative error calculated from the measured data points from Nezu et al. and the newly proposed equations in the current study (see Equations 4.31, 4.34 and 4.36). From this table, we found that the values of relative error obtained from proposed equations are lower than those obtained from Nezu et al.'s equations. According to these lower errors obtained from developed equations in the present study than Nezu et al.'s equations, the agreement is reasonably for unsteady flow. From the above comparison, it can be concluded that the newly proposed Equations 4.31, 4.34 and 4.36, together with the influence of flow

acceleration, are able to predict the horizontal/vertical turbulence intensities and Reynolds shear stress distributions in the entire water depth.

Table 4.3: Comparison of the determination of relative error between the measurement obtained from Nezu et al. (1997) and present study.

Turbulence characteristics	Series run	Nezu et al.'s Equation E (%)	Proposed Equation E (%)
Normalized horizontal turbulence intensity $(u^{'}/u_{*})$	SC3T1/ t=36s	16	12
	SC3T1/t=48s	13.7	9.45
	SC3T1/ t=84s	17	12.3
	SC3T1/t=96s	21.2	13.5
Normalized vertical turbulence intensity $(v^{'}/u_{*})$	SC3T1/ t=36s	20.5	16.5
	SC3T1/t=48s	23.11	20.5
	SC3T1/ t=84s	30.3	13
	SC3T1/t=96s	21.2	13.5
Normalized Reynolds shear stress $(-\overline{u'v'}/u_{*}^{2})$	SC3T1/ t=36s	32.7	19
	SC3T1/t=48s	33.3	20.9
	SC3T1/ t=84s	30.8	20.3
	SC3T1/t=96s	39	30.3

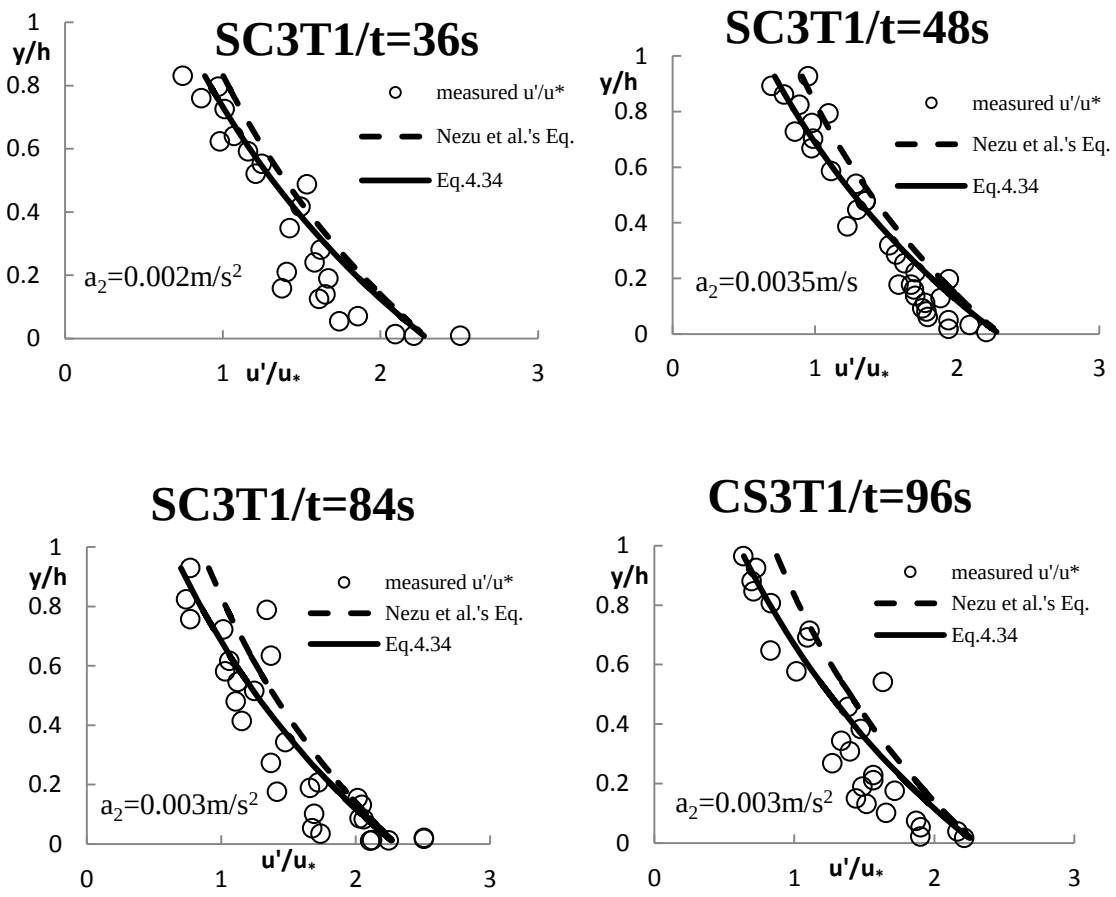

Figure 4.44: Comparison of measured and computed horizontal turbulence intensities profiles for unsteady flow (data from Nezu et al.'s paper).

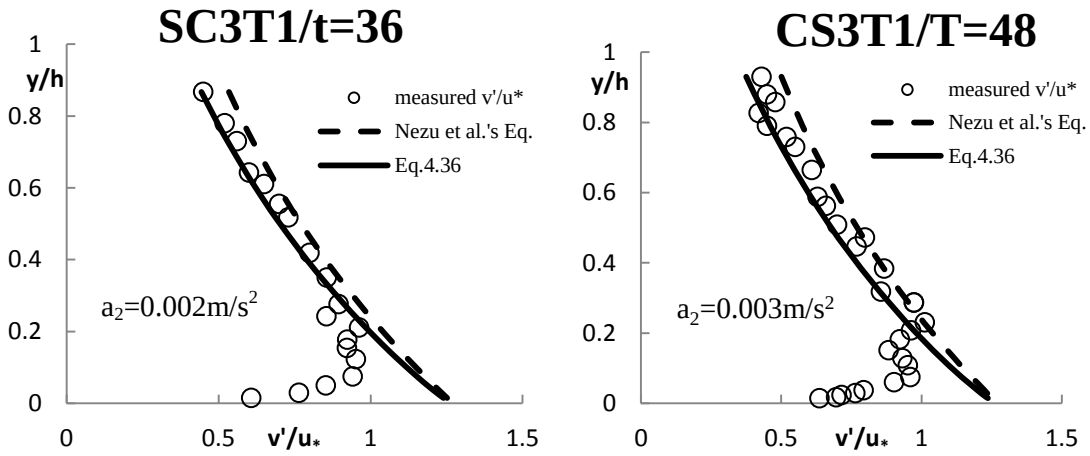

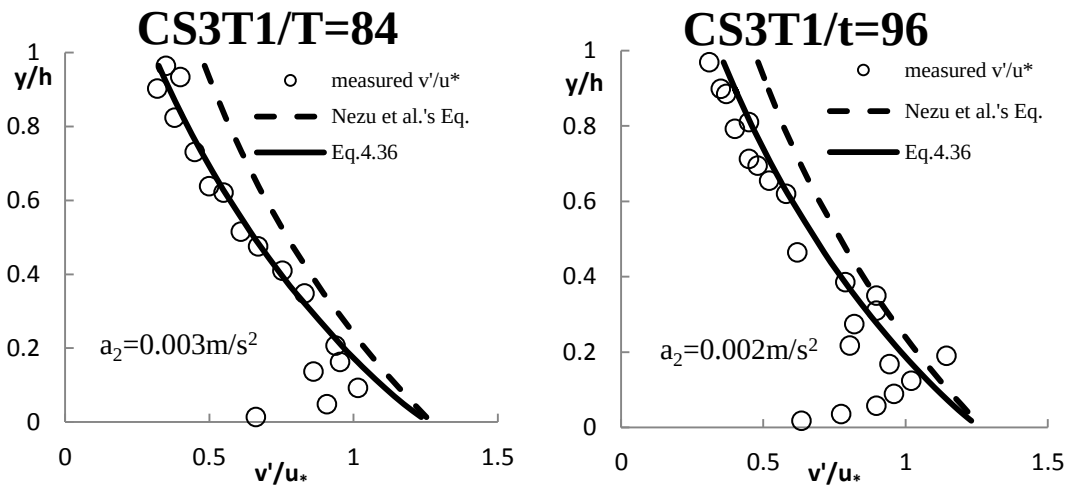

Figure 4.45: Comparison of measured and computed vertical turbulence intensities profiles for unsteady flow (data from Nezu et al.'s paper).

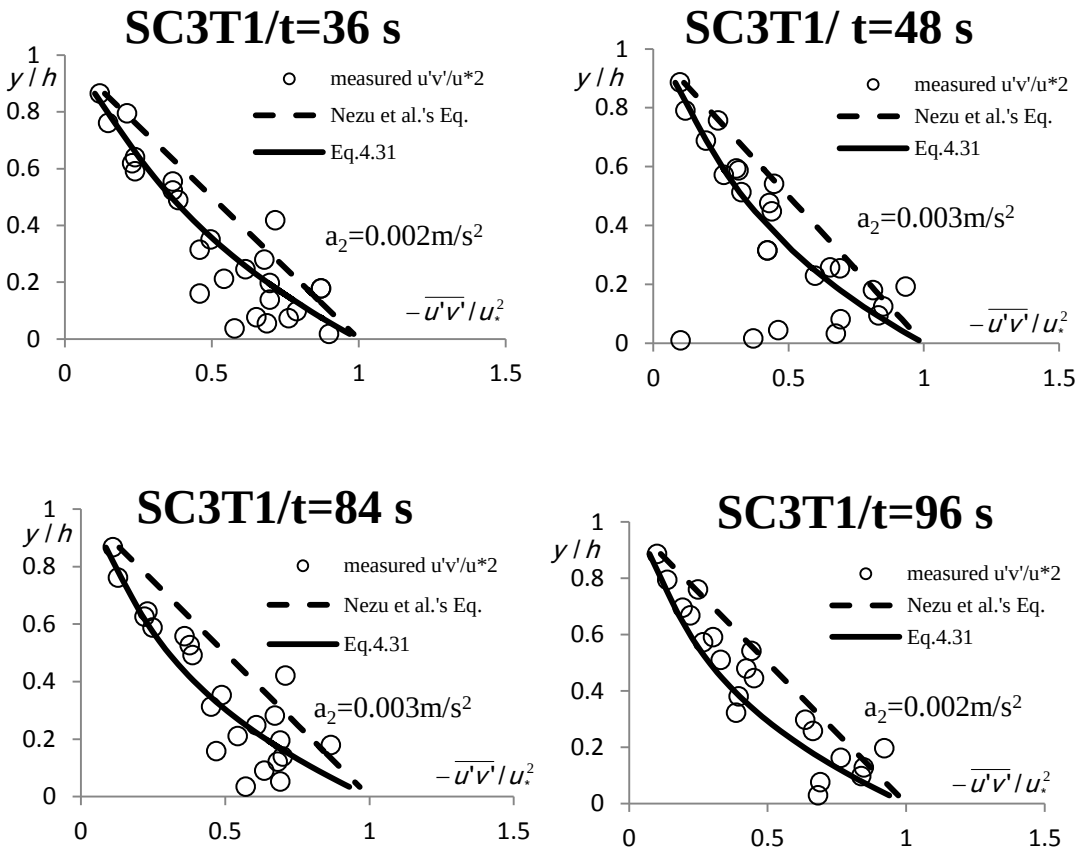

Figure 4.46: Comparison of measured and computed Reynolds shear stress profiles for unsteady flow (data from Nezu et al.'s paper).

4.11 Comparison with Song and Chiew's (2001) experimental data

In this study, reliable experiments carried out by Song and Chiew (2001) are used to verify the proposed models. Their experiments were conducted in a 0.6m wide, 0.8m high and 18m long recirculating flume under a rough bed with a uniformly sediment diameter i.e. d_{50}=2.6mm. Song and Chiew measured the full profiles of turbulence characteristics in non-uniform accelerating and decelerating steady flow using an Acoustic Doppler Velocimeter (ADV). These measurements were conducted at five cross-sections, which were located at x=5, 7, 9, 11 and 13m along the flume. Different bed slope was used, S_0= - 0.2%, 0% to investigate the accelerating flow while S_0= 0.3%, 0.6% and 0.75% to investigate the decelerating flow. From their measurements, they obtained positive values of vertical velocity in a decelerating flow and negative values in an accelerating flow. The turbulence intensities and Reynolds shear stress are different from those in uniform flow. In an accelerating flow, they have a concave form and the maximum value occur close to the bed. For a decelerating flow, the measured Reynolds shear stress and turbulence intensities distribution become convex and its minimum value occurs at the water surface while the maximum occurs above the bed at $y > 0$.

In this datasets, the flow acceleration for each flow condition was not measured but it can be determined based on the measured vertical velocity using Equation 4.21. Figures 4.47 and 4.48 show the comparisons between the proposed Equations, i.e. 4.31, 4.34, 4.35, 4.36 and 4.37 with measured datasets selected from Song and Chiew (2001), in which the solid lines represent the determined Reynolds shear stress and turbulence intensities, and the open circles are the measurements of these turbulence characteristics. In each figure, there are different legends. The letters "A and D" refer to

the accelerating and decelerating flows respectively, S_0 is the bed slope, Q is the flow discharge (m^3/h) and the letters II, III and V are measuring section numbers from the outlet.

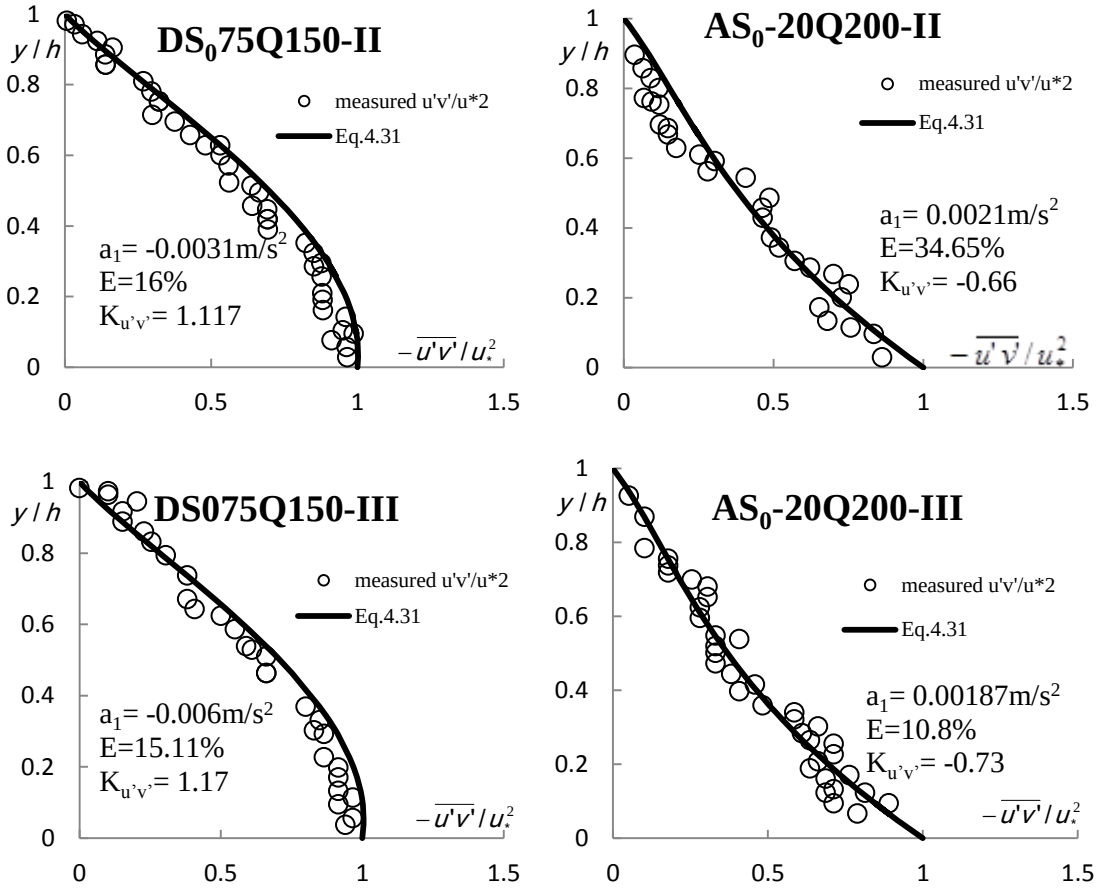

Figure 4.47: Comparison of measured and computed Reynolds shear stress profile for non-uniform accelerating and decelerating flows (data from Song and Chiew's paper).

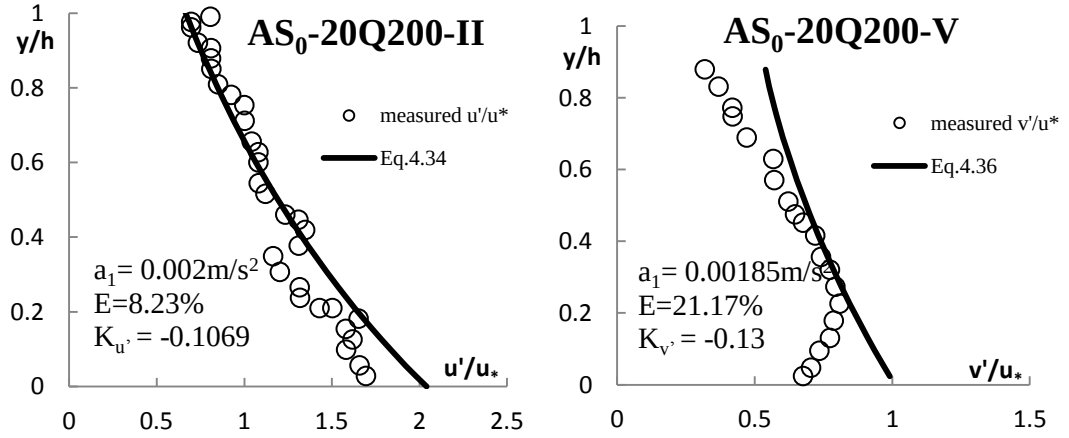

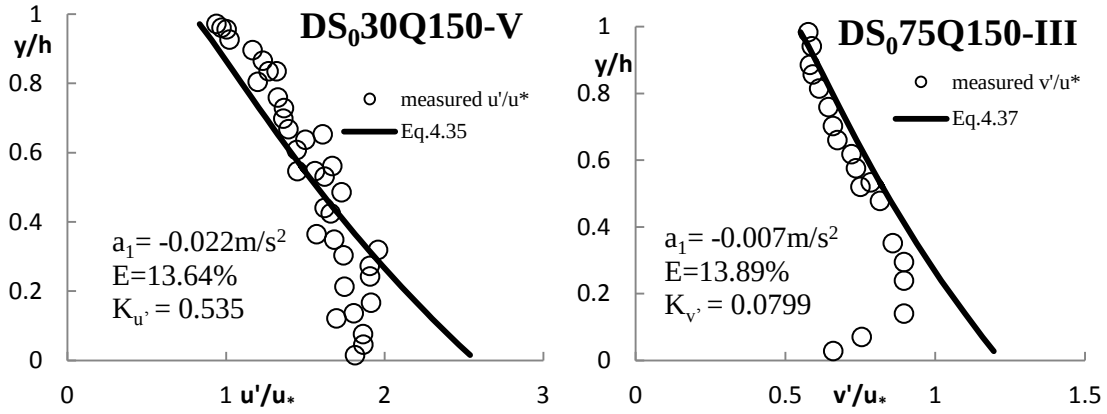

Figure 4.48: Comparison of measured and computed turbulence intensities profiles for non-uniform accelerating and decelerating flows (data from Song and Chiew's paper).

The comparisons between the measured and computed data points for the prediction of Reynolds shear stress and horizontal/vertical turbulence intensities are presented in Figures 4.47 and 4.48, in which the measured the full profiles of Reynolds shear stress ($\overline{u'v'}/u_*^2$) and horizontal/vertical turbulence intensities i.e. u'/u_* and v'/u_*, respectively, which are represented as the open circles and the solid lines present the developed model using Equations 4.31 and 4.34-4.37. In each figure, the acceleration a_1, the relative error, E and the predicted values of $k_{\overline{u'v'}}$, $k_{u'}$ and $k_{v'}$ are presented. Based on these figures, it is clearly shown the good agreement between the measured and determined data points of these specific turbulence characteristics.

4.12 Comparison with Emadzadeh et al.'s (2010) experimental data

Emadzadeh et al. (2010) experimentally investigated the influence of accelerating and decelerating steady flows on Reynolds shear stress distribution under incipient sediment motion. Their experiment was conducted in 14m long, 0.6m wide and 0.6m deep flume using three uniform sediments with median sizes, i.e. d_{50}=1.8, 1.3 and 0.8mm. An Acoustic Doppler Velocimeter (ADV) was fixed in three cross-sections 5, 7 and 9m

from the flume entrance. The authors used negative bed slopes i.e. (-0.7%, -0.9%, -1.25% and -1.5%) to generate accelerating flow and positive bed slope i.e. (0.7%, 0.9%, 1.25% and 1.5%) to generate decelerating flow. Their results showed that Reynolds shear stress associated with decelerating flow is larger than accelerating flow. In decelerating flow, the maximum value of shear stress is larger than that obtained when the flow is accelerating. Unfortunately, the flow acceleration was not measured in this study and it cannot be determined using the developed Equation i.e. 4.21 because no vertical velocity profiles were measured. Thus, the value of acceleration is assumed in this selected datasets.

The comparison for the prediction of Reynolds shear stress using the developed Equation i.e. 4.31 is presented in Figure 4.49. In this figure, there are two different datasets, the open circle samples relate to the prediction of Reynolds shear stress in decelerating flow, the triangle one is the measured Reynolds stress in accelerating flow and their prediction values using the developed equations are represented by the solid lines. In each legend, the letters "A" and "B" denote accelerating and decelerating flows, respectively and the letters I, II and III refer to sediment diameter selected in each flow condition, for example d_{50} =1.8, 0.8 and 1.3mm respectively. For these selected datasets, the assumed values of flow acceleration (a), the determined values of relative errors using $E = \left| \overline{u'v'}_m - \overline{u'v'}_c \right| / \overline{u'v'}_m * 100$ and the computed values of $k_{-\rho\overline{u'v'}}$ using Equations 4.23 and 4.33 are represented in Table 4.4.

Table 4.4: The determinations of $k_{-\rho\overline{u'v'}}$ and E with the assumed a for these selected datasets from Emadzadeh et al. (2010).

Experiment runs	a (m/s^2)	$k_{-\rho\overline{u'v'}}$	E
D-I-0.007-5	-0.0135	16.86	11.56
A-I-0.015-9	0.001	-1.52	13.24
D-II+0.0125-5	-0.0095	20.34	9.15
A-II-0.0125-5	0.0002	-1.023	23.9
DIII+0.0125-7	-0.0085	11.32	8.14
AIII-0.0125-7	0.0002	-1.012	20.9

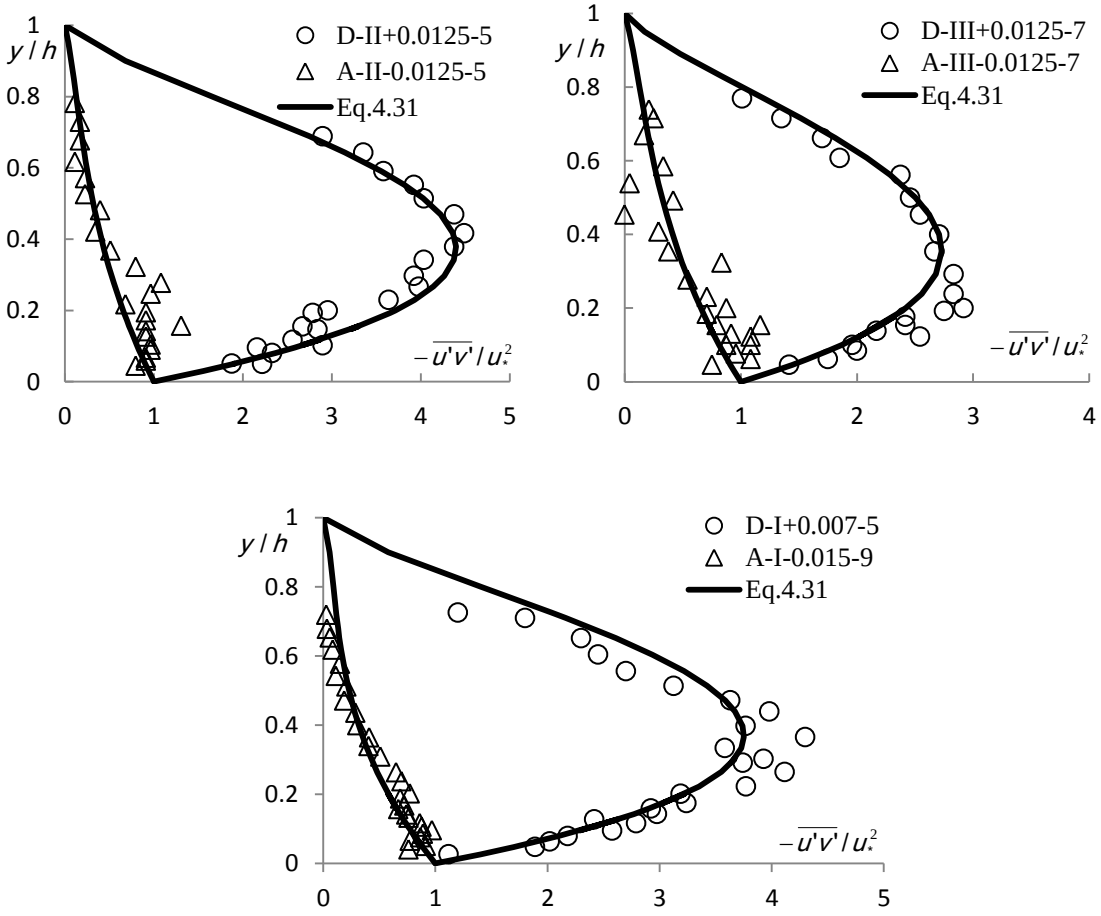

Figure 4.49: Comparison of measured and computed Reynolds shear stress profiles for accelerating and decelerating steady flows (data from Emadzadeh et al.'s paper).

It can be seen from Figure 4.49 that Equation 4.31 is close to the measured data which means that the proposed Equation 4.31 is able to predict the full profile of Reynolds shear stress in accelerating and decelerating flows based on the influence of flow acceleration.

4.13 Other method to predict the distribution of turbulence intensities

In this section, another method to estimate turbulence intensities in unsteady flow is proposed. This method was firstly proposed by Yang and Chow (2008) who developed a new formula to express the similarity between horizontal and vertical turbulence intensities with Reynolds shear stress, they investigated these similarities for steady non-uniform flow only. In this study, this relationship between turbulence intensities and Reynolds shear stress will be extended to unsteady flow. The experimental data from Song's (1994) are plotted in Figure 4.50, in the form of normalised turbulence intensities versus the normalised Reynolds shear stress. This normalization is made with respect to the calculation of turbulent intensities and Reynolds shear stress in uniform flow.

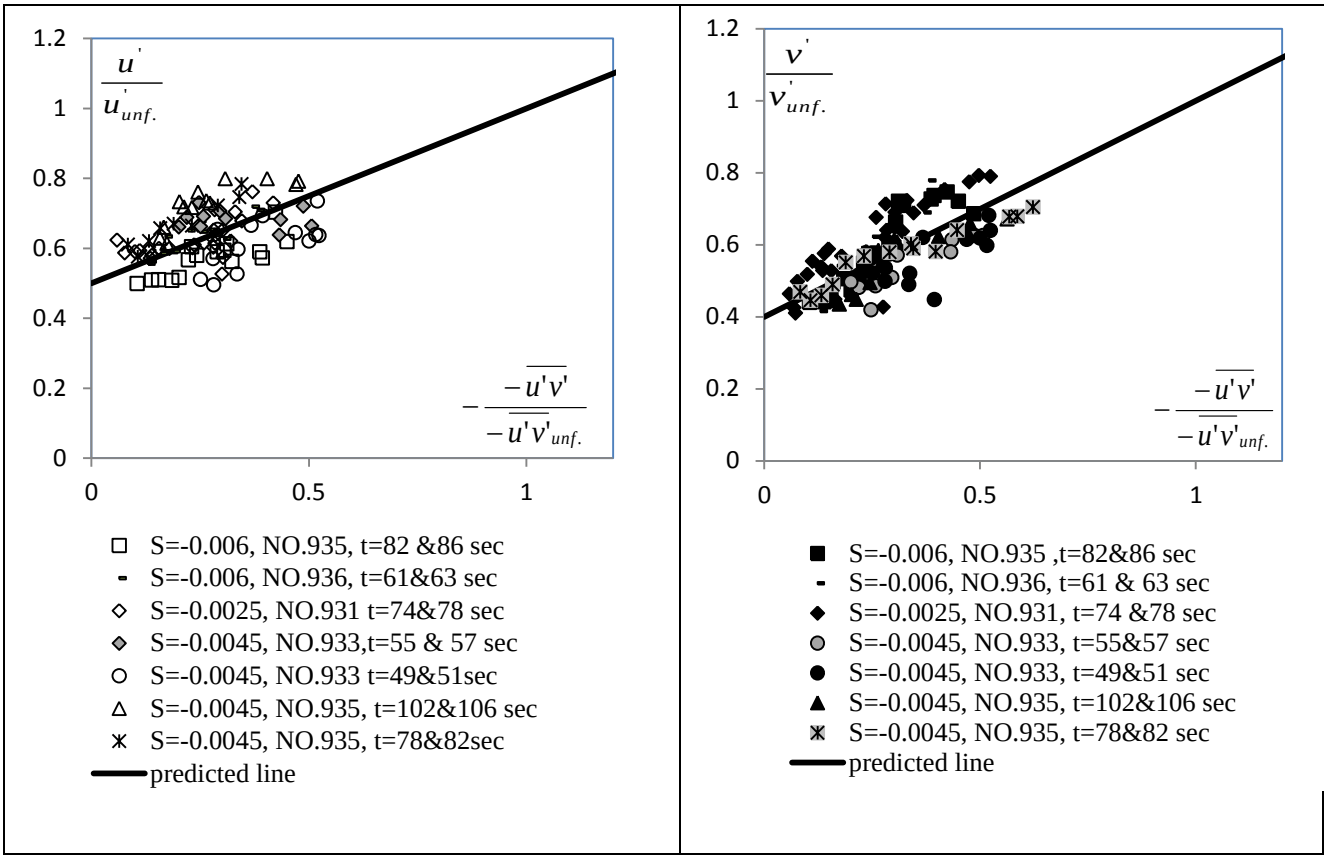

Figure 4.50: Relationship between horizontal and vertical turbulence intensities and Reynolds shear stress in unsteady non-uniform flow based on selected data sets from Song's (1994) where solid lines refer to the predicted Equations 4.45 and 4.46.

As Yang and Chow's (2008) observation about the relationship between relative turbulence intensities and Reynolds shear stress in non-uniform flow, in the present study, we found similar relationships in unsteady flow which can be approximated by:

$$\left(\frac{u'}{u'_{unf.}}\right) = 0.5 + 0.5 * \left(\frac{-\overline{u'v'}}{-\overline{u'v'}_{unf.}}\right) \tag{4.45}$$

$$\left(\frac{v'}{v'_{unf.}}\right) = 0.4 + 0.6 * \left(\frac{-\overline{u'v'}}{-\overline{u'v'}_{unf.}}\right) \tag{4.46}$$

Equations 4.45 and 4.46 describe the relative horizontal $u'/u'_{unf.}$ and vertical $v'/v'_{unf.}$ turbulence intensities in unsteady flow with respect to these turbulences in uniform flow. These two equations demonstrate the values of these turbulence intensities depending on the relative Reynolds shear stress in unsteady flow with respect to

uniform flow, i.e. $-\overline{u'v'}/\overline{u'v'}_{unf.}$. This means that if Reynolds shear stress deviates from the linear distribution, then turbulence intensities will be different from that in uniform flows. If the value of Reynolds shear stress in unsteady flow is less than that in uniform flow, i.e., follows concave distribution, then similar for turbulence intensities distribution can be expected, vice versa. Therefore, the comparisons of measured and predicted turbulence intensities in unsteady flow are plotted in Figure 4.51.

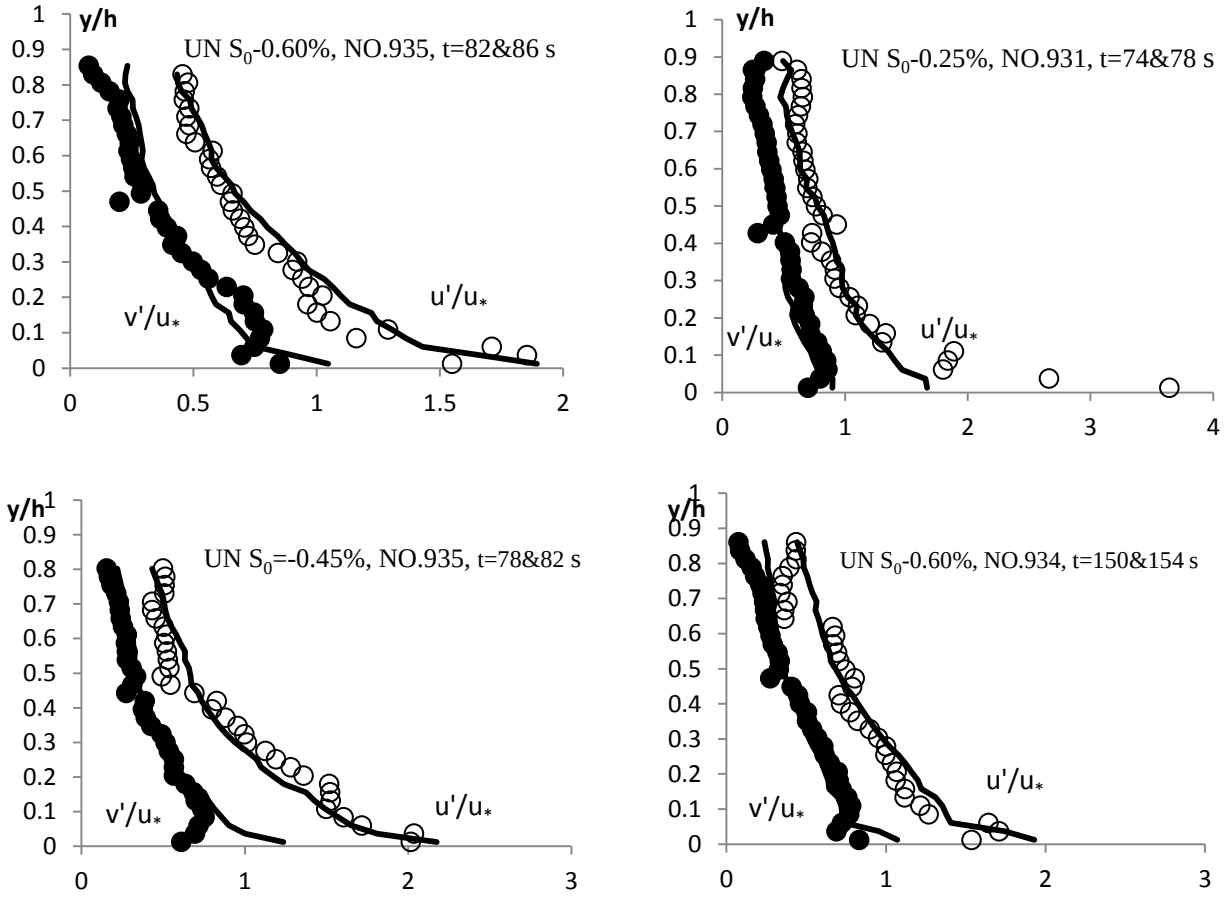

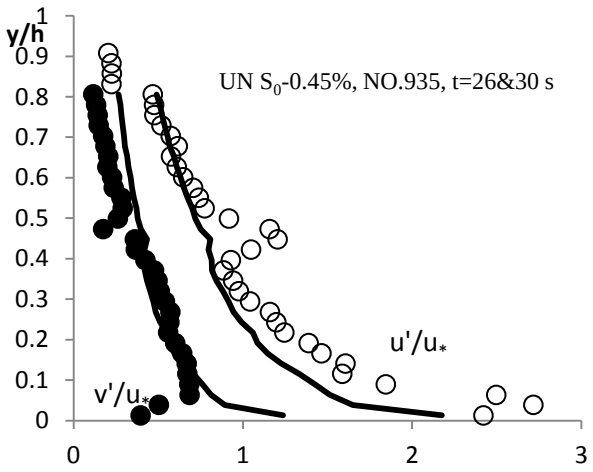
y/h
UN S0-0.45%, NO.935, t=26&30 s
u'/u*
v'/u*

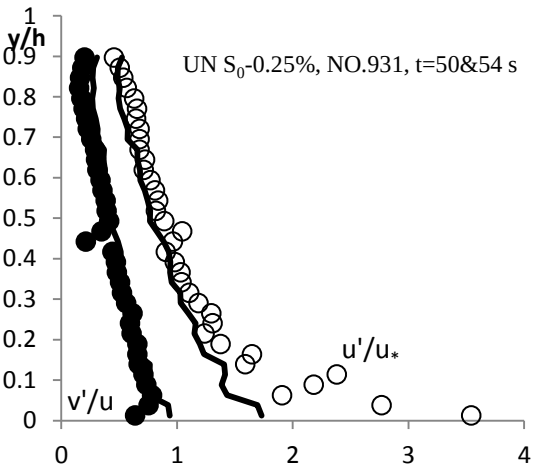
y/h
UN S0-0.25%, NO.931, t=50&54 s
u'/u*
v'/u

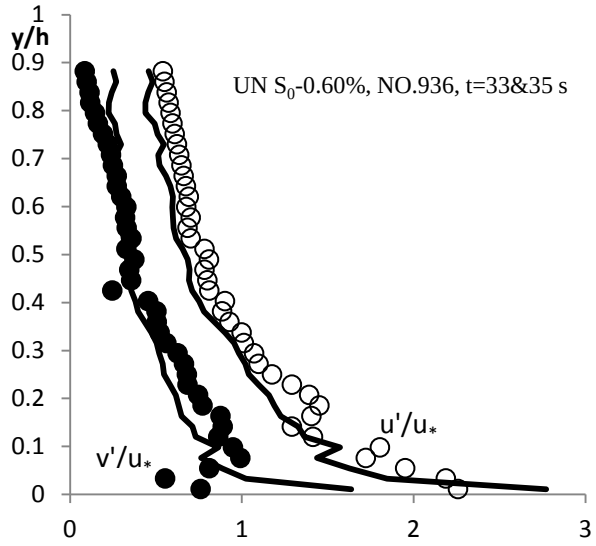
y/h
UN S0-0.60%, NO.936, t=33&35 s
u'/u*
v'/u*

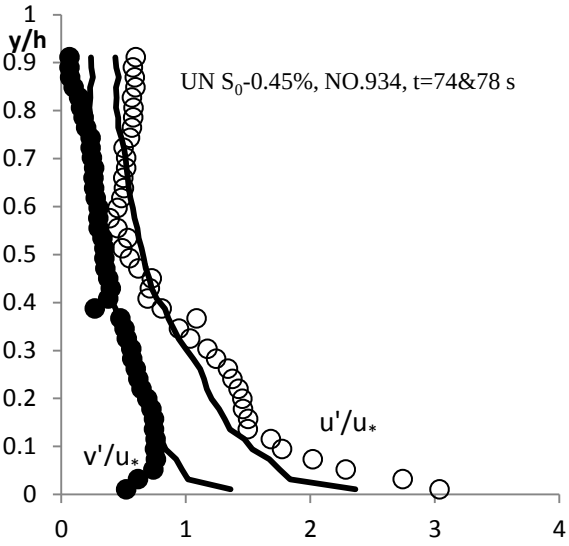
y/h
UN S0-0.45%, NO.934, t=74&78 s
u'/u*
v'/u*

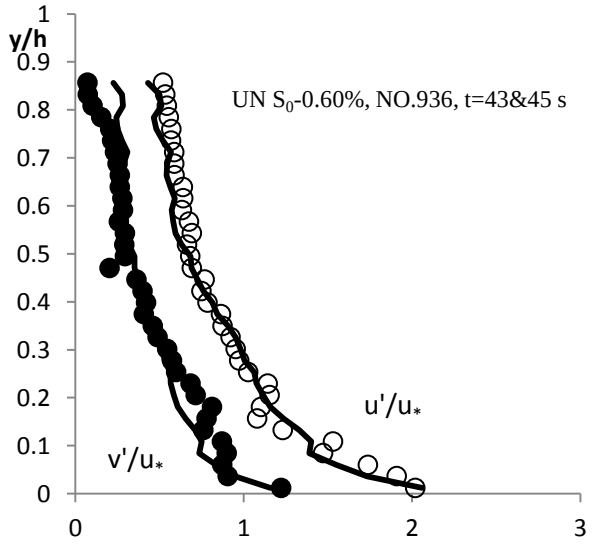
y/h
UN S0-0.60%, NO.936, t=43&45 s
u'/u*
v'/u*

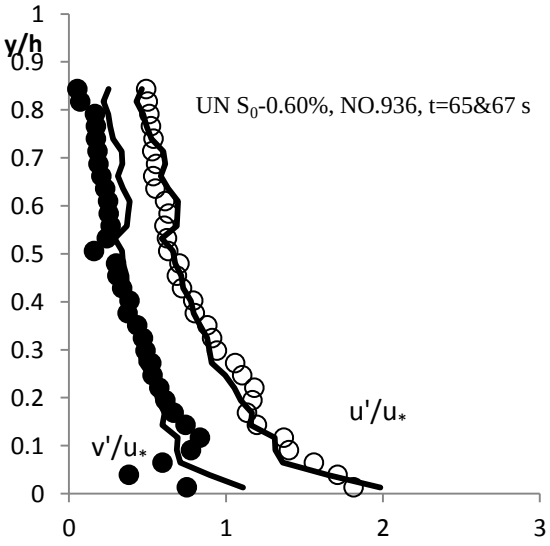
y/h
UN S0-0.60%, NO.936, t=65&67 s
u'/u*
v'/u*

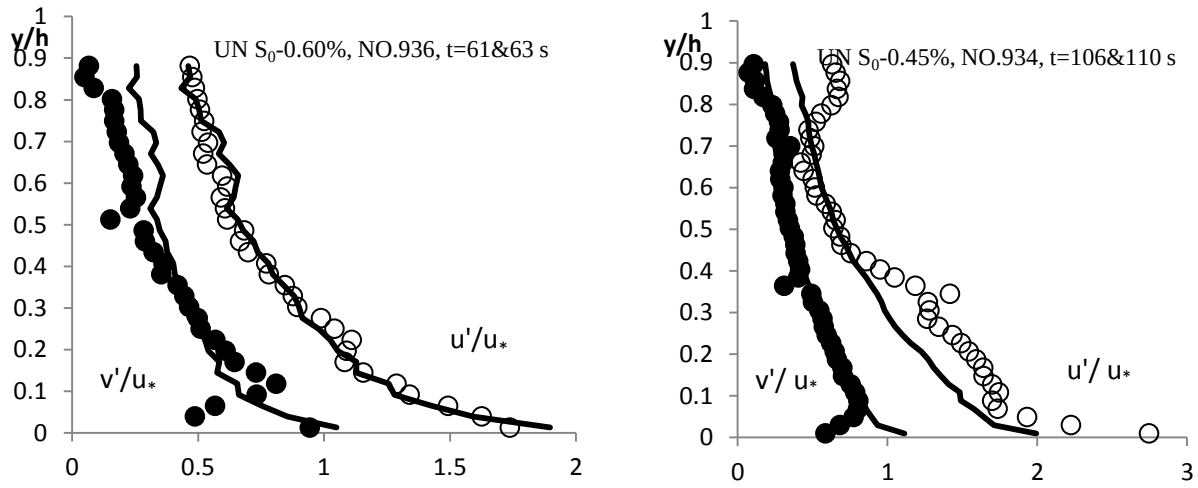

Figure 4.51: Comparison of measured and predicted turbulence intensities in unsteady flow based on Song's (1994) experimental data.

Figure 4.51 shows the comparisons of measured and predicted turbulence intensities in unsteady flow based on Song's (1994) experimental data, where the open circles represent the measured (u'/u_*), the solid circles are the measured (v'/u_*), and the lines are the calculated values from Equations 4.45 and 4.46. It is clearly seen that the agreement between the measured and predicted values are acceptable.

Nezu et al.'s experimental data sets will be used to verify Equations 4.45 and 4.46. Figure 4.52 shows the comparison between the measured and calculated values using the empirical Equations 4.45 and 4.46. Based on these equations, the measured Reynolds shear stress is the main factor to predict other turbulence characteristics, such as (u' and v'). Therefore, the predicted values of these turbulence intensities shown in Figure 4.52 do not appear as smooth lines. Figure 4.52 presents the measured turbulence intensities as open and solid circles and the calculated values as solid lines. Overall, the agreements between the calculated values and experimental measurements are very reasonable.

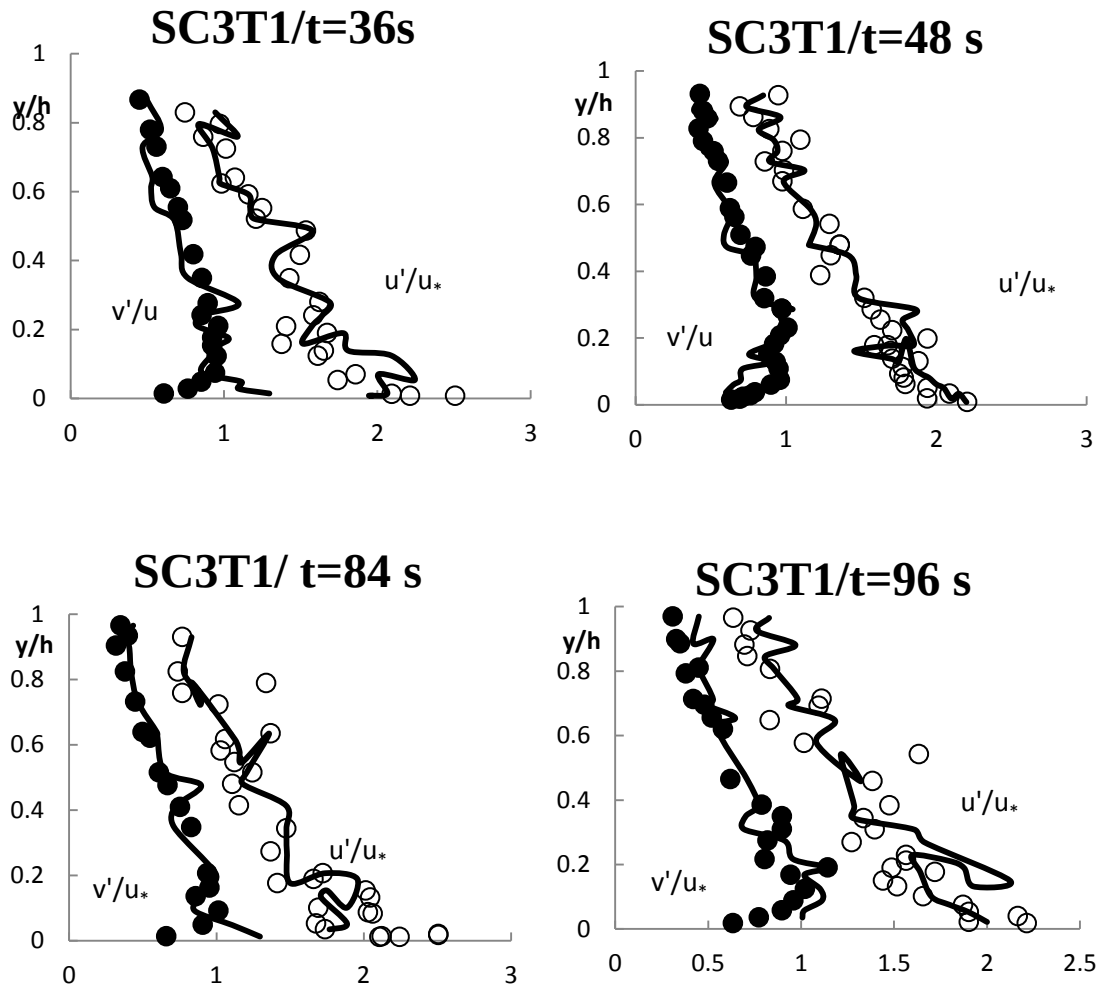

Figure 4.52: Comparison of measured and predicted turbulence intensities in unsteady flow based on Nezu et al. (1997) experimental data.

4.14 Summary

This chapter investigates turbulence characteristics in steady and unsteady non-uniform open channel flows. Specifically, it deals with the re-evaluation of horizontal and vertical velocity, Reynolds shear stress and horizontal and vertical turbulence intensities in non-uniform flows and the development of new formulas for these characteristics. These predicted formulas are associated with the deviations of these turbulence characteristics in steady and unsteady non-uniform flows from that in uniform flow.

CHAPTER 4 THE PREDICTION OF TURBULENCE CHARACTERISTICS IN STEADY AND UNSTEADY FLOWS

For the prediction of mean horizontal velocity, it has been widely reported that the velocity distribution deviates from the classical Log law in steady and unsteady non-uniform flows. In this study, we attribute the deviations to the accelerations of flow. In accelerating non-uniform flow, the longitudinal velocity increases along the open channel, and this leads to positive flow acceleration. In contrast, the decrease of longitudinal velocity generates a negative acceleration, and therefore this flow is decelerating. All data points of longitudinal velocity are higher or lower than Log law's prediction in accelerating or decelerating flows. Therefore, a new empirical equation that combine Log law, Cole's Wake law and Dip law with flow acceleration in both steady and unsteady flows has been proposed, in which two k factors that depend on dimensionless acceleration are determined. The one factor of k is introduced for the Cole's Wake law and the other for the Dip law.

Song's experimental data was used to verify the relationship between the flow acceleration and the values of k. Comparing Equation 4.4 with experimental data by Song (1994), Kironoto and Graf (1995) and Nezu and Nakagawa (1997), good agreements between the measured velocity profiles and predicted values were found using the value of flow acceleration.

The distributions of Reynolds shear stress and turbulence intensities in non-uniform steady and unsteady flows have been predicted. As observed from the literature, the distribution of Reynolds shear stress and turbulence intensities in non-uniform flow deviate from the linear distribution of uniform flow (Song, 1994; Kironoto & Graf, 1995; Song & Chiew, 2001). Song's (1994) experimental results were used to develop the relationships between the dimensionless flow acceleration and values of k for each turbulence characteristics. In both Reynolds shear stress and turbulence intensities, the

positive acceleration (accelerating flow) generates negative value of k while the negative value of flow acceleration (decelerating flow) generates positive value of k. Comparing the determined Reynolds shear stress using Equation 4.31 and the developed turbulence intensities using Equations 4.34, 4.35, 4.36 and 4.37 with experimental data by Song (1994), Kironoto and Graf (1995), Nezu and Nakagawa (1997), Song and Chiew (2001) and Emadzadeh et al.(2010), the agreements between the measured and determined profiles were found to be good.

The vertical velocity in non-uniform steady and unsteady flows was also discussed based on the influence of flow acceleration on the deviation of vertical velocity profiles in non-uniform flows from that in uniform flow. In uniform flow, the distribution of vertical velocity along the water depth is negligible while in accelerating and decelerating non-uniform flows, the value of vertical velocity at the bed is equal to zero when there is no seepage force acting on sediment and then increases until it reaches the maximum value at the water surface. From Song's experimental data, we obtained two empirical Equations, i.e. 4.43 and 4.44, to determine the value of k in accelerating and decelerating flow, respectively depending on the flow acceleration. When the effect of flow acceleration is considered, the agreement between the measured and estimated vertical velocity profiles in steady and unsteady flows is found to be good.

Based on these empirical equations, the turbulence characteristics in unsteady flow, such as longitudinal and vertical velocity, Reynolds shear stress and turbulence intensities were predicted without taking the time factor into the account. This means that the time factor can be ignored to solve any theoretical or experimental problem related to the unsteady flow.

CHAPTER 4 THE PREDICTION OF TURBULENCE CHARACTERISTICS IN STEADY AND UNSTEADY FLOWS

In this study, Yang and Chow's (2008) work was extended to express the relationships between Reynolds shear stress and turbulence intensities in unsteady flow. Based on Song's experimental data, this relationship has been established in unsteady flow. It was found that the deviation of turbulent intensities in non-uniform from uniform flow depends on the ratio of Reynolds shear stress in the non-uniform flow to that in uniform flow. A good agreement between the measured and predicted turbulence intensities in unsteady flow have been achieved depending on the measured Reynolds shear stress.

This study had two main aims: to investigate the effects of accelerating and decelerating non-uniform flows on the incipient motion of sediment transport (Section 5.1); to develop empirical formulas to estimate turbulence characteristics across the full depth of a channel in steady and unsteady flows (Section 5.2).

5.1 The incipient motion of Sediment transport for non-uniform steady flows

Estimation of incipient motion of sediment transport by Shields diagram is well established in the literature. This diagram shows the relationship between sediment diameter and critical shear stress, where the sediment begins to move. However, this diagram is only valid for uniform flow. In non-uniform flow, experimental data sets show significant deviations from Shields curve. The value of critical shear stress in accelerating flow appears higher than expected by Shields while its value in decelerating flow appears below Shields's observation.

In this study, new equations have been developed by modifying Shields criterion for non-uniform flow taking in to account the vertical velocity at the interface between the fluid and porous media. From the literature review, it was clear that non-uniform flow in a channel generates vertical velocity. The profile of vertical velocity along the depth of a channel has negative values when the flow is accelerating and takes positive values when the flow is decelerating. This difference in the value of vertical velocity affects sediment settling velocity. Accelerating flow (decreased water depth along the channel) enhances the sediment settling velocity because the direction of vertical velocity is the same as settling velocity, and therefore, sediment particles become heavier. In contrast, decelerating flow (increased water depth along the channel) generates a positive value

of vertical velocity which has an opposite direction to the settling velocity and therefore, sediment particles become lighter.

A new concept of vertical velocity has been introduced to modify the Shields diagram. This concept is a function of vertical velocity generated from the main flow (V) and the vertical velocity generated from injection or suction seepage (V_s). Each vertical velocity has a relationship with the dimensionless critical shear stress. This relationship depends on the proposed parameter Y which is dependent on the values of vertical velocity from the flow or from the seepage case with the fall velocity. Based on the experimental data sets selected from the previous work in the incipient motion in non-uniform flow or in the seepage case, a good agreement between the measured and determined critical shear stress was achieved. The developed formulas in this study have been predicted well the incipient motion of sediment transport for both non-uniform flows and seepage case. Thus, this is a significant contribution to the body of knowledge on sediment transport in channel flows.

5.2 The development of empirical formulas for turbulence characteristics in steady and unsteady flows

The second aim of this study was to develop empirical formulas to predict the turbulence characteristics in steady and unsteady flows and to observe the impact of flow acceleration on the deviation of measured turbulence characteristics in non-uniform flow from those in uniform flow. The primary purpose is to simplify the study of unsteady flow.

The mean horizontal velocity is the most important flow parameter in steady and unsteady flows. It is clearly understood by previous researchers that Log law cannot predict the full horizontal velocity profile from the bed to the free surface except the

inner region ($y/h < 0.2$). In accelerating flow, the measured data fall below the Log law while it has higher value when the flow is decelerating. The reason for this is attributed to the negative or positive flow acceleration in decelerating or accelerating non-uniform flow, respectively.

Log law was combined with Cole's Wake law and Dip law. This connection is dependent on the relationship between the flow acceleration and the predicted values of k_1 and k_2. Song's experimental data was used to verify these relationships. It is found that for both positive and negative flow accelerations, the values of k_1 and k_2 are positive. According to the data sets from Song (1994), Nezu et al. (1997) and Kironoto and Graf (1995), a good agreement was obtained between the measured and predicted value of velocity profiles depending on the existence of flow acceleration.

In a similar manner, a number of empirical relationships were developed for the other turbulence characteristics, such as Reynolds shear stress ($-\rho\overline{u'v'}$), horizontal and vertical turbulence intensities, i.e. (u' and v'), respectively, and vertical velocity ($\bar{v}$). These empirical formulas were developed dependent on the impact of flow acceleration on the deviation of these turbulence characteristics in non-uniform steady and unsteady flows from those in uniform flow. In each turbulence characteristic, different empirical formulas of k were developed for both accelerating and decelerating flows based on Song's experimental data. Using these values of k, the distribution of Reynolds shear stress, turbulent intensities and vertical velocity across the whole water depth were then predicted. The experimental data from Song (1994), Kironoto and Graf (1995), Nezu et al. (1997), Song and Chiew (2001) and Emadzadeh et al. (2010) support these predictions.

According to all these developed equations, the variation of turbulence characteristics across the entire water depth in steady and unsteady flows were predicted considering the effect of flow acceleration. This means that the prediction of these turbulence characteristics in unsteady flow have been made without referencing to a time factor, which means primary purpose was achieved.

In the current study, another method to predict turbulent intensities in unsteady flow is achieved. This prediction depends on the ratio of Reynolds shear stress in non-uniform flow to that in uniform flow, as developed in Equations 4.45 and 4.46. A good agreement is obtained when compared the measured turbulence intensities from Song (1994) and Nezu et al. (1997) with the calculated values using Equations 4.45 and 4.46.

It can be concluded that the developments and verifications of new empirical equations for turbulent structures in steady and unsteady open channel flows are considered to be further significant contribution coming from this work and adds value to the existing body of technical information available.

5.3 Recommendations for further research

In this research, the influence of steady non-uniform flow on sediment transport especially in the incipient sediment motion was investigated according to the various distribution of vertical velocity generating from steady non-uniform flow or from the seepage case. It is shown that a positive linear distribution of vertical velocity from the bed to water surface was assumed when the flow is non-uniform, and the upward vertical velocity enhances sediment transport. A downward vertical velocity by accelerating flows suppresses sediment transport. These high and low sediment transports are obtained in the incipient sediment motion (see Chapter 3). These different values of vertical velocity are also found in unsteady flow (Song, 1994). Therefore, it is

recommended that the influence of vertical velocity on sediment transport needs to be checked using predicted formula including the influence of vertical velocity on sediment transport.

It is also recommended that a comprehensive laboratory measurement of vertical velocity profiles are undertaken using 3-D LDA technique to verify some of the assumptions made in deriving the formulas. Another aspect discussed in this study was the similarity between steady and unsteady flow. This similarity was demonstrated based on experimental data from Song (1994) who used a changing bed slope to generate non-uniform flow. However, there is another way to do this, which involves changing the laboratory flume width to generate non-uniform flow. It is recommended that the similarity between steady and unsteady flows needs to be experimentally determined when the flume width is either increased or decreased in order to generate non-uniform flow. Changing channel slope and changing channel width are two different geometric configurations and it is likely that the turbulent characteristics they each generate may or may not be different.

REFERENCES

Afzalimhr, H, Dey, S and Rasoulianfar, P 2007, "Influence of decelerating flow on incipient motion of a gravel-bed stream", *Sadhana*, vol. 32, no. 5, pp 545–559.

Andrews, E D and Kuhnle, R A 1993, "Incipient motion of sand-gravel sediment mixture", *Journal of Hydraulic Eng*ineering, vol. 119, pp 1400-1415.

Andrews, E D 1994, "Marginal bed load transport in a gravel-bed stream", *Water Resources Research,* Sagehen Creek, California, vol. 30, pp 2241–2250.

Ashida, K & Bayazit, M 1973, "Initiation of motion and roughness of flows in steep channels", *International Association for Hydraulic Research,* vol.15 TH PT V.1, pp. 475-484.

Bathurst, J C 1987, "Critical Conditions for Bed Material Movement in Steep Boulder-bed Streams", *Erosion and Sedimentation in the Pacific Rim*, no.165, pp 309-318.

Bagheriniyab, F and Lemmin, U 2011," Turbulence and fine sediment suspension in accelerating and decelerating open channel flow",*34th IAHR World Congress – Balance and Uncertainty and 33rd Hydrology and Water Resources Symposium and 10th Hydraulics Conference*, Australia, pp 3365-3369.

Buffington, J M and Montgomery, D R 1997, "A systematic study of eight decades of incipient motion studies with special reference to gravel-bedded rivers", *Water Resources Res*earch, vol.33, no.8, pp 1993-2029.

Cardoso, AH, Graf, WH and Gust, G 1990, "Uniform flow in a smooth open channel", *Journal of Hydraulic Research,* vol. 27, no.5, pp 603-616.

Cardoso, AH, Graf, WH and Gust, G 1991," Steady gradually accelerating flow in a smooth open channel', *Journal of Hydraulic Research,* vol.29, no. 4, pp 525–543.

Carling, PA. 1983, "Threshold of coarse sediment transports in broad and narrow natural streams, *Erath Surface Processes and Landforms,* vol.8, pp1-18.

Cengel, Y.A. and Cimbala, J.M. 2010, Fluid mechanics: fundamentals and application, 2 nd ed., Mc Graw-Hill education, New York.

Chien, N and Wan, Z, 1999, Mechanics of sediment transport, Am. Soc. Civ. Eng. Reston, Va.

Chiew, Y M and Parker, G 1994, "Incipient sediment motion on non-horizontal slopes", *Journal of Hydraulic Research,* vol. 32, pp 649–660.

Cheng, N S and Chiew, Y M 1999, "Incipient sediment motion with upward seepage", *Journal of Hydraulic Research,* vol. 37, no. 5, pp 665-681.

Chow, V T 1959, Open channel hydraulics, Mc Graw-Hill Book Co., New York, NY.

Church, M, Hassan, M A and Wolcott, J F 1998, "Stabilizing self-organized structures in gravel-bed streams", *Water Resource Research,* vol. 34, pp 3169–3179.

REFERENCES

Cipra, B. 1996, "A new theory of turbulence causes a stir among experts", *Science*, vol. 272, no. 5264, pp 951.

Coleman, N L and Alonso, CV 1983, "Two dimensional channel flows over rough surfaces", *Journal of Hydraulic Engineering*, vol. 109, no.2, pp 175-188.

Coles, D 1956, "The law of the wake in turbulent boundary layer", *Journal of Fluid Mech*anics, vol.1, pp. 191-226.

Dey, S, and Debnath, K 2000, "Influence of stream-wise bed slope on sediment threshold under stream flow", *Journal of Irrigation Drainage Engineering*, vol.126, pp 255-263.

Dey, S and Raju, U 2002, "Incipient motion of gravel and coal beds", *Sadhana*, vol. 27, pp 559-568.

Emadzadeh, A, Chiew, YM & Afzalimehr , H 2010, "Effect of accelerating and decelerating flows on incipient motion in sand bed streams", *Advances in Water Resources* ,vol. 33, pp 1094-1104.

Everts, CH 1973, "Particle overpassing on flat granular boundaries", *Journal of the Waterways Harbors and Coastal Engineering Division*, vol. 99, pp 425-439.

Francis, J.B. 1878, "On the cause of the maximum velocity of water flowing in open channels being below the surface", *Trans. ASCE.*, May.

Francalanci, S., Parker, G. and Solari, L 2008, "Effect of seepage – induced non-hydrostatic pressure distribution on bed-load transport and bed morphodynamic", *Journal of Hydraulic Engineering*, vol.134, no.4, pp378-389.

Fernandez Luque, R and Van Beek, R 1976, "Erosion and transport of bed- load sediment", *Journal of Hydraulic Research*, vol.14, no.2, pp127-144.

Garde, R J, Ranga Raju 1985, Mechanics of sediment transportation and alluvial stream problems, 2nd ed. (New York: Wiley).

Gaucher, J, Marche, C and Mahdi, TF 2010, "Experimental investigation of the hydraulic erosion of non-cohesive compacted soils", *Journal of Hydraulic Engineering*, vol. 136, no. 11, pp 901-913.

Graf, WH and Suszka, L1987, "Sediment Transport in Steep Channels", *Journal of Hydroscience and Hydraulic Engineering*, vol.5, no. 1, pp 11-26.

Graf, WH and Altinakar, M 1993, Hydrauliqe Fluvial (Tome1), presess Polytechniques et universities Romandes, Lausanne, Switzerland.

Grass, A.J. 1971, "Structure feature of turbulent flow over smooth and rough boundaries", *Journal of Fluid Mechanics*, vol. 50, pp 233-255.

Griffiths, G.A. and Sutherland, A.J. 1977, "Bed load transport by translation waves", *Journal of Hydraulic Division, American Society Civil*, vol. 103, no. 11, pp1279-1291.

REFERENCES

Hammond, FDC, Heathershaw, AD and Langhorne, DN 1984, "A comparison between Shields threshold criteria and the movement of loosely packed gravel in a tidal channel", *Sedimentology,* vol. 31, pp 51-62.

Henderson, FM 1966, Open channel flow, Macmillan, London.

Huffman, G D, and Bradshaw, P, 1972, " A note on von Karman's constant in low Reynolds number turbulent flows", *Journal of Fluid Mechanics,* vol. 53, no.1, pp 45-60.

Ikeda, S. 1982, "Incipient Motion of Sand Particles on Side Slopes", *Journal of Hydraulics Division ASCE ,* vol.108, no.1, pp 95-114.

Iwagaki, Y 1956, "Fundamental study on critical tractive force", *Trans. Jan. Soc. Civil Engineering,* no. 41, pp 1-21.

Johnston, C E, Andrews, E D, and Pitlick, J 1998, "In situ determination of particle friction angles of fluvial gravels", *Water Resource Research,* vol. 34, no. 8, pp 2017-2030.

Julien, PY 1995, Erosion and Sedimentation, Cambridge University Press.

Kavcar, P.C., and Wright, S.J. 2009, " Experimental results on the stability of non-cohesive sediment beds subject to vertical pore water flux, *Proc. World Environmental and Water Resources Congress 2009: Great Rivers,* vol. 342, pp. 3562-3571, DOI: 10.1061/41036.

Keulegan, G H, 1938, "Law of turbulent flow in open channels", *Journal of Nat. Bureau of Standards, Research,* vol. 21, no. 1151, pp 707-740.

Kirchner, J W, Dietrich, W E, Iseya, F and Ikeda, H 1990, "The variability of critical shear stress, friction angle, and grain protrusion in water worked sediments", *Sedimentology,* vol. 37, pp 647-672.

Kirkgöz, M. S. and Ardiçlioğlu M. 1997, "Velocity Profiles of Developing and Developed Open Channel Flow", *Journal of Hydraulic Eng*ineering, vol.123, no. 12, pp 1099-1105.

Kironoto, B 1992, Turbulence characteristics of uniform and non-uniform, rough open channel flow, Doctoral thesis, Ecole Polytechnique Federale de Lausanne.

Kironoto, B and Graf, WH 1994, "Turbulence characteristics in rough uniform open-channel flow", *In: Proceedings of the institution Civil Engineering Water, Maritime and Energy,* vol. 106, pp 333-344.

Kironoto, B and Graf, WH 1995, "Turbulence characteristics in rough non uniform open channel Flow", *In: Proceedings of the institution Civil Engineering Water, Maritime and Energy,* UK, vol. 112, pp 336-348.

Klebanoff, P S 1954, "Characteristics of turbulence in a boundary layer with zero pressure gradient", *NACA Technical Notes No.3178,* Washington, D.C.

REFERENCES

Ladson, A. 2008, Hydrology: an Australian Introduction, Oxford University Press, Victoria, Australia.

Lamb, M.P., Dietrich, W.E. and Venditti, J.G 2008, "Is the critical Shields stress for incipient sediment motion dependent on channel-bed slope?", *Journal of Geophysical Research*, vol. 113, F02008, pp 1-20.

Lavelle, J W, Mofjeld, H O 1987, "Do critical stresses for incipient motion and erosion really exist?", *Journal of Hydraulic Engineering*, vol. 113, pp 370-385.

Liu, X.X. and Chiew, Y.M. 2012, "Effect of seepage on initiation of cohesionless sediment transport", *Acta Geophysica*, vol. 60, no. 6, pp. 1778-1796, DOI: 10.2478/s11600-012-0043-7.

Lu, Y, Chiew, Y M and Cheng, N S 2008, "Review of seepage effects on turbulent open-channel flow and sediment entrainment", *Journal of Hydraulic* Research, vol. 46, no. 4, pp 476-488.

Mays, LW 2005, Water Resources Engineering, USA.

Monty, J. P., Hutchins, N., Ng, H. C. H., Marusic, I. and Chong M. S. 2009, "A comparison of turbulent pipe, channel and boundary layer flows", *Journal of Fluid Mechanics*, vol.632, pp 431–442.

Mueller E R, Pitlick J, Nelson JM 2005, "Variation in the reference Shields stress for bed load transport in gravel-bed streams and rivers", *Water Resource Re*search, vol. 41:W04006, (doi: 10·1029/2004WR003692).

Neill, C 1967, " Mean-Velocity Criterion for Scour of Coarse Uniform Bed-Material", *International Association for Hydraulic Research*, pp 46-54.

Nezu, I 1977, "Turbulence structures in open channel flow (translation)", Doctoral dissertation, Dep. Civil Engineering, Kyoto University, Japan.

Nezu, I and Rodi, W 1986, "Open channel flow measurements with a laser Doppler anemometer", *Journal of Hydraulic Engineering*, vol. 112, no. 5, pp 335-355.

Nezu, I and Nakagawa, H 1991, " Turbulence structures over dunes and its role on suspended sediments in steady and unsteady open flows, *Intern., Symp on the transport of suspended sediments and its mathematical modeling*, Florence, Italy, pp 165-190.

Nezu, I and Nakagawa, H 1993, "Turbulence in open channel flows", *Monograph of IAHR, A.A.* Balkema publishers, Brookfield, USA.

Nezu, I, Kadota, A and Nakagawa, H 1997, "Turbulent structures in unsteady depth-varing open channel flows", *Journal of Hydraulic Engineering*, vol. 123, no. 9, pp 752-763.

Nikuradse, J 1932, "Gesetzma¨ssigkeiten der turbulenten stromung in glatten rohren. Forschg. *Arb. Ing.-Wes*, vol. 356, no. X, xx–yy.

Paintal, A 1971, "Concept of Critical Shear Stress In Loose Boundary Open Channels", *Journal of Hydraulic Research*, pp 91-109.

REFERENCES

Patel, P L, and Ranga Raju, K G 1999, "Critical tractive stress of non-uniform sediments", *Journal of Hydraulic Research,* vol. 37, pp 39–58.

Prandtl, L 1925, Uber die ausgebildete turbulenz. *ZAMM*, vol. 5, no. 136.

Ramakrishna Rao, A, and Nagaraj, S 1999, "Stability and mobility of sand-bed channel affected by seepage", *Journal of Irrigation Drainage Engineering*, vol. 125, no. 6, pp 370-379.

Reynolds, JA 1974, Turbulence flows in engineering, J. Wiley, London.

Sarker, LK and Hossain, MM 2006, "Shear stress for initiation of motion of median sized sediment of no uniform sediment mixtures, *Journal of Civil Engineering (IEB),* vol.34, no. 2, pp 103-114.

Shields, A 1936, Application of similarity principles, and turbulence research to bed-load movement, California Institute of Technology, Pasadena (translate from German).

Shvidchenko, AB. & Pender, G. 2000, "Flume study of the effect of relative depth on the incipient motion of coarse uniform sediments" *Water Resources Research,* vol. 36, no.2, pp 619-628.

Simons, DB and Senturk, F 1976, "Sediment transport technology", *Water Resources Publications*, Fort Collins, CO.

Song, TC1994, "Velocity and turbulence distribution in non-uniform and unsteady Open - channel flow", *Doctoral dissertation, Ecole Polytechnique Federale de Lausanne,* Switzerland.

Song, T and Graf, WH 1994, "Non uniform open channel flow over a rough bed", *Journal of Hydyroscience and Hydraulic Engineering*, Japan Society of Civil Engineering , Tokyo, vol. 12, no. 1, pp 1-25.

Song, TC and Chiew, YM 2001, "Turbulence measurement in non uniform open-channel flow using Acoustic Doppler velocimeter", *Journal of Hydraulic Engineering*, vol. 127, no. 3, pp 219-232.

Steffler, P M, Rajaratnam, N and Peterson, A W 1985, "LDA measurements in open channel", *Journal of Hydraulic Engineering*, vol. 111, no. 1, pp 119-130.

Sturm, TW 2010, Open Channel Hydraulics, 2nd ed., Mc Graw-Hill companies.

Suszka, L 1987, "Sediment transport in steep channel a laboratory investigation draft for a doctoral dissertation", *Ecole polytechnique federale,* Lausanne, Suisse.

Townsend, A. A. 1956, The structures of turbulent shear flow, Cambridge University Press, New York.

US Army corps of engineers 1996, River Hydraulics, American Society of Civil Engineers.

Van Rijn, LC 1984 a, "Sediment transport, part I: bed load transport", *Journal of Hydraulic Engineering*, vol. 110, no. 10, pp 1431-1456.

Van Rijn, LC 1984 b, "Sediment transport, part II: suspended load transport, *Journal of Hydraulic Engineering*, vol. 110, no. 11, pp 1613-1641.

Van Rijn, 1993, Principles of sediment transport in rivers, estuaries and coastal seas, Bariet, Ruinen, The Netherlands.

White, S J. 1970, "Plane bed thresholds of fine grained sediment", *Nature*, vol.228, pp 152-153.

Wiberg, P L, and Smith, J D 1987, "Calculations of the critical shear stress for motion of uniform and heterogeneous sediments", *Water Resource Research*, vol. 23, pp 1471-1480.

Wilcock, P.R. 1987, Bed-load transport in mixed-size sediment, PhD. Thesis, MIT, Cambridge.

Wilcock, P. R. 1988, "Methods for estimating the critical shear stress of individual fractions in mixed-size sediment", *Water Resource* Research, vol. 24, pp 1127-1135.

Wilcock, P. R. 1992, "Flow competence: A criticism of a classic concept", *Earth Surf. Processes Landforms*, vol. 17, pp 289-298.

Wilcock, PR and Mcardell, BW 1993, "Surface – based fractional transport rates: mobilization thresholds and partial transport of a sand – gravel sediment", *Water Recourse Research*, vol.29, no.4, pp.1297-1312.

Yalin, M.S. and Silva, A.M.F. 2001, Fluvial processes. IAHR, Delft, the Netherlands.

Yang, CT 1973, "Incipient motion and sediment transport", *Journal of the Hydraulics Division*, vol. 99, no. 10, pp 1679-1704.

Yang, C.T 1996, Sediment transport: theory and practice, *Mc Graw-Hill*, Sydney.

Yang, SQ, Tan, SK, and Lim, SY 2004, "Velocity distribution and Dip – phenomenon in smooth uniform open channel flows", *Journal of Hydraulic Engineering*, vol. 130, no. 12, pp 1179-1186.

Yang, SQ and Lee, JW 2007, "Reynolds shear stress distributions in a gradually varied flow", *Journal of Hydraulic Research*, vol. 45, no. 4, pp 462-71.

Yang, SQ and Lim SY 2003, "Total load transport formula for flow in alluvial channels", *Journal of Hydraulic Engineering*, vol. 129, no. 1, pp 68-72.

Yang, SQ 2005, "Prediction of total bed material discharge", *Journal of Hydraulic Research*, vol. 43, no. 1, pp 12-22.

Yang, SQ and Chow, AT 2008, "Turbulence structures in non uniform flows", *Advances in Water Resources*, vol. 31, pp 1344-1351.

Yang, SQ 2009, "Conditionally averaged turbulent structures in 2D channel flow", *Proceedings of the institution of Civil Engineers, Water Management*, vol. 162, issue WMI, pp 1-10.

Zagarola, M. 1996, Ph.D. thesis (Princeton University, Princeton).

APPENDIX A MODIFIED CRITICAL SHEAR STRESS

This appendix contains the original values of dimensionless critical shear stress τ_* and particle diameter d_* collected from Neil (1967), Everts (1973), Cheng and Chiew (1999), Afzalimhr et al. (2007), Kavcar & Wright (2009), Gaucher et al. (2010), Emadzadeh et al. (2010), and Liu and Chiew (2012). This appendix also contains the calculated values of τ_* from the Shields curve which is needed to determine τ'_c / τ_c especially for the data of main flow without seepage, while the seepage data has u_*c and u_*o (m/s) which are referred to critical shear velocity with and without seepage, respectively. Other parameters, such as the variation of water depth dh/dx, U/ω and V_s/ω are also presented.

Table 1 presents these determined parameters and the original values of τ_* and d_* selected from Afzalimhr et al. (2007):

d_{50} (mm)	τ_*	d_*	u_* m/s	dh/dx	τ_* from Shields curve	U/ω	τ'_c / τ_c
8	**0.0242**	**202.26**	**0.056**	**0.003855**	**0.05353**	**0.10689**	**0.45242**
8	**0.0251**	**202.26**	**0.057**	**0.003387**	**0.05357**	**0.10085**	**0.46839**
8	**0.0251**	**202.26**	**0.057**	**0.003171**	**0.05357**	**0.09802**	**0.46839**
8	**0.0234**	**202.26**	**0.055**	**0.00362**	**0.05349**	**0.11408**	**0.43672**
8	**0.0193**	**202.26**	**0.05**	**0.003797**	**0.05326**	**0.12355**	**0.36246**
8	**0.0269**	**202.26**	**0.059**	**0.016185**	**0.05364**	**0.44454**	**0.50118**
8	**0.0225**	**202.26**	**0.054**	**0.01595**	**0.05345**	**0.45741**	**0.42131**
8	**0.0193**	**202.26**	**0.05**	**0.015812**	**0.05326**	**0.47857**	**0.36246**
8	**0.0287**	**202.26**	**0.061**	**0.015519**	**0.05370**	**0.46088**	**0.53509**

Table 2 presents these determined parameters and the original values of τ_* and d_* selected from Everts (1973):

d_{50} (mm)	τ_*	d_*	u_* m/s	dh/dx	τ_* from Shields curve	U/ω	τ'_c/τ_c
1.79	0.0226	45.262	0.041	0.001	0.044	0.034	0.519
1.79	0.0252	45.262	0.043	-0.001	0.044	-0.046	0.572
1.79	0.0191	45.262	0.038	-0.001	0.043	-0.037	0.446
1.79	0.0166	45.262	0.035	-0.003	0.042	-0.065	0.393
0.895	0.0173	22.633	0.027	0.004	0.035	0.129	0.492
0.895	0.0211	22.633	0.031	0.003	0.036	0.107	0.587
0.895	0.0177	22.633	0.027	0.003	0.035	0.090	0.503
0.895	0.0197	22.633	0.030	0.000	0.036	0.007	0.552
0.508	0.0197	12.847	0.023	0.004	0.033	0.172	0.602
0.508	0.0243	12.847	0.026	0.004	0.033	0.161	0.742
0.508	0.0224	12.847	0.025	0.003	0.033	0.130	0.683
0.508	0.0249	12.847	0.027	0.002	0.033	0.083	0.759
0.359	0.0293	9.079	0.024	0.004	0.033	0.233	0.881
0.359	0.0258	9.079	0.023	0.004	0.033	0.210	0.771
0.359	0.0274	9.079	0.024	0.004	0.033	0.188	0.821
0.359	0.0229	9.079	0.022	-0.001	0.034	-0.029	0.679
0.254	0.0323	6.424	0.022	0.004	0.037	0.321	0.881
0.254	0.0348	6.424	0.023	0.004	0.036	0.305	0.961
0.254	0.0411	6.424	0.025	0.003	0.035	0.232	1.172
0.18	0.0388	4.553	0.020	0.004	0.044	0.482	0.886
0.18	0.0463	4.553	0.023	0.003	0.041	0.393	1.121
0.127	0.0521	3.212	0.020	0.004	0.055	0.845	0.953
0.127	0.0521	3.212	0.020	0.004	0.055	0.772	0.954
0.127	0.0399	3.212	0.018	0.002	0.058	0.219	0.686
0.18	0.0559	4.553	0.038	0.001	0.034	0.225	1.621
0.18	0.0563	4.553	0.039	-0.001	0.034	-0.158	1.639
0.18	0.0620	4.553	0.038	-0.002	0.035	-0.428	1.792
0.127	0.0577	3.212	0.032	0.003	0.041	0.945	1.403
0.127	0.0597	3.212	0.033	0.003	0.041	0.838	1.469
0.127	0.0594	3.212	0.033	0.002	0.040	0.617	1.469
0.127	0.0627	3.212	0.035	0.001	0.040	0.213	1.572
0.09	0.0572	2.276	0.027	0.004	0.055	1.783	1.034
0.09	0.0704	2.276	0.031	0.002	0.051	1.263	1.379
0.09	0.0579	2.276	0.028	0.003	0.055	1.237	1.052
0.09	0.0811	2.276	0.033	-0.001	0.049	-0.565	1.644

Table 3 presents these determined parameters and the original values of τ_* and d_* selected from Gaucher et al. (2010):

d_{50} (mm)	τ_*	d_*	u_* m/s	dh/dx	τ_* from Shields curve	U/ω	τ'_c/τ_c
0.91	**0.03**	**23.012**	**0.021**	**0.010**	**0.034**	**0.368**	**0.885**
1.06	**0.032**	**26.805**	**0.023**	**0.009**	**0.035**	**0.397**	**0.907**
1.88	**0.031**	**47.538**	**0.031**	**0.009**	**0.042**	**0.339**	**0.745**
2.2	**0.03**	**55.629**	**0.033**	**0.009**	**0.043**	**0.326**	**0.691**
3.57	**0.02**	**90.266**	**0.034**	**0.009**	**0.047**	**0.264**	**0.421**
4.36	**0.02**	**110.238**	**0.038**	**0.008**	**0.049**	**0.245**	**0.405**

Table 4 presents these determined parameters and the original values of τ_* and d_* selected from Emadzadeh et al. (2010):

d_{50} (mm)	τ_*	d_*	u_* m/s	dh/dx	τ_* from Shields curve	U/ω	τ'_c/τ_c
1.8	**0.11**	**45.52**	**0.02**	**-0.01**	**0.04**	**-0.26**	**2.98**
1.8	**0.13**	**45.52**	**0.02**	**-0.01**	**0.04**	**-0.28**	**3.41**
1.8	**0.15**	**45.52**	**0.02**	**-0.01**	**0.04**	**-0.30**	**3.95**
1.8	**0.07**	**45.52**	**0.01**	**-0.01**	**0.04**	**-0.26**	**1.90**
1.8	**0.09**	**45.52**	**0.02**	**-0.01**	**0.04**	**-0.30**	**2.38**
1.8	**0.10**	**45.52**	**0.02**	**-0.01**	**0.04**	**-0.34**	**2.62**
1.8	**0.05**	**45.52**	**0.01**	**-0.01**	**0.03**	**-0.29**	**1.54**
1.8	**0.06**	**45.52**	**0.01**	**-0.01**	**0.04**	**-0.34**	**1.78**
1.8	**0.07**	**45.52**	**0.01**	**-0.01**	**0.04**	**-0.41**	**2.04**
1.8	**0.08**	**45.52**	**0.02**	**-0.02**	**0.04**	**-0.38**	**2.22**
1.8	**0.06**	**45.52**	**0.01**	**-0.02**	**0.04**	**-0.45**	**1.74**
1.8	**0.11**	**45.52**	**0.02**	**-0.02**	**0.04**	**-0.54**	**2.92**
0.8	**0.08**	**20.23**	**0.01**	**-0.01**	**0.03**	**-0.22**	**2.49**
0.8	**0.09**	**20.23**	**0.01**	**-0.01**	**0.03**	**-0.23**	**2.76**
0.8	**0.10**	**20.23**	**0.01**	**-0.01**	**0.03**	**-0.24**	**3.03**
0.8	**0.08**	**20.23**	**0.01**	**-0.01**	**0.03**	**-0.26**	**2.55**
0.8	**0.09**	**20.23**	**0.01**	**-0.01**	**0.03**	**-0.29**	**2.63**
0.8	**0.10**	**20.23**	**0.01**	**-0.01**	**0.03**	**-0.30**	**3.14**
0.8	**0.11**	**20.23**	**0.01**	**-0.01**	**0.03**	**-0.41**	**3.23**
0.8	**0.12**	**20.23**	**0.01**	**-0.01**	**0.03**	**-0.45**	**3.75**
0.8	**0.14**	**20.23**	**0.01**	**-0.01**	**0.03**	**-0.53**	**4.27**
0.8	**0.10**	**20.23**	**0.01**	**-0.02**	**0.03**	**-0.52**	**3.10**
0.8	**0.13**	**20.23**	**0.01**	**-0.02**	**0.03**	**-0.61**	**3.82**

0.8	0.17	20.23	0.01	-0.02	0.03	-0.73	5.28
1.3	0.05	32.87	0.01	-0.01	0.03	-0.16	1.50
1.3	0.06	32.87	0.01	-0.01	0.03	-0.17	1.77
1.3	0.07	32.87	0.01	-0.01	0.03	-0.19	2.20
1.3	0.09	32.87	0.01	-0.01	0.03	-0.27	2.62
1.3	0.10	32.87	0.01	-0.01	0.03	-0.29	2.93
1.3	0.11	32.87	0.02	-0.01	0.03	-0.32	3.22
1.3	0.05	32.87	0.01	-0.01	0.03	-0.28	1.44
1.3	0.06	32.87	0.01	-0.01	0.03	-0.33	1.74
1.3	0.07	32.87	0.01	-0.01	0.03	-0.36	2.09
1.3	0.06	32.87	0.01	-0.02	0.03	-0.35	1.90
1.3	0.09	32.87	0.01	-0.02	0.03	-0.41	2.56
1.3	0.09	32.87	0.01	-0.02	0.03	-0.53	2.56
1.8	0.01	45.52	0.01	0.01	0.04	0.23	0.18
1.8	0.01	45.52	0.02	0.01	0.04	0.22	0.23
1.8	0.01	45.52	0.02	0.01	0.04	0.21	0.27
1.8	0.01	45.52	0.02	0.01	0.04	0.34	0.27
1.8	0.01	45.52	0.01	0.01	0.04	0.31	0.18
1.8	0.01	45.52	0.01	0.01	0.04	0.27	0.19
1.8	0.01	45.52	0.02	0.01	0.04	0.44	0.28
1.8	0.01	45.52	0.01	0.01	0.04	0.37	0.18
1.8	0.00	45.52	0.01	0.01	0.03	0.34	0.11
1.8	0.00	45.52	0.01	0.02	0.03	0.50	0.11
1.8	0.00	45.52	0.01	0.02	0.03	0.43	0.11
1.8	0.00	45.52	0.01	0.02	0.03	0.37	0.13
0.8	0.01	20.23	0.01	0.01	0.03	0.17	0.19
0.8	0.01	20.23	0.01	0.01	0.03	0.15	0.20
0.8	0.00	20.23	0.01	0.01	0.04	0.14	0.13
0.8	0.00	20.23	0.01	0.01	0.04	0.26	0.10
0.8	0.01	20.23	0.01	0.01	0.03	0.23	0.23
0.8	0.01	20.23	0.01	0.01	0.03	0.21	0.17
0.8	0.01	20.23	0.01	0.01	0.03	0.39	0.23
0.8	0.01	20.23	0.01	0.01	0.03	0.32	0.25
0.8	0.01	20.23	0.01	0.01	0.03	0.29	0.23
0.8	0.01	20.23	0.01	0.02	0.03	0.51	0.28
0.8	0.01	20.23	0.01	0.02	0.03	0.42	0.22
0.8	0.01	20.23	0.01	0.02	0.03	0.38	0.15
1.3	0.00	32.87	0.01	0.01	0.03	0.17	0.15
1.3	0.00	32.87	0.01	0.01	0.03	0.16	0.12
1.3	0.01	32.87	0.01	0.01	0.03	0.14	0.16
1.3	0.01	32.87	0.01	0.01	0.03	0.23	0.20
1.3	0.01	32.87	0.01	0.01	0.03	0.21	0.31
1.3	0.01	32.87	0.01	0.01	0.03	0.19	0.27
1.3	0.01	32.87	0.01	0.01	0.03	0.35	0.21

1.3	**0.01**	**32.87**	**0.01**	**0.01**	**0.03**	**0.30**	**0.18**
1.3	**0.01**	**32.87**	**0.01**	**0.01**	**0.03**	**0.25**	**0.17**
1.3	**0.01**	**32.87**	**0.01**	**0.02**	**0.03**	**0.43**	**0.29**
1.3	**0.01**	**32.87**	**0.01**	**0.02**	**0.03**	**0.35**	**0.21**
1.3	**0.00**	**32.87**	**0.01**	**0.02**	**0.03**	**0.30**	**0.08**

Table 5 presents these determined parameters and the original values of τ_* and d_* selected from Neil (1967):

d_{50} **(mm)**	τ_*	d_*	u_* **m/s**	dh/dx	τ_* from Shields curve	U/ω	τ'_c/τ_c
6.2	**0.04**	**153.19**	**0.06**	**0.00**	**0.05**	**0.10**	**0.82**
6.2	**0.05**	**153.19**	**0.07**	**0.00**	**0.05**	**0.04**	**0.98**
6.2	**0.05**	**153.19**	**0.07**	**0.01**	**0.05**	**0.16**	**1.01**
6.2	**0.05**	**153.19**	**0.07**	**0.01**	**0.05**	**0.24**	**1.00**
6.2	**0.05**	**153.19**	**0.07**	**0.01**	**0.05**	**0.27**	**0.96**
6.2	**0.05**	**153.19**	**0.07**	**0.01**	**0.05**	**0.30**	**0.99**
6.2	**0.05**	**153.19**	**0.07**	**0.01**	**0.05**	**0.31**	**1.00**
6.2	**0.06**	**153.19**	**0.07**	**0.01**	**0.05**	**0.33**	**1.10**
6.2	**0.04**	**153.19**	**0.06**	**0.01**	**0.05**	**0.30**	**0.81**
6.2	**0.05**	**153.19**	**0.06**	**0.01**	**0.05**	**0.31**	**0.85**
8.5	**0.05**	**209.10**	**0.08**	**0.03**	**0.05**	**0.70**	**0.96**
8.5	**0.04**	**209.10**	**0.07**	**0.00**	**0.05**	**-0.10**	**0.82**
8.5	**0.04**	**209.10**	**0.07**	**0.01**	**0.05**	**0.13**	**0.69**
8.5	**0.04**	**209.10**	**0.07**	**0.01**	**0.05**	**0.18**	**0.76**
8.5	**0.04**	**209.10**	**0.07**	**0.01**	**0.05**	**0.21**	**0.73**
8.5	**0.04**	**209.10**	**0.07**	**0.01**	**0.05**	**0.23**	**0.80**
8.5	**0.05**	**209.10**	**0.08**	**0.01**	**0.05**	**0.24**	**0.97**
8.5	**0.05**	**209.10**	**0.08**	**0.01**	**0.05**	**0.25**	**0.85**
8.5	**0.05**	**209.10**	**0.08**	**0.01**	**0.05**	**0.26**	**0.86**
8.5	**0.04**	**209.10**	**0.07**	**0.01**	**0.05**	**0.26**	**0.72**
10.6	**0.04**	**261.90**	**0.08**	**-0.02**	**0.05**	**-0.63**	**0.81**
10.6	**0.04**	**261.90**	**0.08**	**0.00**	**0.05**	**-0.10**	**0.82**
10.6	**0.05**	**261.90**	**0.09**	**0.00**	**0.05**	**-0.04**	**0.86**
10.6	**0.05**	**261.90**	**0.09**	**0.00**	**0.05**	**0.03**	**0.92**
10.6	**0.06**	**261.90**	**0.09**	**0.00**	**0.05**	**0.06**	**1.02**
10.6	**0.05**	**261.90**	**0.09**	**0.00**	**0.05**	**0.15**	**0.95**
10.6	**0.05**	**261.90**	**0.09**	**0.01**	**0.05**	**0.18**	**0.96**
10.6	**0.05**	**261.90**	**0.09**	**0.01**	**0.05**	**0.21**	**0.98**
20	**0.05**	**491.96**	**0.12**	**0.03**	**0.05**	**0.63**	**0.95**
20	**0.06**	**491.96**	**0.13**	**0.03**	**0.05**	**0.68**	**1.06**
20	**0.05**	**491.96**	**0.12**	**0.03**	**0.05**	**0.76**	**0.93**

20	0.05	491.96	0.12	0.05	0.05	1.34	0.91
20	0.04	491.96	0.11	-0.01	0.05	-0.27	0.81
20	0.05	491.96	0.13	-0.01	0.05	-0.36	0.97
23.8	0.06	585.42	0.14	0.03	0.05	0.67	1.06
23.8	0.06	585.42	0.14	0.03	0.05	0.70	1.06
29.1	0.06	715.78	0.16	0.03	0.05	0.74	1.11
29.1	0.06	715.78	0.16	0.03	0.05	0.82	1.15
29.1	0.06	715.78	0.16	0.04	0.05	1.21	1.11
5	0.04	122.19	0.06	0.01	0.05	0.25	0.81
5	0.04	122.19	0.05	0.01	0.05	0.27	0.77
5	0.04	122.19	0.06	0.01	0.05	0.29	0.81
5	0.05	122.19	0.06	0.01	0.05	0.31	0.88
5	0.04	122.19	0.05	0.01	0.05	0.30	0.77
5	0.04	122.19	0.06	0.01	0.05	0.31	0.81
5	0.05	122.19	0.06	0.01	0.05	0.33	0.86
5	0.04	122.19	0.05	0.01	0.05	0.31	0.77
16	0.06	392.71	0.12	0.04	0.05	1.15	1.17
16	0.06	392.71	0.12	-0.02	0.05	-0.77	1.18
6.4	0.05	92.68	0.03	0.01	0.05	0.26	0.95
6.4	0.05	92.68	0.03	0.01	0.05	0.28	0.93
6.4	0.04	92.68	0.03	0.01	0.05	0.27	0.85
6.4	0.05	92.68	0.03	0.01	0.05	0.30	0.98
6.4	0.05	92.68	0.03	0.01	0.05	0.31	0.96
6.4	0.05	92.68	0.03	0.01	0.05	0.31	0.93
6.4	0.05	92.68	0.03	0.01	0.05	0.32	0.96
6.4	0.05	92.68	0.03	0.01	0.05	0.33	0.99
6.4	0.06	92.68	0.03	0.01	0.05	0.34	1.10
6.4	0.06	92.68	0.03	0.01	0.05	0.36	1.09

Table 6 presents these determined parameters and the original values of τ_* and d_* selected from Cheng and Chiew (1999):

d_{50} (mm)	τ_*	d_*	u_*o (m/s)	u_*c (m/s)	dh/dx	V_s/ω	τ'_c/τ_c
1.95	0.015	49.3	0.032	0.0217	0.008	0.043	0.460
1.95	0.030	49.3	0.032	0.0309	0.009	0.000	0.932
1.95	0.010	49.3	0.032	0.0181	0.009	0.045	0.320
1.95	0.033	49.3	0.032	0.0325	0.009	0.000	1.031
1.95	0.020	49.3	0.032	0.0249	0.008	0.042	0.605
1.95	0.014	49.3	0.032	0.0207	0.008	0.043	0.418
1.95	0.007	49.3	0.032	0.0152	0.009	0.060	0.226
1.95	0.002	49.3	0.032	0.0076	0.010	0.075	0.056
1.95	0.002	49.3	0.032	0.0087	0.010	0.080	0.074
1.95	0.004	49.3	0.032	0.0109	0.009	0.084	0.116

1.95	0.006	49.3	0.032	0.0132	0.009	0.081	0.170
1.95	0.009	49.3	0.032	0.0168	0.009	0.061	0.276
1.95	0.020	49.3	0.032	0.025	0.009	0.023	0.610
1.95	0.003	49.3	0.032	0.0099	0.009	0.080	0.096
1.95	0.004	49.3	0.032	0.0116	0.009	0.072	0.131
1.02	0.003	25.8	0.021	0.0065	0.010	0.055	0.096
1.02	0.001	25.8	0.021	0.003	0.010	0.057	0.020
1.02	0.001	25.8	0.021	0.0044	0.010	0.055	0.044
1.02	0.002	25.8	0.021	0.0056	0.010	0.050	0.071
1.02	0.003	25.8	0.021	0.0072	0.010	0.051	0.118
1.02	0.024	25.8	0.021	0.0199	0.010	0.000	0.898
1.02	0.008	25.8	0.021	0.0117	0.010	0.032	0.310
1.02	0.028	25.8	0.021	0.0215	0.010	0.000	1.048
1.02	0.013	25.8	0.021	0.0149	0.010	0.022	0.503
1.02	0.011	25.8	0.021	0.0134	0.010	0.029	0.407
1.02	0.015	25.8	0.021	0.0155	0.010	0.027	0.545
1.02	0.006	25.8	0.021	0.0098	0.010	0.050	0.218
1.02	0.005	25.8	0.021	0.0091	0.010	0.048	0.188
1.02	0.005	25.8	0.021	0.0091	0.010	0.048	0.188
1.02	0.011	25.8	0.021	0.0133	0.010	0.036	0.401
1.02	0.011	25.8	0.021	0.0137	0.010	0.040	0.426
0.63	0.005	15.9	0.017	0.0071	0.010	0.013	0.174
0.63	0.012	15.9	0.017	0.0112	0.010	0.014	0.434
0.63	0.011	15.9	0.017	0.0106	0.010	0.012	0.389
0.63	0.002	15.9	0.017	0.0041	0.010	0.013	0.058
0.63	0.008	15.9	0.017	0.0092	0.010	0.014	0.293
0.63	0.028	15.9	0.017	0.0169	0.010	0.000	0.988
0.63	0.008	15.9	0.017	0.009	0.010	0.016	0.280
0.63	0.005	15.9	0.017	0.0068	0.010	0.017	0.160
0.63	0.002	15.9	0.017	0.005	0.010	0.016	0.087
0.63	0.010	15.9	0.017	0.01	0.010	0.014	0.346
0.63	0.005	15.9	0.017	0.007	0.010	0.017	0.170
0.63	0.004	15.9	0.017	0.006	0.010	0.017	0.125
0.63	0.001	15.9	0.017	0.0038	0.010	0.019	0.050
0.63	0.001	15.9	0.017	0.0025	0.010	0.020	0.022
0.63	0.011	15.9	0.017	0.0105	0.010	0.013	0.381
0.63	0.006	15.9	0.017	0.0079	0.010	0.019	0.216
0.63	0.004	15.9	0.017	0.0066	0.010	0.019	0.151
0.63	0.002	15.9	0.017	0.0048	0.010	0.019	0.080
0.63	0.012	15.9	0.017	0.0112	0.010	0.014	0.434

Table 7 presents these determined parameters and the original values of τ_* and d_* selected from Kavcar and Wright (2009):

d_{50} (mm)	τ_*	d_*	u_*o (m/s)	u_*c (m/s)	dh/dx	V_s/ω	τ'_c/τ_c
0.16	0.067	4.047	0.013	0.013	0.010	0.000	1.000
0.16	0.065	4.047	0.013	0.013	0.010	0.002	0.974
0.16	0.060	4.047	0.013	0.012	0.010	0.003	0.889
0.16	0.062	4.047	0.013	0.013	0.010	0.005	0.920
0.16	0.110	4.047	0.013	0.017	0.010	-0.003	1.636
0.16	0.096	4.047	0.013	0.016	0.010	-0.006	1.431
0.5	0.029	12.645	0.015	0.015	0.010	0.000	1.000
0.5	0.025	12.645	0.015	0.014	0.010	0.001	0.851
0.5	0.024	12.645	0.015	0.014	0.010	0.002	0.832
0.5	0.024	12.645	0.015	0.014	0.010	0.002	0.817
1.2	0.025	30.345	0.022	0.022	0.010	0.000	1.000
1.2	0.018	30.345	0.022	0.019	0.010	0.009	0.704
1.2	0.017	30.345	0.022	0.018	0.010	0.014	0.679
1.2	0.018	30.345	0.022	0.019	0.010	0.018	0.717
1.2	0.036	30.345	0.022	0.026	0.010	-0.012	1.422
1.2	0.047	30.345	0.022	0.030	0.010	-0.021	1.848

Table 8 presents these determined parameters and the original values of τ_* and d_* selected from Liu and Chiew (2012):

d_{50} (mm)	τ_*	d_*	u_*o (m/s)	u_*c (m/s)	dh/dx	V_s/ω	τ'_c/τ_c
0.9	0.052	22.759	0.022	0.028	0.010	-0.030	1.638
0.9	0.055	22.759	0.022	0.028	0.010	-0.026	1.716
0.9	0.047	22.759	0.022	0.026	0.010	-0.015	1.464
0.9	0.046	22.759	0.022	0.026	0.010	-0.011	1.440
0.9	0.031	22.759	0.022	0.021	0.010	0.000	0.980